UNIVERSITÉ DE STRASBOURG

ÉCOLE DOCTORALE DES SCIENCES CHIMIQUES (ED 222)
ICPEES, UMR 7515 CNRS

THÈSE
présentée par

Cuong DUONG-VIET

Soutenue le 23 Juillet 2015

Pour obtenir le grade de

Docteur de l'université de Strasbourg

Discipline/ Spécialité: Chimie /Chimie Physique

Synthèse et mise en forme des catalyseurs «sans métaux» à base de nanotubes de carbone dopés à l'azote pour les procédés d'oxydation sélective de l'H$_2$S

Synthesis and processing of nitrogen-doped carbon nanotubes

as metal-free catalyst for H$_2$S selective oxidation process

Membres du jury:

Dr. Cuong PHAM-HUU	Directeur de thèse, Université de Strasbourg
Dr. Claude ESTOURNES	Rapporteur externe, CIRIMAT, Université de Toulouse
Dr. Andrei KHODAKOV	Rapporteur externe, UCCS, Université de Lille
Pr. Ovidu ERSEN	Examinateur, IPCMS, Université de Strasbourg

Acknowledgements

Contents

Chapter 2. Nitrogen-doped carbon nanotubes decorated silicon carbide as a metal-free catalyst for partial oxidation of H₂S...73

Chapter 3. A highly N-doped carbon phase "dressing" of macroscopic supports for catalytic applications...101

Résumé - Abstract

Depuis l'article publié par Iijima [1] en 1991 portant sur l'observation des nanotubes de carbone présents en tant que sous-produits dans les matériaux synthétisés par arc électrique, un nombre sans cesse croissant de travaux de recherches a été focalisé sur ce sujet, allant des méthodes de synthèse, caractérisations, mécanisme de croissance, jusqu'aux modifications chimiques de la surface ou directement dans la matrice carbonée elle-même pour des applications multiples [2-5].

En effet, en raison de leurs propriétés physiques et chimiques exceptionnelles, les nanomatériaux à base de carbone pourraient être utilisés dans de nombreux domaines d'applications potentiellement prometteuses (biochimiques, mécaniques, électrodes, et catalyse…) [2, 4, 6-12]. En catalyse, ils peuvent être efficacement utilisés en tant que support de catalyseurs pour diverses phases actives, et plus récemment, en tant que catalyseurs « sans métaux » dans divers procédés catalytiques, allant de l'oxydation à l'hydrogénation en passant par la déshydrogénation sélective.

Plusieurs récents rapports ont été publiés concernant les avantages de l'utilisation des nanomatériaux à base de carbone dopés (azote, oxygène) directement comme catalyseurs « sans métaux » dans de nombreux procédés catalytiques pertinents [6-12]. Dans les diverses applications reportées, les matériaux carbonés dopés présentent souvent des performances catalytiques supérieures comparées à celles obtenues sur des catalyseurs traditionnels supportés à base de métaux ou d'oxyde de métaux. Cependant, très peu d'études portent sur la relation entre les paramètres de synthèse, les propriétés physico-chimiques, la mise en forme macroscopique et les performances catalytiques de ces matériaux.

La présente thèse a pour objectif de mettre au point des catalyseurs à base de carbone dopés avec de l'azote pour le procédé d'oxydation partielle des traces de sulfure d'hydrogène (H_2S) en soufre élémentaire, et de dresser la relation structure-activité de ce type de catalyseur. Les résultats obtenus montrent également que ce type de catalyseur « sans métaux » pourrait être utilisé dans d'autres procédés catalytiques en lieu et place des catalyseurs traditionnels et ouvrent ainsi une nouvelle voie de développement intéressant pour la catalyse.

La première partie de cette thèse a consisté à réaliser et optimiser la synthèse des composites carbonés à base de nanotubes de carbone, soit sous forme massique, soit sous forme supportée, dopés ou non avec de l'azote, et leurs caractérisations physico-chimiques adéquates, afin de déterminer l'influence des paramètres de synthèse sur les propriétés physico-chimiques des matériaux ainsi obtenus. Nous développons également une nouvelle voie de synthèse qui permet l'obtention d'une nouvelle phase à base de carbone mésoporeux dopé avec de l'azote qui pourrait avantageusement replacer les nanotubes de carbone dopés à l'azote en tant que catalyseur « sans métaux » dans les procédés catalytiques portant sur l'oxydation sélective.

La seconde partie de cette thèse porte sur l'utilisation de ces nanomatériaux ainsi synthétisés en tant que catalyseurs « sans métaux » dans le procédé d'oxydation partielle d'H_2S en soufre élémentaire. Les performances catalytiques seront étudiées en fonction des différents paramètres réactionnels, tels que la température de réaction, la vitesse spatiale horaire et le ratio oxygène/H_2S. Nous étudierons également la stabilité du catalyseur en fonction de la durée de test et la possibilité de régénérer ces catalyseurs en vue d'applications industrielles ultérieures.

1. Synthèse des composites à base de nanotubes de carbone (NTC) dopés avec de l'azote comme catalyseurs « sans métaux » pour la réaction d'oxydation sélective de l'H_2S.

La première partie de cette thèse porte sur la synthèse des composites à base de nanotubes de carbone dopés avec de l'azote (N-NTCs), soit sous forme massique, soit supportés sur des structures hôtes macroscopiques à base de carbure de silicium (SiC extrudés et mousse alvéolaire). La synthèse est réalisée par la méthode dite de Chemical Vapor Deposition (CVD) utilisant un mélange gazeux de C_2H_6/H_2/NH_3 avec des proportions variables, et un catalyseur de croissance à base de Fe/Al_2O_3 avec une charge massique en fer de 20 %. La synthèse est réalisée à différentes températures, allant de 700 à 800 °C, avec des durées variables. Les N-NTC sont récupérés après synthèse et purifiés par un traitement basique puis acide afin d'éliminer les résidus du catalyseur de croissance. Les analyses par microscopie électronique à transmission (MET) des N-NTC sont présentées sur la Fig. 1, et montrent l'absence de carbone amorphe et de nanoparticules de carbone dans l'échantillon, confirmant ainsi la forte sélectivité de la synthèse.
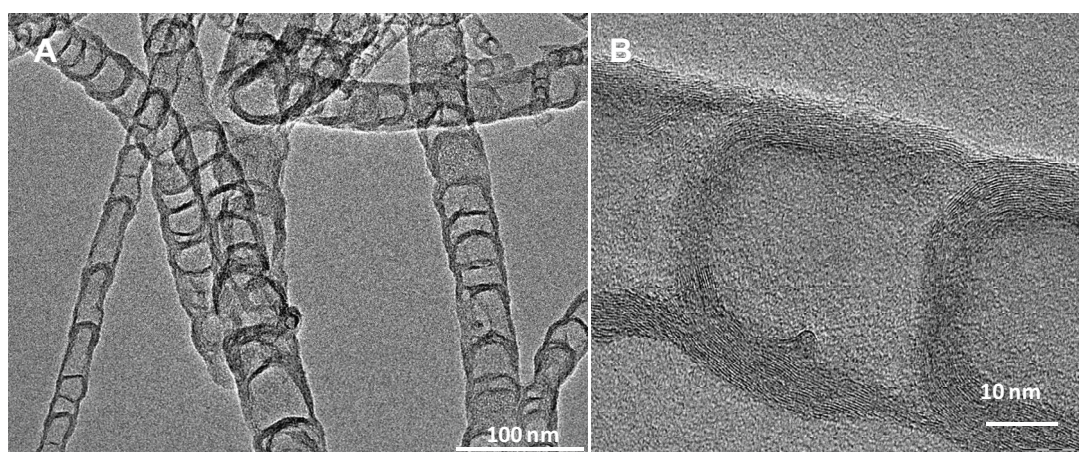
Fig. 1. Images MET des nanotubes de carbone dopés avec de l'azote montrant la morphologie particulière en forme de bambou de ces matériaux et une bonne graphitisation des murs.

Les N-NTCs ainsi synthétisés possèdent des surfaces spécifiques relativement élevées, de l'ordre de 150 à 200 $m^2.g^{-1}$ grâce à leur dimension nanométrique mais aussi à la présence de nombreux défauts structuraux sur la surface qui jouent le rôle de sites d'adsorption. Les conditions optimales de synthèse ont été déterminées en comparant les différents résultats obtenus: concentration de $C_2H_6/H_2/NH_3$ de 50/50/20 $mL.min^{-1}$, une température de synthèse de 750 °C et une durée de synthèse de 3h. Pour des durées de synthèse plus longues le rendement en N-NTCs diminue due en partie à l'encapsulation des sites métalliques de croissance. Les analyses de surface obtenues par spectroscopie de photoélectrons induits par rayons X (XPS) ont montré que l'azote est engagé dans la structure carbonée sous diverses formes: pyridinique, pyrrolique, quaternaire et incorporé (ou oxyde d'azote) (Fig. 2) [13]. La concentration des groupements azotés peut être modifiée en fonction des paramètres de synthèse ou des traitements thermiques ultérieurs.
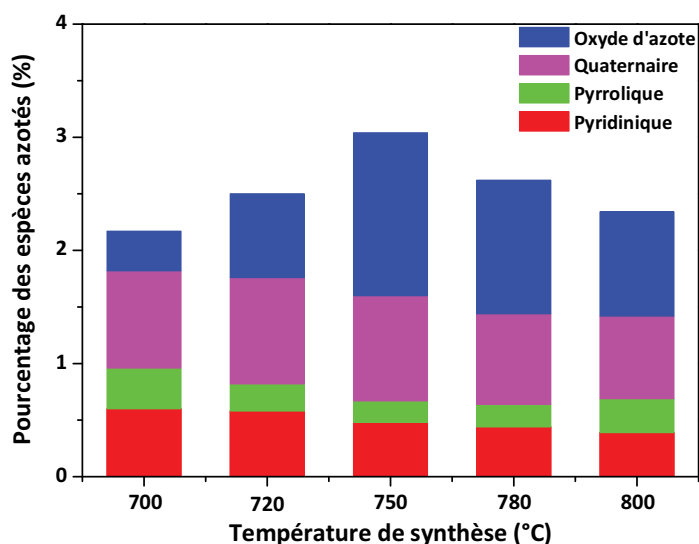
Fig. 2. Diagramme montrant les répartitions des groupements azotés présents dans le N-NTC obtenues par XPS en fonction de la température de synthèse.

Les mêmes conditions de synthèse ont été appliquées avec succès pour la synthèse des N-NTCs supportés sur des structures hôtes macroscopiques à base de SiC, en remplaçant le catalyseur de croissance Fe/Al_2O_3 par du Fe/SiC. Néanmoins, dans le cas du SiC la concentration de fer dans le catalyseur de croissance (Fe/SiC) a dû être ramenée à 7 % en poids. En effet, pour des concentrations en fer trop élevées une croissance importante des N-NTCs entraînent la destruction du composite après synthèse, ce qui n'était pas le cas pour l'alumine.

Les composites carbones dopés avec de l'azote ont été utilisés comme catalyseurs sans métaux pour la réaction d'oxydation sélective de l'H_2S en soufre élémentaire. Cette réaction a été choisie comme réaction modèle afin d'évaluer les performances catalytiques

de ce type de catalyseur dans des réactions d'oxydation en général. L'influence de l'azote en tant que dopant dans le réseau du carbone a été reportée dans la littérature dans diverses réactions en catalyse.
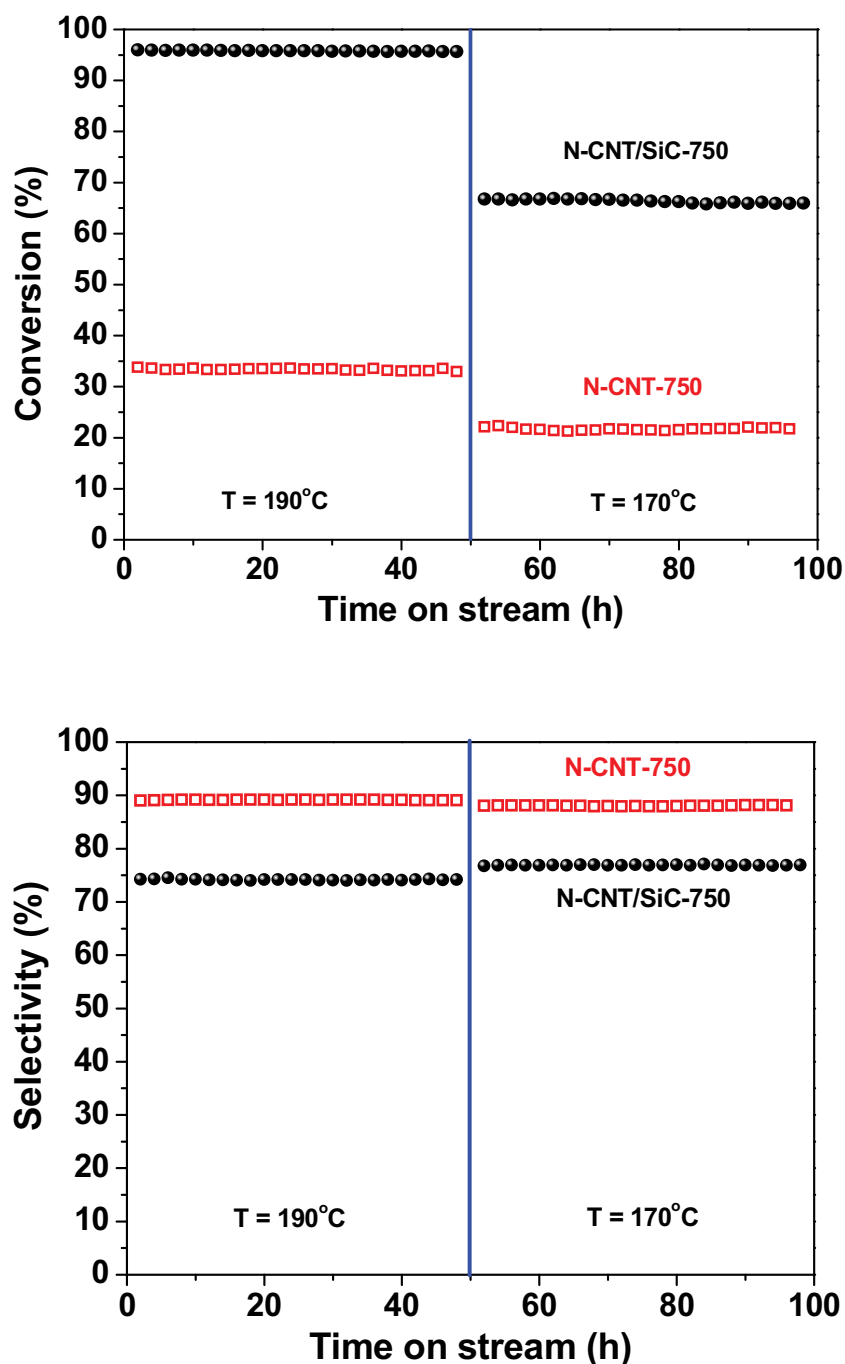
Fig. 3. L'activité en désulfuration de l'H$_2$S en fonction de la température sur des catalyseurs à base de N-NTC/SiC et N-NTCs. Conditions expérimentales: H$_2$S = 1 vol.%; ratio O$_2$/H$_2$S = 2,5; H$_2$O = 30 vol.%; WHSV = 0,6 h^{-1}; M$_{cata}$ (phase active) = 300 mg.

Les divers résultats obtenus ont montré que l'activité désulfurante demeure stable en fonction de la durée du test, et confirme ainsi la forte stabilité des catalyseurs carbonés dopés avec de l'azote par rapport à ceux à base de métal/oxydes supportés où les phénomènes de frittage sont fréquemment observés. Cette forte stabilité a été attribuée au fort ancrage des atomes d'azote dans le réseau du carbone, permettant ainsi d'éviter les migrations des sites actifs au cours de la réaction, et par conséquent une perte de surface active. Selon les résultats obtenus (Fig. 3), les performances catalytiques obtenues sur N-CNT/SiC sont de 94 % en termes de conversion d'H_2S et de 75 % en terme de sélectivité en soufre.

Les performances catalytiques obtenues sur les catalyseurs N-CNTs et Fe/SiC dans les mêmes conditions de réaction (H_2S = 1 vol.%; T = 190 °C; WHSV = 0.6 h^{-1} ; O_2/H_2S = 2.5) sont de 33 et 17 % respectivement en terme de conversion, et de 89 et 87% de sélectivité en soufre, respectivement. La comparaison des performances catalytiques des différents catalyseurs confirme que N-NTC/SiC présente l'activité catalytique la plus importante, grâce notamment à sa surface effective élevée et aux dimensions nanoscopiques des N-NTCs, permettant ainsi une meilleure accessibilité des réactifs aux sites catalytiques.

Les résultats obtenus dans le cadre de ce travail confirment la possibilité de développer des catalyseurs sans métaux à base de N-NTCs pour des applications en catalyse d'oxydation avec une mise en forme spécifique afin de réduire autant que possible les problèmes de perte de charge ou de transport, inhérents aux catalyseurs sous forme de poudre.

2. Composites carbones mésoporeux dopés avec de l'azote comme catalyseurs pour la réaction d'oxydation sélective de l'H_2S en soufre élémentaire

Les études récemment développées dans l'équipe ont permis de développer une nouvelle méthode de synthèse des structures carbonées dopées avec de fort taux d'azote, ainsi qu'une mise en forme macroscopique à volonté, en utilisant comme produits de base des composés alimentaires, donc non-toxiques tels que : dextrose, acide citrique et carbonate d'ammonium. Dans un mode opératoire typique, 2 g de dextrose et 3 g d'acide citrique sont mélangés dans 10 mL d'eau à température ambiante. Ensuite, une quantité fixe de carbonate d'ammonium (par exemple 1, 2 ou 3 g) est ajoutée au mélange obtenu à température ambiante, et une effervescence instantanée est observée en raison de l'évolution des émissions de CO_2. La suspension est agitée jusqu'à obtention d'une solution claire, et sera imprégné par la suite sur 2 g de différents supports (extrudés, poudre, mousses de SiC, et α-Al_2O_3). Les solides humides sont ensuite chauffés à 130 °C sous air pendant 1 h et soumis à une ou plusieurs étapes d'imprégnation jusqu'à ce que la charge souhaitée soit atteinte. Les solides ainsi obtenus seront ensuite traités thermiquement, d'abord 2 heures sous air à 450 °C, puis éventuellement 2 heures sous flux d'hélium à 900 °C lors d'une étape de carbonisation.
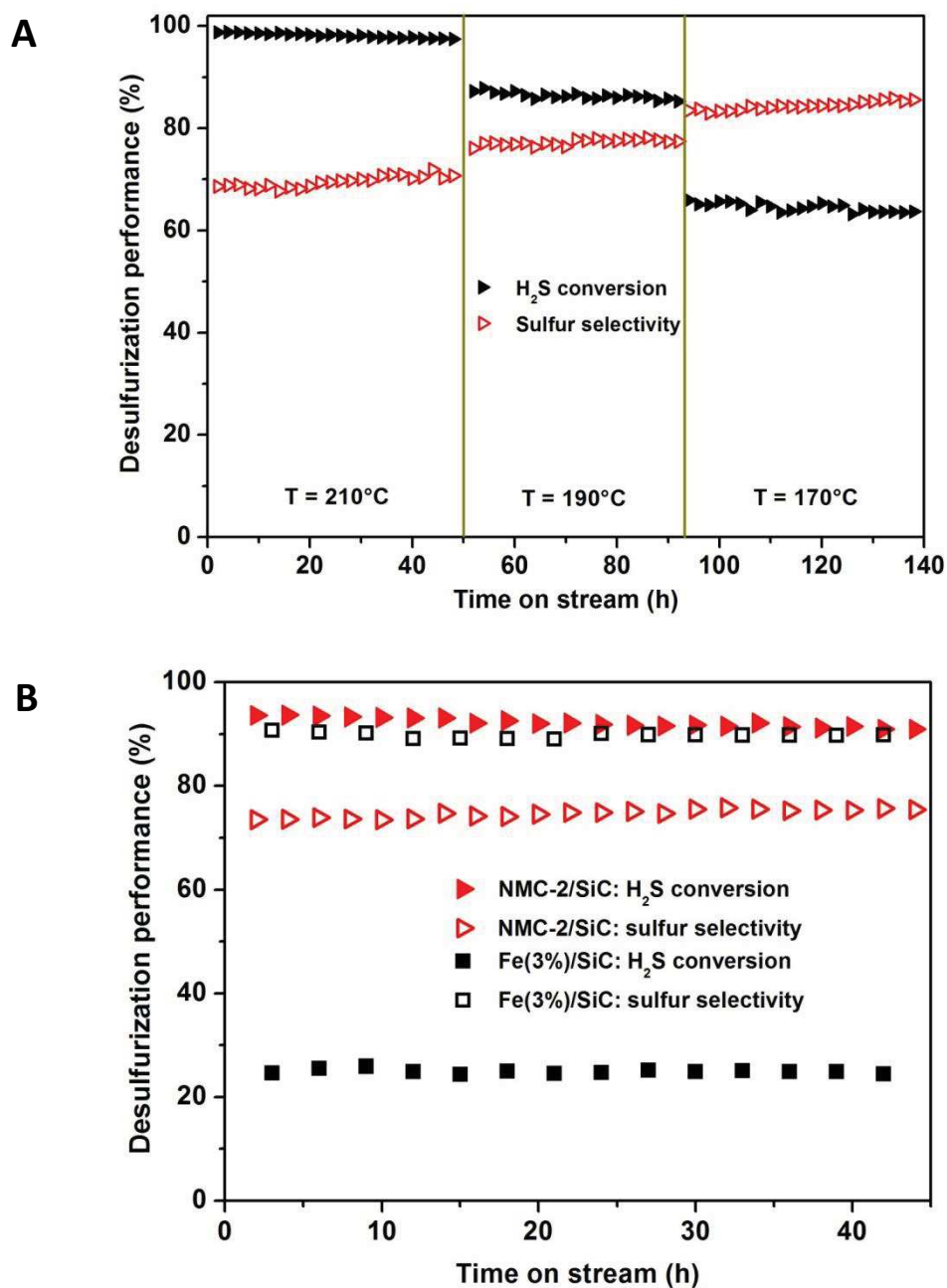
Fig. 4. (A) L'activité en désulfuration de l'H_2S obtenue à WHSV de 0.6 h^{-1} sur des catalyseurs à base de NMC/SiC en fonction de la température de réaction, et (B) en comparaison avec un catalyseur Fe/SiC. Conditions réactionnelles: T = 210 °C; WHSV = 0,6 h^{-1}, H_2S = 1 vol.%; O_2/H_2S = 2,5; H_2O = 30 vol.%; M_{cata} (phase active) = 300 mg.

Les résultats obtenus ont montré que la méthode de synthèse développée permet la transformation d'une solution homogène contenant différents précurseurs, comme l'azote et le carbone, en un film homogène constitué de carbone mésoporeux (taille de pores entre 20 et 60

nm ainsi qu'une petite proportion de micropores) fortement dopé avec de l'azote et présentant également une surface spécifique relativement élevée, > 350 $m^2.g^{-1}$. Les résultats obtenus dans la réaction d'oxydation sélective de l'H_2S ont montré que ce catalyseur présente une activité en désulfuration similaire à celle des catalyseurs à base de N-NTCs étudiés précédemment (Fig. 4). Les avantages de cette nouvelle voie de synthèse sont nombreux tels que la possibilité de réduire l'utilisation des composés chimiques toxiques et coûteux, la facilité dans la mise en œuvre du procédé et l'obtention d'une meilleure concentration de dopant dans le composite final. Dans cette étude nous avons ainsi démontrer que la compréhension de la structure du catalyseur à base de N-NTCs a permis d'initier de nouvelles études d'optimisation, en réalisant des synthèses plus respectueuses de l'environnement.

Un autre avantage non négligeable de ces composés mésoporeux est une meilleure stabilité mécanique sous fortes vitesses spatiales (WHSV = 0,6 - 1,2 h^{-1}), ce qui n'était pas le cas pour des N-NTCs supportés où des pertes de matières ont été observées dans les mêmes conditions de réaction.

3. Composites carbonés contenant des défauts structuraux comme catalyseurs pour la réaction d'oxydation sélective de l'H_2S en soufre élémentaire

Cette étude de la thèse est dédiée au développement d'une nouvelle voie de synthèse de catalyseurs « sans métaux » pour la réaction d'oxydation sélective de l'H_2S mais sans la présence de l'azote. La méthode consiste à créer sur la surface des nanotubes de carbone des défauts structuraux décorés avec des groupements oxygénés qui améliorent grandement l'activité catalytique du système. La synthèse consiste en un traitement des NTCs sous flux gazeux d'HNO_3 à des températures variant entre 180 et 250 °C pendant 12 à 40 h. Les analyses par microscopie électronique à transmission permettent de bien visualiser les sites de défauts sur la surface des NTCs après traitement acide. Ce dernier a également permis d'augmenter d'une manière significative la surface spécifique du matériau passant ainsi de 180 à plus de 300 $m^2.g^{-1}$.

L'activité désulfurante des catalyseurs traités à 250 °C pendant différentes durées est présentée sur la Fig. 5C. La meilleure activité a été obtenue sur le catalyseur traité à 250 °C pendant 24 h. Il est à noter également que l'activité désulfurante est extrêmement stable en fonction de la durée du test, indiquant ainsi que les phénomènes de désactivation couramment rencontrés avec des catalyseurs à base de Fe_2O_3 supportés n'ont pas eu lieu. En effet, les sites catalytiques se trouvant sur les points de défauts sont extrêmement stables et ne sont donc pas sensibles à des phénomènes de frittage rencontrés sur des catalyseurs supportés.
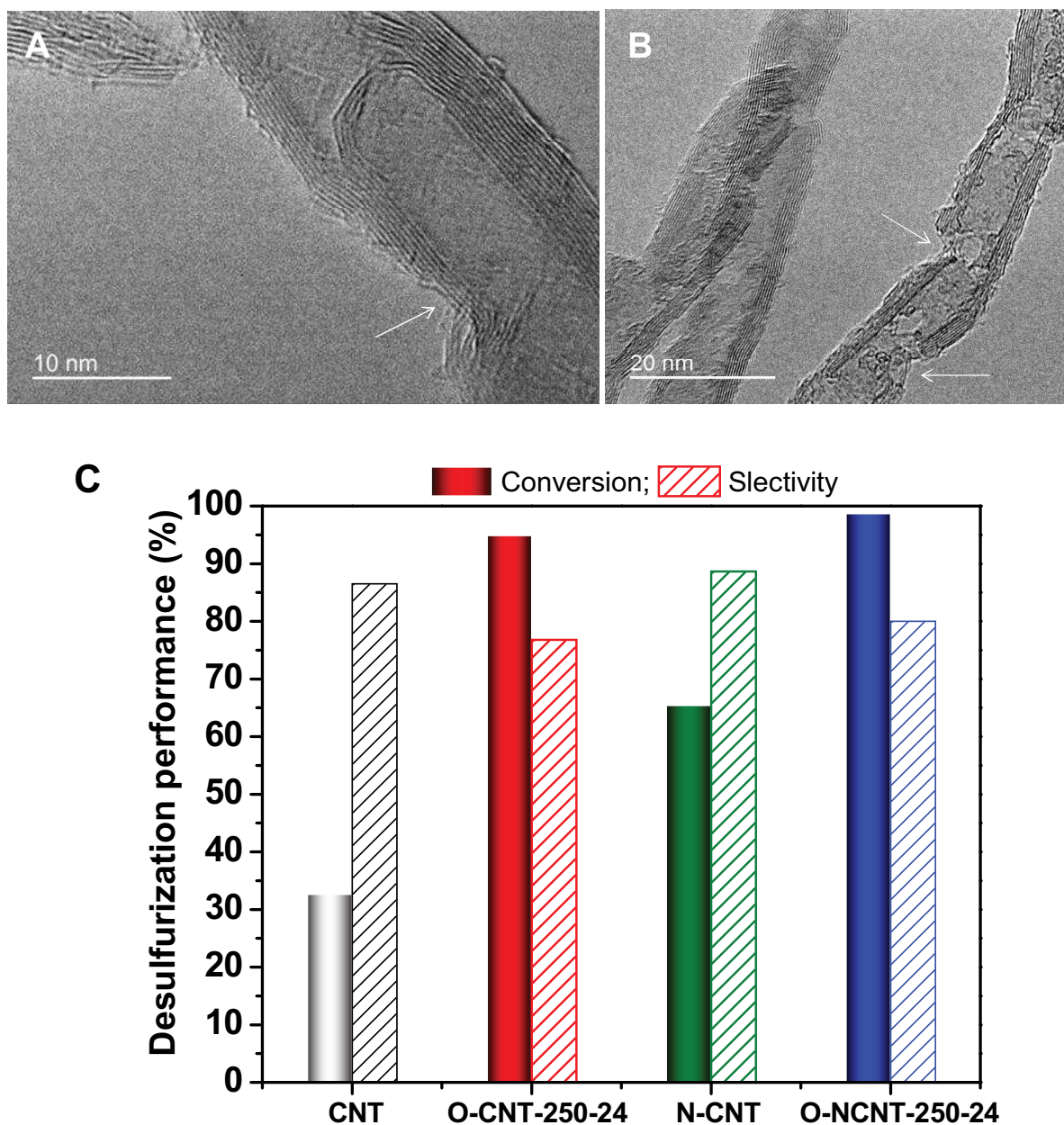
Fig. 5. (A, B) Images MET des nanotubes de carbone présentant des défauts structuraux (indiqués par les flèches) de surface après avoir subi un traitement sous flux gazeux d'HNO₃ à 250 °C pendant 12 et 24 h. (C) Activité désulfurante des catalyseurs sans métaux traités à 250 °C en fonction du temps. L'activité optimale est obtenue avec un catalyseur à base de NTC traités à 250 °C pendant 24 h. Conditions réactionnelles: H_2S = 1 vol.%; H_2O = 30 vol.% ; O_2/H_2S = 2.5; T = 230 °C; WHSV = 0.6 h^{-1}; M_{cata} = 300 mg.

Les récentes études menées ont également montré que les sites défauts ainsi créés peuvent aussi être dopés par la suite avec un précurseur azoté, permettant ainsi d'améliorer d'une manière sensible les performances du catalyseur. Des études complémentaires sont en

cours afin d'optimiser le procédé et de mieux comprendre l'influence des défauts structuraux sur l'activité catalytique.

4. Conclusions et perspectives

Les résultats obtenus dans le cadre de ce travail de thèse ont montré que les catalyseurs à base de nanotubes de carbone dopés avec de l'azote sont des catalyseurs « sans métaux » actifs et relativement sélectifs pour le procédé d'oxydation des traces d'H_2S dans les effluents gazeux, issus des usines de soufre ou de raffineries, afin de satisfaire aux normes sur l'environnement.

Nous avons pu démontrer également dans le cadre de notre travail que les composites carbonés dopés avec de l'azote pourraient également être synthétisés par une voie plus respectueuse de l'environnement, en remplaçant les précurseurs nocifs utilisés dans la synthèse, par exemple l'éthane, l'ammoniac et l'hydrogène, par des précurseurs issus des produits alimentaires non toxiques et nettement moins onéreux. De plus, la méthode de synthèse permet également de produire des catalyseurs « sans métaux » avec des formes macroscopiques contrôlables à volonté en fonction des applications catalytiques ultérieures avec une résistance mécanique accrue.

Enfin, les récentes études que nous avons développées ont permis de montrer que les défauts structuraux jouent également un rôle extrêmement important dans l'adsorption dissociative des réactifs. Le rôle de ces défauts est en cours d'étude et les résultats obtenus permettront de mieux comprendre la nature des sites actifs dans les catalyseurs sans métaux, qui seront probablement les catalyseurs de demain dans de nombreux autres procédés catalytiques.

Les perspectives de ces travaux sont extrêmement nombreuses et on peut citer : le développement de nouvelles générations de catalyseurs « sans métaux » plus actifs et plus sélectifs et qui sont en phase avec les préoccupations environnementales à l'heure actuelle, une meilleure compréhension des relations catalyse-structure qui permettra de développer des catalyseurs à la carte qui pourront s'adapter aux conditions réactionnelles spécifiques. Les catalyseurs à base de carbone dopé à l'azote développés dans cette thèse serviront également comme catalyseur de plateforme pour développer d'autres systèmes en vue des applications qui s'étendre largement au-delà du domaine de la catalyse hétérogène.

References

[1]   S. Iijima, Nature 354 (1991) 56.

[2]   D.S. Su, S. Perathoner, G. Centi, Chem. Rev. 113 (2013) 5782.

[3]   J.-P. Tessonnier, D.S. Su, ChemSusChem 4 (2011) 824.

[4]   P. Serp, M. Corrias, P. Kalck, Appl. Catal. Gen. 253 (2003) 337.

[5]   S. van Dommele, K.P. de Jong, J.H. Bitter, Chem. Commun. Camb. Engl. (2006) 4859.

[6]   G. Tuci, C. Zafferoni, P. D'Ambrosio, S. Caporali, M. Ceppatelli, A. Rossin, T. Tsoufis, M. Innocenti, G. Giambastiani, ACS Catal., 3 (9) (2013), pp. 2108–2111

[8]   C. Nederlof, F. Kapteijn, M. Makkee, Appl. Catal. A: Gen., 417–418 (2012), pp. 163–173

[9]   D. Bégin, G. Ulrich, J. Amadou, D.S. Su, C. Pham-Huu, R. Ziessel, J. Mol. Catal. A: Chem., 302 (2009), pp. 119–123

[10]   C. Chen, J. Zhang, B. Zhang, C. Yu, F. Peng, D.S. Su, Chem. Commun., 49 (2013), pp. 8151–8153

[12]   A. Villa, J.P. Tessonnier, O. Majoulet, D.S. Su, R. Schlögl, Chem. Commun., 29 (2009), pp. 4405–4407

[11]   J. Amadou, K. Chizari, M. Houllé, I. Janowska, O. Ersen, D. Bégin, C. Pham-Huu, Catal. Today, 138 (2008), pp. 62–68

[12]   K. Chizari, A. Deneuve, O. Ersen, I. Florea, Y. Liu, D. Edouard, I. Janowska, D. Begin, C. Pham-Huu, ChemSusChem, 5 (2012), pp. 102–108

[13]   D. Zhong, S. Lin, G. Zhang, E.G. Wang, J. Appl. Phys., 89 (2001), pp. 5939–5943

CHAPTER 1

Introduction about nitrogen-doped carbon composites as metal-free catalysts

● Pyridinic   ● Pyrrolic   ● Graphitic   ● Oxidized
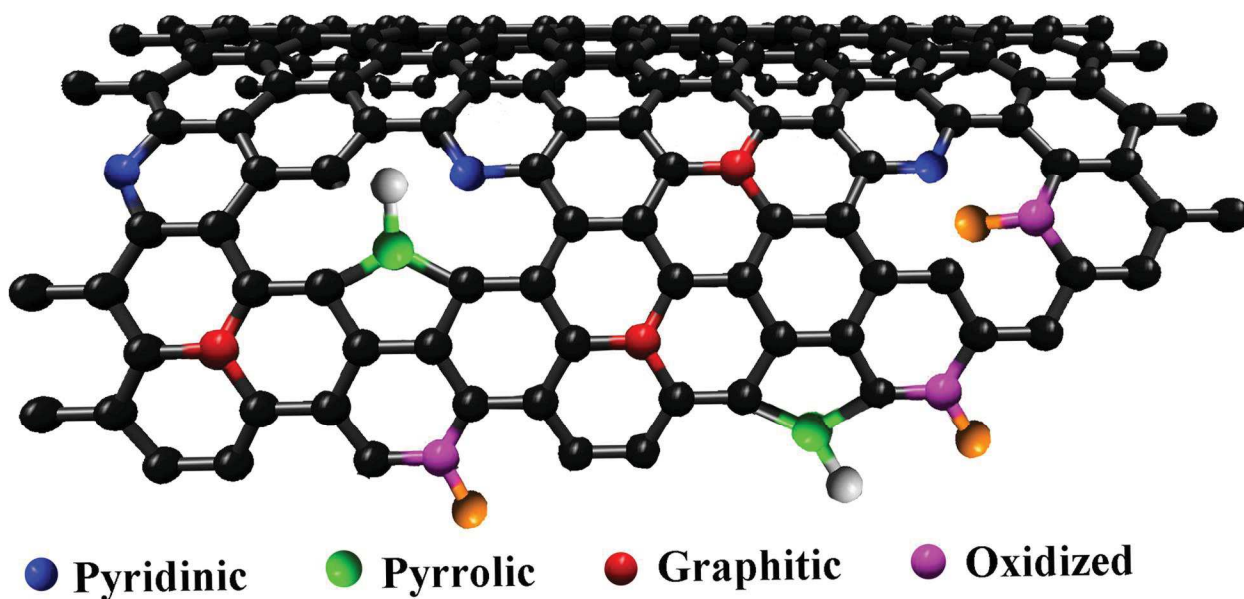
Nitrogen-doped carbon composites as metal-free catalysts

C. Duong-Viet[a,b], Ba H.[a], L. Truong-Phuoc[a], Y.L. Liu[a], J. P. Tessonnier[c]*, J. M. Nhut[a], P. Granger[d]*, C. Pham-Huu[a]*

[a]Institut de Chimie et Procédés pour l'Energie, l'Environnement et la Santé (ICPEES), UMR 7515 CNRS-Université de Strasbourg, 25 rue Becquerel, 67087 Strasbourg Cedex 02, France

[b]Ha-Noi University of Mining and Geology, Co Nhue 2- Bac Tu Liem, Ha-Noi, Viet-Nam

[c]Iowa State University, Department of Chemical & Biological Engineering, 2138 Biorenewables Research Laboratory, Ames, IA 50011-3270 USA

[d]Unité de Catalyse et de Chimie du Solide (UCCS), UMR 8181 CNRS-Université de Lille-1, Bâtiment C3, Université Lille 1, 59655, Villeneuve d'Ascq Cedex, France

1.1. Introduction

Carbon nanomaterials, *i.e.* carbon nanotubes (CNTs) and nanofibers (CNFs), have been synthesized since a long time ago, even the first reports date more than a century, from the action of gaseous hydrocarbon species on a suitable metal catalyst followed by a concomitant decomposition of the adsorbed hydrocarbon into carbon [1,2]. However, it is worthy to note that carbon nanomaterials began to foster a worldwide scientific attention by research groups all around the world for many wide-ranging fields of application only after the publication by Iijima in 1991 on the observation of carbon nanotubes by transmission electron microscopy [3].

The CNTs are constituted by two distinguish classes, namely single-walled (SWCNT) and multi-walled (MWCNT) carbon nanotubes (Fig. 1.1). Indeed, depending on the number of rolled graphene sheets: a single-walled CNTs is formed by rolling a single layer of graphene [4], while multi-walled CNTs is generated by rolling several graphene layers into a single cylinder with multiple concentric graphite walls (MWCNT). The diameter of the SWCNTs can vary from 0.4 to 2.5 nm and the length ranges from few microns to several millimeters depending on the synthesis conditions. Due to the high surface energy of these one-dimensional (1-D) carbon macromolecules, SWCNTs are commonly arranged in bundles in order to minimize the overall energy of the system.
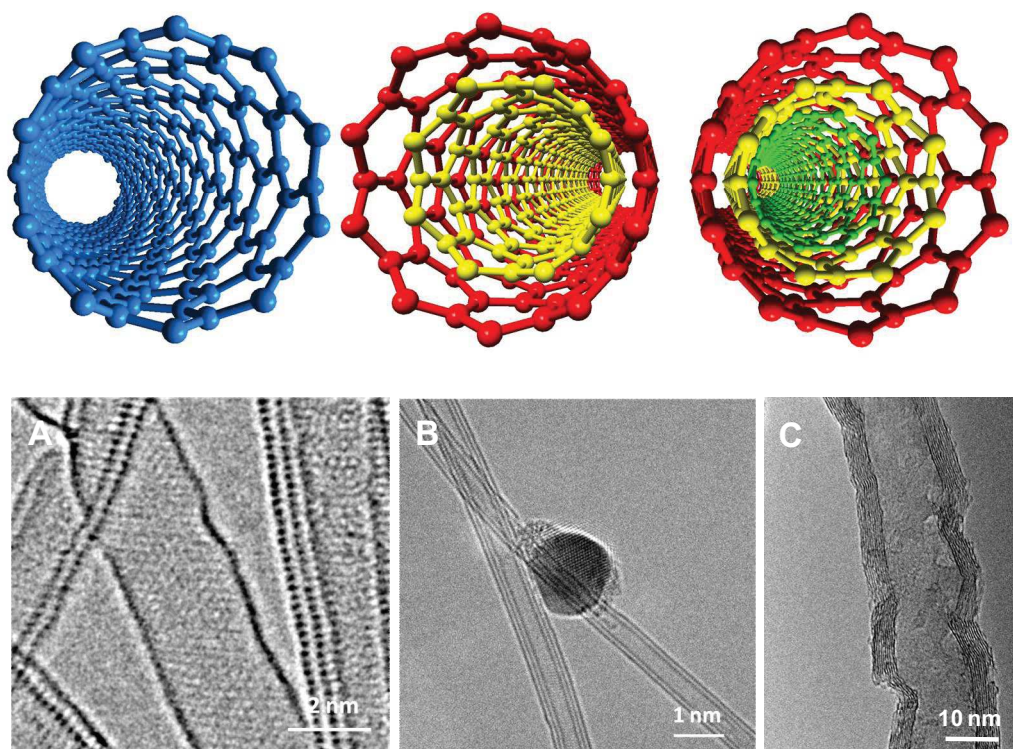
Fig. 1.1. Schematic representation of single-walled, double-walled and multi-walled carbon nanotubes and the corresponding TEM micrographs.

In the case of the MWCNTs the number of walls can vary from two (double-walled carbon nanotubes) to several tens (MWCNT), so that the external diameter can reach 100 nm or even more while the length varies from few micrometers to several millimeters or even longer. The concentric walls are regularly spaced by an interplanar distance of 0.34 nm similar to the one observed in turbostratic graphite materials. The SWCNTs are synthesized generally at a relatively high temperature and thus only contain a very few defects. On the other hand, contrary to SWCNTs, MWCNTs synthesized by catalytic route at lower temperature contain a relatively large amount of structural defects, such as vacancies and terminations, where the carbon atoms are saturated by hydrogen atoms, which exhibiting a much higher reactivity for the functionalization and or doping.

Since the observation of carbon nanotubes inside the products of the arc-discharge materials in 1991 [3], tremendous amount of research had focused on this subject including synthetic methods, advanced characterizations, growth mechanism, chemical modifications and last but not least, potential applications in numerous fields [3, 5–8].
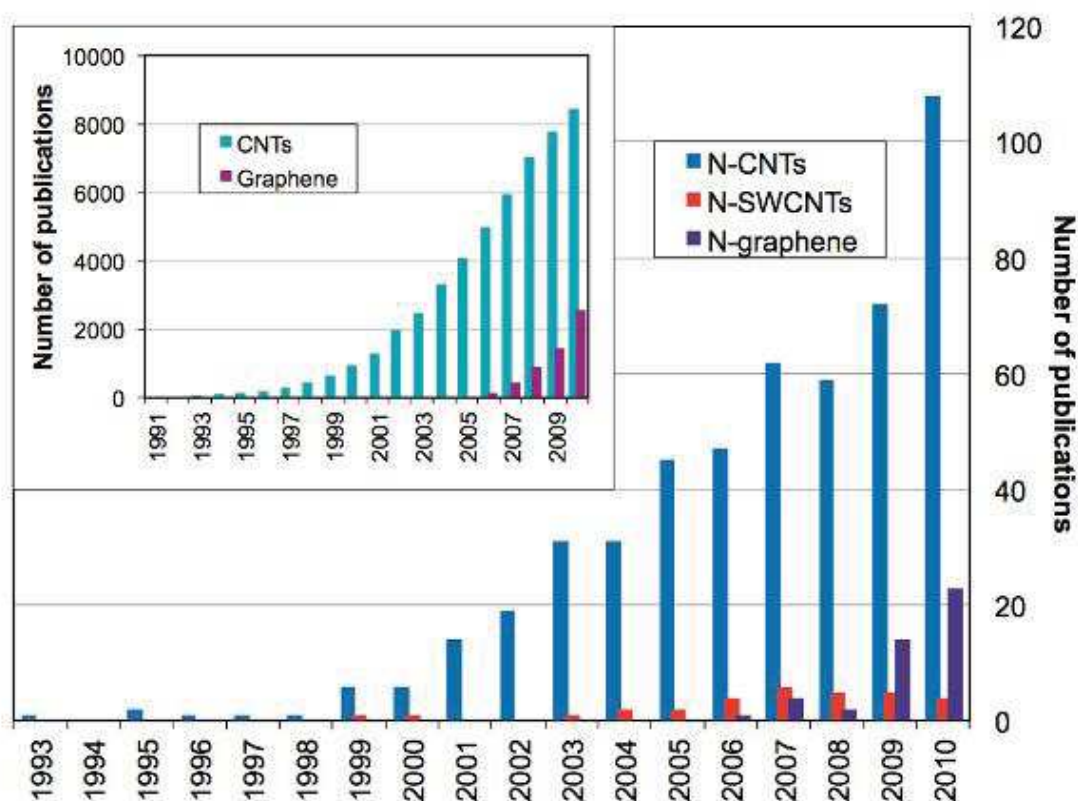
Fig. 1.2. Trends in the number of publications on N-doped carbon nanotubes, N-doped single-walled carbon nanotubes, and N-doped graphene published annually from 1993 to 2010. The inset shows the number of publications on carbon nanotubes and graphene for comparison. Data from the ISI Web of Knowledge reproduced by Toma Sumi [9].

Indeed, carbon nanomaterials hold a huge potential in large application such as biochemical, mechanical, electrodes… due to their excellence physical and chemical properties. In addition, carbon nanomaterials can be efficiently used as catalysis support material or as metal-free catalysts in several relevant catalytic processes [10,11]. The last decade has witnessed an ever increasing amount of publications in this topic according to the results presented in the inset of Fig. 1.2.

In the field of catalysis, the main advantages of the CNTs and CNFs come from their outstanding physical and chemical properties [12]: high effective surface area which provide a higher density of active sites per weight unit, low dimension which significantly reduce the diffusion of the reactants toward the active sites and also for the escaping of the intermediate product, high thermal conductivity which reduce the problem of hot spot formation in the exothermic processes, high chemical inertness which allows them to withstand operating in aggressive medium and to prevent excessive metal-support interaction, and last but not least, the multiple possibilities of surface functionalization or matrix doping with hetero-elements, i.e. N, B and P, to finely tune the surface reactivity and to introduce active sites for catalytic processes. The growing number of publications dealing with the use of nitrogen-doped carbon nanotubes presented in Fig. 1.2 illustrates such trend. It is expected that these doped carbon-based materials will represent a new class of metal-free catalysts holding better catalytic performance as well as long term stability compared to the traditional metal and oxides catalysts for numerous catalytic processes.

The aim of this chapter is to summarize the results obtained on the different fields linked with the research on the nitrogen-doped carbon nanotubes including synthesis, characterization and catalytic applications. The catalytic results will be discussed and compared with those reported for the traditional supported catalysts in order to highlight some critical aspects that have to be developed for the near future. It is expected that such metal-free carbon-based catalysts will open a new era in the field of heterogeneous catalysis which was dominated nowadays by metal and oxides. We will also discuss about some new synthesis routes for producing such nitrogen-doped carbon-based catalysts with non-toxic raw materials which is in line with the environmental concerns. The chapter will end-up with some outlooks regarding the future development of these metal-free catalysts in the field of catalysis.

1.2. Chemical functionalization and doping of carbon nanomaterials

As discussed above the main advantage of the CNTs and CNFs relies on the fact that their surface can be functionalized or doped with various elements to improve the dispersion properties or to introduce new active sites for performing the catalytic reactions afterward. Chemical functionalization of CNTs and/or CNFs is of extreme importance for developing new carbon-based materials with high efficiency for the downstream catalytic applications. It

is expected that the doped carbon nanotubes could represent an important new class of metal-free catalyst with better catalytic performance and improved resistance towards deactivation compared to the traditional metal and oxides supported ones.

To improve their chemical reactivity for dispersing and anchoring the active metal and/or oxides on its surface, the carbon surface can be functionalized by different methods in order to introduce O- or N-containing functional groups on its surface [10,13]. Two main approaches are employed for this purpose and can be described as following: *(1)* direct doping of heteroatom, especially N-, B- and P-containing groups into the carbon nanomaterials matrix during the synthesis, such method is called *"in-situ"* doping method, *(2)* post-treatment of the as-synthesized carbon nanomaterials with an appropriate doping precursor to introduce the doping exclusively onto the carbon surface, such post-treatment method is named *"ex–situ"* doping method. In this method the doping can be carried out in two steps: first, introduction of the oxygen functional groups on the nanocarbon surface through a chemical or thermal treatment involving gaseous, organic molecules, acid in both vapor or liquid phase, containing oxygen, and in the second stage, the oxygenated groups decorated the nanocarbon surface was substituted by the heteroatom doping through thermal treatment, using nitrogen-containing gaseous precursors. The schematic representation of development in the field of nanocarbon materials is illustrated in Fig. 1.3.
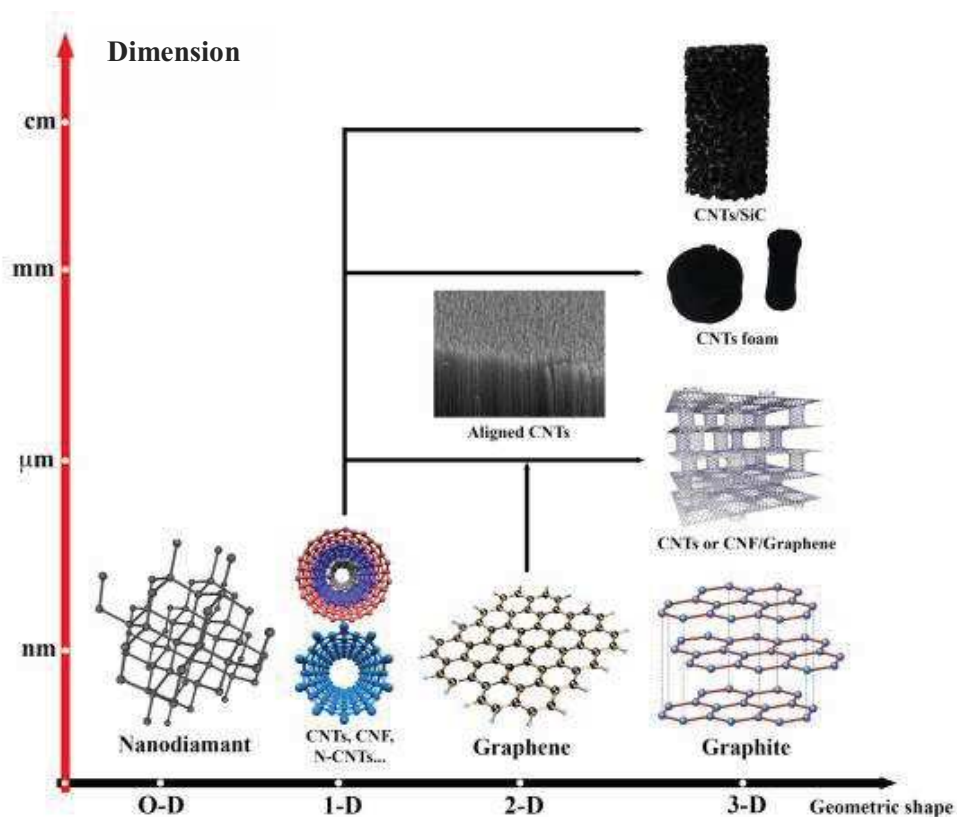
Fig. 1.3. Some ways of the macroscopic based on carbon nanomaterials.

In the first approach, heteroatoms doping were directly introduced on the surface of CNTs during the synthesis by co-feeding the doping precursor with the reactant mixture constituted by carbon source [13]. The doping element in the gaseous doping sources can be chosen amongst nitrogen, boron, phosphorus, sulfur, selenium. The effect of doping on the properties of the carbon nanomaterials is mainly associated with three features of the doping element including: the number of electrons in the external shell, the electro-negativity and the size.

The most common doping element is nitrogen since it has a similar size to carbon and one electron more than carbon in the external shell. Other doping elements, i.e. boron, phosphorus, sulfur… have also been reported but they have not been studied as extensively as nitrogen doping, since a rather large difference in electro-negativity exists between carbon and boron or phosphorus. Boron and phosphorus tend to donate electrons to carbon, thus creating a partial positive charge on the doping atoms.

On the other hand, nitrogen, which has higher electro-negative than carbon, tends to receive electrons from carbon, thus generating a partial positive charge on the carbon atoms. In all cases, the formation of partial positive and partial negative charges can favor the interaction with O_2 and its adsorption on the carbon-doped material. When using sulfur and selenium as doping species, the incorporation of the doping into matrix carbon becomes difficult which could be attributed to the different of electro-negativity between carbon atoms and sulfur or selenium atoms.

Nitrogen can be incorporated into the CNTs matrix leading to different configurations for N bonded to the graphitic network in the common sp^3 or in sp^2 hybridization state for pyridinic and pyrrolic structure.

● Pyridinic ● Pyrrolic ● Graphitic ● Oxidized
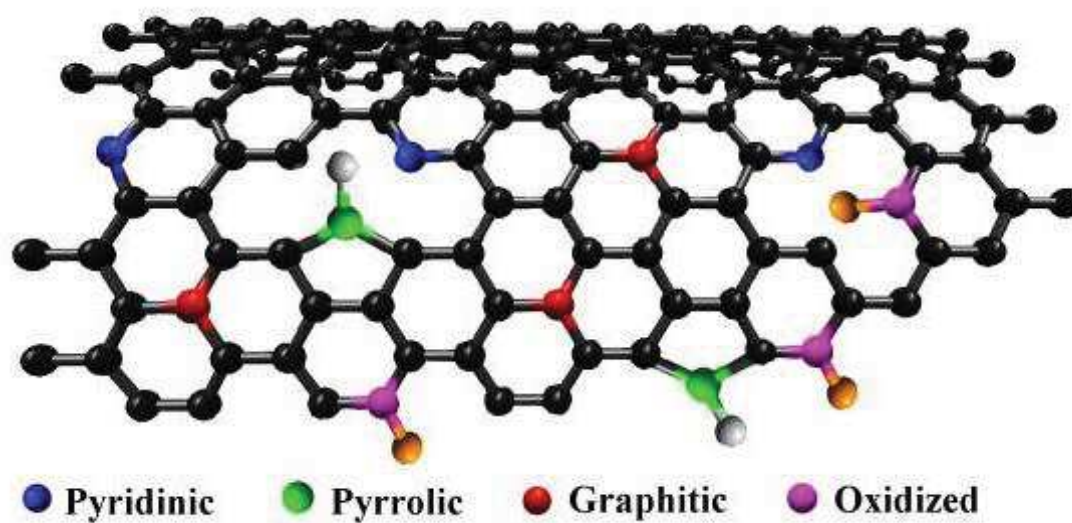
Fig. 1.4. Types of nitrogen species that can be incorporated into graphitic carbon.

In fact, four main bonding configurations (Fig. 1.4) are generally observed including: *(i)* pyridine-like where the nitrogen atom is two-fold coordinated, *(ii)* pyrrole-like where the nitrogen sites substitutionally in a five membered ring, *(iii)* graphitic/substitutional where nitrogen replaces a graphitic carbon atom in the CNTs lattice, and *(iv)* pyridinic oxide structure which pyridinic is oxidized by oxygen. Recently, so-called "wrapping, grafting, or coating" method attracted an increasing attention because it is very simple and facile for synthesis of highly nitrogen-containing CNTs. On the other hand these doped mesoporous carbon can be more active because an ordered interconnected porous structure enhances the surface area (500 - 1900 $m^2.g^{-1}$) [14,15] and the pore volume, which able to allow the reactants to reach the active sites without diffusion limitations. Very recently, Liu et al. [16] have reported the easy way to synthesis of 3D pore structure with high accessible surface area from green materials, non-toxic as dextrose, citric acid, skeleton and carbon nanotubes. The detail description of the different doping methods will be presented and discussed below.

Finally, it is worthy to note that carbon nanomaterials have a nanoscopic dimension which leads to some severe problems linked with their use in conventional gas-phase reactors due to the problem of large pressure drop across the catalyst bed and also for the transport and handling. In the liquid-phase reactions, the difficulty linked with their recovery represents also a concern. It is expected that for the fully development of these nanocarbons a macroscopic shaping step is a prerequisite before any future industrial applications. The easiest route for reaching such macroscopic shaping is the direct growth of CNTs and/or CNFs on a macroscopic host structure previously decorated with the growth catalyst [17]. Another route is the post-synthesis macroscopic shaping with the aid of extra template [16]. Such macroscopic shaping is presented in the schematic presentation in Fig. 1.3. Furthermore, the macroscopic support should not alter the physical properties of the carbon nanostructures deposited on it, *i.e.* high mechanical strength in order to avoid breaking and catalytic bed plugging as well as fine formation, high specific volume in order to afford a high space velocity of the gaseous reactants, high thermal conductivity which is the most important condition for catalyst operating in a highly exothermic or endothermic medium and finally, a high chemical resistance in order to be used in aggressive environments such as highly acidic or basic media [18,19]. Several macroscopic hosts are foreseen such as large pore alumina (α-Al_2O_3)) [20], and ceramic, *i.e.* SiC either pure or doped with foreign elements [21]. The main macroscopic host matrix used in this present work is based on silicon carbide due to its outstanding physical and chemical properties as described below.

1.3. Method for synthesis of nitrogen containing carbon nanotubes

Nitrogen-doped CNTs synthesis can be carried out in two different ways, either directly during synthesis of CNTs (in-situ method) or by post-treatment of the as-synthesized CNTs (ex-situ method). For both approaches various methods such as arc-discharge, laser-ablation, chemical vapor decomposition (CVD), and organo-metallic functionalization have been employed. Among them the CVD method, or low-temperature synthesis, is the most employed thanks to its high flexibility and to the facility for scale up process.

1.3.1. Nitrogen-doped CNTs by in-situ method

1.3.1.1. High temperature synthesis method

Methods such as arc-discharge [22,23], laser-ablation [24,25], solar oven and magnetron sputtering [26] are mainly used for the synthesis of carbon nanomaterials. Among these methods, the arc-discharge is known as the first to be used for the synthesis of carbon nanomaterials and the doping of carbon nanotubes according to the report by Iijima in 1991 [3] and nitrogen and boron doped CNTs by Stéphan et al. in 1994 [27]. In this method, the tubes are grown between two carbon electrodes through evaporation of a graphite rod at temperature more than 3000 °C and under a helium gas atmosphere. The yield and producing selectivity of as-synthesized CNTs depends on several synthesis parameters such as the uniformity of the plasma arc, the temperature of the deposit forming on the carbon electrode and the nature of the gas used (helium, argon, nitrogen, a mixture of hydrogen and nitrogen) as well as the pressure of this later.

Another method, namely laser ablation, was first use to synthesize CNTs in 1996 by Thess and co-workers [28]. In this method, graphite target are evaporated by laser irradiation with a catalyst mixture containing Co and Ni under flowing inert atmosphere at lower temperature, i.e. 1200 °C. The carbon products are swept by the flowing gas and deposit on a water-cooled collector. Substantially, the system is treated in vacuum at 1000 °C in order to remove by-products (C_{60} and other fullerenes). Diameter and size distribution of CNTs can be controlled by adjusting the reaction temperature during the growth procedure and the composition of catalyst.

For the arc-discharge and the laser ablation methods, the obtained carbon nanomaterials contain only fewer defects, usually entangled, heterogeneous with various lengths and diameters and a large percentage of nitrogen incorporation, up to 33 % at [22–25]. However, these synthesis methods are not able to produce neither CNTs nor N-CNTs in large quantities for potential industrial applications. In addition, the product requires further purification to separate the CNTs or N-CNTs from the carbon-based by-products and the residual catalytic metals.

1.3.1.2. Low-temperature synthesis method

Since the reliable reports using the Chemical Vapor Deposition (CVD) method for the synthesis of N-CNTs published in 1997 by Yudasaka et al. [29] and Sen et al. [30] and by Terrones et al. in 1999 [31] the CVD method becomes the most common technique used nowadays to synthesize CNTs and N-CNTs in an industrial scale due to its technical feasibility and its simplicity. Indeed, the CVD method only requires an oven, a tubular reactor, a reactive gas mixture and an appropriate catalyst. In addition, the CVD process is carried out in a continuous mode and at a relatively low temperature compared to the arc-discharge and laser ablation ones. The product is extremely pure and thus, additional purification process is useless which represents a net gain for the cost effectiveness of the process. A schematic diagram of the conventional fixed bed CVD synthesis setup is shown in Fig. 1.5.
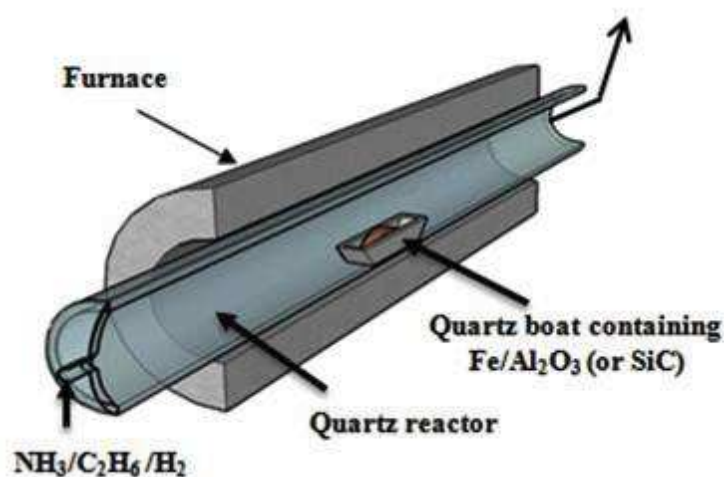
Fig. 1.5. Schematic diagram of fixed bed catalyst CVD apparatus [32].

The CVD procedure is realized by decomposing a gaseous or volatile compounds containing carbon and/or nitrogen precursor onto a catalyst in a tube reactor at temperature from 550 °C to 1100 °C. In the case of CNTs synthesis the most general growth mechanism can be outlined in Fig. 1.6. Firstly, hydrocarbon vapor comes in contact with the "hot" catalyst metal nanoparticles and get decomposition to generate hydrogen and to form elementary carbon atoms which further dissolved into the metal to generate pseudo-liquid metastable carbide (Fig. 1.6a and b). Finally, after saturation of carbon phase within the catalyst particle solid carbon precipitates at the rear side of the catalyst nanoparticles to form a carbon filament with hollow core (Fig. 1.6c). As long as the metal's top is open for fresh hydrocarbon decomposition CNTs continue to grow up. The reaction ceases when the metal tip is fully covered with excess carbon (Fig. 1.6b and c). The CNTs growth operated according to the above described mechanism is called "tip-growth model".
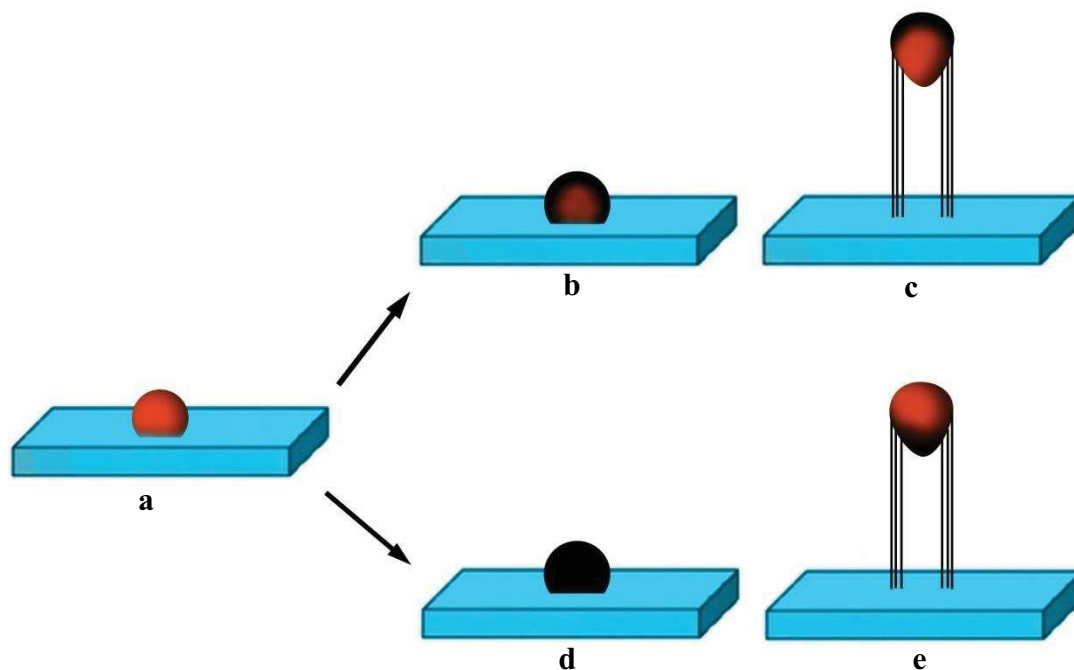
Fig. 1.6. Two ways grow the conventional CNTs in using CVD method: (a) decomposition of the carbon-containing precursor on the surface of the catalyst particles; (b, c) carbon species diffuse only on the surface of the catalyst particle; (d, e) diffusion of carbon atoms through the particles as a solid solution and precipitation of carbon at the metal-support interface and the formation of a nanofiber or a nanotube [33].

In the second growth mechanism carbon crystallizes first out as a hemispherical dome which and then extends up in the form of seamless graphitic. In this case carbon is only present on the outer surface of the catalyst nanoparticle and the growth is controlled by surface carbon diffusion rather than through the bulk of the catalyst nanoparticle (Fig. 1.6d and e). Subsequent hydrocarbon deposition takes place on the lower peripheral surface of the metal, and as dissolved carbon diffuses upward.

However, conventional CNTs growth mechanisms described above cannot explain the presence of regular internal bamboo cavities in the N-CNTs. Hence, an alternative model has been proposed by Torrenes et al. [31] and by Reyes et al. [34] and received a general agreement of the groups working in the field. According to the proposed mechanism, the CN_x species are generated and deposited on the metal catalyst particles during synthesis, where they react exothermically. Diffusion of CN_x species through the metal catalyst particle is responsible for the subsequence N-CNTs growth, and encapsulation of N_2 is caused by the decomposition of unstable reactive intermediates. The compartmentalized structure is a result of the different precipitation rates of different CN_x species. When precipitation is slow, and

there is a lack of material to maintain inner N-CNTs growth, layers will suddenly close leading to the formation of periodically bamboo-like structure.
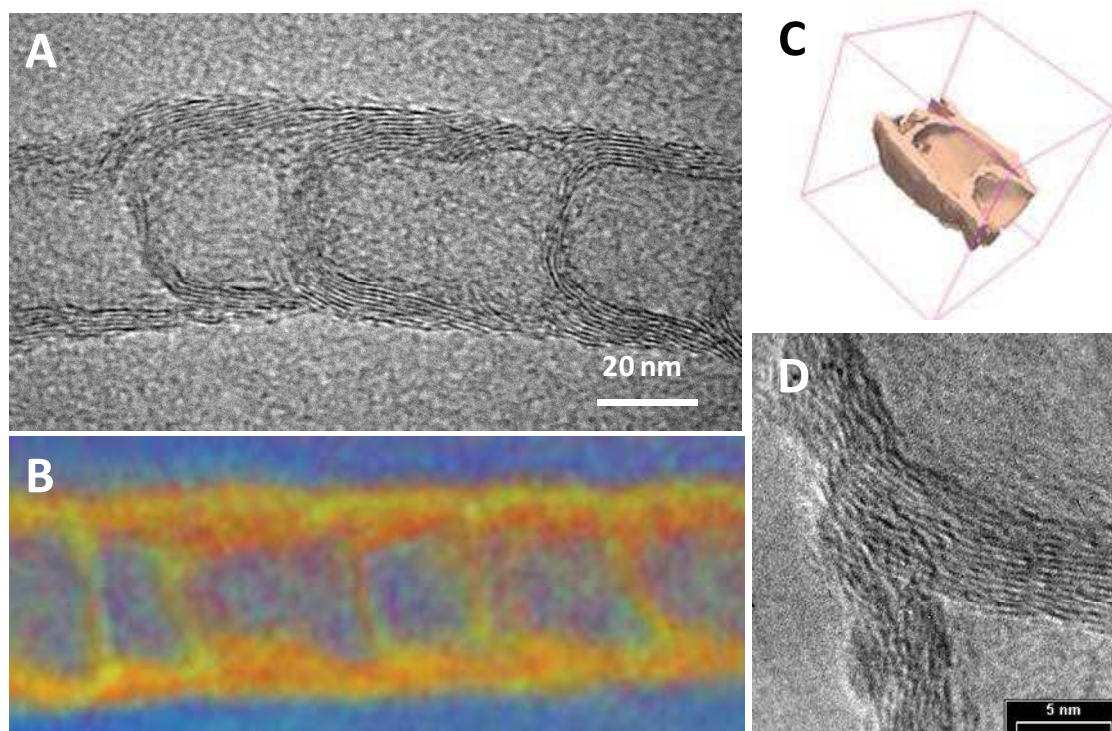
Fig. 1.7. (A) High-resolution TEM micrograph of the arches presented inside the N-CNT axis. (B) STEM-EELS results evidencing an enrichment of nitrogen in the area close to the arch. (C, D) TEM tomography and high-resolution TEM investigation of the microstructure of the N-CNTs evidencing the absence of pores or channel inside the arch.

TEM micrograph in Fig. 1.7A shows the periodical arches along the tube axis. Ersen et al. [35,36] have recently discussed this growth mechanism in detail based on the use of transmission electron microscopy coupled with an Energy Electron Loss Spectroscopy (STEM-EELS) and in a tomography mode (TEM-3D). According to the results the nitrogen concentration is higher in the tube's arch which is directly linked with the proposed growth mechanism (Fig. 1.7B). The reconstruction of the TEM tomography also allows one to figure out the fact that the arch is well closed and thus, no matter can be transferred from one compartment to another along the tube axis (Fig. 1.7C).

The complete absence of metal nanoparticles inside the N-CNTs channel or compartments is evidenced by TEM tomography analysis and the results are presented in Fig. 1.8. The 2D TEM micrograph (Fig. 1.8A) shows the dense and homogeneous decoration of the N-CNTs by palladium nanoparticles. The 3D TEM section views in the XY plane are presented in Fig. 1.8B to D. According to these results palladium nanoparticles are

exclusively localized on the outer surface of the nanotubes which confirms the complete closure between the inner and the outer surface of the N-CNTs.
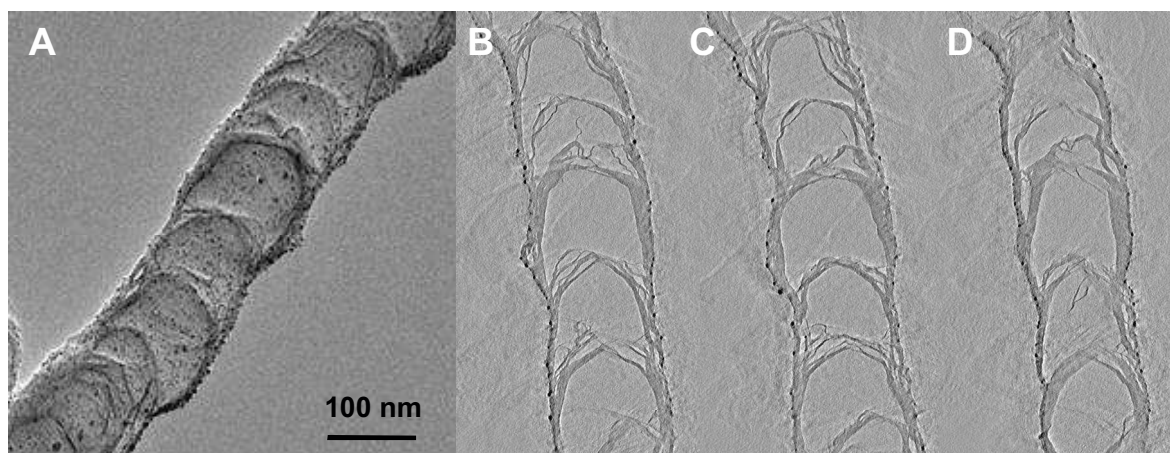
Fig. 1.8. (A) 2D TEM micrograph of the Pd/N-CNTs with 5 wt % loading. (B to D) 3D TEM sections showing the complete absence of Pd nanoparticles inside the N-CNT compartments.

The amount and type of nitrogen incorporated into the CNTs depending on the synthesis conditions, particularly the precursors, catalyst, reaction temperature and duration, and gas flow.

- Carbon and nitrogen source:

Up to now, a large gaseous or organic compounds are used as carbon and nitrogen sources in the synthesis of CNTs and N-CNTs such as CH_4 [37], C_2H_2 [38], C_2H_6 [39,40], C_3H_6 [41], CO [42], N_2 [43], NH_3 [44], benzene [45], xylene [46], alcohol [47], pyridine [30], acetonitrile [48], melamine [31,49,50], dimethylformamide [51], $C_3N_3Cl_2NH_2$ [52], $NiC_{32}N_8H_{16}$ [26,29], $FeC_{32}N_8H_{16}$ [53] and benzylamine [54]. The selection of carbon and nitrogen containing precursors depend mainly on the CVD method employed (fixed bed catalyst CVD or floating catalyst CVD method) and the final requirements on the chemical – physical properties and also type of CNTs (single, double or multi- walled). The carbon precursors consisted with small hydrocarbon such as CH_4, C_2H_6, C_2H_2, C_2H_5OH and CO are usually preferred than liquid or solid hydrocarbons due to it selective decomposition on the surface of the metal nanoparticle of the catalyst while fluid or solid hydrocarbon lead to a complete encapsulation of the metal and as a consequence, a rapid deactivation of the metal centers for subsequence growth. In general and according to the adsorption behavior described above the CNTs yield is much higher using small hydrocarbon precursors than the others.

In the case of nitrogen precursor, ammonia is the most used nitrogen source for the synthesis of N-CNTs because it is present in a gaseous form at room temperature and can be

easily incorporated in the matrix of CNTs during the synthesis even at low temperature and is less toxic than one other precursor. Amadou at al. [55] have synthesized N-CNTs by using a mixture of $C_2H_6/NH_3/H_2$ over an alumina supported Fe catalyst with nitrogen content up to 7 %. Lee et al. [56] have reported that nitrogen-content range are between 2 and 6 at.% being varied with a flow rate of ammonia while using methane/ammonia as gas precursors. This result is similar to the results obtained by Chizari et al. [40] using a ethane/ammonia mixture for the large scale synthesis of N-CNTs. On the other hand the nitrogen incorporation was promoted to some extent with using a liquid or solid precursors, i.e, nitrogen content up to 20 % has been reported using acetonitrile as the nitrogen source [48]. It is absolutely agree in the literature that the nature of the carbon and nitrogen precursors play a key role in the synthesis of nitrogen doped carbon nanotubes.

- Catalyst and catalyst support:

The catalysts used for the CVD synthesis of CNTs and N-CNTs are commonly transition metal such as Fe, Co, Ni, Mo and their binary alloys such as Fe-Mo [57]. In most case, these metal catalysts are usually deposited on different supports such as silica (SiO_2), alumina (Al_2O_3), zeolites and magnesium oxide (MgO) [57]. The role of the support is of great interest through the interaction with the deposited metal active phase: *(i)* it allows the formation of metal nanoparticles with a narrow size distribution and to avoid excessive sintering of metal particles during the CVD process and in turn, lead to the formation of CNTs and/or N-CNTs with narrow diameter distribution and higher yield; *(ii)* it permits an easy handling of the catalyst; the size of the support can be tuned and optimized to allow the fluidization of the catalyst when using the fluidized bed technology for continuous CNTs and/or N-CNTs production; and the support defines the macroscopic shape of the final CNTs/N-CNTs composites for subsequence applications as powdery materials are unlikely for industrial developments.

As reported elsewhere the interface between transition metal and CNTs is of paramount importance. Different configurations have been envisioned regarding the configuration of this contact simply by deposition where the metal will interact with the sidewall. Alternately, the configuration where the CNTs terminated at the metal contact can lead to different behaviors due to changes in metal work function [58]. Jones et al. considered that a better understanding of this metal-CNTs interface is essential for optimising the CNTs nanoelectronic devices but they also stated that even a full understanding will not be able to perfectly relate chiraltity and electronic properties since it is not possible to control the chirality for instance during CVD growth. In a recent study, Jones et al. [59] investigated the interface structure of Fe-CNTs showing a weak sensibility of the nature of the interface to the band gap and the position of the Fermi level. On the other hand these authors showed significant perturbation when boron interacts with CNTs becoming metallic and the formation of a Ohmic contact.

Liquid or solid organometallic complexes or organometallocenes, such as ferrocene, cobaltocene, nickelocene etc., are also widely used as a growth catalyst for CNTs growth, because they liberate metal nanoparticles in-situ, which catalyze the hydrocarbon decomposition more efficiently. However, these growth catalysts are mostly used for the production of vertically-aligned CNT-s and/or N-CNTs while for the randomly CNT-s and/or N-CNTs the supported metal catalysts are the most preferred.

- *Synthesis temperature and duration:*

Liu et al. [60] has investigated the influence of synthesis temperature from 750 °C to 1000 °C to the synthesis N-CNTs using the mixture of pyridine/ferrocene/pure NH_3 or pyridine/ferrocene/NH_3 diluted in Ar, while Chizari et al. [69, 88] used the mixture of ethane/NH_3/H_2. The results obtained indicated that the synthesis temperature plays an important role on the N-CNTs growth. At low temperature, i.e. 650 °C, the N-CNTs growth rate was relatively low, which could be assigned to the low decomposition rate of the precursors leading to the formation of solid carbon which will further diffuse inside the metal center to generate carbon source for the N-CNTs growth. As the growth temperature increases, *i.e.* 750 to 800 °C, the length and population density of the N-CNTs increased considerably which is attributed to the balance between the precursor decomposition rate and the carbon nanotubes nucleation through the metal catalyst. At higher temperatures (850 - 950 °C), the N-CNTs population density was still high, but the diameter distribution was less homogeneous as nanotubes with bigger diameter become preponderant within the as-synthesized sample. For example, the average diameter of the carbon nanotubes grown at 750 °C is about 40±10 nm, while the average diameter of the carbon nanotubes grown at 950 °C is about 65±10 nm while at 1000 °C carbon nanotubes with diameter higher than 100 nm are predominant. It is also worthy to note that the N-CNTs yield is significantly decreased at high temperature which could be attributed to the gasification of the formed carbon by the hydrogen generated during the growth process. The increase of the N-CNTs diameter as a function of the synthesis temperature can be attributed to the migration and sintering of the iron catalyst at high temperatures leading to a growth centers with bigger size. These larger catalyst particles will lead to the formation of CNTs with larger diameters. At medium synthesis temperature the diameter of the growth catalyst is smaller leading to the formation of N-CNTs with small and more homogeneous diameter. The smaller average diameter of N-CNTs at lower temperatures can be also related to the lower activity of large iron particles at low temperatures. Therefore, the majority of the catalysts responsible for the growth of N-CNTs would be the particles with smaller sizes.

On the other hand, these authors reported that the synthesis temperature also significantly affects the incorporation of nitrogen into the matrix of CNTs. Indeed, the nitrogen containing in the N-CNTs decreased as increasing the synthesis temperature. This

trend can be attributed to the higher number of defects and lower crystallinity of the N-CNTs synthesized at lower temperatures, which leads to an easier incorporation of foreign elements into its structure. The high-temperature synthesis could also leads to the reverse reaction between nitrogen and other gaseous species and thus, lowering the total incorporated nitrogen within the carbon matrix.

1.3.2. Nitrogen-doped CNTs by ex-situ method

For the *ex-situ* doping three main approaches were employed such as: *(1)* by heat treatment of un-doped nanocarbon under nitrogen-containing precursor (for example, NH_3 atmosphere) at medium to high temperatures; *(2)* by "grafting or wrapping" of nitrogen containing functionalization groups on the surface of CNTs; *(3)* by exposed the as-synthesized CNTs to a N_2^+ ion beam originating from a cold cathode ion source (carbon annealing by plasma method).

In the first and second approaches, owing to the poor chemical reactivity of the CNTs surface a preliminary step consisted by a chemical modification of the nanocarbon surface is required. The functionalization step consists of performing an oxidation of CNTs with different oxidizing agents in order to improve their physico-chemical properties was employed. The treatment allows the incorporation of oxygenated functional groups on the CNTs surface which can be subsequently reacted with the nitrogen gaseous precursor to generate nitrogen-doped CNTs. The oxidative treatment could carry out in both liquid- or gas-phase medium. The illustrations of the setup used for (A) liquid-phase functionalization and (B) gas-phase functionalization of CNTs are showed in Fig. 1.9.
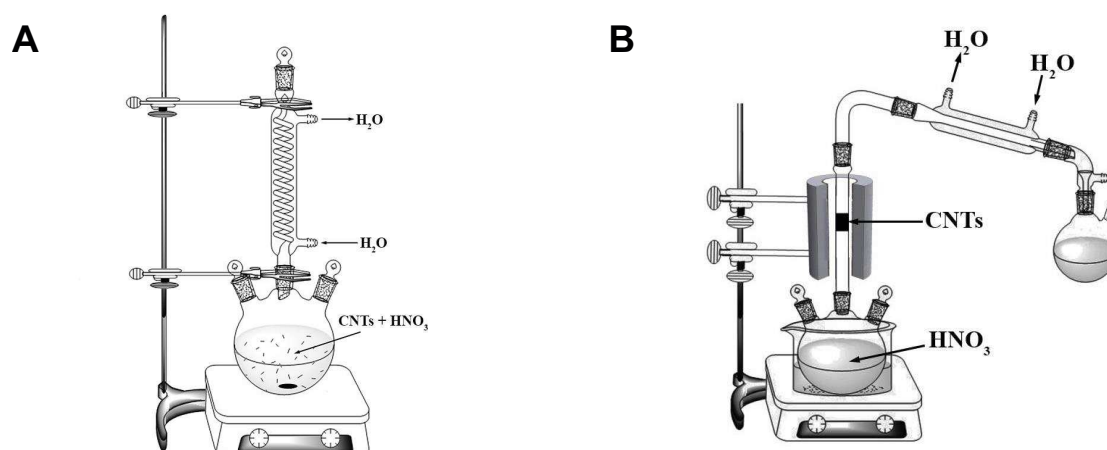
Fig. 1.9. Illustration of the setup used for (A) liquid-phase, where the CNTs are treated at the same temperature in the presence of the oxidizing agent, and (B) gas-phase functionalization of CNTs where the pre-treatment temperature of the CNTs can be tuned with respect to the temperature of the oxidizing chemical agent.

In the liquid-phase functionalization of CNTs, the purify sample and oxidizing agents were added into a two-necked, round-bottom glass flask, equipped with a condenser, the homogenization of the liquid medium is ensured by either a magnetic stirrer or by sonication, and a thermometer was mounted in the pre-heated oil bath for controlling the pre-treatment temperature. The functionalization process was carried out at different temperature and duration. The as-treated CNTs were further filtrated and washed with distilled water to remove the loosely adsorbed chemical species before drying step. The main disadvantages of this method are the un-selective functionalization of the CNTs surface by various oxygen-containing groups on the defect sites of the sidewalls and open caps of CNTs and last but not least, the destruction of the initial macroscopic structure of the material. The use of large amount of water to wash out the residual chemical species and the final filtration process represent also drawbacks for such process despite its wide utilization. It is also worthy to note that for the liquid-phase functionalization the treatment temperature cannot be varied in a large range in order to avoid the thermal decomposition of the functionalized liquid medium.

In contrast to the liquid-phase method the gas-phase treatment allows the avoidance of any of the drawbacks described above. In the gas-phase pre-treatment process the CNTs were loaded inside a reactor, equipped with the same setup as used for the liquid-phase pre-treatment, and the pre-treatment was carried out by passing the oxidizing vapor through the CNTs bed. The temperature of the liquid-phase containing the oxidizing agent was keep at a constant temperature while the treatment temperature can be varied on a large range allowing the functionalization of the CNTs with different degrees. In addition, the gas-phase treatment also presents a net advantage as it allow one to preserve the macroscopic structure of the pre-treated sample unlikely to the liquid-phase pre-treatment where macroscopic structure lost is frequently encountered. The gas-phase pre-treatment also avoid the post-reaction processing, i.e. washing and filtering, which could represent an additional cost for the process.

Up to now, numerous articles have been published on the synthesis of N-CNTs, however, the direct comparison of them is not straightforward due to the various experimental conditions and also to the nature of the carbon and nitrogen sources. In Table 1.1 are reported the different representative results obtained in the literature.

Table 1.1. Summary of the different reported synthesis methods of N-CNTs.

Synthesis method	Catalyst	Precursor	Dopant content (at.%)	Refs
Pyrolysis	Fe	Melamine	< 7	[50]
Pyrolysis	Ferrocene	Melamine	10	[31]
CVD	Ferrocene	Benzylamine	< 5	[54]
CVD	Acetylacetonate	Acetonitrile, tetrahydrofuran	20	[48]
CVD	Fe	CH_4/N_2	15 - 17	[43]
CVD	Ferrocene	Pyrdine/xylene/NH_3	10	[61]
Pyrolysis	Fe	Dimethylformamide	2 - 16	[51]
Pyrolysis	Co	Pyridine	2	[62]
Pyrolysis	Ferrocene	NH_3	4.8 - 8.8	[60]
CVD	Fe	$C_2H_6/NH_3/H_2$	7	[36,40,55]
CVD	Ni	C_2H_6/NH_3	< 12.8	[63]
CVD	Ni/SiO_2/Si	NH_3/CH_4	4	[64]
CVD	Etched SiO_2/Si	NH_3/CH_4	3.6	[65]
CVD	Ni	Pyridine	6.6	[66]
Thermal treatment	-	Oxidized CNTs, NH_3	2.9 - 6	[67]
N_2^+ treatment	-	CNTs, N_2^+	1.5 – 11.3	[68]
Thermal treatment	-	OMCs, NH_3	3.6 – 6.0	[15]

1.4. Properties of CNTs with different functionalization groups on the surface

1.4.1. Structure features

Nitrogen-doped CNTs can be synthesized either directly during synthesis or by post-synthetic treatment methods as described above. However, post-treatment method of carbon materials often yields just surface functionalization, and thus does not change the bulk material properties. In contrast, *in-situ* doping of carbons during the synthesis by using nitrogen-containing precursors can yield a homogeneous incorporation of nitrogen into the

entire carbon matrix with a concomitant modification of the overall physical properties of the final composites such as electrical conductivity, basicity, oxidation stability, and catalytic activity compared with those of the un-doped CNTs. There are at least three different types of nitrogen incorporation found in N-CNTs structure, according to the XPS results from different research groups [69,70], which are most reported in the literature such as: pyridinic (pyridine-like nitrogen), pyrrolic (pyrole-like nitrogen) and graphitic type of nitrogen. The last nitrogen species, named oxidized or encapsulated nitrogen, is expected to play only a minor role. The representative XPS N1s spectrum recorded on the N-CNTs is presented in Fig. 1.10.
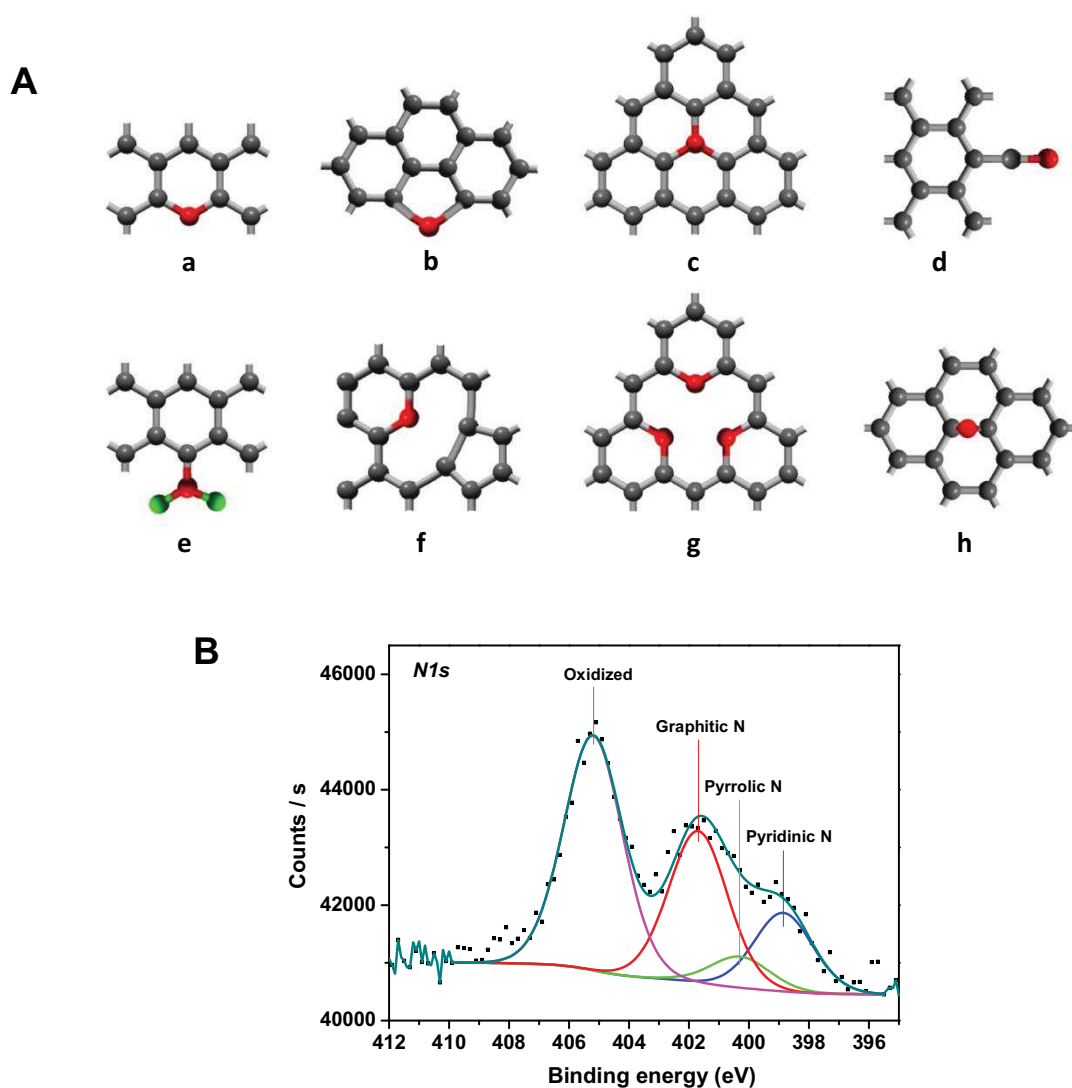
Fig. 1.10. (A) Different nitrogen bonding configuration in graphitic carbon network, (a) pyridine-like N, (b) pyrrole-like N, (c) quaternary or graphitic N, (d) nitrile -C≡N, (e) amine group –NH$_2$, (f) pyridinic N-vacancy complex, (g) pyridinic N3-vacancy, (h) interstitial N. (B) XPS N*1s* analysis showing the presence of the different nitrogen species incorporated in the carbon matrix.

One characteristic feature that is normally associated with the presence of N doped CNTs produced by in-situ doping is the formation of the so-called bamboo-like structure inside the tube axis as briefly discussed above. As can be seen in Fig. 1.11, the inner tube is not hollow, as found in a typical CNTs but is consisted with periodical compartments localized along the tube axis. The bamboo-like shape depends on the synthesis conditions such as nitrogen content, precursors, catalyst, and the synthesis temperature. According to the TEM micrographs showed in Fig. 1.11 the separation between two individual bamboo compartments decreased with an increasing of nitrogen content in the CNTs. However, it is worthy to note that if the nitrogen content is very low or when Co and Ni were used as growth catalyst instead of Fe no compartments or bamboo-like structure are observed in the as-synthesized N-CNTs.
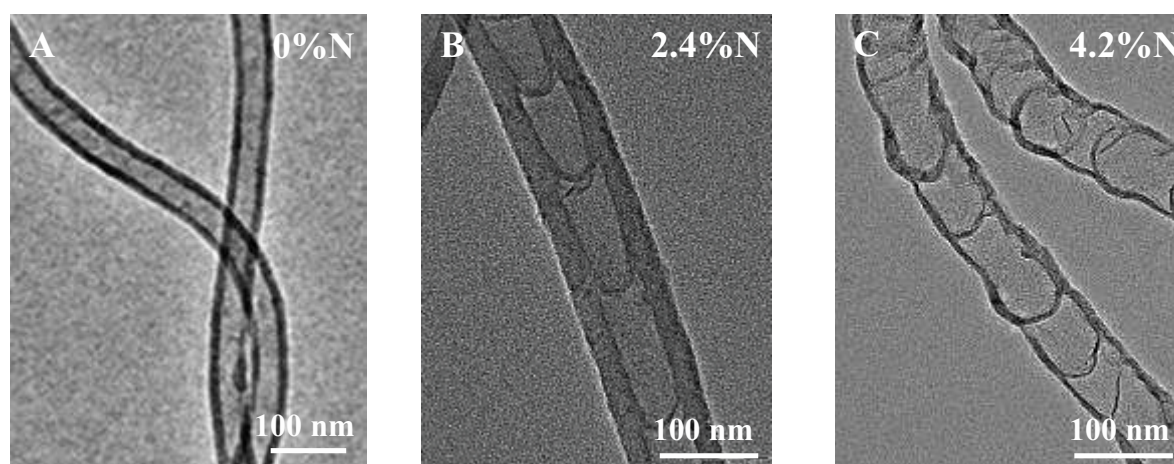
Fig. 1.11. TEM micrograph display the compartment of various nitrogen concentrations doped carbon nanotube by CVD method with using $C_2H_6/NH_3/H_2$ as carbon and nitrogen source and Fe/Al_2O_3 catalyst.

On the other hand, the atomic dimensions of carbon, nitrogen and oxygen as well as the bond length in aromatic structures do not differ very much which makes the latter two elements very suitable for incorporation into the CNTs matrix. However, the C-N bond is shorter as compared to the C-C and C-O bond lengths. Therefore, incorporation of nitrogen into the carbon matrix may distort a perfectly ordered graphitic matrix leading to possible modification of the overall electronic properties of the material. It was shown that low concentrations of nitrogen, i.e., N/C < 0.17, can be incorporated in the graphene layer without changing the graphitic properties and tube morphology in a large extend [71]. Thus nitrogen is able to release strain in the structure of the CNTs, this might be the reason why nitrogen is found around defects [72] and why their concentration in the inner layers was found to be higher than on the outer layers [73].

1.4.2. Electrical properties

Exhaustive studies concerning electronic properties of CNTs indicated that they behave like two types depending on the temperature: at high temperature their electrical conductivity may be described by semi-classical models already used for graphite, whereas at low temperature they reveal 2D-quantum transport features. On the other hand their electrical properties also depend on the rolled up of the graphene layers (armchair, zigzag or chiral) and the presence of defects on the surface of the walled of tubes [12].

The N-doped CNTs not only changes the surface chemistry, but also changes the structural and electrical properties of CNTs. Electrical properties of N-CNTs depend on the nitrogen bond configuration. The three most common bonding configurations of nitrogen doped CNTs as displayed in the Fig. 1.10. However, only the quaternary or graphitic N and pyridine-like N are the most common types. In the case of the graphitic N, where a nitrogen atom is directly substituted to a carbon atom in the hexagonal network, the incorporation of nitrogen can significantly alter the electronic structures, which strongly depend on the bonding configurations [74,75] but they mainly generates an electrical donor state [76,77]. In the case of the pyridine-like structure, N-doped carbon nanotubes are metallic and exhibit strong electron donor states near Fermi level [78]. Two valence electrons of N take part in σ-bonding with neighboring C atoms, two others form a lone pair, and the rest stays in the π-state [74], due to the vacancy site, the equivalent π-electron system is missing, which leads to the p-type doping effect for graphene or metallic CNTs, and the acceptor state in the band gap of semiconducting SWCNTs [74,79].

Many theoretical researches have also demonstrated that N-CNTs obtained by in-situ method will result in localized states above the Fermi level [80–82]. However, it is also distinct from post-synthesis techniques for introducing heteroatoms into the lattice such as thermochemical substitution reactions [83,84] and ion-implantation [85,86].

A similar effect can be observed in the case of the generation of oxygen functional groups on the CNTs surface, which also changes the electronics properties of CNTs. Ago et al. [87] shows that pure CNTs were found to have a slightly lower work function than graphite, i.e. 4.3 eV instead of 4.4 eV. But CNTs after oxygen plasma treatment the density of states were affected and the work function increased up to 4.8 eV. It has been also reported that with increasing oxygen exposure the carbon 2p-π states at 3 eV below the Fermi level diminished, while the 2p-σ states around 6 eV significantly increased. Moreover, CNTs annealing also appeared to increase the density of states around the Fermi level.

In heterogeneous catalysis field, CNTs were used mainly as catalysis supports. Their interaction with the deposited metals is absolutely differences compared to the activated carbon, and mainly related to the interaction of transition metal atoms with CNTs. It has been demonstrated that the binding sites are depending on the structure of the support, for example

the studies conducted over nickel show that the most stable anchoring sites vary sensibly between graphite and SWNT due to the different curvature of the surfaces where the active species can be deposited. The curvature also affects significantly the values of magnetic moments on the nickel atoms on the wall and the charge transfer direction between nickel and carbon can be inverted [12].

1.4.3. Mechanical and thermal properties

Carbon nanomaterials such as CNTs and CNFs have an excellent mechanical resistance, which would be one hundred times higher than the steal while the weight is six times less [12] due to the presence of covalently C-C bond. Furthermore, the mechanical resistance of carbon nanomaterials is hardly influenced by the post-synthesis treatment. Nitrogen doping has a detrimental effect on the mechanical strength of CNTs [88] since C–N bonds are weaker than C–C bonds. Cruz-Silva et al. [79] has reported that the incorporation of nitrogen in the CNTs network led to a reduction in the elongation upon fracture is up to 50 % while the Young Modulus decreased 7 – 8 % compared to the pristine CNTs. N-CNTs also could be oxidized at lower temperatures since the presence of heterogeneous atoms, the defects on the surface of the tube [89]. The presence of residual metal or defects on the surface could lead to a decreased the oxidative resistant of carbon nanomaterials. However, the oxidative resistance properties of the carbon nanomaterials are still higher than active carbon but less than graphite.

1.4.4. Adsorption properties

The adsorption properties of carbon nanomaterials, either on their internal or external surfaces, have attracted increasing attention due to the possibility of using these materials for many applications, especially in gas storage, chemical sensors and heterogeneous catalysis. The interaction of carbon nanomaterials with their environment and in particular with gases or doping species such as metal atoms, oxygen-, nitrogen- species depend on the porous nature and the active sites of these materials. Unlikely to the activated carbon which mainly contained micropores [90–94] the carbon nanomaterials present mainly the mesopores and macropores. Different studies dealing with the adsorption of nitrogen on carbon nanomaterials have evidenced that the pores in carbon nanotubes can be mainly divided into inner hollow cavities of small diameter (narrowly distributed, mainly 3 – 6 nm) and aggregated pores (widely distributed, 20 – 40 nm) formed by interaction of isolated MWCNT. These researches also indicated that the adsorption of carbon nanotubes mainly occur in the aggregated pores, inside the tube or on the external walls, and at the defects [95–97].

In heterogeneous catalysis field, the medium to large-pore carbons with a high total pore volume are preferred in order to increase the contact surface between the reactants and the active sites. The nitrogen doped CNTs lead to the more active support for gas adsorption. Peng

et al. reported that N-CNTs could be used as gas sensors for CO and water while CNTs are not sensitive to these molecules [98].

1.4.5. Catalytic activity

In catalysis field, incorporation of heteroatom such as nitrogen, oxygen, phosphorus, boron, sulfur, in carbon nanotubes matrix is expected to result in the formation of metal-free catalysts which can find application in numerous relevant catalytic processes. Among of these heteroatoms, nitrogen doped CNTs have attracted an increasing studies for many application due to the presence of various functional groups in the surface of CNTs, especially of pyridine-like N, quaternary or graphitic N. The incorporation of the heteroatoms into a CNTs can effectively modify the electronic and surface properties of CNTs, thereby enhancing its catalytic activity. The incorporation of nitrogen in the carbon matrix leads to the formation of a stable basic catalyst. The enhanced basicity can be assigned to the lone electron pair of pyridine-like N, and with graphitic N can be attributed to the presence of more electrons of in the delocalized π-orbitals of the carbon framework due to the higher number of electrons of nitrogen atoms. π-electrons can perform a nucleophilic attack with other molecular such as oxygen leading to the more π-electrons the system contains on the surface of CNTs.

Similarly, oxygen can be also incorporated effectively into the carbon surface by different approaches, *i.e,* HNO_3 treatment. Three types commonly of oxygen-containing groups are C=O type oxygen, C–O type oxygen, and charged oxygen O^-. The presentation of these functional groups led to an easy wrapping, grafting or coating of other functional groups as the site active for various applications. Recently, a few studies also reported the relatively high catalytic activity of oxidized CNTs using directly as metal-free catalyst. However, the roles of oxygen functionalized species are on the catalytic performance is still unclear.

Up to now, almost researches assumed that pyridine-like N is at the origin of the relatively high catalytic activity of N-CNTs [99], while graphitic nitrogen species have been proposed by other research groups [61,100]. In the same with oxygen functional groups, the catalytic roles of carboxyl, carboxylic acid, carboxylic anhydride, and phenol groups are also unclear. Thus, the exact nature of the active sites in N-, or O- doped CNTs is still a matter of debate between the different researches groups involved in this field. In addition, it has also been observed that other properties besides the type of nitrogen site influence the catalytic activity, like the amount of carbon edge sites (*i.e.,* influenced by the type of metal catalyst used in the synthesis of carbon nanotubes), the total N content, the surface area and the degree of graphitization (lower defects) [101,102].

1.5. Catalytic processes applications

1.5.1. N-CNTs as catalyst support

Few applications of the used N-CNTs as catalyst support in some fields have been reported such as in fuel cells, energy storages, and in heterogeneous catalysis. Notably in fuel cells, using N-CNTs as catalyst support early attracted an interesting due to the high active catalyst for the oxygen reduction reaction (ORR) in a proton exchange membrane (PEM) fuel cell environment and possibly using as a cathode material for the ORR in alkaline medium.

While N-doped CNTs make them attractive candidate as metal-free catalysts they can also contribute to modify the electronic structure of nano particles from electron transfer from graphitic nitrogen to metallic particle as recently reported on Pt [103] and on Pt-Ru [104]. Up to now the mechanism of this promoting effect is not clearly elucidated. Previous investigations clearly showed the beneficial effect of N-doped carbon nanotubes for improving the Pt dispersion with uniform distribution providing excellent electrochemical activity of Pt/N-CNT in methanol oxidation [105]. More recently, it was found that promotional effect through electron transfer can drastically increase the intrinsic activity of Pt nano particle. For instance Pt clusters on N-doped systems, having an average particle size lower than 0.75 nm ($\leqslant$1 wt.%) exhibit a remarkable catalytic activity for H_2 production from the decomposition of formic acid, 10 times higher than those measured on un-doped systems [106]. A shift on B.E. of the Pt 4f core level was also observed on the N-doped systems tentatively ascribed to the formation of 2D electron-deficient sub-nm Pt clusters stabilized by pyridinic nitrogen on vacancy sites. Hence, based on this comparison, the electron transfer from pyridinic structure to Pt particles may strongly depend on structural considerations. Changes in the nitrogen concentration at the surface and/or subsequent alteration of the electronic properties after H_2O_2 oxidation can modify the donor-acceptor interactions and the electron-deficiency of Pt particles. A correlation between the Turn-Over-Frequency in glycerol oxidation and the B.E. value of the Pt 4f core level can be established showing the highest intrinsic catalytic properties for the lowest B.E. value. To get more insight into the nature of interaction set between Pt particles and nitrogen groups, the authors investigated the electro-oxydation of CO since CO is recognized to inhibit the rate of numerous reactions due to strong adsorption. Interestingly a rise in catalytic activity is discernible with an increase in B.E. level reflecting a higher electron density due to the electronegativity of oxygen.

According to the results on Pt supported N-CNTs obtained by Vijayaraghavanet al. [107] the catalytic activity and durability enhance with a presence of nitrogen incorporation in the CNTs matrix. Chen et al. [108] have shown that Pt loaded on N-CNTs with different concentration of nitrogen (1.5, 5.4, and 8.4 at.% N) have advantages comparison with C-Vulcan or pristine CNTs. According to these results Pt/N-CNTs have a higher stability than Pt/C and Pt/CNTs after 4000 cycles. Similar studies were done by Maiyalagan and co-workers [109].

The Pt/N-CNTs electrodes exhibited a greater electrochemical surface than the Pt/CNT electrodes as well as higher single-cell performance in a H_2O_2 fuel cell. They were loaded Pt catalysts on three different supports: graphite, CNTs, and N-CNTs (% N = 0 – 16.7).

Many studies also indicated that beside the influence of nitrogen the ORR activity and stability also depend on the metal particle distributions on the N-CNTs support, metal-support interactions, number of edge sites (surface of defects) as well as nitrogen species containing in the N-CNTs. Recently, interesting studies using the combine N-doped carbon materials with various catalytic transition metals such as Fe [110], Co [111], Pd [112] and metal oxides *i.e.,* Fe_3O_4 [113], MnO_2 [114], and $TiSi_2O_x$ [115] in order to replace the high cost Pt have been reported. These metal catalysts also exhibits a more positive onset potential, higher current density, lower peroxide yield, and better durability than the commercial Pt/C catalyst.

N-CNTs as catalyst support material is not only used for ORR but can also be used in other catalytic reactions as listed in Table 1.2. The high activity performance of metal/N-CNTs mainly assigned to the presence of basis sites and the highly dispersion of metal on the CNTs surface compared to that observed on the un-doped CNTs. Amadou et al. [55] and Chizari et al. [36] reported that N-CNTs support allows the significant improvement on the dispersion of the palladium nanoparticles due to the electronicalteration of the carbon matrix after introducing nitrogen atoms. Representative TEM micrographs of the Pd/N-CNTs are presented in Fig. 1.12 and evidence the high and homogeneous dispersion of the Pd nanoparticles on the N-CNTs surface. The Pd nanoparticles have an average size of around 3 ± 1 nm which highlighted the strong interaction with the support. In comparison the average particle size of the Pd supported on CNTs is ranged between 6 to 10 nm. Similar observation has been reported by different research groups working in the field [10,12,116].
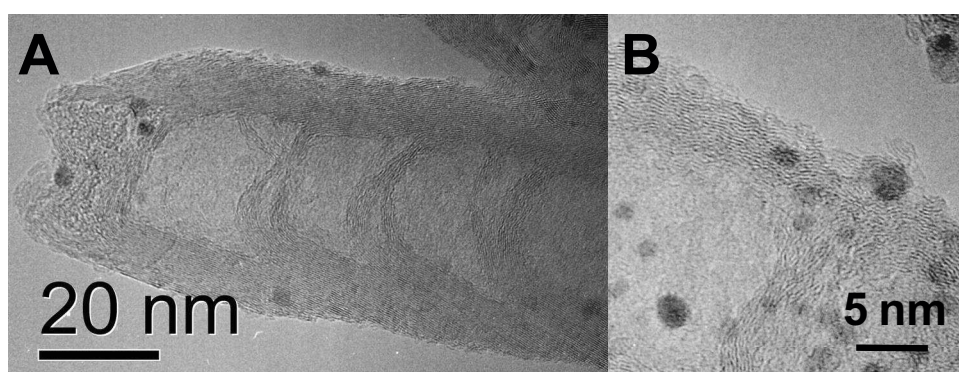
Fig. 1.12. Representative TEM micrographs of the Pd/N-CNTs catalyst used in the selective liquid-phase hydrogenation of cinnamaldehyde [55].

Table 1.2. Application of Metal/N-CNTs as catalyst support in the literature.

Catalyst support	N content (wt.%)	Catalytic reaction	Properties of catalyst support	Refs
Ru/N-CNTs	4.0	NH$_3$ decomposition	Activity of a Ru/N-CNTs catalyst depends on the electron transfer ability and the dispersion of Ru nanoparticles	[117]
Pd/N-CNTs	7.0	Liquid-phase hydrogenation of cinnamaldehyde	Pd/N-CNTs showed C=C bond led to the activity and selectivity higher than that found for the undoped CNTs	[55]
Ni/N-CNTs	3.0 – 3.9	Butyronitrile hydrogenation	Higher electron density delivered by nitrogen on the surface of CNTs leading to an enhanced catalytic activity	[118]
Pd/N-CNTs	1.0 – 1.6	Hydrogen oxidation	Highest Pd dispersion and greatest activity.	[119]
Pt or Pd/ Carbon nitride	16.1 - 60	Cyclohexene or Phenol hydrogenation	Semiconductor-metal heterojunction, stable and uniform dispersion of Pd or Pt	[120, 121]
TiO$_2$ or CdS/N-CNTs	2.0	Photocatalyst	Enhance the photocatalyst activity and modify the intrinsic band-gap by the modulation of electronic structures	[122, 123]

1.5.2. N-CNTs as metal - free catalysts

Carbon nanomaterials, especially N-CNTs, have long been used as catalyst support in the field of heterogeneous catalysis as mentioned above while their direct use as metal-free catalyst has only been reported recently. Some catalytic reaction carried out on heterogeneous atoms doped carbon nanomaterials as listed in Table 1.3. One can see that N-CNTs as metal-free catalyst has received an ever increasing academic interest since the last decade and the catalytic processes involving N-CNTs are continuously expanded with time. Part of the results obtained is summarized in some recent reviews dealing with the use of these metal-free catalysts in the field of heterogeneous catalysis [10,116,124,125].

Table 1.3. Application of heteroatom doped-CNTs as catalyst support in the literature.

Catalyst	Catalytic reaction	Active sites	Properties of catalyst	Refs
O-CNTs or P-CNTs	Oxidative dehydrogenation (ODH) of n-butane to butenes	- C=O groups - Phosphorus as a promoter	- The yield increased: V/MgO < CNTs < O-CNTs < P-CNTs - High selectivity for long-term test (100 hours)	[126]
MWCNT	Direct hydroxylation of benzene to phenol	- Defects - Active oxygen generated by H_2O_2 decomposition	Low benzene conversion (6%) but very high phenol selectivity (99%)	[127]
O-CNTs	Reduction of nitrobenzene	Carbonyl species groups	- The advantages of lower environmental impact and corrosion problems due to using green oxidized H_2O_2 - Better catalytic performance than that for HNO_3 oxidized	[128]
CNTs	Oxidation of cyclohexane with O_2 to cyclohexanol, cyclohexanone	- Oxyen - Redox metal used to synthesize CNTs	- The advantages of lower environmental impact (NO_x and N_2O emissions) and corrosion problems. - The yields (< 70 %) lower than those obtained using HNO_3 - The quality of produced is poor	[128, 129]
N-CNTs	Oxidation of cyclohexane	- Nitrogen species - Defects	Reaction rate increased about 5 times with respect to AC and 2 times compared to un-doped CNTs	[130]
N-, B-, P-, O- doped CNTs	ORR in alkaline media	- Functionalization groups - The graphitic edge plan or defects	- High electrocatalytic - Good stability	[13,15,60, 100,131–133]

In 2006, van Dommele et al. [99] reported that nitrogen doped CNTs can catalyze the Knoevenagel condensation reaction of benzaldehyde and ethylcyanoacetate and the activity performance of N-CNTs increased with increasing amount of pyridine-like species. Since this pioneering work an ever growing research interest has been focused on the use of N-doped carbon nanomaterials as metal-free catalysts in several relevant catalytic processes. Gong et al. [134] recently reported that vertically aligned N-doped CNTs could be efficiently used as a metal-free catalyst for performing oxygen reduction reaction in alkaline medium with an activity comparable to that of the commercial platinum-based catalyst. The high activity of the N-CNTs was attributed to the electronic modification of the carbon atoms located next to the nitrogen one which modifies the adsorption mode of the oxygen. The work of Gong et al. [125] fostered a huge and unprecedented scientific interest in the development of metal-free catalyst for replacing the costly noble metal in the ORR process since the last years from several research groups around the world. It is worthy to note that the ORR field of research is nowadays the biggest fields of investigation for the N-CNTs so far. The results obtained in this field are well documented in several detailed reviews [13,124,131,134]. Recent works have shown that the ORR performance is influenced by the pyridinic nitrogen species present on the N-CNTs surface as well as the total nitrogen doping (Fig. 1.13).
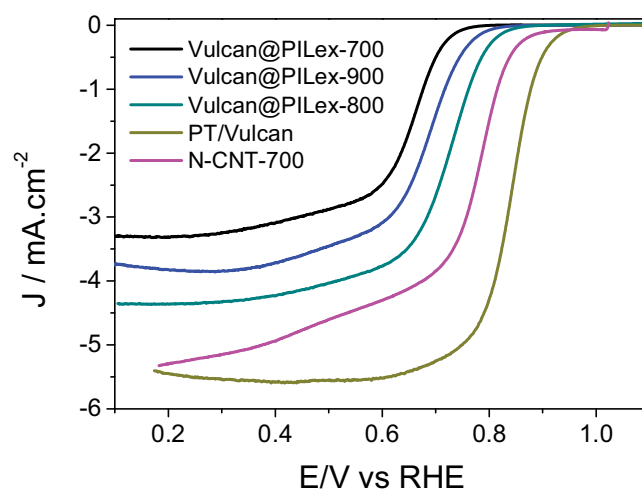
Fig. 1.13. ORR performance of the different N-CNTs and the commercial Pt/Vulcan catalysts. N-CNT-700: nitrogen-doped carbon nanotubes synthesized by a CVD method at 700°C, Vulcan@PILex-X: nitrogen-doped carbon layer synthesized from a thermal decomposition of the polymerized ionic liquids (PILs) at different temperatures.

However, some key points remains still none elucidated regarding the contribution of the different N-containing species on the overall activity of N-CNT in ORR [135]. This can be possibly due to their different coordination with the carbon matrix and/or the ability to

create defective sites at increasing N concentration [136]. As above-mentioned, it was found that pyridinic can play a determining role in the activity in ORR catalyzing the direct reduction of O_2 to H_2O through a four electron pathway whereas graphitic N species would activate preferentially a two-electron pathways. It is worthy to note that the residual iron growth catalyst could also play a role in the ORR performance.

Giambastiani and co-workers [132] have reported that N-CNTs, doped by organic precursor compounds containing specific nitrogen-species at low temperature, exhibit an ORR activity close to the commercial Pt/C catalyst under alkaline medium, although still negatively shifted from the onset potential with respect to the Pt/C catalyst. It is worthy to note that the N-CNTs, synthesized by an in-situ method, contain several nitrogen species which render extremely difficult for the establishment of a direct relationship between the nitrogen species nature and the ORR activity. The main advantage of the doping method by Giambastiani and co-workers [132] is that it allows the precise control of the nitrogen species incorporated on the carbon matrix and thus, allow one to make a clear trend on the influence of each nitrogen species on the ORR performance.

Jiang et al. [133] have recently reported the use of nitrogen-doped nanoporous carbon nanocables as an efficient metal-free catalyst for ORR. The composite is constituted by a CNT core covered by a N-doped nanoporous carbon shell (Fig. 1.14) organized in a 3D structure with high mass transfer and conductive network.
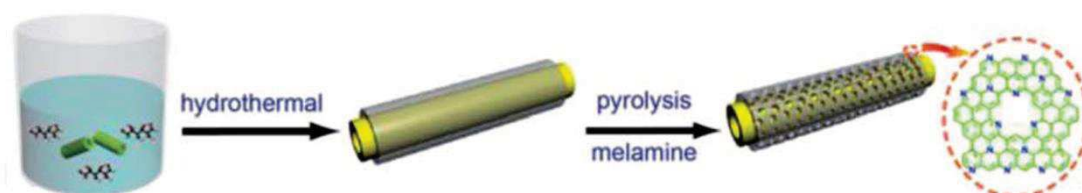
Fig. 14. Schematic representation of the core-shell nanocables synthesis method developed by Jiang et al. [133]

Kruusenberg et al. [137] have reported that nitrogen-doped carbon composite is an efficient metal-free catalyst in the alkaline direct methanol fuel cell. Nitrogen-doped carbon catalyst is also developed for the microbial fuel cells process [138].

Nitrogen-doped CNTs have also been reported recently by Pham-Huu and co-workers as an efficient metal-free catalyst in the partial oxidation of H_2S into elemental sulfur [139]. Such reaction is mostly catalyzed by the iron-based catalyst supported on different carriers such as silica, alumina and silicon carbide [140,141]. The high catalytic stability as displayed in Fig. 1.15 could be attributed to the fact that nitrogen species are well anchored into the

carbon matrix and, as a consequence the active phase sintering is unlikely to occur even under severe reaction conditions. Regarding the large amount of sulfur containing gaseous effluents to be treated in different industrial sectors it is expected that such robust metal-free catalyst will face a large scientific and industrial interest in the near future. It is expected that robustness catalyst will significantly reduce the needs for spent catalyst recycling which is an economic and environmental issues of concern for operating the plant.
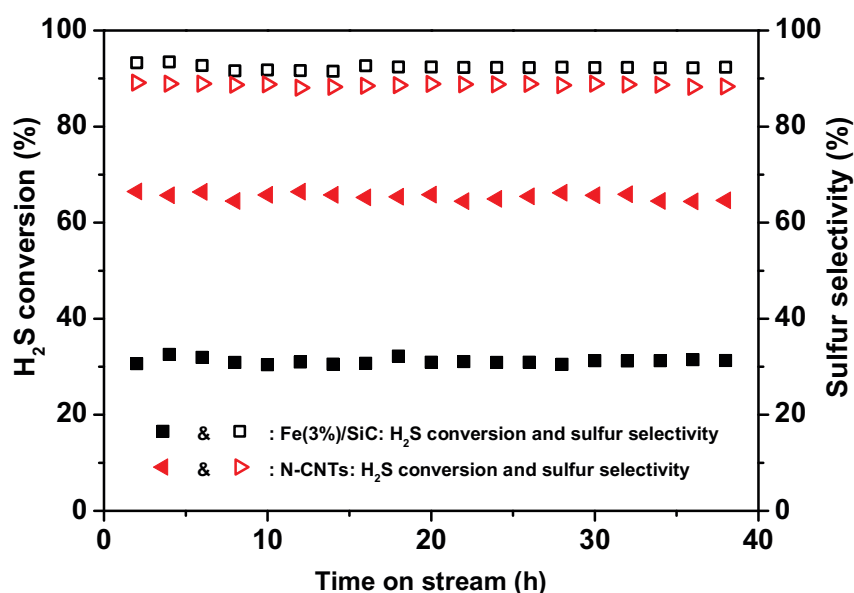
Fig. 1.15. Desulfurization performance on the N-CNTs and Fe_2O_3/SiC catalysts. Reaction conditions: reaction temperature = 230°C, O_2-to-H_2S molar ratio = 2.5, WHSV = 0.6 h^{-1}, steam = 30 vol.%. Results reproduced according to [142].

Yu et al. [129] have reported that N-CNTs significantly improve the cyclohexane oxidation rate compared to those obtained on the corresponding activated charcoal and un-doped CNTs. The use of N-CNTs as selective oxidation metal-free catalyst has been reported by Su and co-workers [143] in the oxidative dehydrogenation of light alkane. The authors have observed that the dehydrogenation rate of propane to propene is proportional to the nitrogen content on the catalyst surface. Despite a loss of ~25% of nitrogen content revealed from XPS analysis, no significant deactivation was detected. Such data was explained by the fact that some of the nitrogen species present on the catalyst surface was not active for the reaction and thus, it degradation during the course of the reaction imparts negligible activity lost. According to the XPS analysis the graphitic nitrogen is an active phase for the oxidative dehydrogenation of propane. It is expected that the graphitic nitrogen atoms donate electrons to the graphitic sheet which improving the electron mobility from the carbon basal plane to the intermediate O_2^- and finally, to an enhancement of the dissociation of O_2 to nucleophilic O^{2-} species. The high selectivity of the N-CNTs towards propene is attributed to the repulsion

between the electron-rich graphitic surface and unsaturated C=C bonds of propene favoring the propene desorption. Gao et al. [144] reported that doping of carbon matrix with nitrogen significantly increase the rate as well as the selectivity towards acetophenone in the oxidation of ethylbenzene with tert-butyl hydroperoxide. In all these reports the dependence of reaction rate versus the concentration of quaternary nitrogen species has been established. The similar dependency, between the quaternary nitrogen and the catalytic performance, has again been reported by Wei and co-workers [145] on the N-CNTs with medium loading for the most demanded industrial hydrochlorination of acetylene to produce vinyl chloride. The results indicate that the hydrochlorination can be carried out on the N-CNTs despite with a reaction rate somewhat lower than those reported for the Au/AC, Hg/AC and Cu/AC catalysts. In addition, the N-CNTs display a better resistance towards deactivation as a function of time on stream compared to the other metal-based catalysts. Indeed, under similar reaction conditions the non-precious metal-based catalysts, *i.e.* 5 wt.% Bi/AC and 2wt.% Cu/AC, steadily deactivate while the N-CNTs remain much more stable and even better than that of the precious metal Au/AC catalyst. The results obtained by Zhou et al. [145] have evidenced that nitrogen-doped CNTs can also catalyze other reactions than those involved with oxygen and thus, significantly widen the panel of applications for those metal-free catalysts.

Tessonnier and co-workers [146] have reported that nitrogen-doped CNTs can be efficiently employed as a metal-free base catalyst in the liquid-phase transesterification reaction between methanol and glyceryltributyrate.
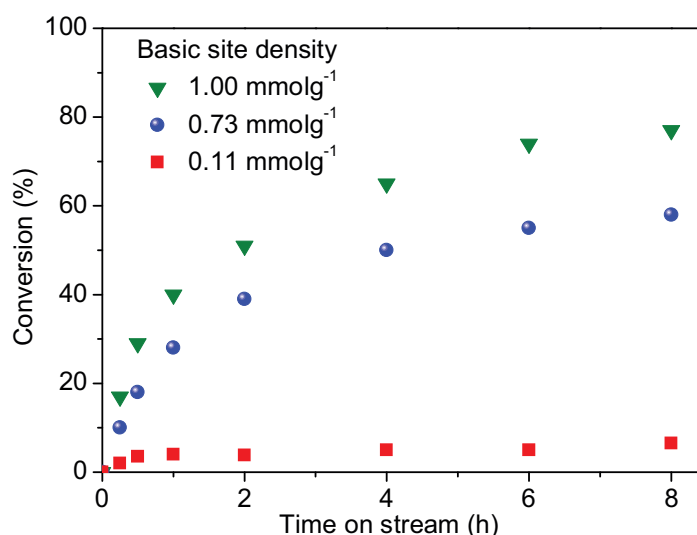
Fig. 1.16. Effect of the amount of grafted triethylamine on the transesterification activity, expressed in terms of glyceryltributyrate conversion, on the nitrogen-grafted CNTs catalysts. Reaction conditions: Temperature = 60°C, glyceryltributyrate to methanol ratio = 1:12, catalyst weight= 2 wt.% versus the reactant mixture. Results reproduced from [146].

The nitrogen-grafted CNTs were synthesized by treating the CNTs with *n*-BuLi followed by an electrophilic attack with a bromoalkylamine. Acido-basic titration indicates a basic character of the samples. The transesterification activity is proportional to the density of the basic groups present on the catalyst (Fig. 1.16). In addition, the nitrogen-grafted catalyst also shown an extremely high transesterification activity compared to that of the N-CNTs, synthesized by high-temperature doping in the presence of ammonia [147]. Indeed, under similar reaction conditions the conversion of the glyceryltributyrate on the nitrogen-grafted catalyst was amounted to 77 % whereas it was only 3 % on the N-CNTs. The main drawback of the process is the post-reaction separation step to recover the vinyl chloride as methanol was used in excess with respect to the glyceryltributyrate.

Rocha et al. [148–150] have also reported recently that the N-CNTs and N-doped graphene can also be efficiently used as metal-free catalyst in the ozonation and advanced oxidation processes to remove organic compounds presented in wastewater. According to the results obtained the introduction of nitrogen into the carbon matrix leads to an improvement of the oxidation of oxalic acid for the catalytic wet air oxidation (CWAO). On the other hand, the nitrogen-based sites allow a higher mineralization of phenol during the ozonation process. The promising catalytic performance and robustness of these nitrogen-doped metal-free catalysts are of high interest for the possibility to replacing traditional metal/oxides catalysts with lower activity and stability in the field of wastewater treatment. Some preliminary catalytic results have obtained by the same group using N-CNTs produced through a ball-milling process. Additional work based on the use of macroscopic shaped nitrogen-based catalyst will be conducted for the future use of these metal-free catalysts in an industrial plant.

Similar results have also reported by Sun et al. [151] in the use of nitrogen-doped carbon composite for the most demanded catalytic oxidation of organic pollutant in wastewater. The authors have reported that doping of CNTs with nitrogen leads to a significant improvement of the phenol oxidation rate, 100 % of phenol conversion was obtained on the N-CNTs after 45 min compared to 76 % on the un-doped CNTs. The modification of sp^2 carbon by nitrogen atoms, both as direct graphitic nitrogen doping and nitrogen decorating defective sites were advanced to explain the activity improvement.

Nitrogen-doped carbon composites have also reported by Chen et al. [152] to be a theoretical efficient metal-free catalyst in the dehydrogenation of ammonia borane compounds.

In light of the literature results reported above one can assume that nitrogen-doped carbon nanotubes materials could represent a new variety of metal-free catalysts with a high catalytic performance and improved stability in numerous important catalytic processes. However, the use of N-CNTs represents also some drawbacks due to its nanoscopic shape which could pose serious problems for its handling and transport and also for its use in industrial catalytic reactors. Indeed, N-CNTs can be used as such in its nanoscopic shape in

the ORR process as it is only require a good dispersion of the N-CNTs in an ink medium before processing whereas for the other applications, the N-CNTs should be shaped in a macroscopic form in order to avoid the problem of pressure drop across the catalyst bed (Fig. 1.17) and also to facilitate the problem of reactor charging and discharging. The macroscopic shaping not only minimizes the pressure drop but also improves heat and mass transfer during the reaction by adapting the macroscopic shape to the reaction conditions. In this aim research projects have been conducted to develop N-CNTs supported on different macroscopic host structures, *i.e.* Al_2O_3, SiO_2, carbon and SiC, for different catalytic processes. The supports should also be produced in an industrial way in order to avoid the costly development of new infrastructure and to reduce as much as possible the time to market of the process.
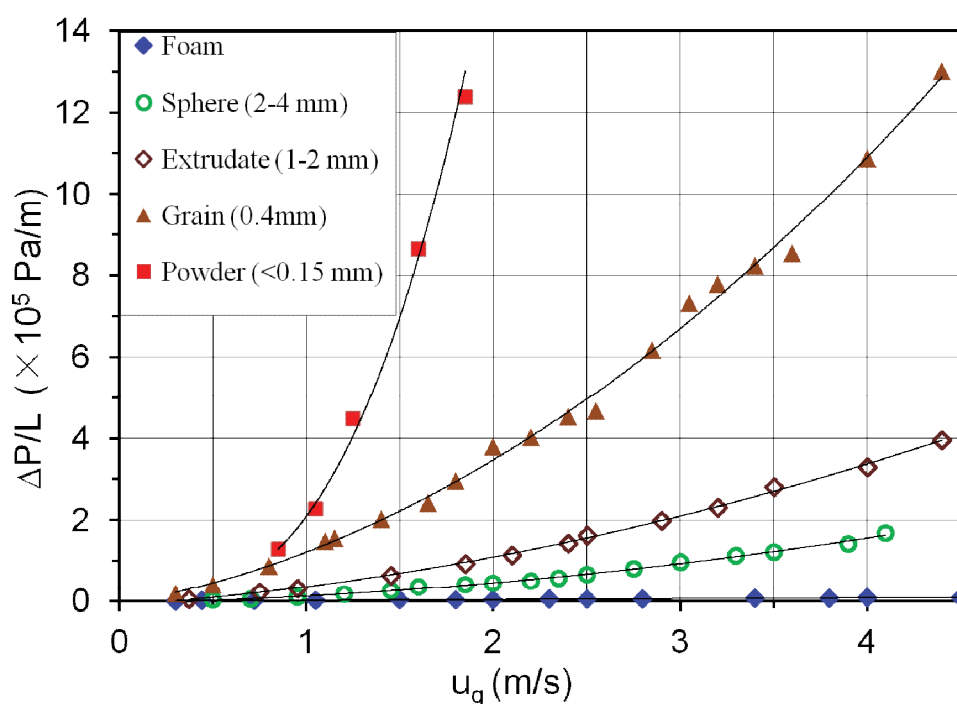
Fig. 1.17. Pressure drop measurements on the various macroscopic composites with different shapes.

The following part of this work will be devoted to the use of these macroscopic shaped nitrogen-doped CNTs and mesoporous carbon for catalysis applications. It is worthy to note that the reports deal with the use of these macroscopic N-CNTs remain scarce nowadays despite their high potential of application. However, it is worthy to note that the results obtained indicate that this new family of metal-free catalysts will play a key role in the relentless development race of future catalysts with better catalytic performance alongside with low carbon footprint.

1.5.3. Metal-free catalyst with macroscopic shaping

Nitrogen-doped CNTs with macroscopic shaped catalysts have received an ever increasing scientific interest as they represent a viable alternative for the future industrial development of these metal-free catalysts in several potential applications. For some catalytic processes these metal-free catalysts outperform the catalytic activity of traditional ones along with a better stability as a function of time on stream. The most developed synthesis process is the Chemical Vapor Deposition (CVD) of the N-CNTs on a macroscopic host structure containing the growth catalyst similarly to that operated for the synthesis of CNTs with macroscopic shaping developed first by Vieira et al.[17,153] for subsequence use as catalyst support in several catalytic processes ranged from hydrazine decomposition to selective hydrogenation [21,154,155]. However, despite a large scientific and industrial interest reports deal with the development of these metal-free catalysts with a macroscopic shaping remain scarce nowadays and most of the catalytic experiments are carried out with the powdery catalysts.

Pham-Huu and co-workers [139] have used the CVD method to synthesize N-CNTs decorated silicon carbide macroscopic structures, *i.e.* grains, pellets and foam, for the selective oxidation of H_2S into elemental sulfur. The N-CNTs exhibit a relatively high anchorage mechanical strength which allows them to be efficiently used in a fixed-bed reactor under a relatively high gaseous flow rate. The N-CNT/SiC catalysts, either supported on SiC pellets or foam, display a net improvement in terms of desulfurization activity compared to that obtained on the unsupported N-CNT catalyst (Fig. 1.18). The improved catalytic rate can be attributed to the fact that most of the N-CNTs are located on the outer surface of the support and thus, the pore diffusion process can be neglected which could significantly increase the reactant access rate leading to a high turn-over frequency. However, the improvement of the desulfurization activity is accompanied by a slight decrease of the sulfur selectivity on the supported N-CNTs catalyst compared to that of the unsupported ones (Fig. 18). The decrease of the sulfur selectivity could be attributed to several facts: *(i)* high entanglement of the as-grown N-CNTs which could led to a high residence time favoring the consecutive oxidation process to form SO_2, *(ii)* some residual acidity on the SiC surface which could contributes to the retro-Claus reaction. Work is underway to uncover the mechanism of the reaction and to control the sulfur selectivity regarding possible industrial developments. The influence of the support shape and size on the desulfurization performance represents also an intensive area of research.
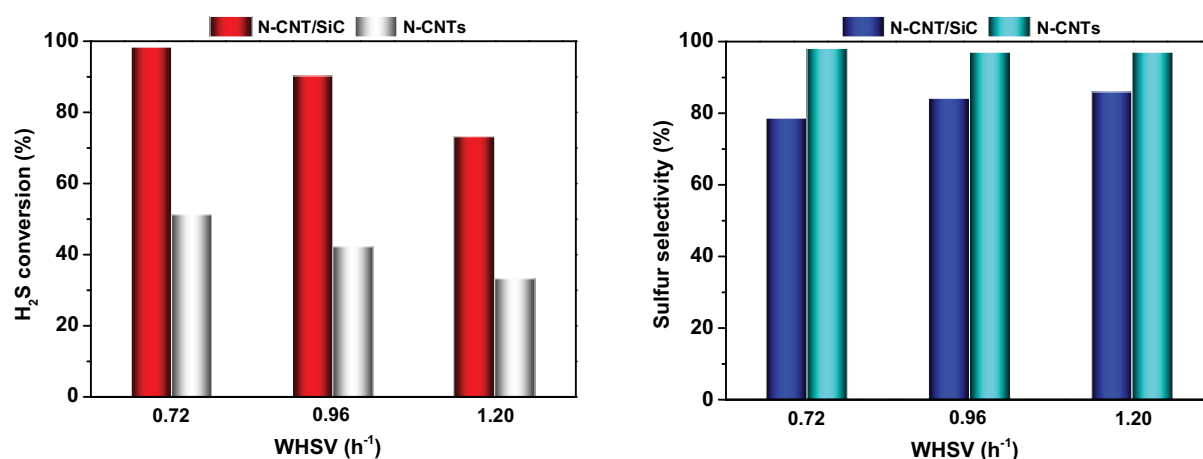
Fig. 1.18. Desulfurization performance, expressed in terms of H_2S conversion, on the N-CNT/SiC and N-CNT catalysts. Reaction conditions: reaction temperature = 190 °C, O_2-to-H_2S molar ratio = 2.5, steam = 30 vol.%.

Recent work deals with the use of nitrogen-doped porous carbon supported on silicon carbide granules has also been reported by Bao and co-workers [156] for the hydrochlorination of acetylene. The authors have reported that pyrollic nitrogen species can activate acetylene in the presence of HCl to produce vinyl chloride. Under similar reaction conditions the SiC@N-C catalyst displays an acetylene conversion of about 80 % while on the nitrogen-free SiC@C only 20 % of acetylene has been converted. Such results confirm the catalytic activity of the nitrogen doping in the hydrochlorination process. Both experimental and theoretical studies indicate that the active site for the hydrochlorination of acetylene is the carbon atom bonded with pyrollic nitrogen species. Such results are somewhat different from those reported before by Wei and co-workers [145] where graphitic nitrogen species were advanced to explain the catalytic activity. Such discrepancy in the nature of the nitrogen active phase could be attributed to the fact that the CVD synthesis is not selective for a type of nitrogen species and thus, a direct relationship between the active site nature and the catalytic performance is not straightforward to build. In addition, it is also worthy to note that XPS analysis cannot allows one to unambiguously ascribe the nitrogen species present on the catalyst surface to a catalytic result and that some other factors should be also taken into account, i.e. amorphous phase, cooperative active ensemble and or degree of graphitization. It is expected that more investigation is needed to uncover the real nature of the active site and perhaps, the influence of its surrounding as well, on the whole catalytic performance.

In the work of Bao and co-workers [156] the possibility to support the nitrogen-doped carbon active phase on the macroscopic SiC carrier also represents another advantage for the process as for industrial exploitation as powdery catalyst is not suitable due to the problem of pressure drop. The main drawback of this work is the use of CCl_4 at high temperature to remove the silicon atoms on the SiC surface which could hinder it industrial development.

1.5.4. Other applications

Beside of the catalysis field applications mentioned above, N-CNTs were also employed for many other applications included: the protection of natural environment for removing sulfur compounds, nitrogen oxides and carbon dioxide; purification of wastewater by selective adsorption of heavy metal ions, aromatic compounds and dye molecules, energy storage…, due to their high adsorption capacities and the presence of different functional groups species on the surface. The presence of acidic oxygen functional groups on CNTs surface mainly occurs by capacity of ion exchange mechanism with proton displacement, while that on nitrogen-containing groups occurs via an interaction with polar adsorbents.

In the purification of wastewater, oxygen-, nitrogen-doped CNTs displayed a highly adsorptions capacities for heavy metal ion (Cr^{3+}, Zn^{2+}, Ni^{2+}, Pb^{2+}, Ag^+, Hg^{2+}) [157,158], phenol [159], toluene, chloroform [16] and organic acid (uric acid) [160]. Nitrogen-containing CNTs showed high adsorption capacities for these metal ions because of their coordination to nitrogen-containing groups, while the π–π interactions between the phenol, chloroform and organic and the graphene layers or the high porous carbon surface led to an increasing adsorption capacities between organic solvent and adsorbents.

In addition, nitrogen-containing CNTs also show excellent adsorption and gas separation properties for polar or acidic gas molecules. Tanada et al. [161] reported that the adsorbed amount of formaldehyde increases with increasing introduced amino groups and depends on the interaction formaldehyde to amino groups on the activated carbon surface. These results are in good agreement with those reported by Song et al. and Rong and co-worker when they used polyacrylonitrile-based activated carbon fibers [162] or rayon-based activated carbon fibers [163] for removing formaldehyde. On the other hand, many studies reported that oxygen-, nitrogen-rich porous carbon can also adsorb highly the harmful gases such as: NO_x [164,165], CS_2, SO_x…, even at ambient temperature. Moreover, the excellence adsorption capacities of N-doped CNTs were employed for gas adsorption and CO_2 capture. Very recently, Dai et al. reported that nitrogen-rich carbon with specific surface areas of more than 500 $m^2.g^{-1}$ exhibited high adsorption capacity for CO_2 and selectivity for CO_2/N_2 separation, while Sevilla et al. reported a high CO_2 adsorption rate (95 % CO_2 uptake in 2 min) and a high adsorptive selectivity (CO_2/N_2 = 12) when they used N-rich doped CNTs (10.1 %N), most of which are pyrrolic-like N species with a small proportion of pyridine-like N species and narrower micropore sizes for CO_2 capture.

In the hydrogen storage field, many studies indicated that the porous structure of carbon nanomaterials can be extremely favorable for adsorption of hydrogen at low operation temperature (-196 °C) [166]. The presence of nitrogen on the CNTs surface led to a beneficial at low coverage (low hydrogen uptake) but detrimental at high coverage (high hydrogen uptake). Zhu et al. predicted that nitrogen might attract the electrons of the neighboring

carbon atoms leading to electron deficient, and so that adsorption capacity of hydrogen increased at the optimum N/C ratio. Contrary, nitrogen would have a negative effect on the hydrogen adsorption at high nitrogen content due to the increase in electron-rich sites [152].

1.6. Supports for the macroscopic shaping of N-CNTs

Up to now, two families of support commonly used in the most field of heterogeneous catalyst are *(i)* amphoteric or acidic oxides, such as graphite [168,169], silicon [170,171], alumina [172,173], silica [174,175], alumino-silicate (zeolite) [176,177], and *(ii)* carbon or carbon-like supports [178]. However, these supports have displayed some drawback in industry applications and especially for the highly exothermic reactions. For insulator supports such as alumina and silica and related composites, which operated in an exothermic reaction, the main problem concerns the heat transfer from the catalytic site to the support body. It is worthy to note that the problem of heat transfer can be even problematic in a laboratory setup where temperature runaway could lead to the destruction of the catalyst and compromise the security of the setup. In these exothermic processes, the support plays an important role by reducing heat gradient within the catalyst particle but also to prevent temperature run away within the catalyst bed. In the case of insulator support, the intraparticle temperature gradients could also be present leading to a large different of temperature between the outermost surface of the catalyst and the catalyst body. This fact led to the drastic modifications of the support and the nature of the active phase. In the second point, drawbacks of carbon – based material are mainly relative to the low mechanical stability and low oxidation resistance along with the presence of micropores, which could hinder their application at high temperature under an oxidative atmosphere and the full accessibility of the reactants to the active sites.

Porous silicon carbide, crystallized in a cubic structure (β-SiC), has overcame the problems faced with the conventional supports described above due to its high thermal conductivity, high resistance towards oxidation, high mechanical strength, high porosity with mostly meso- and macro-pores network and chemical inertness [179–185]. The porous beta SiC was synthesized according to the recipe reported by Ledoux and co-workers [186–188] using the so-called "Shape Memory Synthesis" method (SMS). The SiC was formed by a gas-solid reaction between the gaseous SiO and the solid carbon at reaction temperature around 1300 °C. The side-product is CO, which was actively pumped-off from the reaction chamber allowing the shifting of the reaction towards the SiC formation. The reaction process can be summarized by Equations (1.1) and (1.2). According to the SMS synthesis method, porous beta SiC with medium to high specific surface area, ranging from 10 to 90 $m^2.g^{-1}$, was obtained.

$$Si(s) \; + \; SiO_2(s) \; \rightarrow \; 2\,SiO(g) \qquad\qquad (1.1)$$

$$SiO(g) \; + \; 2\,C(s) \; \rightarrow SiC(s) \; + \; CO(g) \qquad\qquad (1.2)$$
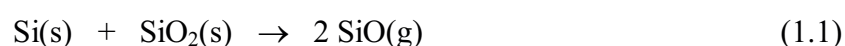
The SMS method also allows the production of beta SiC with various macroscopic shapes, i.e. grains, pellets, foams, rings… which can be easily adapted to the downstream applications. Since the first laboratory synthesis of beta SiC additional researches conducted within different partners companies have lead to a new synthesis method which can be operated at industrial scale (2.2z, 2.2w). In this synthesis the SiC materials were prepared by using stoichiometric mixture of micronized (< 20 µm) metallic silicon and carbon (carbon black from Cabot and high carbon yield binder as carbon source). Temporary binder, i.e. methyl cellulose, polyvinyl alcohol, polyethylene glycol, sodium silicate, SiO_2 sol, can be also added to the precursor for tuning the final pore size of the material. After mechanical mixing of the raw materials, the SiC precursor is shaped into green bodies using standard technologies, like extrusion, spheronisation, granulation, pelletizing and so on. To produce open cell foams or 3D structures, the replica method is used [189]: a slurry is prepared using the same raw materials but the amount of temporary binder is increased and rheological additives are used to meet the required viscosity/thixotropy for the slurry. The preparation is then coated onto polyurethane foam or onto 3D fiber fabric. The green body is then dried overnight at room temperature following a thermal treatment at atmospheric pressure under argon in an electrical furnace up to 1360 °C. The thermal treatment was lasted for 1 h in order to synthesize self-bonded porous silicon carbide materials. The reaction temperature is kept under the silicon melting point (< 1400 °C). During the thermal treatment, the high carbon yield resin is pyrolized into amorphous carbon binding the carbon black and the silicon particles together. Above 1000 °C, the metallic silicon will then react with residual traces of oxygen to form $SiO_{(g)}$ which further react with the carbon structure to form SiC according to Eq. (1.3), whereas the CO releases by the reaction is reacted with metallic silicon to form SiC according to Eq. (1.4).

$$SiO(g) + 2C(s) \rightarrow SiC(s) + CO(g) \qquad\qquad (1.3)$$

$$CO(g) + 2Si(s) \rightarrow SiO(g) + SiC(s) \qquad\qquad (1.4)$$

After synthesis the SiC material was submitted to an oxidative treatment in air at 800 °C for 2 h in order to remove the residual un-reacted carbon species in its matrix. The as-synthesized silicon carbide is "self-bonded" and highly porous which allows it to be fully used as catalyst support. This general experimental procedure enable us to produce a large panel of well controlled SiC materials with controlled size and shape with medium to high specific surface area and adaptable morphology regarding the downstream catalytic applications. The beta-SiC materials synthesized by a gas-solid reaction at an industrial scale (50 tons per annum) with controlled size and shape are presented in Fig. 1.19.

Fig. 1.19. Digital photo of β-SiC synthesized by SMS method with different macroscopic shapes, i.e., grains, pellets, foams, rings, tubes. Courtesy by http://www.sicatcatalyst.com/.

After synthesis and after calcinations the SiC surface was covered with a thin layer of SiO_2 and SiO_xC_y [190] which will play an importance role as anchorage site for dispersing metal nanoparticles on its surface. Recently, such passivity layer consisted by a mixture of SiO_2 and SiO_xC_y was replaced by a TiO_2 one which presents a higher interaction with the metal salt precursor and, as a consequence, significantly improve the final dispersion of the active phase on the SiC surface.

The medium to high surface area beta SiC synthesized according to the gas-solid reaction described above is used as support catalyst in several relevant catalytic reactions such as: hydrodesulfurization (HDS), automotive exhaust-pipe [191], isomerization of linear saturated hydrocarbons [192], dehydrogenation and isomerization of n-butane [192,193], Fischer-Tropsch synthesis [194,195], dehydration of methanol to dimethyl ether (DME) [196,197] and the selective oxidation of H_2S into elemental sulfur [141]. According to these results SiC support exhibit higher catalytic performance compared to that obtained on the traditional supports [21].

1.7. Partial oxidation of hydrogen sulfide (H$_2$S) into elemental sulfur

1.7.1. Hydrogen sulfide and elemental sulfur

Hydrogen sulfide is a highly toxic and corrosive environmental pollutant for human and animals with an obnoxious smell, the removal of which is necessary for pollution control and processing requirements within industry. The content of H$_2$S in crude petroleum, biogas, gas by-products from petroleum refineries and natural gas is significantly different and in general varies from 0.005 % up to 90 % in volume, respectively. Due to its toxicity, in addition to the corrosion problems that could occur within industrial plants, its removal from gas is crucial before releasing the effluents into atmosphere. The maximum admissible operative concentration of H$_2$S in industrial gas flows is 1000 ppm, with the maximum concentration allowed in a gas flow which releases into the environment set at 5 ppm. Hydrogen sulfide in gaseous are dangerous for the environment since it is as a precursor to rain acid.

In the petrochemical domain, hydrogen sulfide is a poison for catalysts, which generally consist of metals or metal oxides (catalytic processes are numerous in the refining and petrochemical). The reaction between H$_2$S and the active phase (metals and oxides) leads to the formation of sulfide(s), which significantly lower the overall catalytic activity.

According to the short description above the H$_2$S must be removed from the different effluent gaseous before their releasing into atmosphere. The most common process is the selective conversion of H$_2$S into elemental sulfur through different thermal and catalytic processes as described below.

The mainly as-received elemental sulfur formed from the desulfurization processes has many industrial applications. Through its main derivatives as sulfuric acid (H$_2$SO$_4$), sulfur is considered to be one of the most important elements used as industrial raw materials. It is most important for all sectors of the world economy. Sulfur is used in batteries, detergents, rubber vulcanization, and in the manufacture of phosphate fertilizers.

Sulfur is a big market. In 2010, global production of sulfur was at 67.80 million tons. At present, China, the USA and Russia are the main sulfur manufacturers with 15 %, 13 % and 11 % shares (Fig. 1.20). However the prices are really volatile as sulfur is a co-product of oil and gas production and processing, supply cannot respond to weakening demand. Thus they are very dependent of the phosphates market.
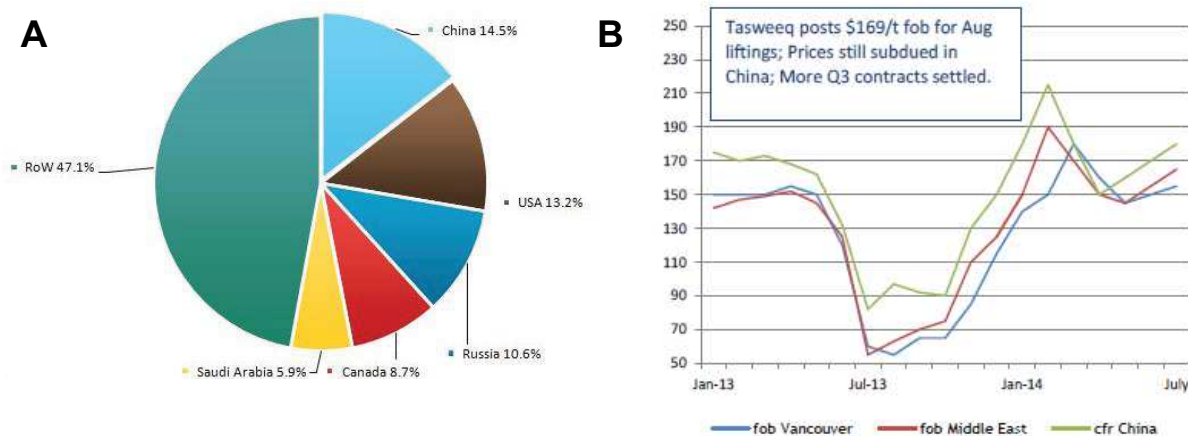
Fig. 1.20. (A) Global sulfur production in 2013; (B) Sulfur price comparison

1.7.2. Desulfurization process and Supper Claus process

The first industrial solution to get rid of hydrogen sulfide was incineration. However the combustion of H_2S leads to the formation of sulfur dioxide SO_2 which is another harmful sulfur-based compound. Therefore, units for hydrogen sulfide reduction or also called sulfur recovery have been developed. These units transform the sour gases in sulfur and water. Due to thermodynamic limitations, the process is often operated in several steps: there is first a main thermal desulfurization process then a tail gas selective oxidation unit to convert the remaining H_2S containing gas into elemental sulfur.

1.7.2.1. Desulfurization process

Concentration levels of H_2S in the effluent gaseous vary significantly depending upon their source. H_2S produced from absorption processes, such as amine treating of natural gas or refinery gas, can contain 50 – 75 % H_2S by volume or higher. Many other processes can produce H_2S with less than 0.01 % concentration, but in large quantities, which preclude the gases from being vented without further treatment.

The large variations in the H_2S concentrations and effluent flows require different methods for H_2S removal and sulfur recovery. For relatively small quantities of H_2S/sulfur, scavenger processes are often used. For sulfur quantities up to approximately 5 long tons per day (LTD) of sulfur, liquid reduction-oxidation (Redox) processes are commonly employed. Direct oxidation can sometimes be utilized for low H_2S concentrations to produce high quality liquid sulfur. Fig. 1.21 is a Sulfur Recovery Process Applicability Chart, which presents the relative ranges of technology applications.
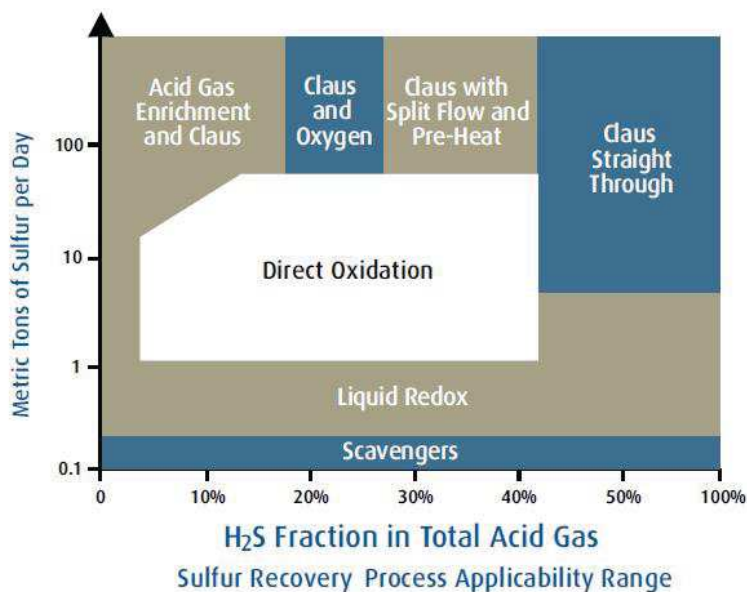
Fig. 1.21. Comparative chart of hydrogen sulfide conversion technologies [198].

At large scales, the most economical technology for converting hydrogen sulfide into sulfur is the Claus process. The Claus process was first presented by Claus in a patent in 1883 (Piéplu, Claus Catalysis and H_2S Selective Oxidation) and then was improved and developed worldwide (El-Bishtawiet Oxygen Based Claus Process for Recovery of Sulfur from H_2S Gases).

This well-established process uses partial combustion and catalytic oxidation to convert about 98 % of the H_2S containing in the effluent gas to elemental sulfur. But standards for discharges of sulfur-based compounds into the atmosphere are becoming more and depending on the size of the desulfurization unit, and the Claus process is not efficient enough to meet the thresholds of these releases due to the thermodynamic limitations. Thus a whole series of desulfurization processes for residual gas waste has been developed: Tail Gas Clean Up. In a typical application, an amine treatment unit concentrates the H_2S before it enters the Claus unit, and a tail gas treatment unit removes the remaining 2 % of the H_2S after it exits from the Claus unit, *i.e.* Super-Claus process. In the Super-Claus process the residual H_2S is directly oxidized by the catalyst in presence of air into elemental sulfur and water. As there are no thermodynamic limitations, the conversion of H_2S is complete. However, the exothermic character of the reaction leads also to the formation of SO_2 as by-product and thus, a compromise should be found in order to maximize the overall sulfur yield of the process. The detailed description of these different processes will be presented below.

Fig. 1.22 shows a schematic of the Claus process. First the H_2S is separated from the host gas stream using amine extraction, then it is fed to the Claus unit where it is converted in two steps: in the first thermal step, the H_2S is partially oxidized with air to form SO_2 (one-

third). This is done in a reaction furnace at high temperatures (1000 - 1400 °C) according to the following reaction:

$$H_2S + 3/2\ O_2 \rightarrow SO_2 + H_2O \qquad (1.5)$$

The unburned H_2S (remaining 2/3) reacts with the SO_2 formed from Eq. (1.5) to yield elemental sulfur vapor and water (Eq. (1.6)). This reaction is referred to as the Claus reaction, which is limited by the equilibrium:

$$2\ H_2S + SO_2 \leftrightarrow 3/n\ S_n + 2H_2O \qquad (1.6)$$

In this thermal conversion step, 60 - 70 % of the total H_2S was converted into elemental sulfur. This latter is condensed and the unconverted H_2S is then processed in the catalytic step.
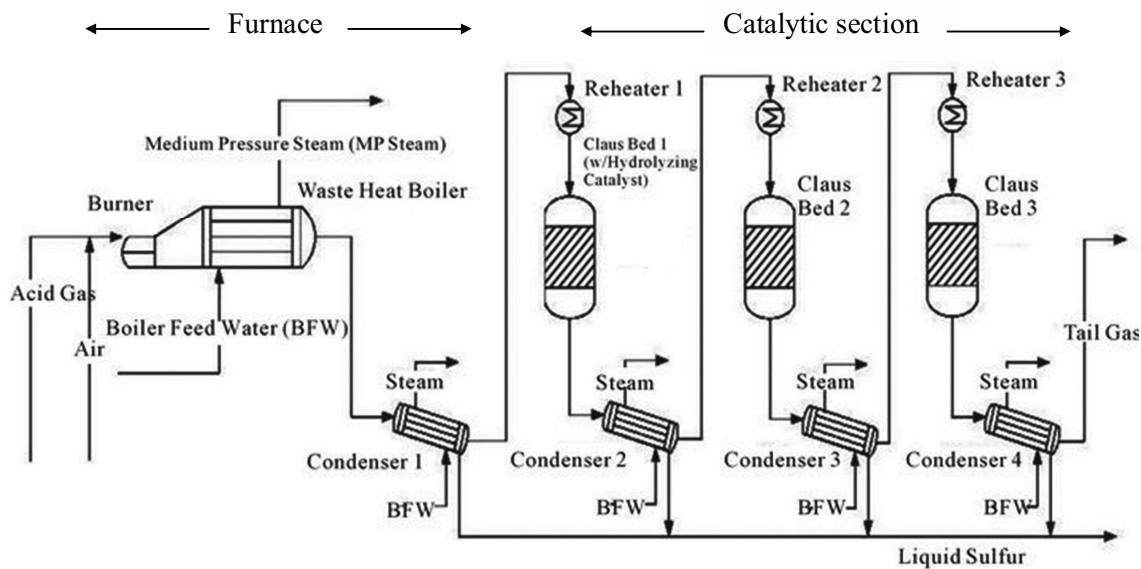
Fig. 1.22. Schematic flow diagram representation of the Claus process.

In the second step, catalytic section consisted of a series of three steps: reheating, catalytic conversion, and cooling/condensing through a series of catalytic beds. Sulfur is then produced by the Claus reaction in the presence of activated alumina as a catalyst. This catalytic section of the Claus process is favored by low temperatures, 200 – 350 °C. In general, three catalytic converters are normally considered optimum, and 96 - 97.5 % overall conversion can be achieved. A small amount of H_2S (about 3 vol.%) invariably remains in the tail gas. This residual quantity, together with other trace sulfur compounds, is usually dealt with in a tail gas unit.

1.7.2.2. Tail gas units

The most commonly used tail gas clean-up processes can be divided into three categories and were developed in comparisons as described in Fig. 1.23.
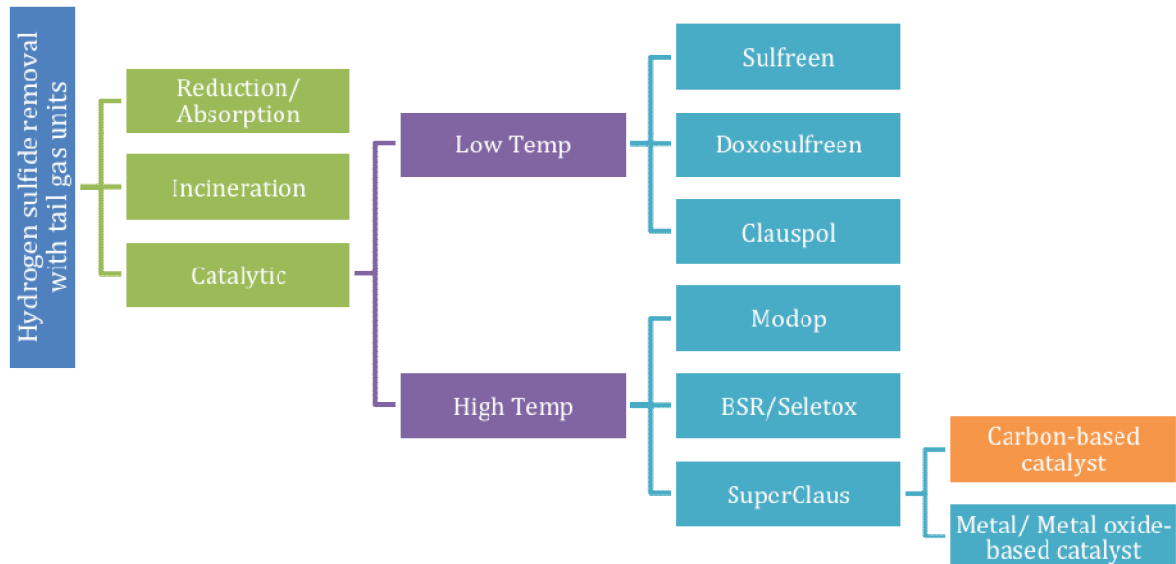
Fig. 1.23. Processes developed for hydrogen sulfide removal in tail gas.

- Tail gas hydrogenation/hydrolysis followed by either selective catalytic oxidation (*i.e.* BSR/Selectox, BSR/Hi-Activity), or selective amine coupled with acid gas recycle (*i.e.* BSR/MDEA, BSR/Flexsorb, SCOT).

- Direct oxidation of H_2S to elemental sulfur (*i.e.* SuperClaus).

- Sub-dewpoint Claus (*i.e.* MCRC, CBA, Sulfreen, OxoSulfreen, Clauspol).

It is not a simple task to rank the tail gas processes in terms of recovery or in terms of costs. Some units alter the recovery in Claus or integrate the tail gas unit with Claus, making it impossible to evaluate all processes on a common basis. Operating companies will need to perform studies to determine which TGCU (Tail-Gas Claus Unit) best meet their recovery requirements.

Currently most sulfur recovery applications require either an overall recovery of about 99.0 % or of 99.8 % based on environmental regulations. For 99.0 % recovery, the processes of choice are the subdewpoint processes (CBA, MCRC™, and Sulfreen™) and Superclaus™. For 99.8 % recoveries, SCOT or its equivalent is universally used.

The post-Claus treatment units are divided in three categories (Table 1.4). The first, which is currently the most commonly used (because of its effectiveness and its control at

industrial scale), is based on the neutralization/absorption; the second one is based on catalytic processes and the last one is based on the outlet gas treatment after incineration.

Table 1.4. Comparative table of post-Claus processes.

Process		Catalyst	Yield (%)
Adsorption Reduction	SCOT		99.8
	LS-SCOT	Co-Mo et MDEA	99.95
	Super-SCOT		
Catalytic	Sulfreen (T < 180)	Ni-FE/Al$_2$O$_3$	98 - 99.5
	Doxosulfreen(T < 180)	TiO$_2$ or Cu-Al$_2$O$_3$	99.9
	Clauspol-300 (T < 180)		99.8 - 99.9
	SuperClaus (T > 180)	Fe-Cr/α-Al$_2$O$_3$ also on SiO$_2$ and on SiC	99.0 - 99.5
Gas treatment after incineration	Cominco	Ammonium sulfite	99.0
	Elsorb	Ammonium phosphate	99.9
	Wellman-Lord	Na$_2$SO$_3$	99.8

Super-Claus is one of the most developed tail gas process up to date and represents an example of selective oxidation process for final sulfur removal. The process involves a slightly modified two stage Claus units followed by a third stage catalytic reactor to oxidize the remaining H$_2$S (resulted from the thermodynamic equilibrium) to elemental sulfur. Reactor 1 to 2 uses the standard Claus catalyst whereas the third reactor contains the selective oxidation catalyst. The Claus unit itself is operated under thermodynamic limitations so that the gas that exits the second reactor contains between 0.8 to 3 vol.% H$_2$S. In the last reactor sufficient air is added to this exit gas to keep the oxygen level in the 0.5 to 2 vol.% range depending to the H$_2$S inlet concentration. It is also worthy to note that steam generated during the Claus reactors was not removed and thus, a relatively high amount of steam is present in the tail-gas to be treated in the last reactor.

The Super-Claus unit is one of the most installed unit in the tail-gas treatment, and represents the most attractive option, because it is available as an upgrade retrofit to a third bed of an existing Claus unit, while other tails units need the construction of an entirely new reactor. The Super-Claus is a combined process that represents a convenient solution for existing sulfur recovery units to increase the overall sulfur recovery to at least 99.5 % without

any further tail gas clean up. The SUPER-CLAUS® process achieves high sulfur recovery levels by suppressing SO_2 formation in the Claus stages, and selectively oxidizing H_2S in the presence of oxygen over a proprietary catalyst. The mixture then goes to the third reactor where the following catalytic reaction occurs:

$$2\ H_2S + O_2 \rightarrow 2\ S + 2\ H_2O \tag{1.7}$$

$2H_2S + SO_2 \rightarrow\ 3S + 2H_2O$ $2H_2S + SO_2 \rightarrow\ 3S + 2H_2O$ $H_2S + \frac{1}{2}\ O_2 \rightarrow S + H_2O$

$3H_2 + SO_2 \rightarrow H_2S + 2H_2O$

$2H_2 + SO_2 \rightarrow S + 2H_2O$
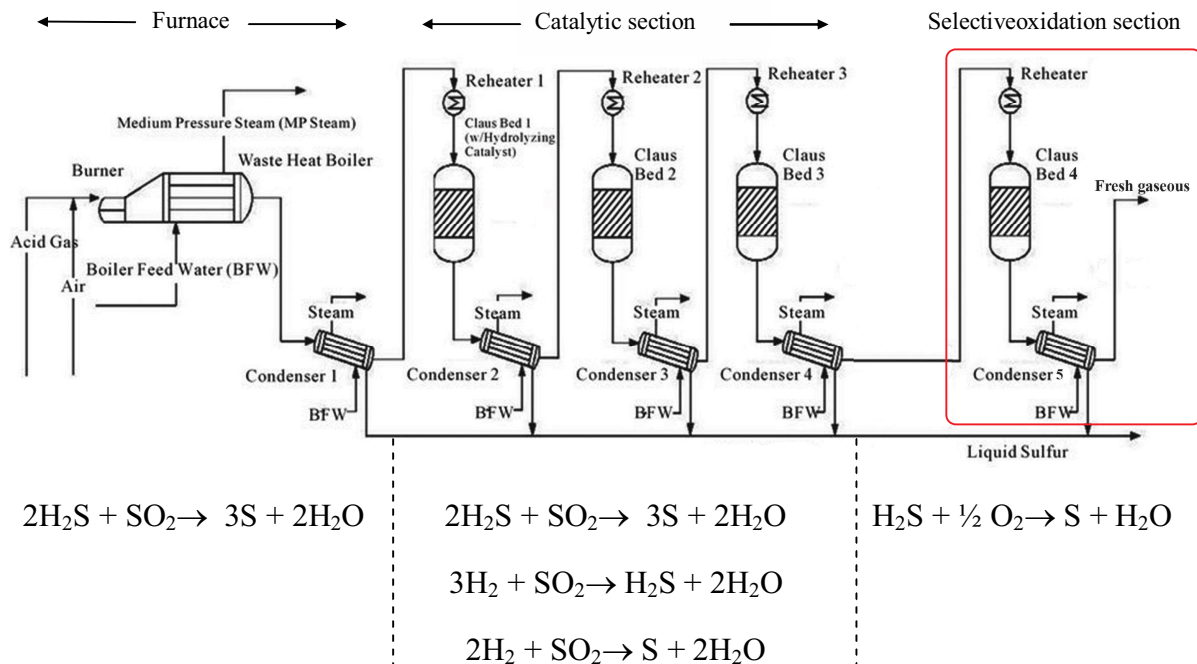
Fig. 1.24. Connecting Supper-Claus process with Claus plans process for the ultimate sulfur recovery.

1.7.2.3. Catalysts for direct oxidation process and Super-Claus process

Tail gas catalysts have rapidly evolved in order to cope with an ever strict legislation for environment. The first generation catalysts were based on hydrotreating catalysts; the second generation catalysts were specifically developed as systems featured by high activity, high porosity and long-catalytic life; the third generation catalysts are nowadays represented by those systems capable to operate under moderate reaction conditions (low temperature operating catalysts). Modern units make use of catalysts capable to operate with low temperatures without a burner for their pre-heating. Additional properties to be considered are their higher mechanical strength, the bulk density, the pressure drop and the catalyst resistance to aging.

The transition metal oxide-based catalysts such as MgO, Al_2O_3, TiO_2, Bi_2O_3, Sb_6O_{13}, V_2O_5, Cr_2O_3, Mn_2O_3, Fe_2O_3, CoO, CuO…are the most employed in the continuous process of selective oxidation of H_2S. A series of H_2S-selective oxidation activities by oxygen ($H_2S/O_2 =$

0.5) can be represented as $V_2O_5 > Mn_2O_3 > CoO > TiO_2 > Fe_2O_3 > Bi_2O_3 > Sb_6O_{13} > CuO > Al_2O_3 = MgO = Cr_2O_3$. Among them, V_2O_5, MgO, and Mn_2O_3 are considered to be the most selective catalysts. Notably, iron- and vanadium-based catalysts have induced a larger amount of research effort in past decades compared with other metal oxide-based catalysts. Davidov et al. [199] reported that desulfurization performance over V_2O_5 catalyst is 16 times more active than TiO_2 and 73 times more active than Al_2O_3 used as the main components of the Claus process at the same reaction conditions. Iron oxide has relatively high activity for H_2S oxidation [200,201], but its sulfur selectivity is quite low because of the excess oxygen requirement. However, the selectivity and catalytic performance were significantly increased with a presence of other metal into the iron oxide structure, especially cerium. In particular, a 2Fe-2Ce catalyst exhibits extremely high catalytic activity and sulfur selectivity at 250 °C. H_2S conversion and sulfur selectivity are as high as 99 % under conditions of GHSV = 21.000 h^{-1}, 1 vol.% H_2S, and O_2/H_2S = 0.5 [202]. The high catalytic and sulfur selectivity were mainly attributed to the improved redox ability of cerium and the oxygen offered by the cerium lattice, and iron species are existed mainly in the form of Fe^{3+} clusters and $\alpha\text{-}Fe_2O_3$ crystallites. It is worthy to note that the formation of FeS_2 in the presence of sulfur-based compounds is responsible for the catalyst deactivation.

Recently, one of the most widely used and effective catalyst for the H_2S selective oxidation process is made of metal-oxide nanoparticles (typically Fe_2O_3 NPs) supported on different carriers such as alumina, silica and silicon carbide. According to the report of Terorde et al. Fe_2O_3/SiO_2 catalysts [203] exhibit excellent activity performance with 97 % sulfur selectivity and 94 % sulfur yield at 240 °C under the following reaction conditions: 1 vol.% H_2S, 5 vol.% O_2, 30 vol.% H_2O, and balance He. The high catalytic activity can be assigned to the fact that SiO_2 can significantly stabilize the formed iron (II) sulfate species. On the other hand, various metal oxides such as TiO_2, VO_x loading on SiO_2 were employed. These catalysts also displayed a high desulfurization performance with > 92 % of H_2S conversion and > 90 % of sulfur selectivity depending on the reaction temperature. However, for all these catalysts the sulfur selectivity decreased sharply with the further rise of reaction temperature, which probably due to the reaction between the oxygen and sulfur radical on the SiO_2 support surface. Previous works from our laboratory have shown that the Fe_2O_3/SiC catalyst also exhibits a high activity and selective performance for the above mentioned reaction [204,205,182].

However, all the catalysts cited above suffer from several drawbacks as listed below:

- Sensitivity and selectivity lost as a function of time stream, especially in the presence of impurities [206]. In addition, deactivation also occurs due to the active phase sintering as a function of time on stream.

- Low desulfurization activity when the reaction is operated at high space velocity (WHSV $\geq$ 0.3 h^{-1}) due to the low diffusion of the reactant towards the active sites localized

depth inside the support porosity, which significantly lowers the efficiency of sulfur formation per unit of time versus catalyst weight.

- Difficulty to recycle: The recycling of the iron-containing catalyst is not frequent due to the low intrinsic value of the metal active phase and thus, most of the time the spent catalyst is directly moved to a waste disposal area.

- Addition of expensive and/or toxic metals addictives to enhance its catalytic performance: Vanadium, Chrome…

- By-products synthesis: production of NO_x during the synthesis of Fe - Cr catalysts consecutive to the decomposition of the nitrate precursors.

Other types of catalyst derived from iron can be found, generally doped with a second metal in order to enhance their stability. For example Fe - Cr oxide is a catalyst developed by Lurgi/Air Liquide (FeCr - oxide/Al_2O_3) generally has a H_2S conversion > 85 % and is insensitive to excess air and steam [207]. Zinc oxide and alkaline solids can also remove hydrogen sulfide from gas streams by direct oxidization. For tail gas process, the catalyst used by Comprimo's Super-Claus process is alumina-supported iron oxide/chromium oxide, the catalyst used by Mobil's direct-oxidation process is a TiO_2-based catalyst and for BSR the oxidation of hydrogen sulfide is made by a mixed catalyst based on vanadium and bismuth.

The different operation conditions in terms of the H_2S concentration and contact time on the different catalysts, either supported metal oxide or metal-free catalysts, is presented in Table 1.5. The actived carbon, carbon nanomaterials such as CNTs, CNFs, N-CNTs have received increasing interest for being extensively used as catalyst support or as metal-free catalysts. Particularly for carbon nanomaterials, the completely lack of microporosity in conjunction with the various structures (internal or external diameter and number of graphene layers) and rich surface chemistry (heterogeneous atoms or surface defects) make them a promising material compared with microporous activated carbon, in which the large number of micropores increases diffusion problem. Notably, the tubular morphology of carbon nanotubes can cause peculiar reactivity of the gaseous or liquid reactants when these later passing through the tubules.

Many studies of desulfurization have focused on these metal-modified CNTs or CNFs for the desulfurization at low temperature. According to the literature, Ledoux et al. [17,208,209] have been reported a series of results on the NiS_2 supported on CNTs for the selective desulfurization process. The catalyst displayed a high sulfur storage capacity of up to 1.8 $g_{H2S}.g^{-1}_{catalyst}$ at 60 °C by using the discontinuous desulfurization process and without any deactivation after a 70 h of tests. Chen et al. [210] using Na_2CO_3 supported on SWCNTs at 30 °C were also obtained the same result.

Table 1.5. Comparative table of hydrogen removal catalyst performances.

Catalyst	[H$_2$S] (vol.%)	Temperature (°C)	Yield (%)	Refs
Nb/TiO$_2$	0.5 - 10	170 - 240	80 - 95	GTC Technology
Fe/SiC	0.5 - 1.5	180 - 260	91 - 94	Lurgi
Fe/SiC	2	180 - 260	91 - 94	Elf / Total
N@C/SiC	1	210 - 230	81	DECOrATE
N@C/SiC	2	210 - 230	72	DECOrATE
Other experiments				
Fe$_2$O$_3$/Al$_2$O$_3$	1	260 - 300	86 max	
Fe$_2$O$_3$/SiC	1	230 - 270	94 - 91	
FeCr/SiO$_2$	1	260	92	2nd generation catalyst

The first report deals with the use of N-CNTs as metal-free catalyst in the desulfurization process has been reported by Chizari et al. [139]. In this study, macroscopic N-CNTs and N-CNTs supported on SiC foams were developed and first used for selective oxidation of H$_2$S at high reaction temperature (> 180 °C) with high Weight Hourly Space Velocity (WHSV = 0.09 – 1.2 h^{-1}) by using continuous Supper-Claus process [139]. According to the results, the N-CNTs and N-CNT/SiC foams exhibit excellent stability: both H$_2$S conversion and sulfur selectivity are remaining unchanged after 120 h of test. These results also indicated that macroscopic N-CNTs or N-CNTs/SiC foam absolutely overcame obstacles compared to the metal oxides based catalysts such as: the rapidly deactivation, the problems linked with transport and pressure drop in a fixed bed reactor configuration. However, desulfurization performance depends on the nitrogen containing in the CNTs matrix and details investigation is still needed for the well assessment of such metal-free catalysts in the desulfurization process.

1.7.2.4. Mechanism of selective oxidation reaction of H$_2$S into sulfur on N-CNTs catalyst

Two common types of catalytic mechanisms on carbon nanomaterials have been proposed by Mars-van Krevelen and Langmuir-Hinshelwood [211]. The different between these two mechanisms is in the initiation step. Ghosh and Tollefson [212] claim that H$_2$S is physisorbed on the catalyst surface, whereas Steijns et al. [213] insist that H$_2$S adsorption is

dissociative. However, many researchers agree with the Yan's groups proposal [214]. They confirmed that physisorbed H_2S further dissociates to HS^- and that water plays a key role in the reaction which generally includes physical adsorption, chemical adsorption, and oxidation steps. Therefore, the catalytic mechanism for carbon nanomaterials can be revised by three steps as the following [214–216]:

- ***Physical adsorption step:*** H_2S is first adsorbed on the carbon surface, then H_2S is dissolved in a water film and dissociates in an adsorbed state in the water film, while the carbon atoms located next to the nitrogen atoms in the structure of carbon nanomaterials are active sites for adsorption and activation of oxygen.

$$H_2S_{\,gas} \rightarrow H_2S_{\,ads}$$

$$H_2S_{\,ads} + H_2O \rightarrow HS^-_{\,ads} + H_3O^+$$

$$O_{2\,gas} \rightarrow O_{2\,ads}$$

$$C^* + O_{2\,ads} \rightarrow 2\,C(O^*)_{\,ads}$$
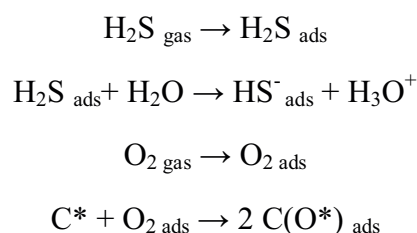
- ***Oxidation and termination steps:*** The adsorbed H_2S reacts with oxygen to produce elemental sulfur or sulfur dioxide, and SO_2 is further oxidized to H_2SO_4 in the presence of water.

$$HS^-_{\,ads} + C(O^*)_{\,ads} \rightarrow C(S^*)_{\,ads} + OH^-$$

$$C(S^*)_{\,ads} + C(O^*)_{\,ads} + H_2S \rightarrow C(SS^*)_{\,ads} + H_2O$$

$$nC(SS^*)_{\,ads} \rightarrow nC + nS_{\,ads}$$

$$SO_{2\,ads} + O_{2\,ads} + H_2O \rightarrow H_2SO_{4\,ads}$$

$$H^+ + OH^- \rightarrow H_2O$$
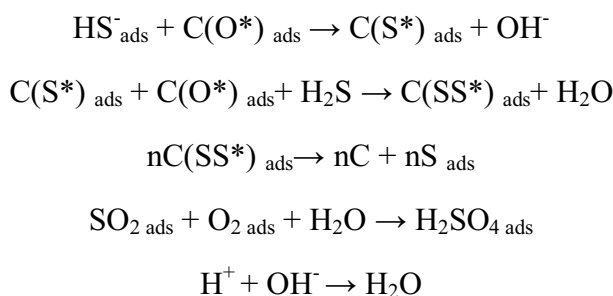
1.8. Scope and outline of this thesis

Although carbon nanomaterials, either undoped or doped with foreign elements, has been attracted many researchers since their discovery it is expected that a large field of application of these materials remains unexplored. Recently, several reports have been published dealing with the advantages of using nitrogen-doped carbon nanomaterials directly as free-metal catalyst in several relevant catalytic processes compared to the traditional catalyt such as metal and/or metal oxide. However, there are scarce reports that systematically investigate the relation between the synthesis parameters, the physical-chemical properties, the macroscopic shaping and the catalytic performance of these metal-free catalysts. The lack of these studies renders the optimization process difficult. The aim of this thesis is to investigate the influence of the physical and chemical properties of the macroscopically shaped N-CNTs, which were synthesized and functionalized by using both *in-situ* and *ex-situ* method, on their catalytic performance in the partial oxidation of trace amount of H_2S into

elemental sulfur. In this study, we have also investigated the influence of the oxygenated functional groups present on the CNTs surface on the desulfurization performance.

The thesis will start with an introduction section recalling the different synthesis routes for N-CNTs and an in-depth discussion of the advantages and drawbacks of these methods. The chapter will also cover the literature survey of the recent developments of the N-CNTs in the field of heterogeneous catalysis, both as catalyst support and as direct metal-free catalyst, and the comparison of the metal-free catalytic performance and that of the traditional supported metal and oxides catalysts. The aim of this first chapter is to provide to the readers a clear view on the potential field of applications of this new family of metal-free catalyst which is expected to face a relentless development in a near future.

Chapter 2 reports on the synthesis of the N-CNTs decorating on different macroscopic silicon carbide (SiC) supports (N-CNT/SiC) for subsequence use as metal-free catalyst in the selective oxidation of H_2S into elemental sulfur. The influence of the synthesis parameters on the final physical and chemical properties of the N-CNTs/SiC composites will be discussed and bench-marked with those reported in the literature. The advantages of using the N-CNTs in a macroscopic shape versus the un-supported ones will be discussed in detail in light of the catalytic performance.

Chapter 3 will focus on a new, facile and simple approach (*ex-situ* method) for the synthesis of a highly nitrogen-doped mesoporous carbon on different macroscopic shapes using food raw materials, *i.e.* ammonium carbonate, glucose and citric acid, as nitrogen and carbon precursors. Such method allows one to avoid the use of traditional CVD methods with significant drawbacks: *(i)* the employ of nitrogen precursors with relatively high toxicity [*i.e.* dicyandiamide, melamine, polypyrrole, ammonia]; *(ii)* tricky reaction environments based on hydrocarbons and/or hydrogen atmosphere (which necessitate specific safety precautions); *(iii)* high operative temperatures. In addition, significant loss of the N- and C-containing precursors, including their partial thermal decomposition into waste and toxic by-products, denote protocols featured by low atom efficiencies, weighty environmental impacts and high production costs. This contribution describes a methodology developed starting from non-toxic, raw and abundant organic building blocks that generate highly N-doped CNMs while facing the major limitations and drawbacks of the existing synthetic procedures. A shape-adaptable, highly N-doped mesoporous carbon phase is properly grown as a "catalytic clothing" at the surface of macroscopically shaped supports. The simple supports "dressing" with a catalytically active and metal-free phase represents a real breakthrough for the creation of a series of tailored sustainable heterogeneous catalysts. The as-synthesized highly nitrogen-doped mesoporous carbon will be evaluated in the partial oxidation of H_2S into elemental sulfur. The relationship between the physical properties and the catalytic performance of this catalyst will be discussed in detail in this chapter.

Chapter 4 is devoted to the oxygen functionalization of carbon nanotube using gas-phase HNO_3 pre-treatment. The generation of defects and the formation the different oxygen species on the surface of the CNTs were controlled by adjusting the treatment duration and temperature. It is worthy to note that this study is the first to date which explores the used of CNTs decorated with oxygenated functional groups as metal-free catalyst. The influence of defects and the presence of oxygen species on the surface of CNTs and their role in the partial oxidation of H_2S into sulfur will be discussed in light of the characterization results.

Finally, **Chapter 5** presents the general conclusions of the work based on the different results obtained along with the different perspectives for future developments of this new class of catalyst.

References

[1] M. Monthioux, V.L. Kuznetsov, Carbon 44 (2006) 1621.

[2] H.W. Kroto, A.W. Allaf, S.P. Balm, Chem. Rev. 91 (1991) 1213.

[3] S. Iijima, Nature 354 (1991) 56.

[4] J. Gavillet, A. Loiseau, F. Ducastelle, S. Thair, P. Bernier, O. Stéphan, J. Thibault, J.-C. Charlier, Carbon 40 (2002) 1649.

[5] R. Andrews, D. Jacques, D. Qian, T. Rantell, Acc. Chem. Res. 35 (2002) 1008.

[6] H. Dai, Acc. Chem. Res. 35 (2002) 1035.

[7] J.E. Fischer, Acc. Chem. Res. 35 (2002) 1079.

[8] S. Niyogi, M.A. Hamon, H. Hu, B. Zhao, P. Bhowmik, R. Sen, M.E. Itkis, R.C. Haddon, Acc. Chem. Res. 35 (2002) 1105.

[9] S. Toma, Nitrogen-Doped Single-Walled Carbon Nanotube Thin Films, Aalto University, 2011.

[10] D.S. Su, S. Perathoner, G. Centi, Chem. Rev. 113 (2013) 5782.

[11] K.P. De Jong, J.W. Geus, Catal. Rev. 42 (2000) 481.

[12] P. Serp, M. Corrias, P. Kalck, Appl. Catal. Gen. 253 (2003) 337.

[13] N. Daems, X. Sheng, I.F.J. Vankelecom, P.P. Pescarmona, J. Mater. Chem. A 2 (2014) 4085.

[14] Y. Xia, R. Mokaya, Chem. Mater. 17 (2005) 1553.

[15] X. Wang, J.S. Lee, Q. Zhu, J. Liu, Y. Wang, S. Dai, Chem. Mater. 22 (2010) 2178.

[16] Y. Liu, H. Ba, D.-L. Nguyen, O. Ersen, T. Romero, S. Zafeiratos, D. Begin, I. Janowska, C. Pham-Huu, J. Mater. Chem. A 1 (2013) 9508.

[17] M.J. Ledoux, R. Vieira, C. Pham-Huu, N. Keller, J. Catal. 216 (2003) 333.

[18] M.-J. Ledoux, C. Pham-Huu, Catal. Today 102–103 (2005) 2.

[19] C. Pham-Huu, M.-J. Ledoux, Top. Catal. 40 (2006) 49.

[20] Y. Liu, T. Dintzer, O. Ersen, C. Pham-Huu, J. Energy Chem. 22 (2013) 279.

[21] L. Truong-Phuoc, T. Truong-Huu, L. Nguyen-Dinh, W. Baaziz, T. Romero, D. Edouard, D. Begin, I. Janowska, C. Pham-Huu, Appl. Catal. Gen. 469 (2014) 81.

[22] R. Droppa Jr., P. Hammer, A.C.M. Carvalho, M.C. dos Santos, F. Alvarez, J. Non-Cryst. Solids 299–302, Part 2 (2002) 874.

[23] S.E. Rodil, W.I. Milne, J. Robertson, L.M. Brown, Appl. Phys. Lett. 77 (2000) 1458.

[24] J. Hu, P. Yang, C.M. Lieber, Phys. Rev. B 57 (1998) R3185.

[25] F. Le Normand, J. Hommet, T. Szörényi, C. Fuchs, E. Fogarassy, Phys. Rev. B 64 (2001) 235416.

[26] K. Suenaga, M. Yudasaka, C. Colliex, S. Iijima, Chem. Phys. Lett. 316 (2000) 365.

[27] O. Stephan, P.M. Ajayan, C. Colliex, P. Redlich, J.M. Lambert, P. Bernier, P. Lefin, Science 266 (1994) 1683.

[28] R.E. Smalley, in:, D.S. Yoshimura, P.R.P.H. Chang (Eds.), Supercarbon, Springer Berlin Heidelberg, 1998, pp. 31–40.

[29] M. Yudasaka, R. Kikuchi, Y. Ohki, S. Yoshimura, Carbon 35 (1997) 195.

[30] R. Sen, B.C. Satishkumar, A. Govindaraj, K.R. Harikumar, M.K. Renganathan, C.N.R. Rao, J. Mater. Chem. 7 (1997) 2335.

[31] M. Terrones, H. Terrones, N. Grobert, W.K. Hsu, Y.Q. Zhu, J.P. Hare, H.W. Kroto, D.R.M. Walton, P. Kohler-Redlich, M. Rühle, J.P. Zhang, A.K. Cheetham, Appl. Phys. Lett. 75 (1999) 3932.

[32] M. José-Yacamán, M. Miki-Yoshida, L. Rendón, J.G. Santiesteban, Appl. Phys. Lett. 62 (1993) 657.

[33] J.-P. Tessonnier, D.S. Su, ChemSusChem 4 (2011) 824.

[34] M. Reyes-Reyes, N. Grobert, R. Kamalakaran, T. Seeger, D. Golberg, M. Rühle, Y. Bando, H. Terrones, M. Terrones, Chem. Phys. Lett. 396 (2004) 167.

[35] I. Florea, O. Ersen, R. Arenal, D. Ihiawakrim, C. Messaoudi, K. Chizari, I. Janowska, C. Pham-Huu, J. Am. Chem. Soc. 134 (2012) 9672.

[36] K. Chizari, I. Janowska, M. Houllé, I. Florea, O. Ersen, T. Romero, P. Bernhardt, M.J. Ledoux, C. Pham-Huu, Appl. Catal. Gen. 380 (2010) 72.

[37] J. Kong, A.M. Cassell, H. Dai, Chem. Phys. Lett. 292 (1998) 567.

[38] B.C. Satishkumar, A. Govindaraj, C.N.R. Rao, Chem. Phys. Lett. 307 (1999) 158.

[39] A. Deneuve, I. Florea, O. Ersen, P. Nguyen, C. Pham, D. Bégin, D. Edouard, M.-J. Ledoux, C. Pham-Huu, Appl. Catal. Gen. 385 (2010) 52.

[40] K. Chizari, A. Vena, L. Laurentius, U. Sundararaj, Carbon 68 (2014) 369.

[41] W.. Li, S.. Xie, L.. Qian, B.. Chang, B.. Zou, W.. Zhou, R.. Zhao, G. Wang, Science 274 (1996) 1701.

[42] P. Nikolaev, M.J. Bronikowski, R.K. Bradley, F. Rohmund, D.T. Colbert, K.A. Smith, R.E. Smalley, Chem. Phys. Lett. 313 (1999) 91.

[43] E.-G. Wang, Adv. Mater. 11 (1999) 1129.

[44] C.J. Lee, S.C. Lyu, H.-W. Kim, J.H. Lee, K.I. Cho, Chem. Phys. Lett. 359 (2002) 115.

[45] R. Sen, A. Govindaraj, C.N.R. Rao, Chem. Phys. Lett. 267 (1997) 276.

[46] B.Q. Wei, R. Vajtai, Y. Jung, J. Ward, R. Zhang, G. Ramanath, P.M. Ajayan, Nature 416 (2002) 495.

[47] Y. Murakami, Y. Miyauchi, S. Chiashi, S. Maruyama, Chem. Phys. Lett. 377 (2003) 49.

[48] M. Glerup, M. Castignolles, M. Holzinger, G. Hug, A. Loiseau, P. Bernier, Chem. Commun. (2003) 2542.

[49] S. Trasobares, O. Stéphan, C. Colliex, W.K. Hsu, H.W. Kroto, D.R.M. Walton, J. Chem. Phys. 116 (2002) 8966.

[50] M. Terrones, P. Redlich, N. Grobert, S. Trasobares, W.-K. Hsu, H. Terrones, Y.-Q. Zhu, J.P. Hare, C.L. Reeves, A.K. Cheetham, M. Rühle, H.W. Kroto, D.R.M. Walton, Adv. Mater. 11 (1999) 655.

[51]   C. Tang, Y. Bando, D. Golberg, F. Xu, Carbon 42 (2004) 2625.

[52]   M. Terrones, N. Grobert, J. Olivares, J.P. Zhang, H. Terrones, K. Kordatos, W.K. Hsu, J.P. Hare, P.D. Townsend, K. Prassides, A.K. Cheetham, H.W. Kroto, D.R.M. Walton, Nature 388 (1997) 52.

[53]   X. Wang, W. Hu, Y. Liu, C. Long, Y. Xu, S. Zhou, D. Zhu, L. Dai, Carbon 39 (2001) 1533.

[54]   M. Terrones, R. Kamalakaran, T. Seeger, M. Rühle, Chem. Commun. (2000) 2335.

[55]   J. Amadou, K. Chizari, M. Houllé, I. Janowska, O. Ersen, D. Bégin, C. Pham-Huu, Catal. Today 138 (2008) 62.

[56]   Y.T. Lee, N.S. Kim, S.Y. Bae, J. Park, S.-C. Yu, H. Ryu, H.J. Lee, J. Phys. Chem. B 107 (2003) 12958.

[57]   Y. Liu, W. Wongwiriyapan, K.C. Park, H. Muramatsu, K. Takeuchi, Y.A. Kim, M. Endo, Carbon 47 (2009) 2543.

[58]   F. Léonard, J. Tersoff, Phys. Rev. Lett. 84 (2000) 4693.

[59]   S.L.T. Jones, G. Greene-Diniz, M. Haverty, S. Shankar, J.C. Greer, Chem. Phys. Lett. 615 (2014) 11.

[60]   J. Liu, S. Webster, D.L. Carroll, J. Phys. Chem. B 109 (2005) 15769.

[61]   S. Maldonado, S. Morin, K.J. Stevenson, Carbon 44 (2006) 1429.

[62]   R. Sen, B.C. Satishkumar, A. Govindaraj, K.R. Harikumar, G. Raina, J.-P. Zhang, A.K. Cheetham, C.N.R. Rao, Chem. Phys. Lett. 287 (1998) 671.

[63]   L. Roldán, S. Armenise, Y. Marco, E. García-Bordejé, Phys. Chem. Chem. Phys. 14 (2012) 3568.

[64]   L. Qu, Y. Liu, J.-B. Baek, L. Dai, ACS Nano 4 (2010) 1321.

[65]   L. Feng, Y. Yan, Y. Chen, L. Wang, Energy Environ. Sci. 4 (2011) 1892.

[66]   Y. Ma, L. Sun, W. Huang, L. Zhang, J. Zhao, Q. Fan, W. Huang, J. Phys. Chem. C 115 (2011) 24592.

[67]   T.C. Nagaiah, S. Kundu, M. Bron, M. Muhler, W. Schuhmann, Electrochem. Commun. 12 (2010) 338.

[68]   C. Combadière, W. Raoul, X. Guillonneau, F. Sennlaub, Exp. Eye Res. 111 (2013) 134.

[69]   E.J. Biddinger, D. von Deak, U.S. Ozkan, Top. Catal. 52 (2009) 1566.

[70]   C.P. Ewels, M. Glerup, J. Nanosci. Nanotechnol. 5 (2005) 1345.

[71]   N. Hellgren, M.P. Johansson, E. Broitman, L. Hultman, J.-E. Sundgren, Phys. Rev. B 59 (1999) 5162.

[72]   M. Menon, E. Richter, A. Mavrandonakis, G. Froudakis, A.N. Andriotis, Phys. Rev. B 69 (2004) 115322.

[73]   S.Y. Kim, J. Lee, C.W. Na, J. Park, K. Seo, B. Kim, Chem. Phys. Lett. 413 (2005) 300.

[74]   T. Schiros, D. Nordlund, L. Pálová, D. Prezzi, L. Zhao, K.S. Kim, U. Wurstbauer, C. Gutiérrez, D. Delongchamp, C. Jaye, D. Fischer, H. Ogasawara, L.G.M. Pettersson, D.R. Reichman, P. Kim, M.S. Hybertsen, A.N. Pasupathy, Nano Lett. 12 (2012) 4025.

[75]   L.S. Panchakarla, K.S. Subrahmanyam, S.K. Saha, A. Govindaraj, H.R. Krishnamurthy, U.V. Waghmare, C.N.R. Rao, Adv. Mater. 21 (2009) 4726.

[76]   J.C. Carrero-Sánchez, A.L. Elías, R. Mancilla, G. Arrellín, H. Terrones, J.P. Laclette, M. Terrones, Nano Lett. 6 (2006) 1609.

[77]   J. Robertson, C.A. Davis, Diam. Relat. Mater. 4 (1995) 441.

[78]   R. Czerw, M. Terrones, J.-C. Charlier, X. Blase, B. Foley, R. Kamalakaran, N. Grobert, H. Terrones, D. Tekleab, P.M. Ajayan, W. Blau, M. Rühle, D.L. Carroll, Nano Lett. 1 (2001) 457.

[79]   E. Cruz-Silva, F. López-Urías, E. Muñoz-Sandoval, B.G. Sumpter, H. Terrones, J.-C. Charlier, V. Meunier, M. Terrones, ACS Nano 3 (2009) 1913.

[80]   H.J. Choi, J. Ihm, S.G. Louie, M.L. Cohen, Phys. Rev. Lett. 84 (2000) 2917.

[81]   A.H. Nevidomskyy, G. Csányi, M.C. Payne, Phys. Rev. Lett. 91 (2003) 105502.

[82]   B. Zheng, P. Hermet, L. Henrard, ACS Nano 4 (2010) 4165.

[83]   D. Golberg, Y. Bando, W. Han, K. Kurashima, T. Sato, Chem. Phys. Lett. 308 (1999) 337.

[84]   D. Golberg, Y. Bando, L. Bourgeois, K. Kurashima, T. Sato, Carbon 38 (2000) 2017.

[85]   F. Xu, M. Minniti, C. Giallombardo, A. Cupolillo, P. Barone, A. Oliva, L. Papagno, Surf. Sci. 601 (2007) 2819.

[86]   U. Bangert, A. Bleloch, M.H. Gass, A. Seepujak, J. van den Berg, Phys. Rev. B 81 (2010) 245423.

[87]   H. Ago, T. Kugler, F. Cacialli, K. Petritsch, R.H. Friend, W.R. Salaneck, Y. Ono, T. Yamabe, K. Tanaka, Synth. Met. 103 (1999) 2494.

[88]   Y. Ganesan, C. Peng, Y. Lu, L. Ci, A. Srivastava, P.M. Ajayan, J. Lou, ACS Nano 4 (2010) 7637.

[89]   A.A. Koós, M. Dowling, K. Jurkschat, A. Crossley, N. Grobert, Carbon 47 (2009) 30.

[90]   A.N. Kaliva, J.W. Smith, Can. J. Chem. Eng. 61 (1983) 208.

[91]   V. Meeyoo, D.L. Trimm, N.W. Cant, J. Chem. Technol. Biotechnol. 68 (1997) 411.

[92]   A. Primavera, A. Trovarelli, P. Andreussi, G. Dolcetti, Appl. Catal. Gen. 173 (1998) 185.

[93]   F. Adib, A. Bagreev, T.J. Bandosz, Langmuir 16 (2000) 1980.

[94]   S. Bashkova, F.S. Baker, X. Wu, T.R. Armstrong, V. Schwartz, Carbon 45 (2007) 1354.

[95]   Q.-H. Yang, P.-X. Hou, S. Bai, M.-Z. Wang, H.-M. Cheng, Chem. Phys. Lett. 345 (2001) 18.

[96]   S. Inoue, N. Ichikuni, T. Suzuki, T. Uematsu, K. Kaneko, J. Phys. Chem. B 102 (1998) 4689.

[97]   M. Eswaramoorthy, R. Sen, C.N.R. Rao, Chem. Phys. Lett. 304 (1999) 207.

[98]   S. Peng, K. Cho, Nano Lett. 3 (2003) 513.

[99]   S. van Dommele, K.P. de Jong, J.H. Bitter, Chem. Commun. Camb. Engl. (2006) 4859.

[100]   Y. Shang, J. Zhao, H. Wu, Q. Cai, X. Wang, X. Wang, Theor. Chem. Acc. 127 (2010) 727.

[101]   C.H. Choi, S.H. Park, S.I. Woo, ACS Nano 6 (2012) 7084.

[102] H. Kim, K. Lee, S.I. Woo, Y. Jung, Phys. Chem. Chem. Phys. 13 (2011) 17505.

[103] X. Ning, H. Yu, F. Peng, H. Wang, J. Catal. 325 (2015) 136.

[104] A.-C. Johansson, J.V. Larsen, M.A. Verheijen, K.B. Haugshøj, H. F. Clausen, W.M.M. Kessels, L. H. Christensen, E.V. Thomsen, J. Catal. 311 (2014) 481.

[105] B. Xiong, Y. Zhou, Y. Zhao, J. Wang, X. Chen, R. O'Hayre, Z. Shao, Carbon 52 (2013) 181.

[106] L. Jia, D.A. Bulushev, O.Y. Podyacheva, A.I. Boronin, L.S. Kibis, E.Y. Gerasimov, S. Beloshapkin, I.A. Seryak, Z.R. Ismagilov, J.R.H. Ross, J. Catal. 307 (2013) 94.

[107] G. Vijayaraghavan, K.J. Stevenson, Langmuir 23 (2007) 5279.

[108] Y. Chen, J. Wang, H. Liu, R. Li, X. Sun, S. Ye, S. Knights, Electrochem. Commun. 11 (2009) 2071.

[109] T. Maiyalagan, Appl. Catal. B Environ. 80 (2008) 286.

[110] K. Parvez, S. Yang, Y. Hernandez, A. Winter, A. Turchanin, X. Feng, K. Müllen, ACS Nano 6 (2012) 9541.

[111] A. Pacuła, K. Ikeda, T. Masuda, K. Uosaki, J. Power Sources 220 (2012) 20.

[112] S. Abate, M. Freni, R. Arrigo, M.E. Schuster, S. Perathoner, G. Centi, ChemCatChem 5 (2013) 1899.

[113] Z.-S. Wu, S. Yang, Y. Sun, K. Parvez, X. Feng, K. Müllen, J. Am. Chem. Soc. 134 (2012) 9082.

[114] H.W. Park, D.U. Lee, L.F. Nazar, Z. Chen, J. Electrochem. Soc. 160 (2013) A344.

[115] J.M. Lee, B.-H. Kwon, H.I. Park, H. Kim, M.G. Kim, J.S. Park, E.S. Kim, S. Yoo, D.Y. Jeon, S.O. Kim, Adv. Mater. 25 (2013) 2011.

[116] D. Yu, E. Nagelli, F. Du, L. Dai, J. Phys. Chem. Lett. 1 (2010) 2165.

[117] F.R. García-García, J. Álvarez-Rodríguez, I. Rodríguez-Ramos, A. Guerrero-Ruiz, Carbon 48 (2010) 267.

[118] A. Nieto-Márquez, D. Toledano, P. Sánchez, A. Romero, J.L. Valverde, J. Catal. 269 (2010) 242.

[119] V.Z. Radkevich, T.L. Senko, K. Wilson, L.M. Grishenko, A.N. Zaderko, V.Y. Diyuk, Appl. Catal. Gen. 335 (2008) 241.

[120] S.-W. Bian, Z. Ma, W.-G. Song, J. Phys. Chem. C 113 (2009) 8668.

[121] Y. Wang, J. Yao, H. Li, D. Su, M. Antonietti, J. Am. Chem. Soc. 133 (2011) 2362.

[122] W.J. Lee, J.M. Lee, S.T. Kochuveedu, T.H. Han, H.Y. Jeong, M. Park, J.M. Yun, J. Kwon, K. No, D.H. Kim, S.O. Kim, ACS Nano 6 (2012) 935.

[123] L. Jia, D.-H. Wang, Y.-X. Huang, A.-W. Xu, H.-Q. Yu, J. Phys. Chem. C 115 (2011) 11466.

[124] H. Wang, T. Maiyalagan, X. Wang, ACS Catal. 2 (2012) 781.

[125] P. Ayala, R. Arenal, M. Rümmeli, A. Rubio, T. Pichler, Carbon 48 (2010) 575.

[126] J. Zhang, X. Liu, R. Blume, A. Zhang, R. Schlögl, D.S. Su, Science 322 (2008) 73.

[127] S. Song, H. Yang, R. Rao, H. Liu, A. Zhang, Catal. Commun. 11 (2010) 783.

[128] S. Wu, G. Wen, R. Schlögl, D.S. Su, Phys. Chem. Chem. Phys. 17 (2014) 1567.

[129] H. Yu, F. Peng, J. Tan, X. Hu, H. Wang, J. Yang, W. Zheng, Angew. Chem. Int. Ed. 50 (2011) 3978.

[130] X. Yang, H. Yu, F. Peng, H. Wang, ChemSusChem 5 (2012) 1213.

[131] W. Shen, W. Fan, J. Mater. Chem. A 1 (2012) 999.

[132] G. Tuci, C. Zafferoni, P. D'Ambrosio, S. Caporali, M. Ceppatelli, A. Rossin, T. Tsoufis, M. Innocenti, G. Giambastiani, ACS Catal. 3 (2013) 2108.

[133] W.-J. Jiang, J.-S. Hu, X. Zhang, Y. Jiang, B.-B. Yu, Z.-D. Wei, L.-J. Wan, J. Mater. Chem. A 2 (2014) 10154.

[134] K. Gong, F. Du, Z. Xia, M. Durstock, L. Dai, Science 323 (2009) 760.

[135] S. Yasuda, L. Yu, J. Kim, K. Murakoshi, Chem. Commun. 49 (2013) 9627.

[136] F.J. Pérez-Alonso, M.A. Salam, T. Herranz, J.L. Gómez de la Fuente, S.A. Al-Thabaiti, S.N. Basahel, M.A. Peña, J.L.G. Fierro, S. Rojas, J. Power Sources 240 (2013) 494.

[137] I. Kruusenberg, S. Ratso, M. Vikkisk, P. Kanninen, T. Kallio, A.M. Kannan, K. Tammeveski, J. Power Sources 281 (2015) 94.

[138] Y.-Y. Yu, C.X. Guo, Y.-C. Yong, C.M. Li, H. Song, Chemosphere (n.d.).

[139] K. Chizari, A. Deneuve, O. Ersen, I. Florea, Y. Liu, D. Edouard, I. Janowska, D. Begin, C. Pham-Huu, ChemSusChem 5 (2012) 102.

[140] P.J. van den Brink, R.J.A.. Terörde, J.H. Moors, A.J. van Dillen, J.W. Geus, in:, P. Ruiz and B. Delmon (Ed.), Stud. Surf. Sci. Catal., Elsevier, 1992, pp. 123–132.

[141] N. Keller, C. Pham-Huu, C. Crouzet, M.J. Ledoux, S. Savin-Poncet, J.-B. Nougayrede, J. Bousquet, Catal. Today 53 (1999) 535.

[142] C. Duong-Viet, H. Ba, Y. Liu, L. Truong-Phuoc, J.-M. Nhut, C. Pham-Huu, Chin. J. Catal. 35 (2014) 906.

[143] C. Chen, J. Zhang, B. Zhang, C. Yu, F. Peng, D. Su, Chem. Commun. 49 (2013) 8151.

[144] Y. Gao, G. Hu, J. Zhong, Z. Shi, Y. Zhu, D.S. Su, J. Wang, X. Bao, D. Ma, Angew. Chem. Int. Ed. 52 (2013) 2109.

[145] K. Zhou, B. Li, Q. Zhang, J.-Q. Huang, G.-L. Tian, J.-C. Jia, M.-Q. Zhao, G.-H. Luo, D.S. Su, F. Wei, ChemSusChem 7 (2014) 942.

[146] A. Villa, J.-P. Tessonnier, O. Majoulet, D.S. Su, R. Schlögl, ChemSusChem 3 (2010) 241.

[147] R. Arrigo, M. Hävecker, R. Schlögl, D.S. Su, Chem. Commun. (2008) 4891.

[148] R.P. Rocha, J.P.S. Sousa, A.M.T. Silva, M.F.R. Pereira, J.L. Figueiredo, Appl. Catal. B Environ. 104 (2011) 330.

[149] R.P. Rocha, A.G. Gonçalves, L.M. Pastrana-Martínez, B.C. Bordoni, O.S.G.P. Soares, J.J.M. Órfão, J.L. Faria, J.L. Figueiredo, A.M.T. Silva, M.F.R. Pereira, Catal. Today 249 (2015) 192.

[150] R.P. Rocha, J. Restivo, J.P.S. Sousa, J.J.M. Órfão, M.F.R. Pereira, J.L. Figueiredo, Catal. Today 241, Part A (2015) 73.

[151] H. Sun, C. Kwan, A. Suvorova, H.M. Ang, M.O. Tadé, S. Wang, Appl. Catal. B Environ. 154–155 (2014) 134.

[152] X. Chen, L. Wan, J. Huang, L. Ouyang, M. Zhu, Z. Guo, X. Yu, Carbon 68 (2014) 462.

[153] R. Vieira, M.-J. Ledoux, C. Pham-Huu, Appl. Catal. Gen. 274 (2004) 1.

[154] R. Vieira, C. Pham-Huu, N. Keller, M.J. Ledoux, Chem. Commun. (2002) 954.

[155] R. Vieira, D. Bastos-Netto, M.-J. Ledoux, C. Pham-Huu, Appl. Catal. Gen. 279 (2005) 35.

[156] X. Li, X. Pan, L. Yu, P. Ren, X. Wu, L. Sun, F. Jiao, X. Bao, Nat. Commun. 5 (2014).

[157] A.D. Budaeva, E.V. Zoltoev, Fuel 89 (2010) 2623.

[158] B. Xiao, K.M. Thomas, Langmuir 21 (2005) 3892.

[159] E. Lorenc-Grabowska, G. Gryglewicz, J. Machnikowski, Appl. Surf. Sci. 256 (2010) 4480.

[160] C. Liu, X. Liang, X. Liu, Q. Wang, L. Zhan, R. Zhang, W. Qiao, L. Ling, Appl. Surf. Sci. 254 (2008) 6701.

[161] S. Tanada, N. Kawasaki, T. Nakamura, M. Araki, M. Isomura, J. Colloid Interface Sci. 214 (1999) 106.

[162] Y. Song, W. Qiao, S.-H. Yoon, I. Mochida, Q. Guo, L. Liu, J. Appl. Polym. Sci. 106 (2007) 2151.

[163] H. Rong, Z. Liu, Q. Wu, D. Pan, J. Zheng, Cellulose 17 (2009) 205.

[164] P. Nowicki, R. Pietrzak, Chem. Eng. J. 166 (2011) 1039.

[165] E. Deliyanni, T.J. Bandosz, Langmuir 27 (2011) 1837.

[166] K.M. Thomas, Catal. Today 120 (2007) 389.

[167] Z.H. Zhu, H. Hatori, S.B. Wang, G.Q. Lu, J. Phys. Chem. B 109 (2005) 16744.

[168] R.T.K. Baker, M.A. Barber, P.S. Harris, F.S. Feates, R.J. Waite, J. Catal. 26 (1972) 51.

[169] R.T.K. Baker, P.S. Harris, R.B. Thomas, R.J. Waite, J. Catal. 30 (1973) 86.

[170] K. Hata, Science 306 (2004) 1362.

[171] M. Kumar, K. Kakamu, T. Okazaki, Y. Ando, Chem. Phys. Lett. 385 (2004) 161.

[172] C.L. Cheung, A. Kurtz, H. Park, C.M. Lieber, J. Phys. Chem. B 106 (2002) 2429.

[173] H. Hongo, M. Yudasaka, T. Ichihashi, F. Nihey, S. Iijima, Chem. Phys. Lett. 361 (2002) 349.

[174] B. Kitiyanan, W.E. Alvarez, J.H. Harwell, D.E. Resasco, Chem. Phys. Lett. 317 (2000) 497.

[175] C. Mattevi, C.T. Wirth, S. Hofmann, R. Blume, M. Cantoro, C. Ducati, C. Cepek, A. Knop-Gericke, S. Milne, C. Castellarin-Cudia, S. Dolafi, A. Goldoni, R. Schloegl, J. Robertson, J. Phys. Chem. C 112 (2008) 12207.

[176] I. Willems, Z. Kónya, J.-F. Colomer, G. Van Tendeloo, N. Nagaraju, A. Fonseca, J.B. Nagy, Chem. Phys. Lett. 317 (2000) 71.

[177] M. Kumar, Y. Ando, Carbon 43 (2005) 533.

[178] C. Pham-Huu, R. Vieira, B. Louis, A. Carvalho, J. Amadou, T. Dintzer, M.J. Ledoux, J. Catal. 240 (2006) 194.

[179]   D. Ding, J. Wang, Z. Cao, J. Dai, Carbon 41 (2003) 579.

[180]   T. Murakami, T. Sako, H. Harima, K. Kisoda, K. Mitikami, T. Isshiki, Thin Solid Films 464–465 (2004) 319.

[181]   S. Ivanova, E. Vanhaecke, B. Louis, S. Libs, M.-J. Ledoux, S. Rigolet, C. Marichal, C. Pham, F. Luck, C. Pham-Huu, ChemSusChem 1 (2008) 851.

[182]   N. Keller, C. Pham-Huu, M.J. Ledoux, Appl. Catal. Gen. 217 (2001) 205.

[183]   W. Yu, D.M. France, D.S. Smith, D. Singh, E.V. Timofeeva, J.L. Routbort, Int. J. Heat Mass Transf. 52 (2009) 3606.

[184]   E. Zhang, Y. Tang, Y. Zhang, C. Guo, Phys. E Low-Dimens. Syst. Nanostructures 41 (2009) 655.

[185]   A.M. Morales, C.M. Lieber, Science 279 (1998) 208.

[186]   M.J. Ledoux, S. Hantzer, C.P. Huu, J. Guille, M.-P. Desaneaux, J. Catal. 114 (1988) 176.

[187]   M.J. Ledoux, C. Pham-Huu, Catal. Today 15 (1992) 263.

[188]   N. Keller, C. Pham-Huu, S. Roy, M.J. Ledoux, C. Estournes, J. Guille, J. Mater. Sci. 34 (1999) 3189.

[189]   P. Nguyen, C. Pham, Appl. Catal. Gen. 391 (2011) 443.

[190]   M.J. Ledoux, C. Pham-Huu, CATTECH 5 (2001) 226.

[191]   P.-H. Cuong, S. Marin, M.J. Ledoux, M. Weibel, G. Ehret, M. Benaissa, E. Peschiera, J. Guille, Appl. Catal. B Environ. 4 (1994) 45.

[192]   C. Pham-Huu, P.D. Gallo, E. Peschiera, M.J. Ledoux, Appl. Catal. Gen. 132 (1995) 77.

[193]   M.E. Harlin, A.O.I. Krause, B. Heinrich, C. Pham-Huu, M.J. Ledoux, Appl. Catal. Gen. 185 (1999) 311.

[194]   M. Lacroix, L. Dreibine, B. de Tymowski, F. Vigneron, D. Edouard, D. Bégin, P. Nguyen, C. Pham, S. Savin-Poncet, F. Luck, M.-J. Ledoux, C. Pham-Huu, Appl. Catal. Gen. 397 (2011) 62.

[195]   Y. Liu, B. de Tymowski, F. Vigneron, I. Florea, O. Ersen, C. Meny, P. Nguyen, C. Pham, F. Luck, C. Pham-Huu, ACS Catal. 3 (2013) 393.

[196]   S. Ivanova, E. Vanhaecke, L. Dreibine, B. Louis, C. Pham, C. Pham-Huu, Appl. Catal. Gen. 359 (2009) 151.

[197]   Y. Liu, S. Podila, D.L. Nguyen, D. Edouard, P. Nguyen, C. Pham, M.J. Ledoux, C. Pham-Huu, Appl. Catal. Gen. 409–410 (2011) 113.

[198]   http://www.linde-engineering.de/internet.le.le.deu/de/images/Sulfur%20Process%20Technology563_111155.pdf.

[199]   A.A. Davydov, V.I. Marshneva, M.L. Shepotko, Appl. Catal. Gen. 244 (2003) 93.

[200]   J.H. Uhm, M.Y. Shin, J. Zhidong, J.S. Chung, Appl. Catal. B Environ. 22 (1999) 293.

[201]   E. Laperdrix, G. Costentin, N. Nguyen, F. Studer, J.C. Lavalley, Catal. Today 61 (2000) 149.

[202]   D.D.E. Koyuncu, S. Yasyerli, Ind. Eng. Chem. Res. 48 (2009) 5223.

[203] R.J.A.M. Terörde, P.J. van den Brink, L.M. Visser, A.J. van Dillen, J.W. Geus, Catal. Today 17 (1993) 217.

[204] C. Claude, N. Keller, J. Marc-Ledoux, P.-H. Cuong, S.-P. Sabine, Patents: Method for direct oxidation in sulphur by catalytic process and in vapour phase of low content H2S in a gas, EP1040080 A1.

[205] P. Nguyen, J.-M. Nhut, D. Edouard, C. Pham, M.-J. Ledoux, C. Pham-Huu, Catal. Today 141 (2009) 397.

[206] J.M. Nhut, Réaction d'oxydation selective de l'hydrogène sulfuré (H2S) en soufre élémentaire, Thèse de l'Université Louis Pasteur, 2003.

[207] http://www.ecn.nl/docs/library/report/2012/e12025.pdf.

[208] J.-M. Nhut, R. Vieira, L. Pesant, J.-P. Tessonnier, N. Keller, G. Ehret, C. Pham-Huu, M.J. Ledoux, Catal. Today 76 (2002) 11.

[209] J.-M. Nhut, L. Pesant, J.-P. Tessonnier, G. Winé, J. Guille, C. Pham-Huu, M.-J. Ledoux, Appl. Catal. Gen. 254 (2003) 345.

[210] Q. Chen, J. Wang, X. Liu, X. Zhao, W. Qiao, D. Long, L. Ling, Carbon 49 (2011) 3773.

[211] A. Piéplu, O. Saur, J.-C. Lavally, O. Legendre, C. Nédez, Catal. Rev. 40 (1998) 409.

[212] T.K. Ghosh, E.L. Tollefson, Can. J. Chem. Eng. 64 (1986) 969.

[213] M. Steijns, F. Derks, A. Verloop, P. Mars, J. Catal. 42 (1976) 87.

[214] R. Yan, D.T. Liang, L. Tsen, J.H. Tay, Environ. Sci. Technol. 36 (2002) 4460.

[215] J. Klein, K.-D. Henning, Fuel 63 (1984) 1064.

[216] X. Zhang, Y. Tang, S. Qu, J. Da, Z. Hao, ACS Catal. 5 (2014) 1053.

CHAPTER 2

Nitrogen-doped carbon nanotubes decorated silicon carbide as a metal-free catalyst for partial oxidation of H$_2$S
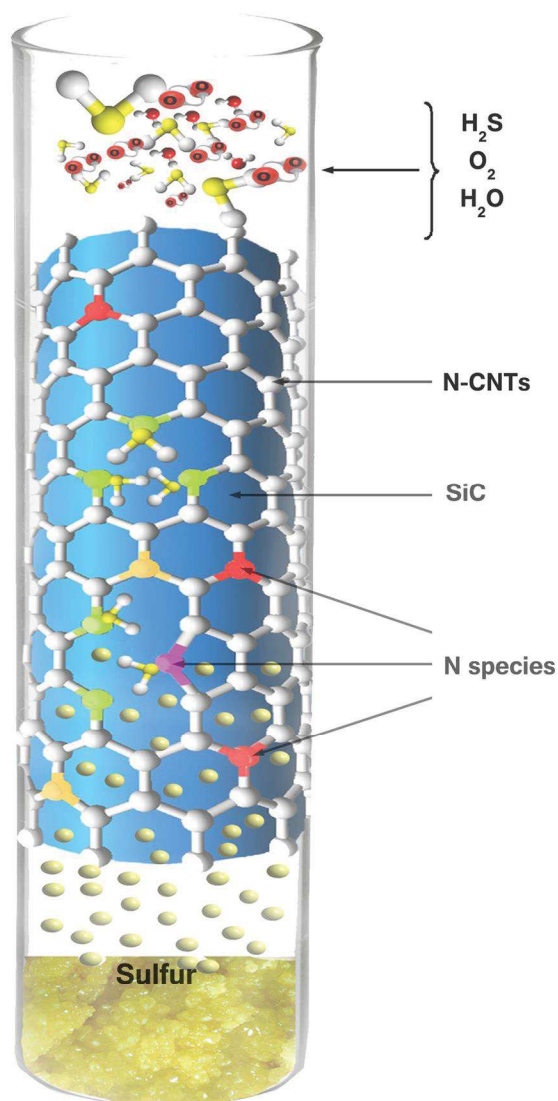
Nitrogen-doped carbon nanotubes decorated silicon carbide as a metal-free catalyst for partial oxidation of H₂S

Duong-Viet Cuong[a,b], Lai Truong-Phuoc[a], Tung Tran-Thanh[a], Jean-Mario Nhut[a], Lam Nguyen-Dinh[c], Izabela Janowska[a], Dominique Begin[a], Cuong Pham-Huu[a*]

[a] Institut de Chimie et Procédés pour l'Energie, l'Environnement et la Santé (ICPEES), ECPM, UMR 7515 du CNRS-Université de Strasbourg, 25 rue Becquerel, 67087 Strasbourg Cedex 02, France.

[b] Ha-Noi University of Mining and Geology, Dong Ngac - Tu Liem - Ha Noi – Viet Nam.

[c] The University of Da-Nang, University of Science and Technology, 54, Nguyen Luong Bang - Da Nang - Viet Nam.

Corresponding author: cuong.pham-huu@unistra.fr (C. Pham-Huu)

Abstract

Hierarchical metal-free catalyst based on the CVD synthesis of nitrogen-doped carbon nanotubes decorated silicon carbide (N-CNTs/SiC) macroscopic host structure has been prepared. The catalyst was evaluated in the partial oxidation of H_2S by oxygen into elemental sulphur in a fixed-bed reactor. The catalytic results indicate that the N-CNTs/SiC catalyst exhibits an extremely high desulfurization performance even under severe reaction conditions such as low temperature, high space velocity and at low O_2-to-H_2S molar ratio. The high desulfurization performance was attributed to the high effective surface area of the catalyst along with a short diffusion length associated with the nanoscopic dimension of the carbon nanotubes. The N-CNTs/SiC catalyst also displays a high stability as a function of time on stream which could be attributed to the strong anchoring of the nitrogen doping within the carbon matrix. The extrudates shape of the SiC support allows the direct macroscopic shaping of the catalyst for use in conventional fixed-bed reactor without facing problems linked with catalyst handling, transportation and pressure drop across the catalyst bed as encountered with nanoscopic carbon-based catalyst.

Keywords:

Catalysis – Nitrogen-doped carbon nanotubes – Silicon carbide – Extrudates – Selective oxidation – H_2S

2.1. Introduction

The last decade has faced an over increasing research on the development of metal-free catalysts for several catalytic applications such as oxygen reduction reaction (ORR) [1], [2] and [3], selective steam-free dehydrogenation and oxidative dehydrogenation [4], [5], [6] and [7], transesterification [8] and [9], and selective oxidation [10], [11] and [12]. Nitrogen-doped carbon nanotubes (N-CNTs) were the most studied metal-free catalysts [13], [14] and [15] due to the very similar size between the nitrogen atom and carbon atom which allows an easy insertion of nitrogen atoms inside the carbon matrix [16]. It is also worthy to note that the metal-free catalysts display a higher activity and stability compared to their counterpart metal and/or metal oxide catalysts. In a recent review, Su et al. [17] have highlighted the advantages of using carbon-based metal-free catalysts for several catalytic reactions with an advantage on the active-site control. Dai et al. [3] have recently reviewed on the development and use of N-CNTs and graphene metal-free catalysts, for the selective dehydrogenation and oxidative dehydrogenation of alkanes and the ORR, which display better activity and stability compared to the metal-based catalysts. Bitter et al. [18] have also reported the high activity of the N-CNTs in the Knoevenagel reaction. Recently, Peng et al. [12] have reported that N-CNTs can be efficiently employed as metal-free catalyst in the selective oxidation of benzyl alcohol to benzaldehyde with molecular oxygen. The N-CNTs catalyst also exhibits an extremely high stability as a function of the cycling tests which could be attributed to the strong incorporation of nitrogen atoms in the carbon host matrix. Similar results have also been reported by Faba et al. [19] in the biomass upgrading processes: acetone aldol and acetic acid decarboxylative condensations. Recently, Su et al. [20] have also reported that sp^2 N-doped graphitic catalysts generate reactive oxygen species which allow one to perform the hydrocarbon activation even at room temperature. The high advantage of using these N-CNTs catalysts versus the traditional metal/metal oxide supported ones is belong to the fact that the nitrogen species are well anchored within the catalyst structure and thus, problems linked with the active phase sintering are unlikely to occur.

The international restrictions concerning the release of sulfur compounds containing gas into the atmosphere are becoming more and more drastic during the last decades [21]. Nowadays, a large amount of hydrogen sulfide (H$_2$S) is released from crude oil, natural gas refineries and metal smelting process in steel production. It is also worthy to note that the coal liquefaction process is also considered to be the major source of H$_2$S emission in the near future [22]. A large part of the H$_2$S was removed via the Claus process [23] while the residual un-reacted H$_2$S will be converted into elemental sulfur at different reaction temperatures through the Super-Claus process [24] and [25]. In a recent study we have reported that N-CNTs and N-CNTs/SiC foam are efficient metal-free catalysts for performing the high

temperature selective oxidation of H_2S into elemental sulfur at a relatively high space velocity [11]. In addition, owing to the well anchorage of the nitrogen species inside the carbon matrix no deactivation was observed for a long-term reaction which was not the case with traditional supported catalyst where deactivation by sintering could occur. The problem linked with the transport/handling and pressure drop across the catalyst bed, belonging to the nanoscopic structure of the N-CNTs, can be avoided by supporting them on a macroscopic host structure of silicon carbide (SiC) [11]. However, the high porous volume of the SiC foam support (> 90 %) presents a drawback for industrial application due to its relatively low active phase loading per unit volume of the reactor. It is of interest to optimize the synthesis process of the hybrid composite and to develop new support with a higher density in order to fulfill the industrial requirements.

The aim of the present study is to report on the high desulfurization performance of the metal-free nitrogen-doped carbon nanotubes (N-CNTs) immobilized on a silicon carbide (SiC) extrudates host structure with high density. It is expected that the macroscopic shaping of the catalyst allows the avoidance of problems linked with handling and pressure drop for applications in a fixed-bed reactor. This hybrid catalyst exhibits an extremely high desulfurization performance along with a low pressure drop even at high reactant weight hourly space velocity (WHSV). The results highlighted the strong influence of the N-CNTs loading on the desulfurization performance which has ever been reported before. The desulfurization performance was also bench-marked with those obtained on the Fe_2O_3/SiC which is one of the most active and selective catalyst for the selective oxidation of H_2S into elemental sulfur [26] and [27].

2.2. Experimental

2.2.1. Silicon carbide supports

Silicon carbide (β-SiC) in an extrudates shape was synthesized via a gas–solid reaction between SiO vapor and dispersed solid carbon. The detailed synthesis of the SiC-based materials is summarized in a recent review [28]. The β-SiC was synthesized by mixing microsized silicon powder with a carbon-containing resin. The paste will be further shaped into desired shape, i.e. extrudates, grains, beads, etc. Examples of the medium to high surface area SiC with different size and shape synthesized by an industrial gas–solid process are presented in Fig. 2.1.
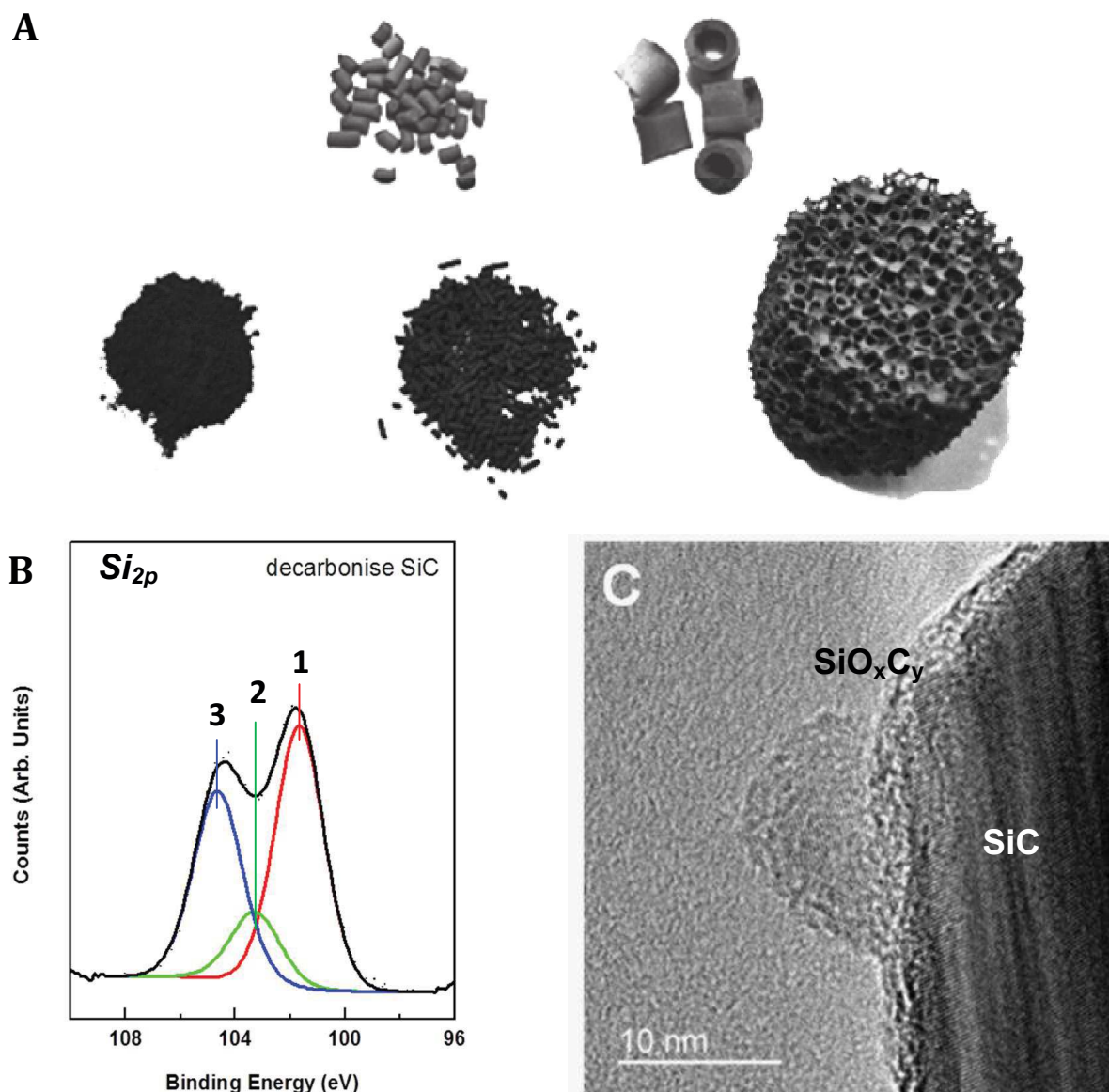
Fig. 2.1. (A) Macroscopic shapes, i.e. grains, extrudates, foams, rings, of silicon carbide synthesized by a gas-solid reaction (www.sicatcatalyst.com). (B) XPS Si$2p$ of the SiC surface after calcinations at 700 °C in air showing the presence of SiC (red-1), SiO_xC_y (green-2) and SiO_2 (blue-3). (C) High-resolution TEM micrograph showing the presence of a thin (2 nm) amorphous layer of SiO_2/SiO_xC_y which was formed during air exposure on the SiC surface.

The carburization process was carried out under flowing argon at temperature around 1350 °C during 1 h. The as-synthesized SiC was further calcined in air at 700 °C for 2 h in order to remove the un-reacted carbon within its matrix. The resulted SiC material was thus

partly covered with a thin layer of SiO_2 and SiO_xC_y (Fig. 2.1B) which could play the role of anchorage site for dispersing metal nanoparticles on its surface [29] and [30].

2.2.2. Synthesis of the N-CNT/SiC composite

The N-CNT/SiC composite was synthesized according to the Chemical Vapor Deposition (CVD) method with iron as a growth catalyst [31] and [32]. The Fe/SiC (7 wt.%) catalyst was synthesized by impregnating the SiC support with an aqueous solution containing $Fe(NO_3)_3$. The solid was dried at room temperature overnight and oven-dried at 110 °C for 24 h. It was then calcined in air at 350 °C for 2 h in order to transform the nitrate precursor into its corresponding oxide. The Fe_2O_3/SiC catalyst was housed in a quartz reactor localized inside an electric furnace. The catalyst was reduced under hydrogen flow (200 mL.min^{-1}) at 400 °C for 2 h and then, the reaction temperature was raised to the synthesis temperature (heating rate of 10 °C.min^{-1}) and the H_2 flow was replaced by a C_2H_6/NH_3/H_2 mixture. The XRD patterns of the iron-based growth catalyst after calcination and reduction (not shown) confirm the complete reduction of the Fe_2O_3 phase. The C_2H_6, NH_3, and H_2 flow rates, used in the synthesis of N-CNT/SiC, were fixed at 50:50:20 sccm.min^{-1}. The synthesis was lasted for 2 h, and the reactor was cooled to room temperature under argon. For the unsupported N-CNTs the Fe/Al_2O_3 growth catalyst was used instead of Fe/SiC and the similar process was used.

For the unsupported N-CNTs, growth from the Fe/Al_2O_3 catalyst, the as-synthesized product was treated by a NaOH (20 wt.%) solution at 80 °C for 24 h followed by an acid treatment (HNO_3, 32 vol.% at 80 °C) for 24 h in order to remove both the support and the growth catalyst. The solid was washed thoroughly with distilled water between the treatment processes. Elemental analysis performed on the treated N-CNTs indicates that about 0.2 wt.% of residual iron remains in the catalyst. Such residual iron could be attributed to the iron encapsulated within the carbon nanotubes which was not being accessible to the acid during the purification process. For the supported N-CNT/SiC sample the solid was only treated with an acid solution under the same conditions. The washed catalyst contains a residual iron of about 0.4 wt.% according to the elemental analysis. TEM-EELS analysis on both samples indicates that the nitrogen concentration was higher in the arches region while lower nitrogen concentration was observed on the tube wall [33] and confirms the similar growth mode on both un-supported and supported materials.

2.2.3. Characterization techniques

The TEM analysis was carried out on a JEOL 2100F working at 200 kV accelerated voltage, equipped with a probe corrector for spherical aberrations, and a point-to-point resolution of 0.2 nm. The sample was grinded and then dispersed by ultrasounds in an ethanol

solution for 5 min and a drop of the solution was deposited on a copper grid covered with a holey carbon membrane for observation.

The scanning electron microscopy (SEM) was carried out on a JEOL 2600F with a resolution of 5 nm. The sample was deposited onto a double face graphite tape in order to avoid the problem of charging effect during the analysis.

The thermal gravimetric analysis (TGA) was carried out on a TA Instruments Model Q-5000. The known amount of sample (10 mg) was loaded into a platinum crucible and heated up in air from room temperature to 1000 °C with a heating rate of 5 °C min^{-1}.

The specific surface area of the support and the catalyst, after reduction, was determined in a Micromeritics sorptometer. The sample was outgassed at 250 °C under vacuum for 14 h in order to desorb moisture and adsorbed species on its surface. The measurements were carried out using N_2 as adsorbent at liquid N_2 temperature at relative pressures between 0.06 and 0.2.

The X-ray photoelectron spectroscopy (XPS) measurements of the support and catalyst were performed by using a MULTILAB 2000 (THERMO) spectrometer equipped with an Al Kα anode ($hv = 1486.6$ eV) with 10 min of acquisition to achieve a good signal to noise ratio. Peak deconvolution was performed with the "Avantage" program from the Thermoelectron Company. The C1s photoelectron-binding energy was set at 284.6 ± 0.2 eV relative to the Fermi level and used as reference to calibrate the other peak positions.

2.2.4. Selective oxidation of H₂S

The catalytic selective oxidation of H_2S by oxygen (Eq. (2.1)) was carried out in an apparatus working isothermally at atmospheric pressure. The temperature was controlled by a K-type thermocouple and a Minicor regulator. The gas mixture was passed downward through the catalyst bed. Before the test, the reactor was flushed with helium at room temperature until no trace of oxygen was detected at the outlet. The helium flow was replaced by the one containing steam. The catalyst was slowly heated up to the reaction temperature, and then the wet helium flow was replaced by the reactant mixture. The gases (H_2S, O_2, and He) flow rate was monitored by Brooks 5850TR mass flow controllers linked to a control unit. The composition of the reactant feed was H_2S (1 vol. %), O_2 (0.625%, 1.25% or 2.5 vol.%), H_2O (30 vol.%) and He (balance). The use of a relatively high concentration of steam in the feed is motivated by the will to be as close as possible to the industrial working conditions as the steam formed during the former Claus units is not removed before the oxidation step and remains in the treated tail gas. Steam (30 vol.%) was fed to the gas mixture by bubbling a helium flow through a liquid tank containing water maintained at 85 °C. The O_2-to-H_2S molar ratio was varied from 0.62 to 2.5 with a WHSV fixed at 0.6 h^{-1}. It is worth to note that the

WHSV used in the present work is extremely high regarding the usual WHSV used in the industrial process for this kind of reaction, i.e. 0.09 h^{-1} (GHSV: 1500 h^{-1}).

Equation (2.1):

$$H_2S + \frac{1}{2} O_2 \rightarrow (1/n)\ S_n + H_2O \qquad \Delta H = -222 \text{ kJ.mol}^{-1} \qquad (2.1)$$

The reaction was conducted in a continuous mode and the sulfur formed during the reaction was vaporized, due to the relatively high partial pressure of sulfur at these reaction temperatures, and was further condensed at the exit of the reactor in a trap maintained at room temperature.

The analysis of the inlet and outlet gases was performed on-line using a Varian CP-3800 gas chromatography (GC) equipped with a Chrompack CP-SilicaPLOT capillary column coupled with a thermal catharometer detector (TCD), allowing the detection of O_2, H_2S, H_2O and SO_2.

2.3. Results and discussion

2.3.1. N-CNT/SiC characteristics

The N-CNTs yield and the specific surface area of the composites synthesized on the Fe–7%/SiC extrudate catalysts as a function of the reaction temperature are presented in Fig. 2.2A. Introduction of the N-CNTs on the SiC host surface leads to a significant increase of the composite specific surface area, from about 20 m^2.g^{-1} to more than 100 m^2.g^{-1}, as shown in Fig. 2.2A with the maximum value of 150 m^2.g^{-1} at the synthesis temperature of 750 °C.
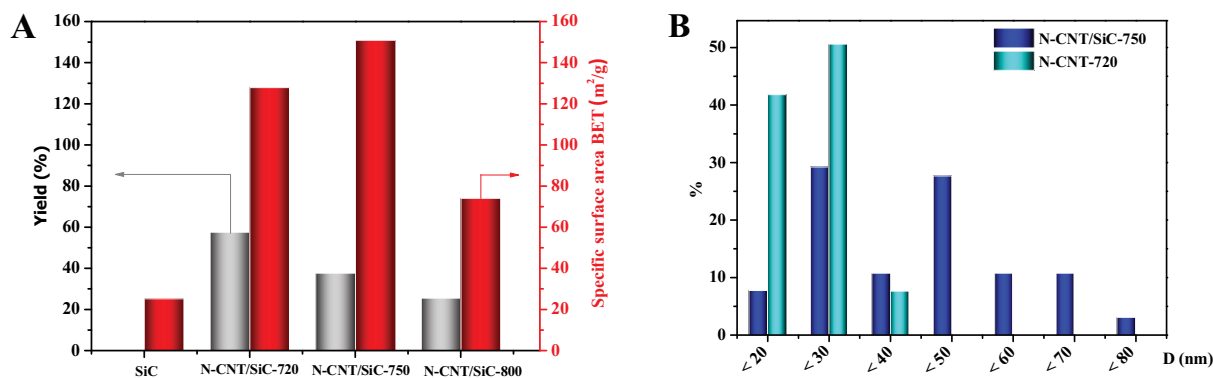

Fig. 2.2. (A) Specific surface area of the pristine SiC and the same after decorating with different N-CNTs as a function of the synthesis temperature. The N-CNTs yield as a function of the synthesis temperature is also reported in the same figure. (B) Average tube diameter of the un-supported and SiC supported N-CNTs synthesized at 750 °C.

The specific surface area increase was directly attributed to the presence of the N-CNTs with high intrinsic surface area [13], [17], [18], [31] and [32]. At higher synthesis temperature the N-CNTs yield and the specific surface area slightly decreased (Fig. 2.2A).

The decrease of the N-CNTs yield as increasing the synthesis temperature could be attributed to the gasification of part of the formed N-CNTs by the hydrogen presence in the reactor while the specific surface area lost was attributed to the generation of a more graphitic material with lower surface area. The N-CNTs yield obtained on the N-CNT/SiC extrudates at 750 °C was about 40 wt.%. The results obtained have shown that at yield higher than 60 wt.%, the macroscopic structure was partly destroyed due to the breakdown of the grain boundary by the formed nanotubes.

The decoration of the SiC surface with a dense layer of N-CNTs also significantly increases the macroscopic shape of the support as evidenced by the digital photos in Fig. 2.3. Such phenomenon has already been reported previously by different groups working on the CVD synthesis of either CNTs or N-CNTs on macroscopic supports [34], [35], [36] and [37] on the alumina-based growth catalyst.
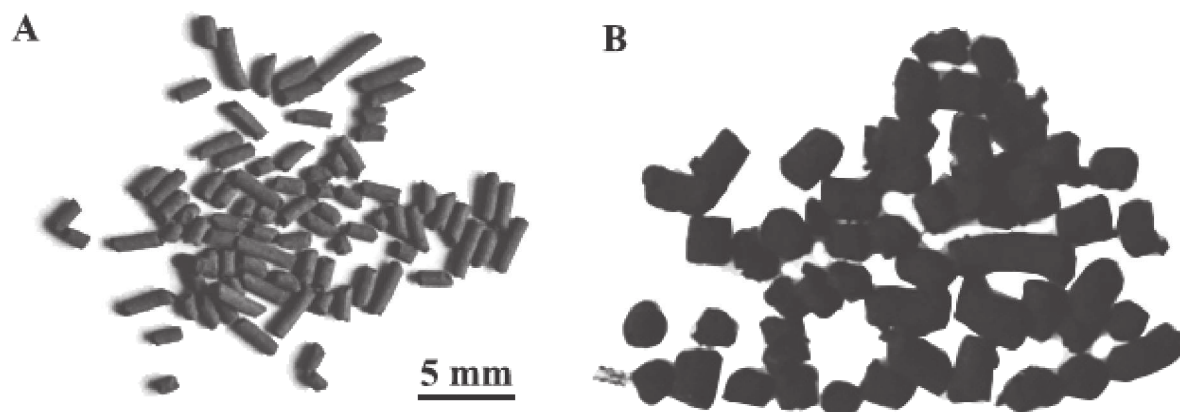
Fig. 2.3. Digital photos of the SiC before (A) and after (B) N-CNTs loading carried out at 750 °C showing the significant increase of the apparent volume of the catalyst due to the formation of a high surface-to-volume N-CNTs.

SEM analysis was extensively employed to characterize the final composite morphology and the coverage of the SiC host structure by the N-CNTs and the representative SEM micrographs are presented in Fig. 2.4. The N-CNT/SiC sample was synthesized at 750 °C. Low magnification SEM micrographs (not shown) indicates that the SiC surface was completely covered by a dense and homogeneous layer of entangled carbon nanotubes providing a high density of active sites and low diffusion catalytic network for performing the

selective oxidation reaction. For comparison the SEM micrographs of the N-CNTs synthesized from the Fe/Al₂O₃ catalyst at 750 °C are also reported in Fig. 2.4A and B. The diameter distribution of the N-CNTs synthesized on the SiC- and alumina-based catalysts is presented in Fig. 2.2B. The N-CNTs synthesized from the alumina-based catalyst exhibit a narrower diameter distribution which is centered between 20 and 40 nm, while those synthesized from the SiC-based catalyst show a much larger diameter distribution ranged from 20 to 80 nm.
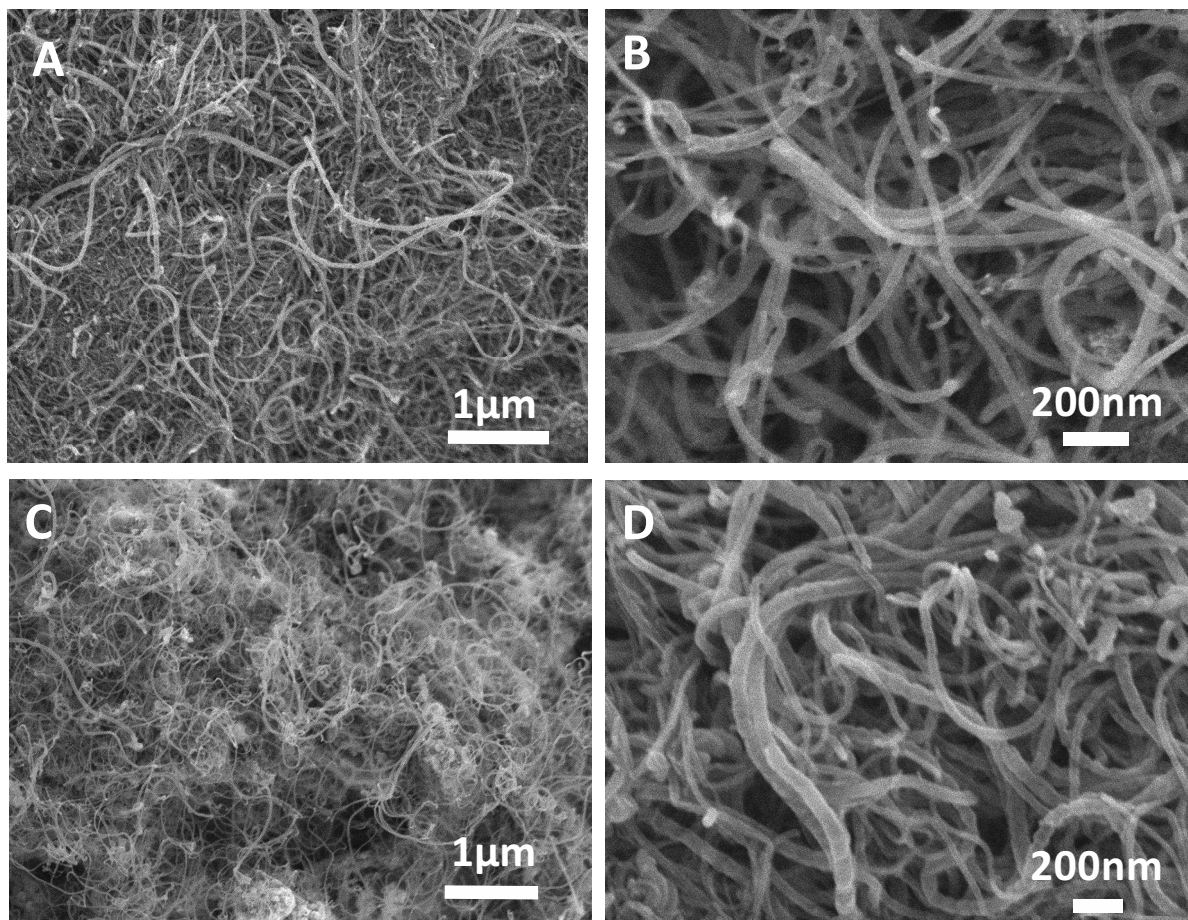
Fig. 2.4. SEM micrographs of the N-CNT/Al₂O₃ synthesized at 750 °C (A and B) and the N-CNT/SiC synthesized at 750 °C (C and D) composites showing the high coverage of the SiC surface by the N-CNT network.

Such result could be attributed to the specific surface area of SiC which is lower than that of alumina and to the low metal-support interaction between the deposited iron nanoparticles and the SiC surface which leads to the sintering of the growth catalyst, during the thermal treatment, and thus, to a larger diameter of the as-growth N-CNTs compared to that observed on the alumina-based catalyst. SEM micrographs also evidence the absence of

carbon nanoparticles in the samples which confirm the high selectivity of the synthesis process to generate nitrogen-doped carbon nanotubes.

It is worthy to note that the composite integrity was strongly depended on the synthesis temperature: low synthesis temperature, i.e. < 750 °C, leads to the relatively high yield (> 40 wt.%) of the N-CNTs which partially break the macroscopic structure of the final composite, while high synthesis temperature leads to the significant reduction of the N-CNTs yield. This low N-CNTs yield could be attributed to the formation of amorphous carbon or to the excessive gasification of the formed carbon by the H_2 generated within the synthesis medium.

The high temperature synthesis also leads to a significant decrease of the nitrogen doping in the material (Table 2.1) which is attributed to the low stability of the nitrogen in the carbon matrix at high temperature. The most appropriate synthesis temperature is set at 750 °C which allows the compromise between yield and morphological stability. For the catalytic process only the catalyst synthesized at 750 °C with a N-CNTs yield of about 40 wt.% will be evaluated.

Table 2.1. Total nitrogen content and nitrogen species composition determined by XPS in the N-CNTs and N-CNTs/SiC as a function of the synthesis temperature.

Synthesis temperature (°C)	N_{total}(*) (%)	$N_{Pyridinic}$ (%)	$N_{Pyrrolic}$ (%)	$N_{Quaternary}$ (%)	$N_{Intercalated}$ (%)
N-CNTs catalysts					
720	2.8	21	20	33	26
750	2.4	21	13	37	30
800	2.2	17	25	29	29
N-CNTs/SiC catalysts					
720	3.1	26	30	28	15
750	4.1	30	20	32	18
800	3.2	21	35	33	11

(*) N_{total} = N/(N+C+O)

The microstructure of the N-CNT/SiC catalyst is also investigated by TEM and the representative TEM micrographs are presented in Fig. 2.5. High-resolution TEM micrographs of the N-CNTs catalyst are presented in Fig. 2.5A and B and again confirm the lack of any

residual iron nanoparticles on the outer surface of the catalyst in good agreement with the assumption that residual iron is mainly localized within the tube channel. The TEM analysis confirms the periodical bamboo-like structure of the nanotube which is typical for the CNTs doped with nitrogen atoms [38], [39] and [40]. It has been reported that nitrogen doping not only modify the physical properties of the nanotubes but also drastically modify the morphology and microstructure of the carbon nanotubes [41] and [42]. Low magnification TEM analysis indicates the complete absence of carbon nanoparticles which again confirm the high selectivity of the synthesis to the formation of N-CNTs.
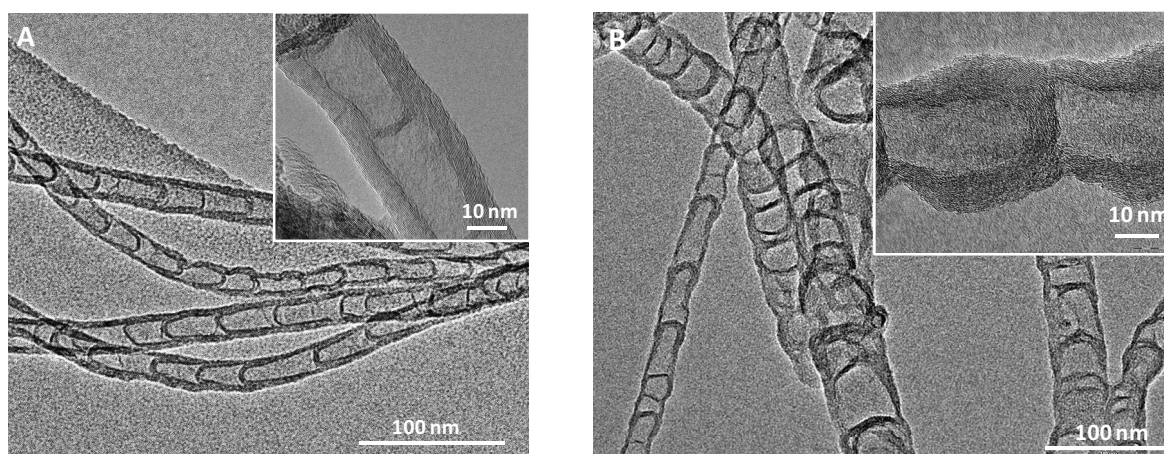
Fig. 2.5. TEM micrographs of the N-CNTs (A) and the N-CNT/SiC (B) synthesized at 750 °C with similar closed periodical bamboo-like structure.

The nitrogen species present in the catalyst are analyzed by XPS and the results are presented in Fig. 2.6. The N1s recorded XPS shows that the N-CNT/SiC synthesized at 750 °C (so far named N-CNT/SiC-750) contains 4.1 at.% of nitrogen presented in Fig. 2.6A and shows the presence of several nitrogen nitrogen-bonded carbon species: pyridinic, pyrrolic, quaternary, and an oxidized type of pyridinic nitrogen [43], [44], [45] and [46]. On the N-CNT/Al₂O₃ synthesized at the same temperature (N-CNT-750) similar results are also observed. The percentages of the different nitrogen species present on the two catalysts are summarized in Table 2.1. The SiC-based catalyst seems to have a higher total N content and also N-pyridinic species compared to the unsupported ones.

The absence of iron particles on the surface of the N-CNTs is also investigated by using XPS. Fe2p XPS spectra of the N-CNT/SiC-750 and N-CNT-750 catalysts are shown in Fig. 2.6B. The atomic percentage of iron in N-CNT/SiC-750 and N-CNT-750, measured by using XPS, is very low, and confirms the almost complete removal of the iron growth catalyst after the acid treatment (Fig. 2.6B). However, one cannot exclude the presence of some residual iron growth catalyst inside the N-CNTs which was not accessible during the acid

treatment. According to the previous results these iron NPs are not accessible to the reactant during the subsequence catalytic reaction as well.

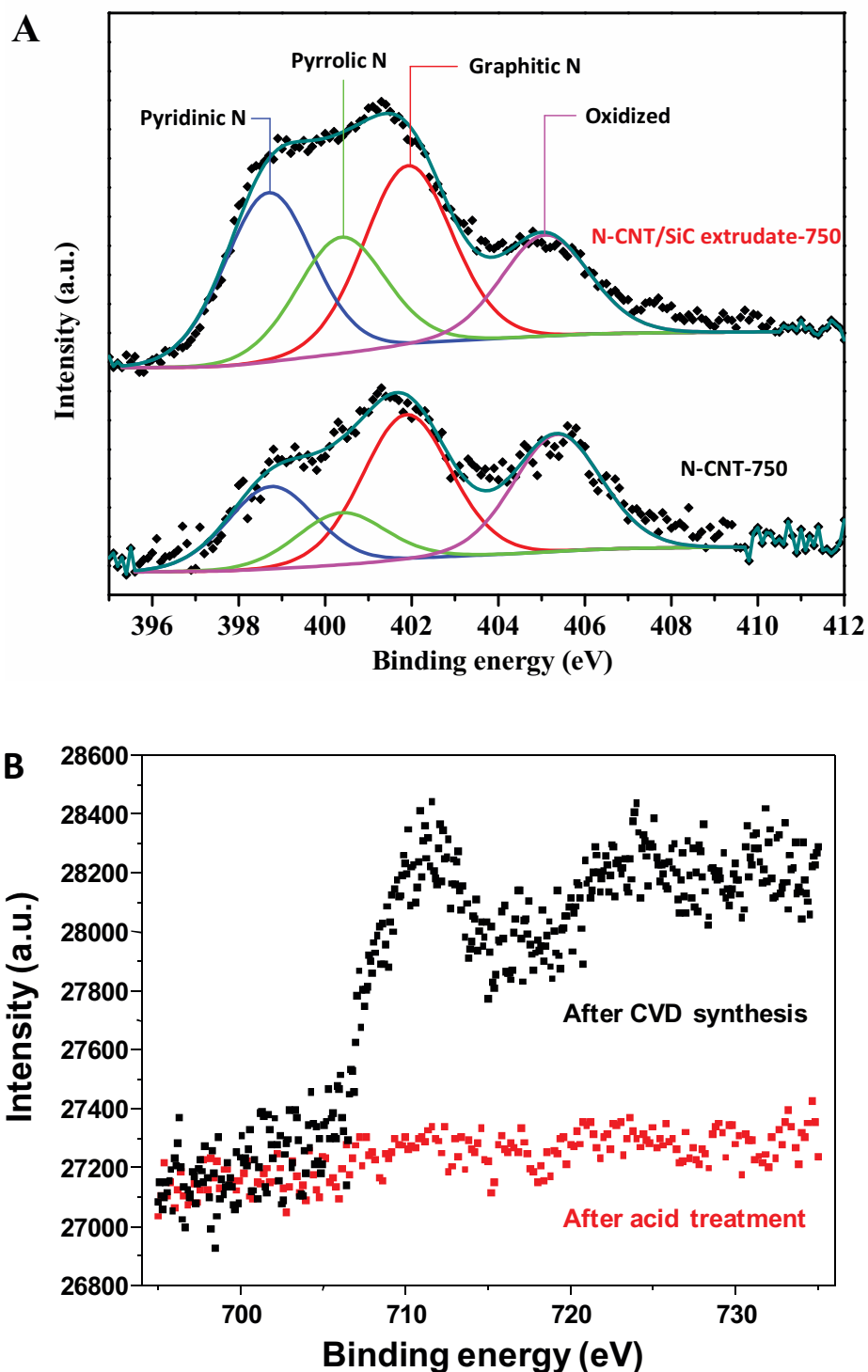**Fig. 2.6.** (A) N1s XPS spectra on the N-CNT/SiC-750 and N-CNT-750 catalysts after acid treatment in HNO_3 (35 vol. %) at 80 °C for 6 h. (B) Fe2p XPS spectra recorded on the N-CNT-750 sample after CVD synthesis and after acid treatment.

2.3.2. Selective oxidation of H_2S

2.3.2.1. Influence of the reaction temperature

The desulfurization tests are carried out on the N-CNT-750 and N-CNT/SiC-750 catalysts at two reaction temperatures, 170 °C and 190 °C, and with the WHSV fixed at 0.6 h⁻¹. The catalysts were evaluated first at 190 °C for about 50 h of test and then, the reaction temperature was lowered from 190 to 170 °C and the test was continued on the same catalyst. The results obtained as a function of time on stream are presented in Fig. 2.7. According to the results the N-CNT/SiC catalyst exhibits a relatively high desulfurization activity compared to the un-supported N-CNTs catalyst regardless of the reaction temperature. The high desulfurization activity could be attributed to the high open porous structure of the N-CNT/SiC, due to the generation of N-CNTs from different SiC grains surface, which provides a high effective surface contact between the reactant and the active sites compared to the unsupported N-CNTs with a more entangled structure which could render difficult the diffusion of the gaseous reactant inside the structure. The high effective surface area of the N-CNT/SiC induces, however, a lower sulfur selectivity compared to the unsupported ones which could be attributed to secondary reactions between the formed sulfur and the oxygen in excess under the reaction conditions applied. Similar results have already been reported in previous work [14].

The desulfurization test on the N-CNT/SiC catalyst was also carried out at higher space velocity in order to check out the influence of the H₂S conversion on the sulfur selectivity (Fig. 2.8). The sulfur selectivity slightly increases from 75 to around 80 % when the H₂S conversion was decreased from 95 to 45 % and remains stable for the whole test. The sulfur selectivity remains unchanged at 80 % even after further decreasing the H₂S conversion from 45 to 30 % which indicates that the sulfur selectivity is directly linked with the catalyst morphology and not only to the H₂S conversion level. It is expected that on the N-CNT/SiC catalyst a direct reaction between H₂S and O₂ could occur, probably through the layer of N-CNTs, which lead to a higher production of SO₂ compared to the unsupported one.
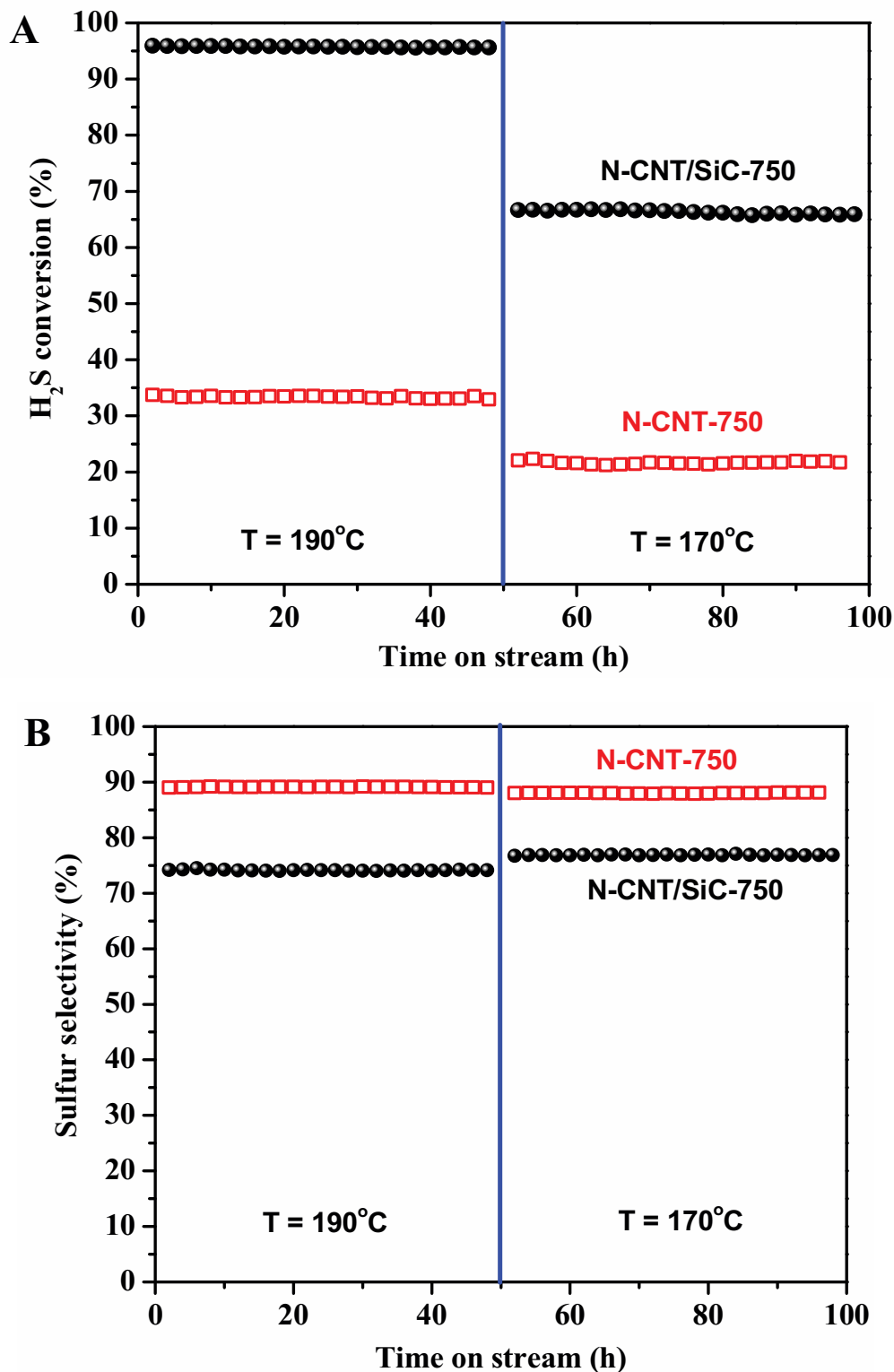
Fig. 2.7. Desulfurization conversion (A) and sulfur selectivity (B) on the N-CNT/SiC-750 and N-CNT-750 catalysts as a function of the reaction temperature. Reaction conditions: catalyst weight = 0.8 g, O_2-to-H_2S molar ratio = 2.5, reaction temperature = 170 – 190 °C, WHSV = 0.6 h^{-1}. The same catalyst was used for both tests.
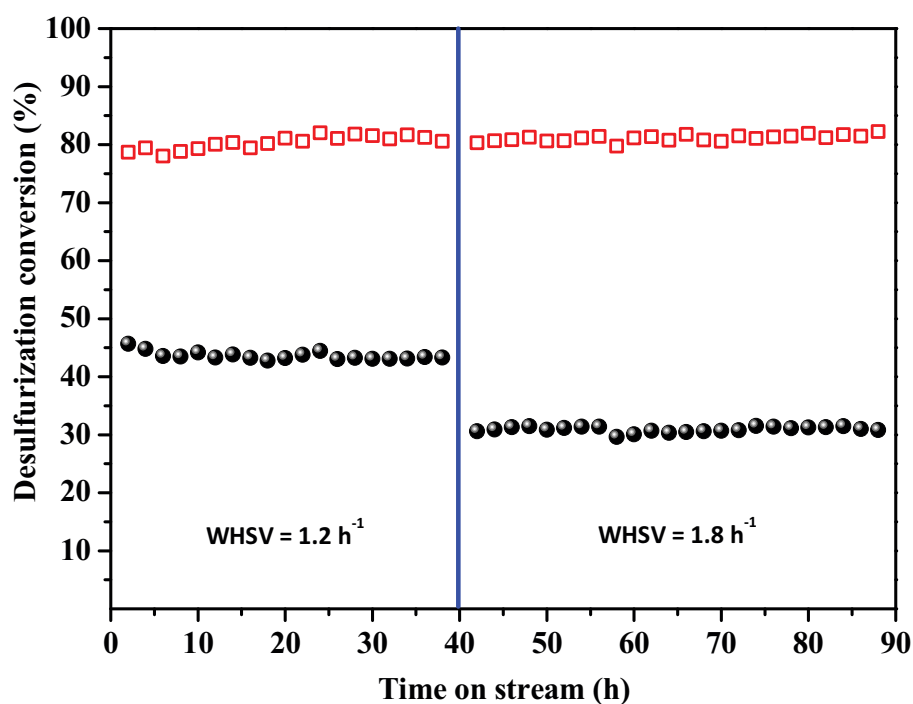
Fig. 2.8. Desulfurization performance at high space velocity on the N-CNT/SiC-750 catalyst. Reaction conditions: catalyst weight = 0.4 g, O$_2$-to-H$_2$S molar ratio = 2.5, reaction temperature = 190 °C, WHSV = 1.2 and 1.8 h^{-1}. The same catalyst was used for both tests.

2.3.2.2. Influence of the N-CNTs loading

The catalytic performance of the N-CNT/SiC-750 catalysts synthesized under the same reaction temperature but with different N-CNTs loading, *i.e.* N-CNTs density and thickness, is also evaluated and the results are presented in Fig. 2.9. According to the results one can stated that high N-CNTs loading, *i.e.* 60 wt.%, leads to a significantly lower desulfurization performance compared to that obtained on the low N-CNTs loading, *i.e.* 40 wt.%.

The low desulfurization activity obtained on the high N-CNTs loading could be attributed to the presence of a much denser N-CNTs network on the catalyst surface, and also to the partial breakdown of the catalyst integrity, which could hinder the accessibility of the reactants toward the inside active site. Similar results have also been observed in the present work on the unsupported N-CNTs with low accessibility. On the lower N-CNTs loading catalyst it is expected that the N-CNTs layer and entanglement degree are less pronounced and thus, leading to a more easy diffusion of the reactants toward the active site. Such explanation was also partly confirmed by the sulfur selectivity obtained, the sulfur selectivity is almost similar on both catalysts: on the low loading catalyst the sulfur selectivity is about 75 % whereas it reached almost 78 % on the high loading catalyst. Such results could be

explained by a lower accessibility of the reactant to the active site in the case of the catalyst with high N-CNTs loading and not to a modification of the active site nature.
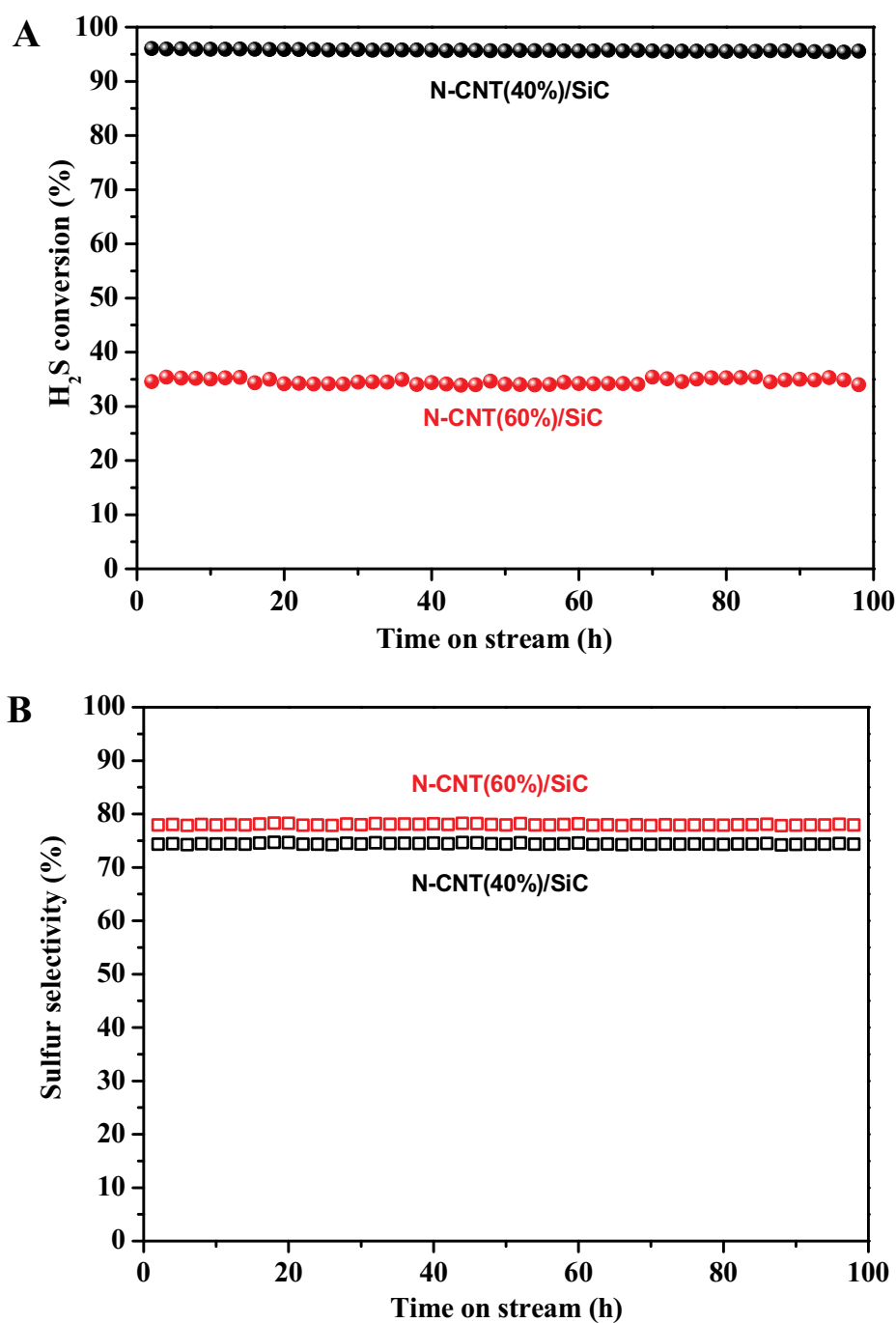
Fig. 2.9. Desulfurization performance, H₂S conversion (A) and sulfur selectivity (B), on the N-CNT/SiC with different N-CNTs loading, *i.e.* 40 and 60 wt.%, catalysts, synthesized at 750 °C. Reaction conditions: O₂-to-H₂S molar ratio = 2.5, reaction temperature = 190 °C, WHSV = 0.6 h⁻¹.

2.3.2.3. Influence of the O₂-to-H₂S molar ratio

The influence of the O_2-to-H_2S molar ratio on the desulfurization performance was also studied in order to evaluate the ability of the N-CNTs to generate active oxygen species for oxidizing H_2S compound. The results obtained at different O_2-to-H_2S molar ratios, i.e. 2.5, 1.25 and 0.625, as a function of time on stream are presented in Fig. 2.10.
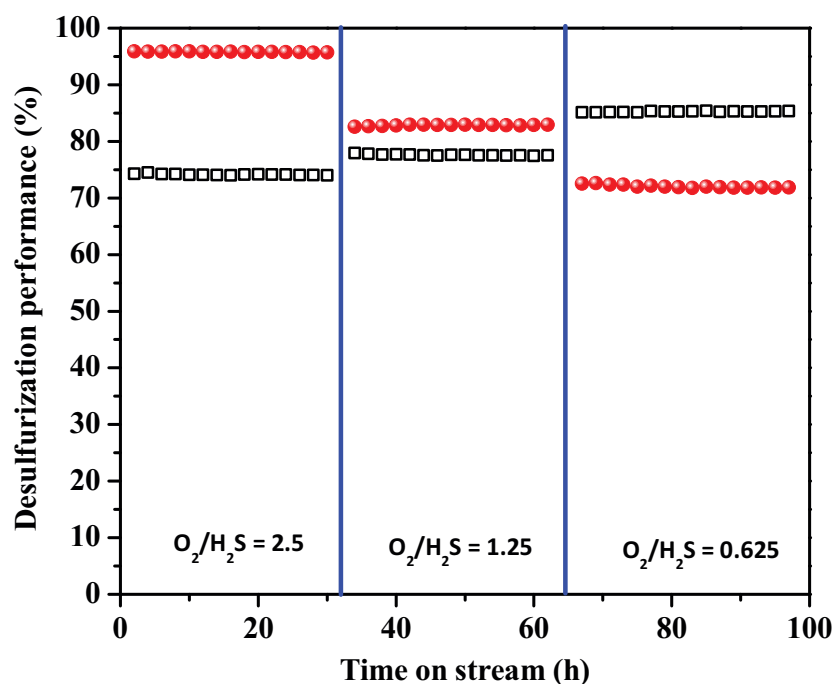
Fig. 2.10. Desulfurization performance, H_2S conversion (black sphere) and sulfur selectivity (red open square), on the N-CNT/SiC catalyst at different O_2-to-H_2S molar ratio. Reaction conditions: catalyst weight = 0.3 g, temperature = 190 °C, WHSV = 0.6 h⁻¹. The same catalyst was used for both tests. (For interpretation of the references to color in this figure legend, the reader is referred to the web version of the article.)

The decreasing of the O_2-to-H_2S molar ratio leads to a slight decrease of the desulfurization performance without any observable deactivation as a function of time on stream. On the other hand, the sulfur selectivity steadily increases as decreasing the O_2-to-H_2S molar ratio. The sulfur selectivity increases was attributed to the low oxygen partial pressure which prevent successive oxidation of the formed sulfur into SO_2. The results indicate that the N-CNT/SiC-750 catalyst exhibits a high activity for oxygen dissociation which provides enough oxygen to perform the selective oxidation of H_2S even at low oxygen concentration in the reactant mixture and under a relatively high space velocity. Such phenomenon is relatively

similar to the oxygen dissociation mechanism reported on the N-CNTs for the ORR [47] and [48].

It is worthy to note that it is the first time that such high desulfurization performance has been reported at high space velocity and low O_2-to-H_2S molar ratio. Desulfurization reaction carried out on supported Fe-based catalysts at higher reaction temperature and lower WHSV has shown that at low O_2-to-H_2S molar ratio the H_2S conversion was severely decreased due to the lack of active oxygen species available for the reaction [26].

2.3.2.4. Desulfurization performance between N-CNT/SiC and Fe_2O_3/SiC catalysts

For comparison the catalytic desulfurization performance of the Fe_2O_3-3%/SiC extrudate catalyst, which is among the most reactive catalyst for the selective oxidation of H_2S [26] and [27], and that of the N-CNT/SiC-750 are also reported in Fig. 2.11. The results show that all the tested catalysts exhibit a high stability as a function of time on stream. The results clearly indicate that the N-CNT/SiC-750 metal-free catalyst is the most active catalyst for performing the selective oxidation of H_2S into elemental sulfur at low reaction temperature range and under high space velocity. Indeed, under the same reaction conditions, the N-CNT/SiC-750 exhibits a conversion of about 97 % compared to < 20 % for the Fe_2O_3/SiC catalyst. The low desulfurization activity of the Fe_2O_3/SiC catalyst could be attributed to the high space velocity of the reaction which significantly affects the diffusion of the reactant inside the SiC pore where the active phase was localized.

On the N-CNT/SiC catalyst the high effective surface area combined with the nanoscopic size of the carbon nanotubes significantly improve the contact surface between the active site and the reactant leading to such a high desulfurization activity. Similar results have also been obtained on the cobalt catalyst deposited on a low surface area alumina decorated with carbon nanotubes for the Fischer-Tropsch synthesis [49]. The Fischer-Tropsch activity was greatly improved compared to the alumina-based catalyst due to the high effective surface area of the carbon-based catalyst for the gas phase reactant. The difference in the specific surface area between the two catalysts, *i.e.* 40 $m^2.g^{-1}$ for the Fe_2O_3/SiC and 145 $m^2.g^{-1}$ for the N-CNT/SiC catalyst, also contributes to the enhancement of the desulfurization performance on the N-CNT/SiC catalyst. The sulfur selectivity on the N-CNT-based catalysts is slightly lower than the one obtained on the iron-based catalyst, *i.e.* 75 % instead of ca. 88 %. This low sulfur selectivity could be attributed to the high activity of the N-CNTs which further oxidize the formed sulfur or the H_2S into SO_2 in the presence of excess oxygen in the stream as observed above.
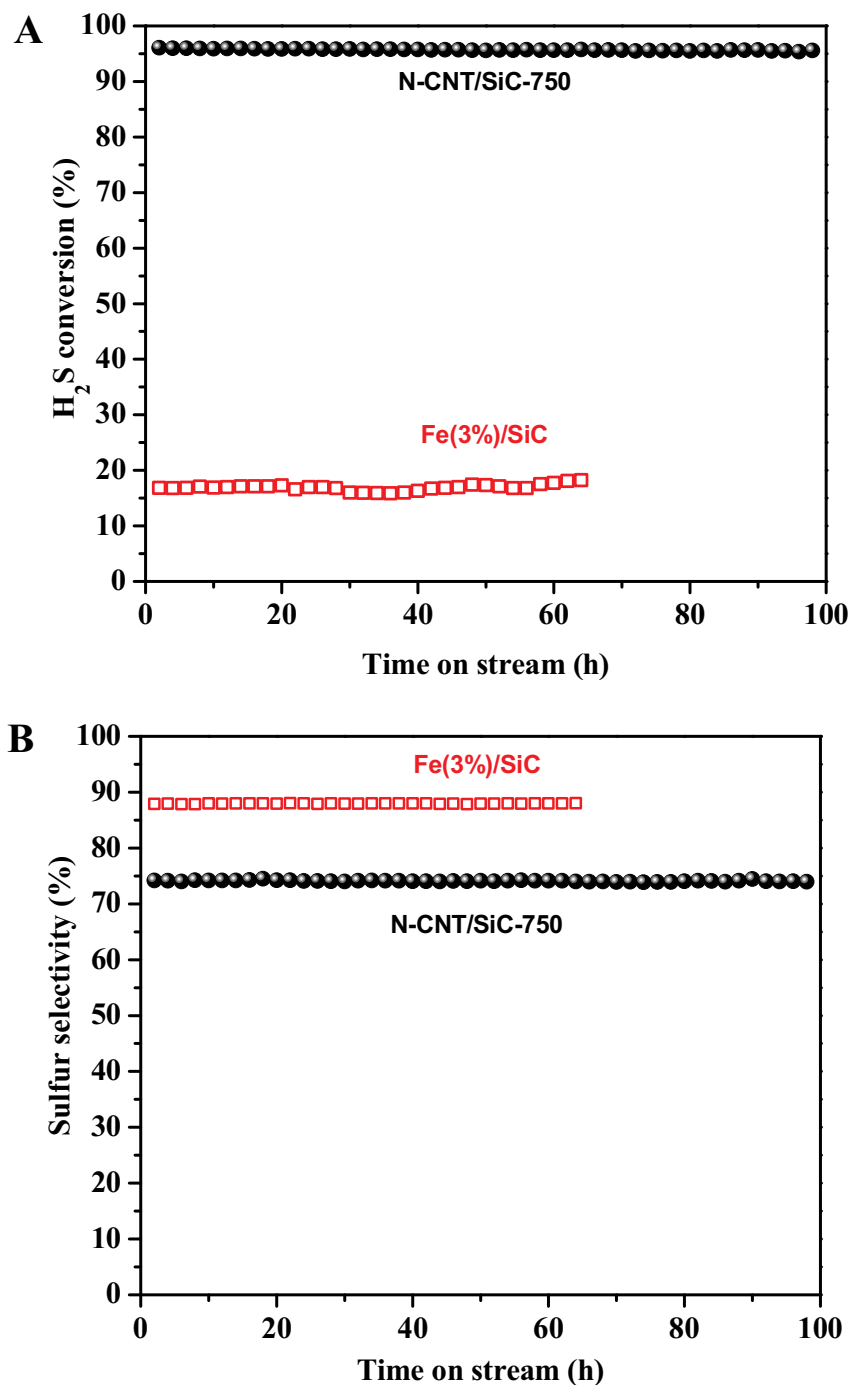
Fig. 2.11. Desulfurization conversion (A) and sulfur selectivity (B) on the N-CNT/SiC-750 and Fe_2O_3-3%/SiC catalysts. Reaction conditions: O_2-to-H_2S molar ratio = 2.5, reaction temperature = 190 °C, WHSV = 0.6 h^{-1}.

The apparent longer sojourn time of the sulfur intermediate within the N-CNTs layer could also favor the secondary oxidation reaction to yield SO_2 and thus, leading to a lower selectivity. According to this result one should expected that the N-CNTs density and thickness could play a significant role on the desulfurization performance. Work is ongoing to

find new structured metal-free catalyst with better activity along with high selectivity by replacing N-CNTs by nitrogen-doped carbon composite with high effective surface area and low diffusion characteristic length, *i.e.* mesoporous-doped carbon generated from thermal decomposition of polymerized ionic liquids (PILs) [50].

2.3.3. Characteristics of the spent catalysts
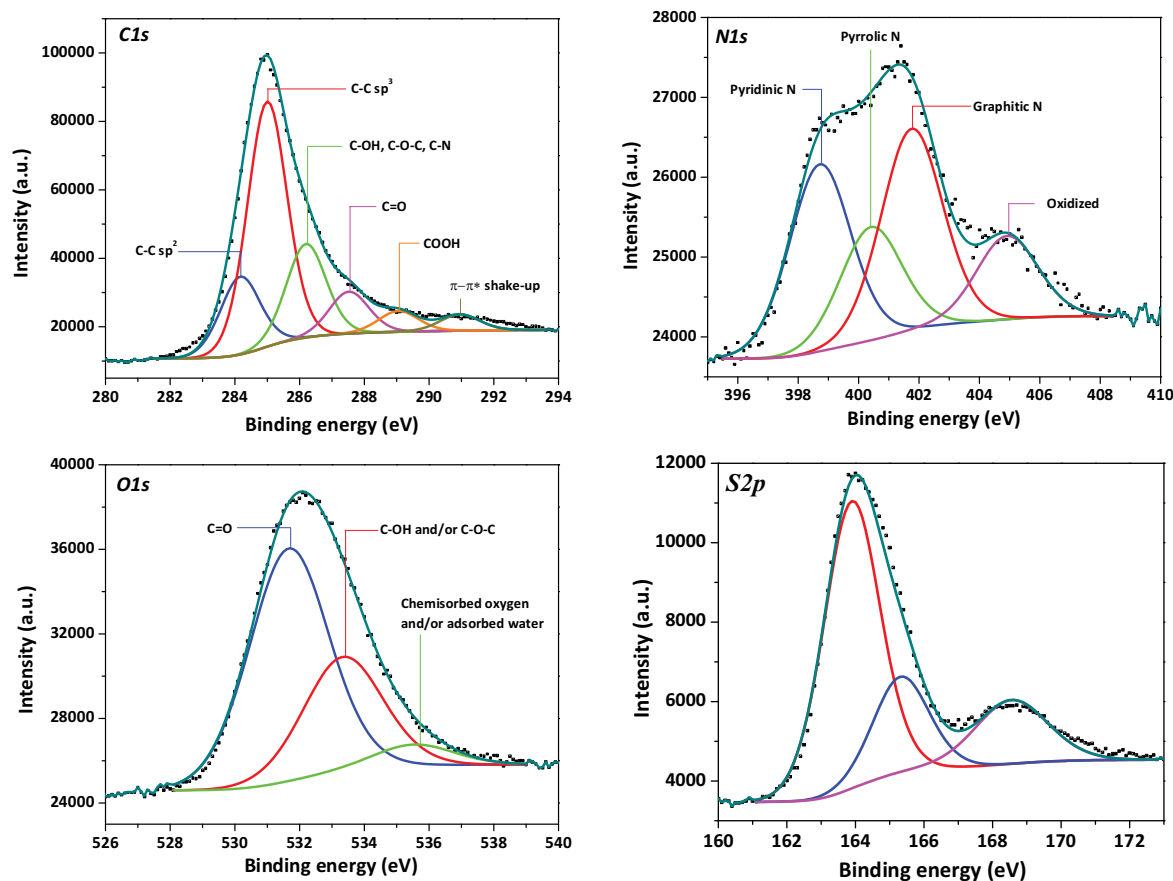
Fig. 2.12. XPS analysis of the N-CNT/SiC-750 catalyst after desulfurization reaction showing the formation of sulfur on the spent catalyst.

The specific surface area of the spent N-CNT/SiC catalyst, measured after more than 200 h of reaction under different reaction conditions, is about two times lower than that of the fresh catalyst, *i.e.* 80 instead of 145 $m^2.g^{-1}$. Such result could be attributed to the deposition of some solid sulfur with low specific surface area within the catalysts porosity which contributes to the lowering of the overall specific surface area of the catalysts. The XPS analysis carried out on the spent catalyst, after more than 200 h on stream, evidences the presence of some sulfur species on the catalyst surface (Fig. 2.12). Such sulfur deposition was

attributed to the low reaction temperature in the present study, *i.e.* 190 °C instead of 230 °C, which is not able to vaporize the totality of the solid sulfur formed during the reaction. As no deactivation was observed as a function of time on stream on the catalysts one should expected that the solid sulfur was mostly deposited on the SiC surface and thus, had no direct effect on the desulfurization activity of the N-CNTs. It is worthy to note that the desulfurization performance can be recovered after a thermal treatment of the spent catalyst under helium flow at 400 °C for 1 h in order to vaporize the residual solid sulfur. The XPS analysis also confirms the high stability of the catalyst as the nitrogen species distribution remains unchanged after the reaction as shown by the N1s spectrum in Fig. 2.12.

2.4. Conclusion

In summary, nitrogen-doped carbon nanotubes supported on a macroscopic host structure of SiC have shown to be an active and selective metal-free catalyst for the low-temperature oxidation of H₂S into elemental sulfur. The macroscopic shaping of the catalyst allows one to avoid the problems linked with the handling and transport of the nanoscopic un-supported N-CNTs catalyst. In addition, this hybrid metal-free catalyst with controlled macroscopic shape can be efficiently employed in a fixed-bed configuration without facing the problem linked with the pressure drop across the catalytic bed. The N-CNTs supported on SiC extrudate catalyst also displays higher desulfurization performance compared to the most active Fe₂O₃/SiC catalyst. The high activity of the N-CNTs-based catalyst for oxygen dissociation also allows the catalyst to operate at low O₂-to-H₂S molar ratio without detrimental lost in catalytic performance. The N-CNT/SiC catalysts were also extremely stable under the employed desulfurization reaction which could be directly attributed to the chemical bonding between the nitrogen and the carbon matrix, which prevent active site lost by sintering. Some surface area lost was observed on the spent catalyst which could be attributed to the presence of some low surface area solid sulfur deposited on the SiC surface during the course of the reaction. However, as no deactivation occurred, even after more than 100 h of test, one can speculate that such solid sulfur deposition has no effect on the overall density of the active site. The results obtained here have shown that hierarchical nitrogen-doped carbon materials with controlled macroscopic shaping can be efficiently employed as metal-free catalyst for several reaction of interest.

Acknowledgements

References

[1]   S. Yasuda, L. Yu, J. Kima, K. Murakoshi, Chem. Commun. 49 (2013) 9627-9629.

[2]   G. Tuci, C. Zafferoni, P. D'Ambrosio, S. Caporali, M. Ceppatelli, A. Rossin, T. Tsoufis, M. Innocenti, G. Giambastiani, ACS Catal. 3 (9) (2013) 2108–2111.

[3]   L. Qu, Y. Liu, J-B. Baek, L. Dai, ACS Nano 4 (2010) 1321-1326.

[4]   C. Nederlof, F. Kapteijn, M. Makkee, Appl. Catal. A: Gen. 417–418 (2012) 163-173.

[5]   D. Bégin, G. Ulrich, J. Amadou, D. S. Su, C. Pham-Huu, R. Ziessel, J. Mol. Catal. A: Chem. 302 (2009) 119-123.

[6]   C. Chen, J. Zhang, B. Zhang, C. Yu, F. Peng, D. S. Su, Chem. Commun. 49 (2013) 8151 – 8153.

[7]   J. Amadou, K. Chizari, M. Houllé, I. Janowska, O. Ersen, D. Bégin, C. Pham-Huu, Catal. Today 138 (2008) 62-68.

[8]   A. Villa, J. P. Tessonnier, O. Majoulet, D. S. Su, R. Schlögl, Chem. Commun. 29 (2009) 4405-4407.

[9]   A. Villa, J. P. Tessonnier, O. Majoulet, D. S. Su, R. Schlögl, ChemSusChem 3 (2010) 241-245.

[10]   Y. Cao, H. Yu, J. Tan, F. Peng, H. Wang, J. Li, W. Zheng, N.-B. Wong, Carbon, 57 (2013) 433-442.

[11]   K. Chizari, A. Deneuve, O. Ersen, I. Florea, Y. Liu, D. Edouard, I. Janowska, D. Begin, C. Pham-Huu, ChemSusChem 5 (2012) 102-108.

[12]   J. Luo, F. Peng, H. Wang, H. Yu, Catal. Commun. 39 (2013) 44-49.

[13]   D. S. Su, S. Perathoner, G. Centi, Chem. Rev. 113 (2013) 5782-5816.

[14]   H. Wang, T. Maiyalagan, X. Wang, ACS Catal. 2 (2012) 781-794.

[15]   D. Yu, E. Nagelli, F. Du, L. Dai, J. Phys. Chem. Lett. 1 (2010) 2165 –2173.

[16]   S. Peng, K. Cho, Nano Lett. 3 (2003) 513-517.

[17]   D. S. Su, J. Zhang, B. Frank, A. Thomas, X. Wang, J. Paraknowitsch, R. Schlögl, ChemSusChem 3 (2010) 169-180.

[18]   S. van Dommele, K. P. de Jong, J. H. Bitter, Chem. Commun. 46 (2006) 4859-4861.

[19]   L. Faba, Y. A. Criado, E. Gallegos-Suarez, M. Perez-Cadenas, E. Diaz, I. Rodriguez-Ramos, A. Guerrero-Ruiz, S. Ordonez, Appl. Catal. A: Gen. 458 (2013) 155-161.

[20]   Y. Gao, G. Hu, J. Zhong, Z. Shi, Y. Zhu, D. S. Su, J. Wang, X. Bao, D. Ma, Angew. Chem. Int. Ed. 52 (2013) 2109-2113.

[21]   L. Connock, Sulphur 34 (1998) 257.

[22]   S. W. Chun, J. Y. Jang, D. W. Park, H. C. Woo, J. S. Chung, Appl. Catal. B Environ. 16 (1998) 235.

[23]   J. W. Estep, G. T. McBride, Jr., J. R. West, Advances in Petroleum Chemistry and Refining, Vol. 6, Interscience. New-York, Chapter 7, (1962) 315.

[24] J. Wieckowska, Catal. Today 24 (1995) 405.

[25] M. J. Ledoux, C. Pham-Huu, N. Keller, J. B. Nougayrède, S. Savin-Poncet, J. Bousquet, Catal. Today 61 (2000) 157-163.

[26] N. Keller, C. Pham-Huu, M. J. Ledoux, Appl. Catal. A: Gen. 217 (2001) 205-217.

[27] P. Nguyen, D. Edouard, J. M. Nhut, M. J. Ledoux, C. Pham-Huu, Appl. Catal. B: Environ. 76 (2007) 300-310.

[28] P. Nguyen, Ch. Pham, Appl. Catal. A 391 (2011) 443-454.

[29] A. Deneuve, O. Ersen, P. Nguyen, Ch. Pham, D. Edouard, D. Begin, M. J. Ledoux, C. Pham-Huu, Appl. Catal. A: Gen. 385 (2010) 52-61.

[30] I. Florea, O. Ersen, Ch. Hirlimann, L. Roiban, A. Deneuve, M. Houllé, I. Janowska, P. Nguyen, Ch. Pham, C. Pham-Huu, Nanoscale 2 (2010) 2668-2678.

[31] K. Chizari, I. Janowska, M. Houllé, I. Florea, O. Ersen, T. Romero, P. Bernhardt, M. J. Ledoux; C. Pham-Huu, Appl. Catal. A: Gen. 380 (2010) 72-80.

[32] J. Amadou, K. Chizari, M. Houllé, I. Janowska, O. Ersen, D. Begin, C. Pham-Huu, Catal. Today 138 (2008) 62-68.

[33] I. Florea, O. Ersen, R. Arenal, D. Ihiawakrim, C. Messaoudi, K. Chizari, I. Janowska, C. Pham-Huu, J. Am. Chem. Soc. 134 (2012) 9672-9680.

[34] J. P. Tessonnier, D. S. Su, ChemSusChem 4 (2011) 824-847.

[35] P. Chen, L. M. Chew, A. Kostka, M. Muhler, W. Xia, Catal. Sci. Technol. 3(2013) 1964-1971.

[36] I. Janowska, G. Winé, M. J. Ledoux, C. Pham-Huu, J. Mol. Catal. A: Chem. 267 (2007) 92-97.

[37] L. Roldan, S. Armenise, Y. Marco, E. Garcia-Bordejé, Phys. Chem. Chem. Phys. 14 (2012) 3568-3575.

[38] M. Terrones, A. M. Benito, C. Manteca-Diego, W. K. Hsu, O. I. Osman, J. P. Hare, D. G. Reid, H. Terrones, A. K. Cheetham, K. Prassides, H. W. Kroto, D. R. M. Walton, Chem. Phys. Lett. 257 (1996) 576-582.

[39] D. Zhong, S. Lin, G. Zhang, E. G. Wang, J. Appl. Phys. 89 (2001) 5939-5943.

[40] K. Chizari, A. Vena, L. Laurentius, U. Sundararaj, Carbon 68 (2014) 369-379.

[41] M. Terrones, P. M. Ajayan, F. Banhart, X. Blase, D. L. Carroll, J. C. Charlier et al., Appl. Phys. A Mater. Sci. Process 74 (2002) 355-361.

[42] C. P. Ewels, M. Glerup, J. Nanosci. Nanotechnol. 5 (2005) 1345-1363.

[43] S. Biniak, G. Szymanski, J. Siedlewski, A. Wiatkoski, Carbon 35 (1997) 1799-1810.

[44] H. C. Choi, J. Park, B. Kim, J. Phys. Chem. B 109 (2005) 4333-4340.

[45] H. C. Choi, S. Y. Bae, J. Park, K. Seo, C. Kim, B. Kim, H. J. Song, H. J. Shin, Appl. Phys. Lett. 85 (2004) 5742-5744.

[46] V. V. Strelko, N. T. Kartel, I. N. Dukhno, V. S. Kuts, R. B. Clarkson, B. M. Odintsov, Surf. Sci. 548 (2004) 281-290.

[47] K. Gong, F. Du, Z. Xia, M. Durstock, L. Dai, Science 323 (2009) 760-764.

[48]   G. Tuci, C. Zafferoni, A. Rossin, A. Milella, L. Luconi, M. Innocneti, L. Truong-Phuoc, C. Duong-Viet, C. Pham-Huu, G. Giambastiani, Chem.Mater. DOI: 10.1021/cm500805c (2014).

[49]   Y. Liu, T. Dintzer, O. Ersen, C. Pham-Huu, J. Ener. Chem. 22 (2013) 279-289.

[50]   Q. Zhao, T. P. Feillinger, M. Antoneitti, J. Yuan, J. Mater. Chem. A 1(2013) 5113-5120.

CHAPTER 3

A highly N-doped carbon phase "dressing" of macroscopic supports for catalytic applications
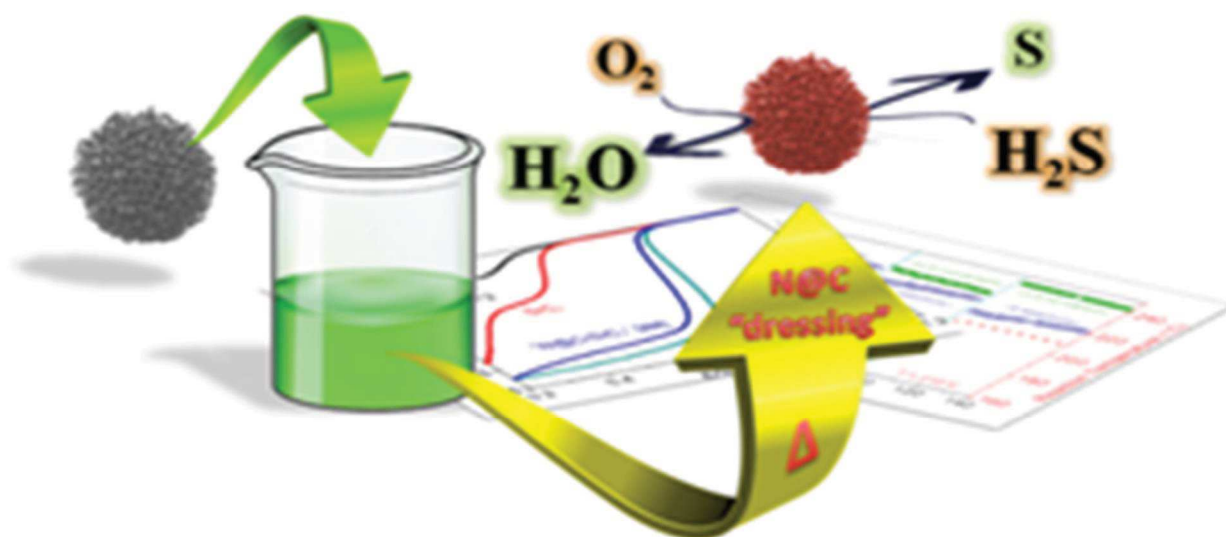
A highly N-doped carbon "dressing" of macroscopic supports for catalytic applications

H. Ba,[1,3,†] Y. Liu,[1,†] L. Truong-Phuoc,[1] C. Duong-Viet,[1] X. Mu,[1] W.H. Doh,[1] T. Tran-Thanh,[1] W. Baaziz,[1] L. Nguyen-Dinh,[2] J.M. Nhut,[1] I. Janowska,[1] D. Begin,[1] S. Zafeiratos,[1] P. Granger,[3] G. Tuci,[4] G. Giambastiani,[4,*] F. Banhart,[5] M.J. Ledoux,[1] C. Pham-Huu[1,*]

[1] *Institut de Chimie et Procédés pour l'Energie, l'Environnement et la Sant*

é (ICPEES), ECPM, UMR 7515 CNRS-Université de Strasbourg, 25, rue Becquerel, 67087 Strasbourg Cedex 02, France.

[2] *The University of Da-Nang, University of Science and Technology, 54 Nguyen Luong Bang, Da-Nang, Viet-Nam.*

[3] *Unité de Catalyse et Chimie du Solide (UCCS), UMR 8181 du CNRS-Université de Lille-1, Bâtiment C3, Université Lille-1, 59655 Villeneuve d'Ascq Cedex, France.*

[4] *Institute of Chemistry of OrganoMetallic Compounds, ICCOM-CNR and Consorzio INSTM, Via Madonna del Piano, 10 – 50019, Sesto F.no, Florence, Italy.*

[5] *Institut de Physique et Chimie des Matériaux de Strasbourg (IPCMS), UMR 7504 CNRS-University of Strasbourg, 23, rue du Loess, 67034 Strasbourg Cedex 02, France.*

Correspondence to: Cuong Pham-Huu (cuong.pham-huu@unistra.fr) and Giuliano Giambastiani (giuliano.giambastiani@iccom.cnr.it)

† These authors contributed equally.

Abstract

We describe the effective synthesis of macroscopic and highly porous nitrogen-doped carbon-based composites with exceptionally high nitrogen content. An aqueous solution of food-processing raw materials, *i.e.* ammonium carbonate, glucose and citric acid, is used as an impregnating pre-catalytic phase where a variety of macroscopically shaped supports are soaked. Successive thermal treatments "dress" the supports with a foamy carbon layer featured by a high density of surface exposed N-sites. The as-prepared composites are employed as heterogeneous metal-free catalysts in gas- and liquid-phase processes, showing excellent catalytic performance compared to that of analogous classical metal/metal-oxide-based composites. Two industrially and technologically relevant catalytic transformations are scrutinized: 1) the electrochemical oxygen reduction reaction (ORR) as a process at the heart of renewable energy technology, and 2) the partial H_2S oxidation to elemental sulfur from refinery tail gas.

One Sentence Summary: Highly N-doped carbon nanomaterials prepared from raw foodstuff components act as catalytically active and metal-free "dresses" for macroscopic supports.

3.1. Introduction

The main challenge of modern and sustainable catalysis stems on re-thinking fundamental metal-based catalytic processes while eliminating critical raw components like expensive noble metals. The exploitation of tailored *metal-free* catalytic architectures designed and fabricated from cheap and easily accessible building blocks may represent a valuable and green alternative. Nitrogen-doped 1D and 2D carbon nanomaterials (N-CNMs), have emerged in the last decade as effective metal-free systems, capable of promoting a high number of catalytic processes [1–8]. Since the pioneering work by Gong *et al.* [1], independent studies have demonstrated how the inclusion of nitrogen(s) in the honeycomb carbon structure breaks the electroneutrality of the Csp^2 network [9,10] and generates charged active sites. Their presence plays a pivotal role in the ultimate material catalytic activity, sometimes offering performance comparable or even better than that observed with classical metal-based systems. Among the synthetic approaches known for the production of N-CNMs systems, Chemical Vapor Deposition (CVD) still remains the most popular technique. At odds with their feasibility, CVD methods suffer from a number of serious drawbacks: *(i)* the use of nitrogen precursors with relatively high toxicity (*i.e.* pyridine [11,12], acetonitrile [13], ammonia [14,15]); *(ii)* tricky reaction environments based on hydrocarbons and/or hydrogen atmosphere (which necessitate specific safety precautions); *(iii)* high operation temperatures. In addition, significant loss of the N- and C-containing gaseous reagents throughout the nanomaterial synthesis, including their partial thermal decomposition into waste and toxic by-products, denotes the CVD as a low atom efficiency protocol with a weighty environmental impact and high production costs. As a result of the joint efforts of chemists, physicists and engineers, recent years have witnessed a wonderful "technological renaissance" towards the development of a number of innovative synthetic tools for the carbon nanomaterials N-decoration [16,17]. Thus, N-doped carbon-based systems, acting as metal-free catalysts in a series of industrially relevant processes, have been prepared and thoroughly characterized. Nonetheless, none of the emerging synthetic technologies fulfills the requirements of a really sustainable and environmentally friendly approach to the large-scale production of N-doped CNMs. Difficult scale-up procedures, sensitivity of the material to high temperatures, high production costs and environmentally unsafe protocols along with difficult materials handling (often caused by their prevalent powdery texture) limit an effective exploitation of N-doped CNMs in catalysis.

3.2. Experimental

3.2.1. Materials

This contribution describes a straightforward and environmentally benign methodology for the preparation of highly N-doped CNMs starting from non-toxic, raw and

abundant organic building blocks while facing all major limitations and drawbacks of the existing synthetic procedures. A shape-adaptable, highly N-doped mesoporous carbon phase is properly grown as a truly metal-free "catalytic clothing" at the surface of macroscopically shaped supports. Various matrices based on silicon carbide (β-SiC) [18,19] in the form of powder (< 40 μm), grains (150 - 400 μm), extrudates (1 x 2 mm) and foams (from mm to cm) or α-Al$_2$O$_3$ beads (mm), are selected as hosting catalyst scaffolds.

Ammonium carbonate [(NH$_4$)$_2$CO$_3$], citric acid (C$_6$H$_8$O$_7$) and glucose are the non-toxic foodstuff constituents of a homogeneous aqueous pre-catalytic phase to be used as an impregnating solution where the selected supports are soaked [20]. A controlled thermal treatment of the impregnated materials generates a carbonaceous, highly N-doped coating as a mesoporous active phase featured by a Specific Surface Area (SSA) higher than that of the pristine host matrices (Fig. S4 and Table S1).

3.2.2. Synthesis of a highly N-doped carbon-based coating (N@C) on a macroscopically shaped of SiC
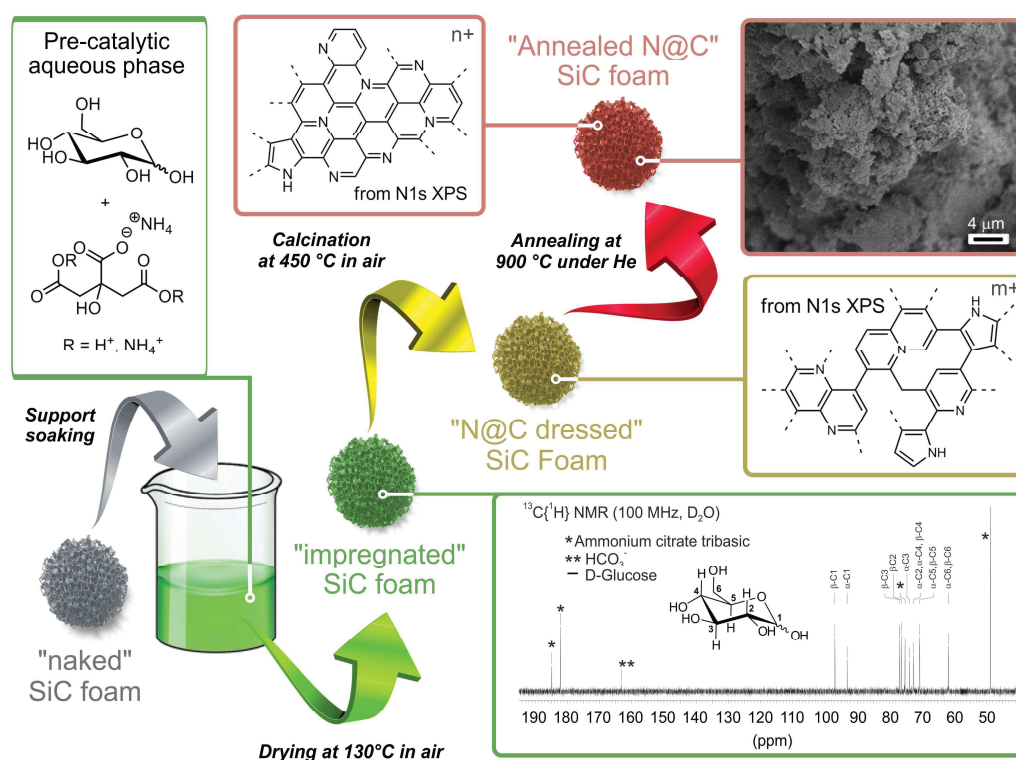

Fig. 3.1. Synthesis of a highly N-doped carbon-based coating (N@C) on a macroscopically shaped host matrix (SiC foam). Arrows refer to the sequential synthetic steps; from the material soaking and drying up to its calcination at 450 °C in air followed by annealing at 900 °C under inert atmosphere.

The soaking of SiC in the aqueous pre-catalytic phase, followed by drying in air at 130 °C, results in a thin pre-catalytic coating of the host scaffolds essentially made of glucose and basic ammonium citrate (Fig. 3.1 and S1). The soaking/drying treatment can be repeated for a number of times at will, thus increasing the thickness of the pre-catalytic deposit (Table S1). Finally, different compositions of the impregnating phase (*i.e.* a different glucose/$(NH_4)_2CO_3$/citric acid molar of the starting mixture) can be adopted to tune the ultimate material composition in terms of C/N ratio and SSA.

3.2.3. Characterizations

The N@C surface coating composition is determined by either $^{13}C\{^1H\}$ NMR spectroscopy (for the water soluble pre-catalytic phase at the surface of the impregnated composite) and N1s XPS analysis for the samples treated at 450 and 900 °C, respectively. NMR and XPS spectra refer to a model pre-catalytic phase prepared dissolving 2 g of D-Glucose, 3 g of citric acid and 2.3 g of $(NH_4)_2CO_3$ in 500 mL of ultrapure Milli-Q water and repeating the soaking/drying phase twice. SEM image refers to the typical porous texture of the N@C phase after material annealing.

3.3. Results and discussion

3.3.1. N@C/SiC characteristics

Two consecutive thermal treatments at 450 °C under air and at 900 °C under inert atmosphere "dress" the support with a N-doped mesoporous carbon phase (N@C) (Fig. 3.1 and S2) (*21*). Besides changing the ultimate material composition (*vide infra*), the annealing at 900 °C induces polymerization/extended conjugation processes which enhance the N@C adhesion to the SiC matrix while improving its electrical and thermal conductivity. Glucose represents the main carbon source in the process, while the basic ammonium citrate (in the forms of tri-, di- or mono-basic, depending on the ammonium carbonate/citric acid molar ratio used) plays the double role of N-reservoir and pore forming agent ("leavening" agent, Fig. S3) throughout the heating. In a general procedure, composites prepared from different shaped SiC matrices are obtained using 2 g of the selected scaffold to be soaked in 500 mL of an aqueous homogeneous solution prepared dissolving 11 mmol of D-Glucose (2 g), 15.6 mmol of citric acid (3 g) and varying the amount of the $(NH_4)_2CO_3$ from 7.8 mmol (0.75 g) to 23.5 mmol (2.30 g), respectively (Table S1). The as-prepared composites are conventionally designated as follows: $^AN@C/SiC_x{}^y$, where the superscript "A" denotes "annealed samples" (treatment at 900°C under inert atmosphere), "N@C/SiC" stands for the material made of a SiC support coated with a N@C active-phase, the "X" subscript illustrates the pristine SiC texture (P = powder; G = grains; E = extrudates) while the "Y" superscript displays the number of

impregnation cycles (soaking/drying). A similar nomenclature is adopted for the α-Al_2O_3-based composites.
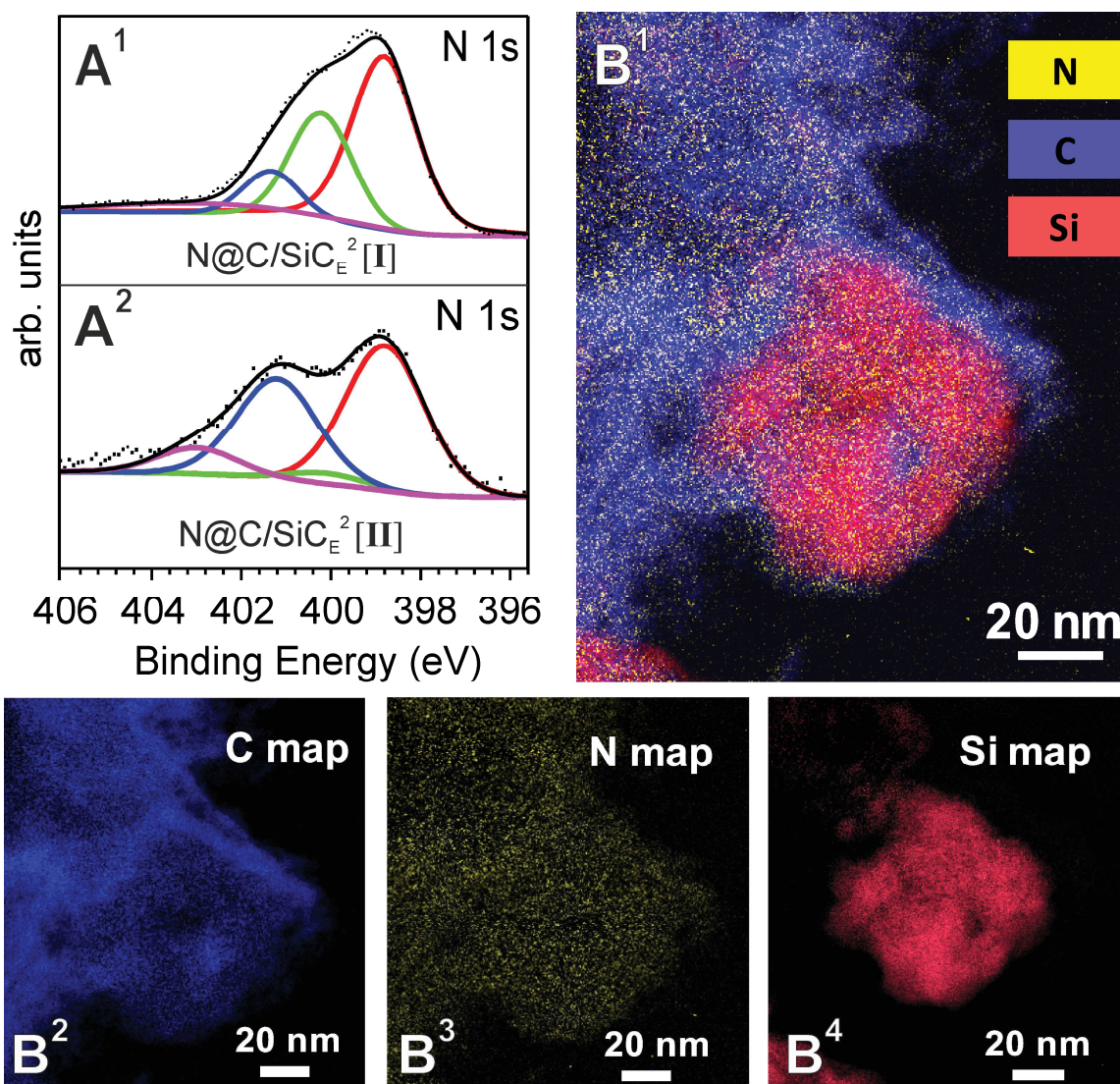
Fig. 3.2. (**A**) High-resolution N1s XPS spectra of two samples prepared from SiC extrudates as support. SiC undergoes two impregnation/drying cycles before being heated at 450 °C in air for 2h (**A^1**) and annealed at 900 °C under inert atmosphere (He) for 1h (**A^2**). (**B**) STEM-EELS analysis of the annealed ^{A}N@C/SiC$_p^2$ [**III**] sample. Colors labeling in the elemental map **B^1** are: yellow for Nitrogen, red for Silicon and blue for Carbon. Separate element maps are shown in Figures **B^2** (carbon), **B^3** (nitrogen) and **B^4** (silicon).

A marked increase of the composites Specific Surface Area (SSA) and basicity with respect to the related pristine SiC supports are observed after the thermal treatments as a

function of the impregnation cycles (Fig. S4 and S5). For the model $^AN@C/SiC_E^2$ composite [**V**] (Table S1, entry 5), the SSA increases up to five times above its original value (Fig. S4, SiC_E, SSA: 29 $m^2.g^{-1}$ *vs.* $^AN@C/SiC_E^2$, SSA: 144 $m^2.g^{-1}$) while the pH of an aqueous dispersion of [**III**] (Table S1, entry 3) grows to 9.6 from the value of 6.6 recorded for the bare SiC_P support (Fig. S5) [21]; this unusual effect [*not* observed in traditionally prepared (CVD) N-doped CNMs] is reasonably ascribed to an unprecedented high density of the surface-exposed basic N-sites.

N1s XPS analysis gives insights on the nature of the N-species available at the N@C phase. As Fig 3.2-**A**^{1} and **A**^{2} shows, the model composites [**I**] and [**II**] present three and two main components, respectively, along with a minor shoulder at higher binding energies (403,1 eV attributed to oxidized N-species). Curve fitting for sample [**I**] is consistent with the presence of pyridinic (398.8 eV – red line; 55 %), pyrrolic (400.2 eV – green curve; 29 %) and quaternary (401.3 eV; 11 %) nitrogens, respectively [Fig. 3.2-**A**^{1}]. Thermal annealing reduces the N-species to pyridinic (398.8 eV; 43 %) and quaternary N-groups (401.3 eV; 37 %) almost exclusively (Fig. 3.2-**A**^{2}). Thermo gravimetric (TGA, Fig. S6) and elemental analyses (Table S1) are then used to determine the N wt. % of the N@C phase for each sample. Measurements unveil remarkably high N-contents (normalized to the N@C mass deposit on the SiC matrix), spanning from 32 wt.% (Table S1, entry 1) for samples treated in air at 450°C to 23 wt.% for annealed composites (Table S1, entry 3). Nature and content (wt.%) of the N-species within each N@C phase is tunable as a function of several factors: *(i)* the ammonium carbonate molar fraction in the impregnating solution (Table S1, entries 1 *vs.* 4); *(ii)* the number of soaking/drying cycles undergone by the SiC matrix; *(iii)* the applied thermal treatment(s) (Table S1, entries 1 *vs.* 2 and 4 *vs.* 5). Electron energy-loss spectroscopy (EELS) in High-Resolution STEM (STEM-EELS) analysis conducted on the model $^AN@C/SiC_P^2$ composite [**III**] (Table S1, entry 3) confirms the high N-concentration at the material topmost surface [(Figs. 3.2B^1 and B^4) and (S7, S8)].

These unique properties make the N@C/SiC composites ideal single-phase candidates to act as metal-free heterogeneous catalysts (with controlled macroscopic shape) in a number of industrially relevant liquid-phase and gas-phase catalytic transformations.

3.3.2. Catalytic application of N@C/SiC as metal-free catalysts

3.3.2.1. Oxygen reduction reaction

As a first trial, a Nafion®-based ink of **III** (Table S1, entry 3), is scrutinized in the model liquid-phase electrochemical oxygen reduction reaction (ORR) under alkaline environment (KOH 0.1 M). Figure 3.3A shows its catalytic performance [rotating ring-disk electrode (RRDE) measurements] along with that of a reference 20 wt.% Pt/C catalyst

(Nafion®-based ink of 20 wt % Pt on Vulcan® XC72) and those of the respective bare supports (Nafion®-based ink of SiC$_p$ and Vulcan® XC72) under identical conditions.
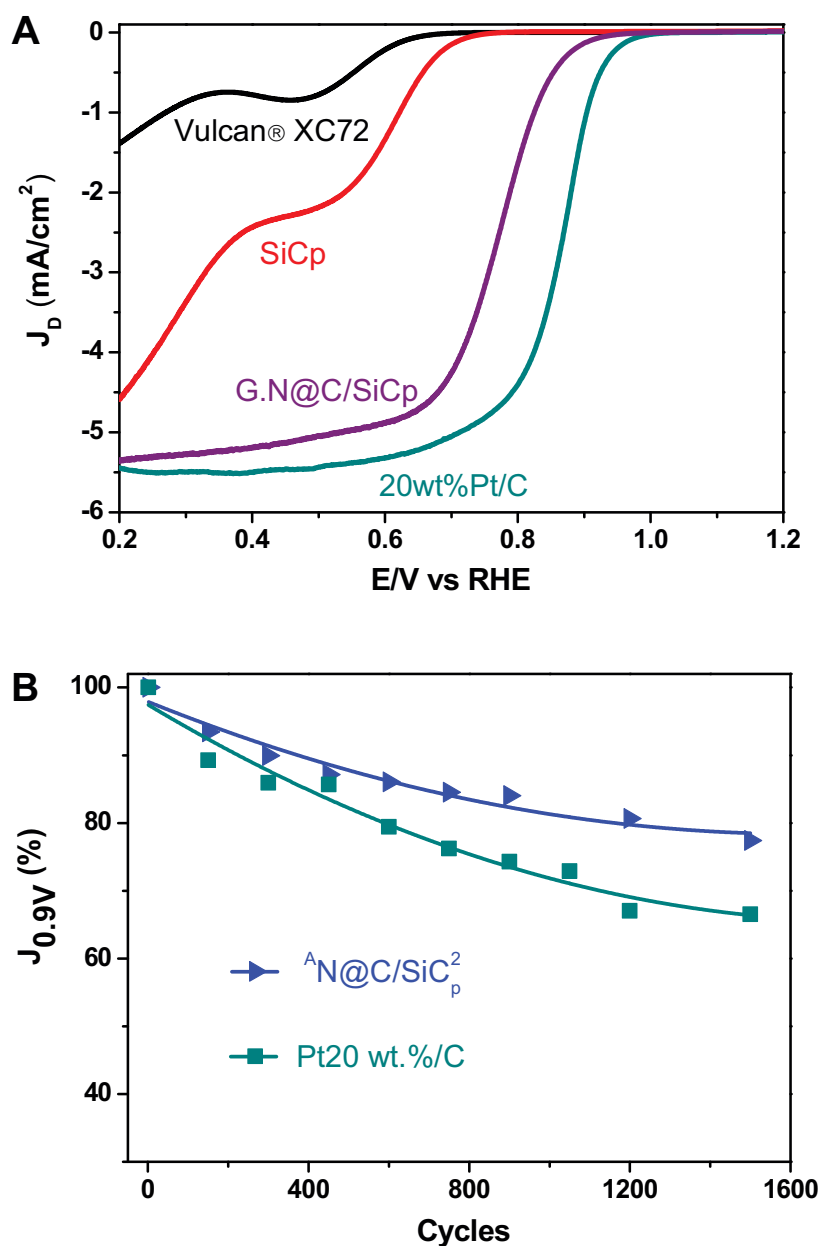
Fig. 3.3. Catalytic applications: (**A**) RRDE potential curves at 25 °C for ORR in O$_2$ saturated 0.1 M KOH solution recorded by a rotating ring-disk GC electrode [GC disk, A = 0.238 cm^2]. Curves recorded at 1600 rpm refer to [**III**] (< 40 µm, 450 µg.cm^{-2}), Vulcan® XC72 (100 µg.cm^{-2}), 20 wt.% Pt/C (Vulcan® XC72, 25 µg$_{Pt}$.cm^{-2}) and SiC$_P$ (< 40 µm, 450 µg.cm^{-2}). (**B**) Long-term stability of [**III**] and 20 wt.% Pt/C catalysts at 25 °C and 1600 rpm in O$_2$ saturated 0.1 M KOH; the test was carried out for 1,500 cycles between 1.0 and 0.6 mV.

The Koutecky-Levich (K-L) plots of both metal-free and Pt/C-based electrocatalysts, as obtained from the respective linear sweep voltammograms (LSVs) at 0.4 V, present similar curve slopes consistent with a four-electron mechanism operating on both systems (Fig. S9A). Further proof of evidence is provided by low Pt-ring currents measured for both systems at the RRDE due to the H_2O_2 % produced throughout the electrochemical processes (Fig. S9B). Accordingly, the average number of electrons transferred (n) per mol of O_2 are calculated in 3.6 and 4 on **III** and on the Pt/C catalysts, respectively.

The onset potential values (E_{on}) are very close to each other (~ 1V), while the half-wave potential ($E_{1/2}$) measured on **III** is fixed about 45 mV down (over potential) to that of the Pt/C-based system. Overall, $E_{1/2}$ and current density values (J) measured at 0.9V reveal only a slightly reduced catalytic performance of the metal-free system compared with the classical Pt-containing one. On the other hand, a remarkably higher stability of **III** compared to that of the Pt/C-based system is observed for long-term cycling RRDE tests (measurements in the 0.6 - 1.0 V range at 100 mV.s^{-1}, 1600 rpm in 0.1 M KOH at 25 °C). As Fig. 3.3B shows, **III** retains about 80 % of its initial ORR activity after 1500 cycles, whereas that of the Pt/C-based system drops down to 65 % of its initial catalytic performance under the same experimental conditions. Such a behavior, similarly observed for the ORR by vertically-aligned, N-doped carbon nanotubes (N-VCNTs) (*1*), strengthens the relevance of the N@C/SiC composites as valuable, cheap and easy-to-make alternative to the platinum-group metal-based catalysts of the *state-of-the-art*.

3.3.2.2. Selective oxidation of H_2S

The high temperature oxidation of H_2S residues from refinery tail gas effluents is selected as a model high-temperature gas-phase reaction to be accomplished on the basis of the developed metal-free catalysts technology, in agreement with the current environmental legislation. The ^{A}N@C/SiC$_E$^{2} composite [**II**] (Table S1, entry 2) is then prepared from extrudate SiC, following the sequential procedure outlined in Fig.3.1.

As Fig. 4A shows, at T = 210 °C with a O_2/H_2S molar ratio of 2.5 and a 0.3 h^{-1} Weight Hourly Space effluent Velocity (WHSV), **II** exhibits a remarkably high desulfurization activity (> 97% of H_2S conversion) with a sulfur selectivity closed to 70 %. Notably, no catalyst deactivation takes place under these severe conditions even after prolonged (> 100 h) reaction times (Fig. 3.4A) that mirrors with negligible leaching effects of the N@C active phase. The metal-free nature of the catalyst active phase (N@C) also prevents undesired sintering side-effects classically responsible for catalysts deactivation in metal-containing systems. For the sake of completeness, the model Fe_2O_3/SiC catalyst is selected as a reference desulfurization benchmark [22,23] and tested under comparative experimental conditions. Despite its high selectivity (> 90 %), the Fe_2O_3/SiC$_E$ catalyst is featured by a markedly lower

desulfurization activity when compared with **II** (Fig. 3.4B). The high surface density of active sites at the N@C catalyst is very likely responsible for the higher H_2S conversion measured ($\approx$ 95 %) with respect to the Fe-based system.

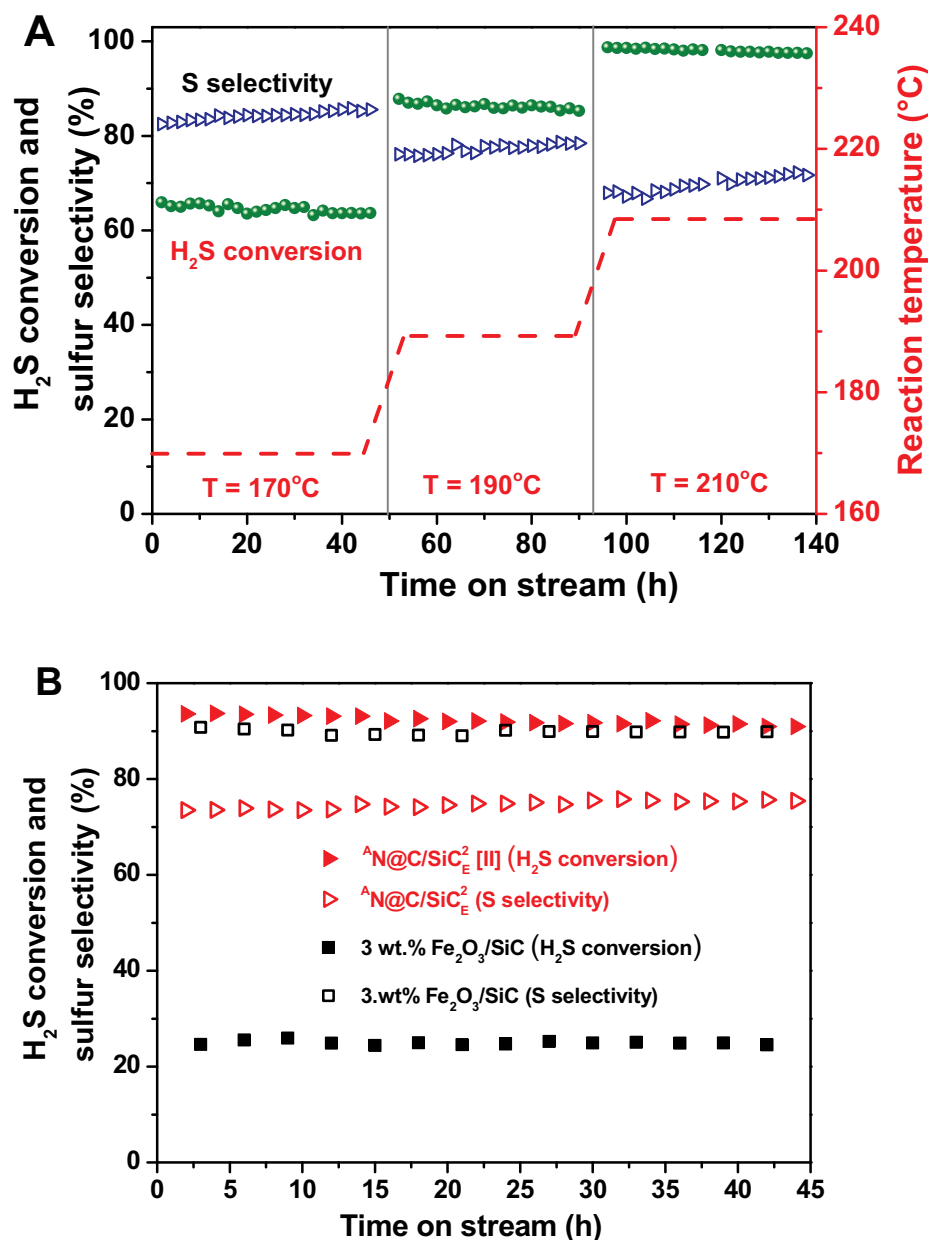**Fig. 3.4.** (**A**) Desulfurization performance on [**II**] as a function of the reaction conditions (1g of [**II**], O_2/H_2S molar ratio = 2.5, WHSV = 0.3 h^{-1}). (**B**) Comparative study of H_2S conversion and sulfur selectivity over [**II**] and 3 wt.% Fe_2O_3/SiC catalysts (operative conditions: T = 210 °C, 1g of catalyst, O_2/H_2S molar ratio = 2.5, WHSV = 0.6 h^{-1}).

On the other hand, the combination of a high active sites density at the material topmost surface with the highly porous structure of the SiC matrix (ideal for optimal reagents mixing degree and catalyst/reagent contacts) translates into a moderate selectivity towards elemental sulfur. Improved catalyst performance (compared to the Fe-based system), both in terms of H_2S conversion and S selectivity, are given by an N@C active phase grown on α-Al_2O_3 beads as an alternative lower surface area hosting support (Table S1, entry 6). Similarly to the SiC-based systems, the N@C/Al_2O_{3B}[2] catalyst (**VI**) is prepared through impregnation/drying/thermal treatment sequences according to the general scheme outlined in Fig. 3.1 and (Table S1, entry 6). Such a result witnesses the high versatility of the proposed "dressing" synthetic procedure, applicable to an assorted range of host matrices that can be selected on the basis of the ultimate catalytic downstream application. As shown in Fig. S10, **VI** provides a remarkably high desulfurization activity (over 7 0% of H_2S conversion) with a sulfur selectivity close to 90 % under regime conditions. In spite of slightly lower H_2S conversions, selectivity higher than 90 % are also achieved with the same catalyst by means of a reduction of the O_2/H_2S molar ratio.

3.4. Conclusion

In summary, the proposed methodology offers a highly sustainable and valuable approach to the generation of highly adaptable N-doped, carbon porous active phases (N@C) capable of "dressing" different macroscopic host supports. The porous N@C carbon phases are conveniently prepared from non-toxic and cheap raw materials such as ammonium carbonate, glucose and citric acid and they are grown in the form of tight coatings on different supports (powders, grains, beads, extrudates and foams) selected on the basis of the specific needs of a gas-phase and/or liquid-phase reactor. At odds with the classical CVD technique, C and N sources for this methodology are solid feedstock, neither toxic nor dangerous or explosive. Most importantly, their conversion into highly N-doped porous carbon phases meets the requirements of atom efficiency, negligible environmental impact and low production costs necessary for the exploitation of a truly metal-free technology for industrial key-processes at the heart of renewable energy technology and environmental protection. The successful use of these basic metal-free N@C catalysts in two fundamental catalytic transformations is also described: 1) the liquid-phase electrochemical oxygen reduction reaction in alkaline environment and 2) the high temperature gas-phase H_2S partial oxidation to elemental sulfur. For both processes, the N@C composites appear as ideal candidates capable of offering high (and to some extent better) catalytic performance and long-term active-phase stability compared to the classical metal-based systems (including platinum-group-metals - PGMs) of the *state-of-the-art*. Finally, the easy and cost-efficient up-scale synthesis of stable N@C active phases on different macroscopic host supports paves the way to further material exploitation in other catalytic processes where the combination of exposed

basic sites with good electrical conductivity and thermal stability of the active phases represents the essential pre-requisite to reach high catalyst performance.

Acknowledgments

References

[1]   K. Gong, F. Du, Z. Xia, M. Durstock, L. Dai, Science 323 (2009) 760.

[2]   Y. Li, W. Zhou, H. Wang, L. Xie, Y. Liang, F. Wei, J.-C. Idrobo, S.J. Pennycook, H. Dai, Nat. Nanotechnol. 7 (2012) 394.

[3]   R. Liu, D. Wu, X. Feng, K. Müllen, Angew. Chem. Int. Ed. 49 (2010) 2565.

[4]   K. Chizari, A. Deneuve, O. Ersen, I. Florea, Y. Liu, D. Edouard, I. Janowska, D. Begin, C. Pham-Huu, ChemSusChem 5 (2012) 102.

[5]   D.S. Su, S. Perathoner, G. Centi, Chem. Rev. 113 (2013) 5782.

[6]   F. Bonaccorso, L. Colombo, G. Yu, M. Stoller, V. Tozzini, A.C. Ferrari, R.S. Ruoff, V. Pellegrini, Science 347 (2015) 1246501.

[7]   S. Yang, X. Feng, X. Wang, K. Müllen, Angew. Chem. Int. Ed. 50 (2011) 5339.

[8]   Y. Lin, X.-Y. Li, A.L. Willis, C. Liu, G. Chen, S.J. Weiss, Nat. Commun. 5 (2014) 3070.

[9]   C. Zhou, J. Kong, E. Yenilmez, H. Dai, Science 290 (2000) 1552.

[10]   X. Wang, X. Li, L. Zhang, Y. Yoon, P.K. Weber, H. Wang, J. Guo, H. Dai, Science 324 (2009) 768.

[11]   C. Shan, W. Zhao, X.L. Lu, D.J. O'Brien, Y. Li, Z. Cao, A.L. Elias, R. Cruz-Silva, M. Terrones, B. Wei, J. Suhr, Nano Lett. 13 (2013) 5514.

[12]   Y. Xue, B. Wu, L. Jiang, Y. Guo, L. Huang, J. Chen, J. Tan, D. Geng, B. Luo, W. Hu, G. Yu, Y. Liu, J. Am. Chem. Soc. 134 (2012) 11060.

[13]   Y. Xia, G.S. Walker, D.M. Grant, R. Mokaya, J. Am. Chem. Soc. 131 (2009) 16493.

[14]   T. Susi, A. Kaskela, Z. Zhu, P. Ayala, R. Arenal, Y. Tian, P. Laiho, J. Mali, A.G. Nasibulin, H. Jiang, G. Lanzani, O. Stephan, K. Laasonen, T. Pichler, A. Loiseau, E.I. Kauppinen, Chem. Mater. 23 (2011) 2201.

[15]   L. Qu, Y. Liu, J.-B. Baek, L. Dai, ACS Nano 4 (2010) 1321.

[16]   W. He, C. Jiang, J. Wang, L. Lu, Angew. Chem. Int. Ed. 53 (2014) 9503.

[17]   Y. Meng, X. Zou, X. Huang, A. Goswami, Z. Liu, T. Asefa, Adv. Mater. 26 (2014) 6510.

[18]   Y. Liu, O. Ersen, C. Meny, F. Luck, C. Pham-Huu, ChemSusChem 7 (2014) 1218.

[19]   P. Nguyen, C. Pham, Appl. Catal. Gen. 391 (2011) 443.

[20]   Y. F. Liu, L. Nguyen-Dinh, et al., Eur. Pat. Appl. No. EP 15-152038 (2015).

[21]   R. Arrigo, M. Hävecker, S. Wrabetz, R. Blume, M. Lerch, J. McGregor, E.P.J. Parrott, J.A. Zeitler, L.F. Gladden, A. Knop-Gericke, R. Schlögl, D.S. Su, J. Am. Chem. Soc. 132 (2010) 9616.

[22]   N. Keller, C. Pham-Huu, M.J. Ledoux, Appl. Catal. Gen. 217 (2001) 205.

[23]   P. Nguyen, D. Edouard, J.-M. Nhut, M.J. Ledoux, C. Pham, C. Pham-Huu, Appl. Catal. B Environ. 76 (2007) 300.

3.5. Supplementary information

S − 1. Materials and methods: General procedure for the synthesis of highly N-doped mesoporous carbon-based coating (N@C) on macroscopically shaped supports

In a typical procedure, 2 g of D-Glucose and 3 g of citric acid were added in 500 mL of ultrapure Milli-Q water at room temperature. A proper amount of ammonium carbonate (*i.e.* 0.75, 1.5 or 2.3 g) was then added in a single portion to the solution at r.t. and an instantaneous effervescence due to CO_2 evolution was observed. The obtained clear solution was exploited as an aqueous pre-catalytic phase for the soaking/impregnation of a series of suitable supports (2 g): SiC extrudates (29 $m^2 \cdot g^{-1}$; SICAT) and powder (25 $m^2 \cdot g^{-1}$; SICAT), SiC foams (30 $m^2 \cdot g^{-1}$; SICAT) and α-Al_2O_3 beads (6 $m^2 \cdot g^{-1}$; Sasol). The wet solids were slowly heated (10 °C·min^{-1}) in air from room temperature to 130 °C and kept at this temperature for 1 h. The as obtained dry solids were further impregnated with the same three component solution for several times at will, until the desired loading is achieved. The solids underwent a thermal treatment in air at 450 °C (2 °C·min^{-1}) for 2 h during which the macroscopic host support was coated with a highly N-doped mesoporous carbon phase. The as-prepared solids can be further heated in He atmosphere at 900 °C (10 °C·min^{-1}) for 2 h in order to increase the graphitization/conjugation degree of the final materials.

S − 2. Materials characterization

^{1}H and ^{13}C{^{1}H} NMR spectra were obtained on either a Bruker Avance DRX-400 spectrometer or a Bruker Avance 300 MHz instrument. Chemical shifts are reported in ppm (δ) relative to TMS.

Thermogravimetric analyses (TGA) were performed under air (100 mL·min^{-1}) on an EXSTAR thermogravimetric analyzer (TG/DTA) Seiko 6200.

The specific surface area of the different samples was measured by the BET method using N_2 as adsorbent at liquid nitrogen temperature (TriStar sorptometer). Before measurement, the samples were outgassed at 200 °C overnight.

XPS measurements were performed on a MULTILAB 2000 (THERMO VG) spectrometer equipped with Al Kα anode (*hv* = 1486.6 eV) with 10 min of acquisition. Peak deconvolution has been accomplished with "Avantage" program from Thermoelectron Company. The C1s peak at 284.6 eV was used to correct charging effects. Shirley backgrounds were subtracted from the raw data.

The gross morphology of the materials was observed by scanning electron microscopy (SEM) on a JEOL F-6700 FEG with an accelerating voltage of 10 kV.

Transmission electron microscopy (TEM) measurements were performed using a JEOL 2100F operating at 200 kV, equipped with GATAN Tridiem imaging filter and an aberration-corrected condenser.

Electron energy-loss spectroscopy (EELS) analysis was performed in the scanning mode (STEM) with 30 mrad convergence angle and 25 mrad collection angle. The spectral image was acquired in 20×33 pixels with an exposure time of 1 s for each pixel. The energy resolution was 1.7 eV. Elemental signals were extracted from the Si-L, C-K, N-K and O-K edges, respectively. Energy-filtered TEM (EFTEM) measurements were acquired by a three-window method with energy slits of 8 eV, 30 eV and 20 eV and acquisition times of 10 s, 30 s and 40 s for Si, C and N, respectively. Prior to the analysis the sample was covered by a thin layer of gold in order to reduce charging during the analysis.

S – 3. Catalytic Reactions

S – 3.1. Oxygen Reduction Reaction (ORR)

Electrochemical studies were performed at 25 °C in a three-electrode cell in 0.1 M KOH supporting electrolyte, using an Autolab PGSTAT30 (Eco Chemie, The Netherlands) potentiostat equipped with an analogue linear sweep generator at a scan rate of 10 mV s^{-1}. Mercury oxide (Hg/HgO) electrode and Pt-wire electrode were used as reference and counter electrode, respectively. Unless otherwise stated, all potentials hereinafter are referred to the reversible hydrogen electrode (RHE). The electrochemical impedance spectroscopic (EIS) is used to determine the resistance of the electrolyte solution.

RRDE (rotating-ring disk electrode) measurements were performed on a Pine electrode (PINE AFE6R2GCPT, glassy carbon disk: 5.5 mm diameter and 0.2376 cm^2 geometrical area, Pt ring: 0.234 cm^2). 10.0 mg of catalyst, 5 mL isopropanol and 50 μL Nafion solution (5 wt.%) were ultrasonically mixed to form a homogenous catalyst ink that was drop-casted onto the GC electrode and dried at room temperature. The reference Pt curve was recorded with a 20 wt.% Pt/VXC-72 (Sigma) catalyst with a loading of 25 μg$_{Pt}$ .cm^{-2}.

All aqueous solutions were prepared using ultrapure water (18 MΩ.cm < 3 ppb TOC) and supra-pure KOH (Sigma-Aldrich). In O_2-reduction experiments oxygen was constantly bubbled through the solution in order to maintain the saturation level and the ring potential was set at 1.2 V *vs*. RHE. Collection efficiency (N) was calculated from the experimental data obtained in 10 mM K_3FeCN_6 in 0.1 M NaOH at standard measurement conditions (potential sweep rate 10 mV.s^{-1}, 25°C). The collection efficiency for the Pt(20%)/VXC-72 electrode was found to be 37 % which displays the same value as reported by Chlistunoff [1].

The catalyst four-electron selectivity was evaluated on the basis of the H_2O_2 yield, calculated from the following equation (Eq. (3.1)):

$$H_2O_2(\%) = 200(J_R/N)/(J_R/N\text{-}J_D) \qquad\qquad (3.1)$$

Here, J_D and J_R are the disk and ring currents density, respectively, and N is the ring collection efficiency.

The electron transfer number can be calculated in two ways. The first is to use the ring current and the disk current (Eq. (3.2)):

$$n = \text{-} 4J_D/(J_R/N\text{-}J_D) \qquad\qquad (3.2)$$

The second way to calculate n is by using the first-order Koutecky-Levich equation (Eq. (3.3)):

$$1/J_D = 1/j_k + 1/j_d \qquad\qquad (3.3)$$

Where: j_k is the kinetic current density and j_d is the diffusion-limited current density through the expression $j_d = Bf^{1/2} = 0.2nF\gamma^{-1/6}D_{O2}{}^{2/3}C_{O2}f^{1/2}$. Here n is the average electron transfer number; F is the Faraday constant; γ is the kinematic viscosity of the electrolyte; D_{O2} is the oxygen diffusion coefficient (1.95×10^{-5} cm^2.s^{-1}); C_{O2} is the bulk oxygen concentration in the electrolyte (1.15×10^{-3} mol.dm^{-3}); f is the angular velocity of the electrode. The kinetic current density (j_k) and the Koutecky-Levich slope ($1/B$) can be obtained from a plot of $1/j$ versus $1/f^{1/2}$.

S – 3.2. Partial Oxidation of H$_2$S into Elemental Sulfur

The catalytic selective oxidation of H$_2$S by oxygen (Eq. (3.4)) was carried out in an all glass tubular reactor working isothermally at atmospheric pressure.

$$H_2S + \tfrac{1}{2}\, O_2 \rightarrow 1/n\, S_n + H_2O \qquad \Delta H = -222 \text{ kJ/mol} \qquad (3.4)$$

A proper amount of catalyst (300 mg) was placed on silica wool in a tubular Pyrex reactor (inner diameter: 16 mm) located inside a vertical tubular electrical furnace. The temperature was controlled by a K-type thermocouple and a Minicor regulator. The gas mixture of the reactant feed including H$_2$S (1 vol.%), O$_2$ (1 to 2.5 vol.%), H$_2$O (30 vol.%) and He (balance) was passed downward through the catalyst bed. The gases flow rates were monitored by Brooks 5850TR mass flow controllers linked to a control unit. The weight hourly space velocity (WHSV) was fixed at 0.3 - 0.6 h^{-1} and the O$_2$/H$_2$S molar ratio was settled to 2.5, unless otherwise stated.

The reaction was conducted in a continuous mode. The sulfur formed in the reaction was vaporized (because of the high partial pressure of sulfur at the adopted temperatures) and then condensed at the exit of the reactor in a trap maintained at room temperature. The analysis of the inlet and outlet gases was performed online using a Varian CP-3800 gas chromatograph (GC) equipped with a Chrompack CP-SilicaPLOT capillary column and a thermal catharometer detector (TCD), which allowed the detection of O$_2$, H$_2$S, H$_2$O and SO$_2$.
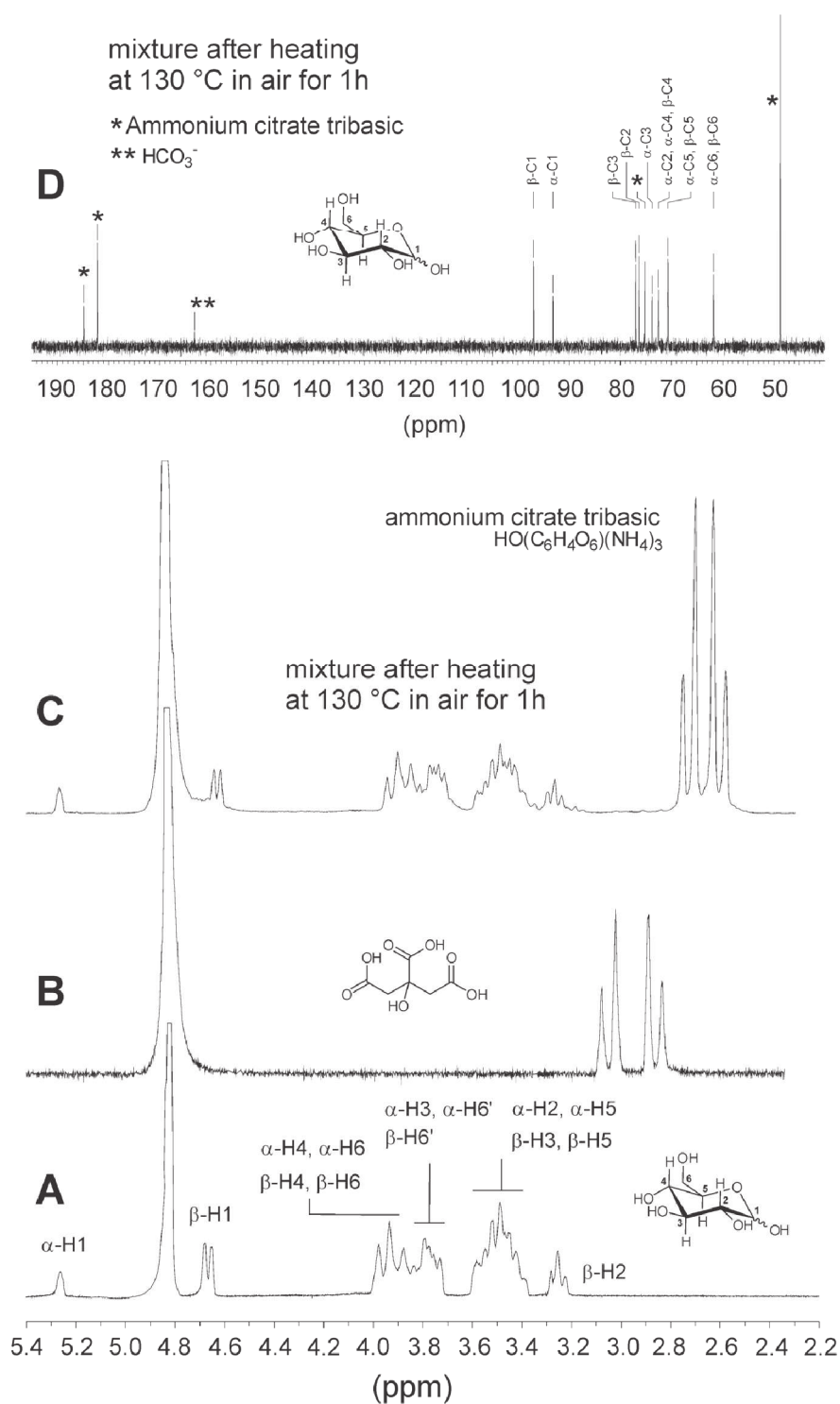
Fig. S1. ^{1}H and ^{13}C{^{1}H} NMR spectra (D$_2$O, 298 K) of the three component mixture after heating at 130 °C for 1h (C, D) and ^{1}H NMR spectra (D$_2$O, 298 K) of the two separate components, D-Glucose (A) and citric acid (B). From a close inspection of the NMR spectra, the first thermal treatment at 130 °C of the three-component aqueous solution results into a homogeneous solid mixture of α,β-D-glucopyranose and ammonium citrate tribasic. Traces of either CO$_3^{2-}$ or HCO$_3^{-}$ are observed after this phase (D).
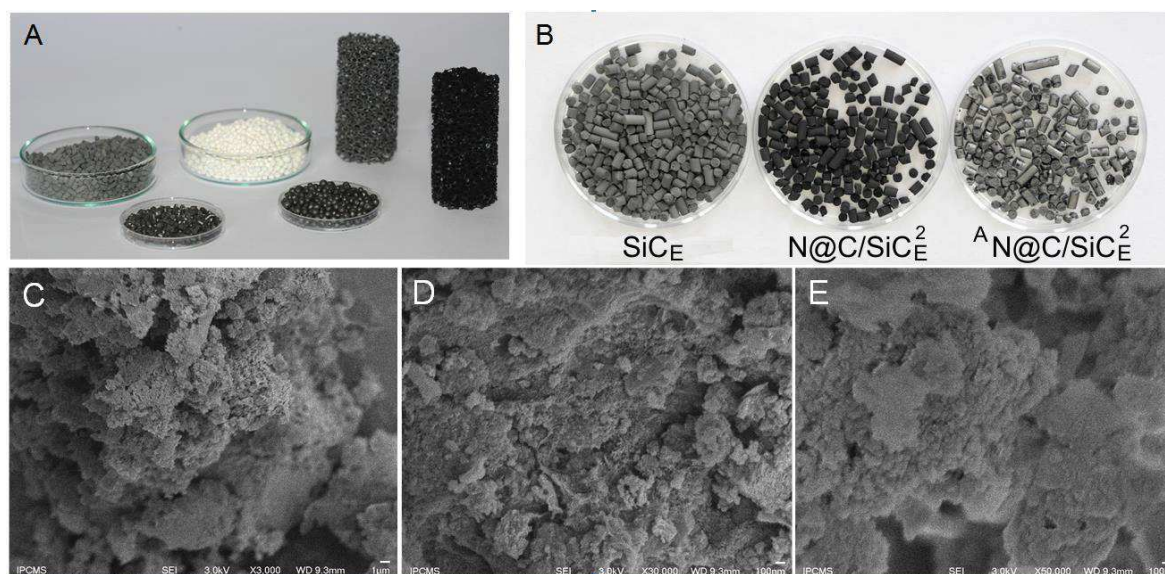
Fig. S2. Digital photos of pristine SiC supports with different macroscopic shapes (A) and SiC extrudate (SiC_E) samples (B) after N@C-coating and thermal treatment at 450 °C in air ($N@C/SiC_E^2$) (Table S1, entry 1) and annealing at 900 °C under He atmosphere ($^AN@C/SiC_E$). Typical SEM images illustrating the N@C porous texture of the $^AN@C/SiC_E^2$ sample (Table S1, entry 2) at different magnifications.
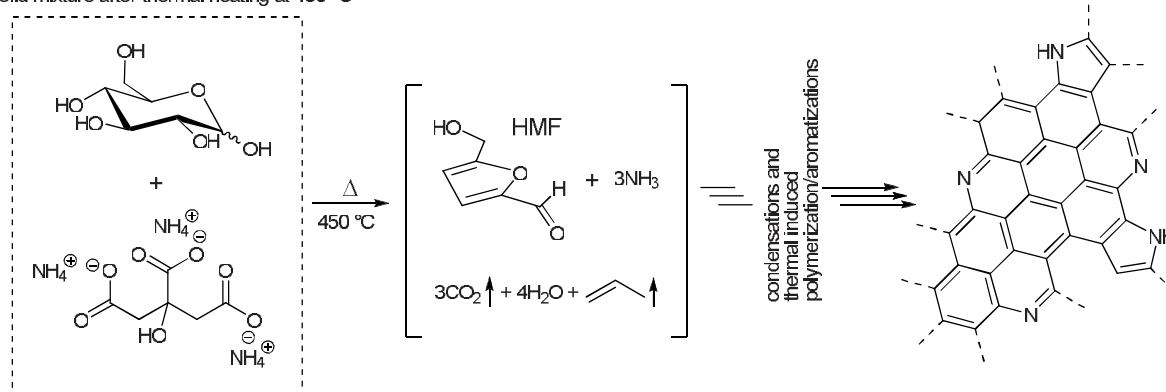
Fig. S3. Proposed mechanism for the thermal transformation of α,β-D-glucopyranose and ammonium citrate tribasic (pre-catalyst phase) into a N-rich, heteroaromatic, graphene-like network (N@C - catalytically active phase). The thermal treatment at 450 °C is supposed to start the progressive dehydration of the sugar into the 5-hydroxymethyl-furfural (5-HMF) [2]. Under these conditions, ammonium citrate tribasic, is expected to act as both a N-reservoir for the generation of N-containing heterocycles [3,4] and a pore-forming agent (due to its complete decomposition into volatiles like NH_3, CO_2, H_2O and propene) thus contributing to the ultimate material mesoporosity.
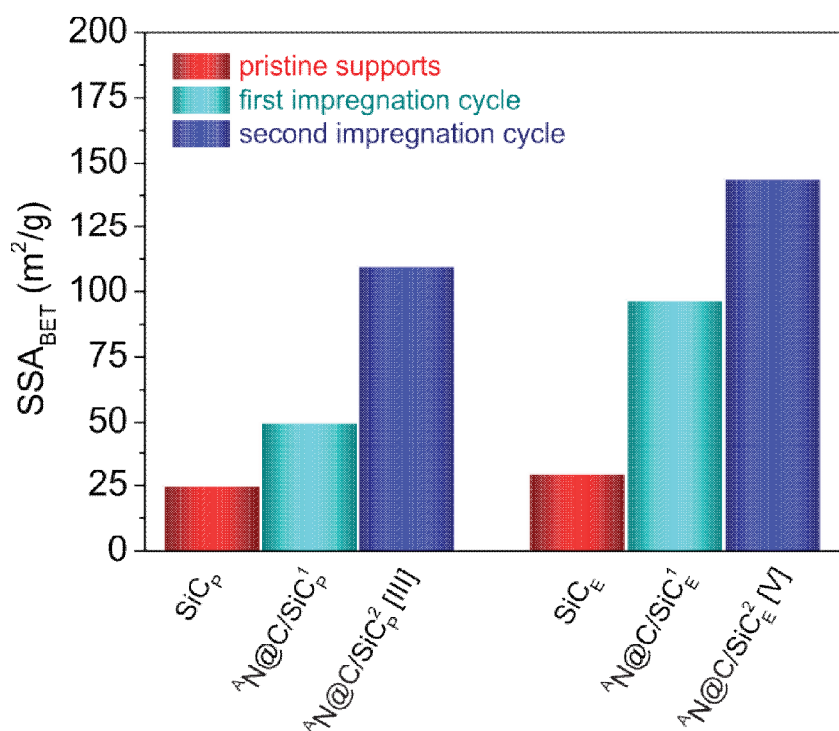
Fig. S4. BET Specific Surface Area of annealed composites after one or two impregnation cycles of differently shaped SiC matrices. For samples [**III**] and [**V**], refer to Table S1.
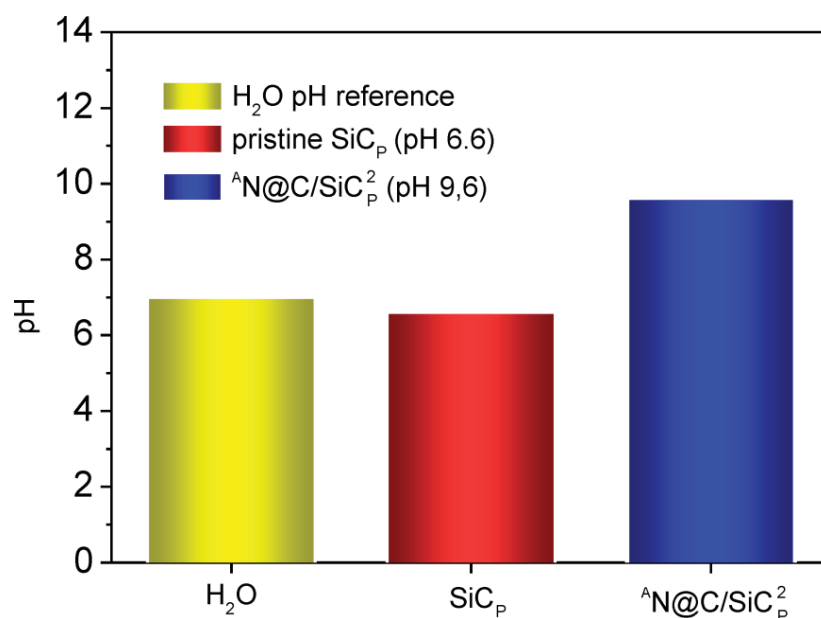
Fig. S5. Acid-basic properties of an aqueous dispersion of [**III**] (Table S1, entry 3) at comparison with its pristine counterpart (bare SiC_P).
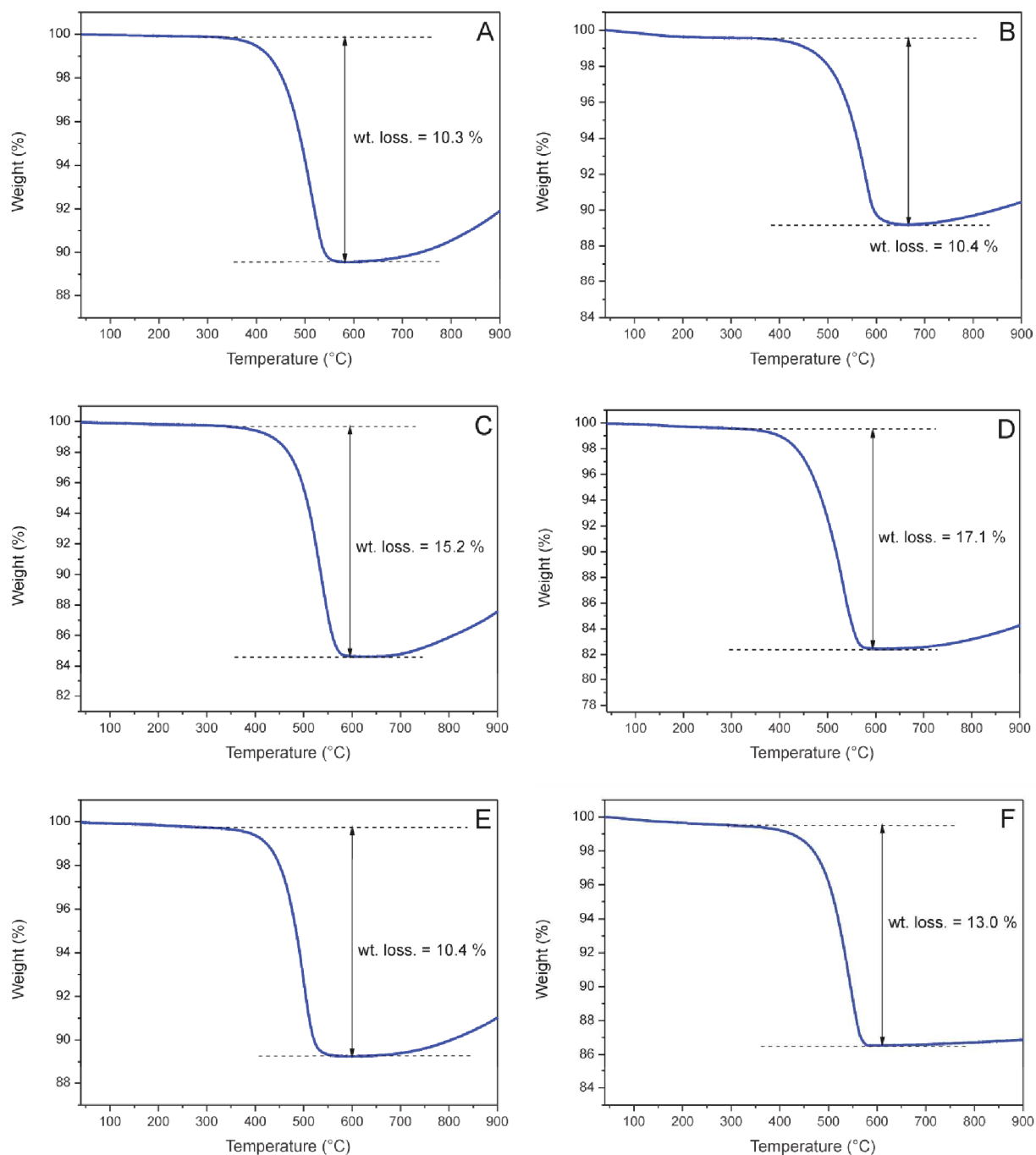
Fig. S6. TGA profiles of N@C/SiC composites (40-900 °C, 5°C/min, air 100 mL/min). All samples are dried at 40°C at 0.05 torr, overnight before each measurement. Weight losses refer to the complete burning of the N@C deposit at the SiC matrices: **A)** N@C/SiC$_E^2$ [**I**], see Table S1, entry 1. B) ^{A}N@C/SiC$_E^2$ [**II**], see Table S1, entry 2. C) ^{A}N@C/SiC$_P^2$ [**III**], see Table S1, entry 3. D) N@C/SiC$_E^2$ [**IV**], see Table S1, entry 4. E) ^{A}N@C/SiC$_E^2$ [**V**], see Table S1, entry 5. F) ^{A}N@C/α-Al$_2$O$_{3B}^2$ [**VI**], see Table S1, entry 6.

Table S1. Physico-chemical characterization of N@C phases of various SiC/Al_2O_3-based composites.[a].

Entry	Sample[b] [Cat. label]	1st impregn. cycle $(NH_4)_2CO_3$ (g)	2st impregn. cycle $(NH_4)_2CO_3$ (g)	Thermal treatment/ atmosphere	N@C wt % loading from TGA	N wt % from EA[c]	N wt % at the N@C phase[d]	SSA (m^2/g)	Pyridinic	Pyrrolic	Graphitic	Oxidized
									Nitrogen species (%)[e]			
1	N@C/SiC$_E^2$ [I]	2.3	0.75	450 °C/Air	10.3	3.34	32.4	108	55.2	28.8	11.2	4.8
2	^{A}N@C/SiC$_E^2$ [II]	2.3	0.75	900 °C/He	10.4	2.12	20.4	109	43.2	7.5	37.2	12.1
3	^{A}N@C/SiC$_P^2$ [III]	2.3	0.75	900 °C/He	15.2	3.55	23.4	110	44.6	17.4	32.4	5.6
4	N@C/SiC$_E^2$ [IV]	2.3	1.5	450 °C/Air	17.1	5.11	29.9	138	45.9	27.6	19.6	6.9
5	^{A}N@C/SiC$_E^2$ [V]	2.3	1.5	900 °C/He	10.4	1.61	15.5	144	38.9	10.5	37.9	12.7
6	^{A}N@C/α-Al$_2$O$_{3B}^2$ [VI]	2.3	0.75	900 °C/He	13.0	1.47	12.9	91	40.6	11.2	35.6	12.6

[a] All $SiC/α-Al_2O_3$-composites are prepared by repeating the soaking/impregnation step of the pristine SiC support twice and using impregnating solutions prepared dissolving 2 g of D-Glucose, 3 g of citric acid and $(NH_4)_2CO_3$ (from 0.75 to 2.3 g) in 500 mL of ultrapure Milli-Q water. [b] Composites are designated as follows: ^{A}N@C/SiC$_x^y$ where superscript "A" denotes "annealead samples" (treatment at 900 °C under inert atmosphere), "N@C/SiC" or "N@C/α-Al$_2$O$_3$" stand for the $SiC/α-Al_2O_3$ material coating with the (N@C) active-phase, "X" subscript illustrates the pristine support form (P = powder; E = exstrudates; B = beads) while "Y" superscript displays the number of impregnation cycles. [c] Elemental analysis: average values calculated over three independent runs per sample. [d] N wt.% normalized to the N@C content (active phase) calculated by TGA analysis. [e] Estimated from fitting of the N 1s XPS profile.
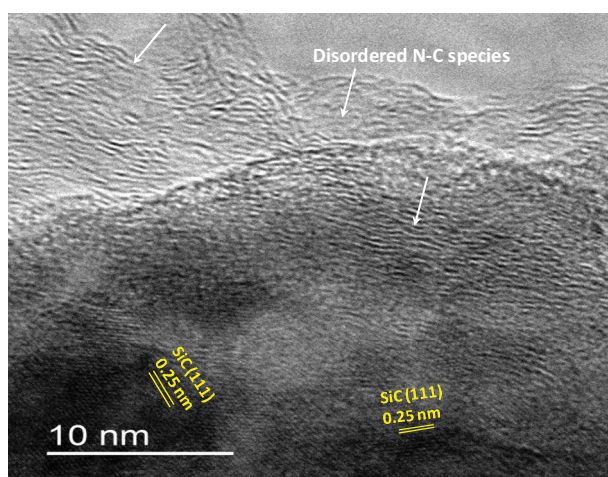
Fig. S7. HR-TEM high-resolution image of the ^{A}N@C/SiC$_p^2$ [**III**] sample (Table S1, entry 3) showing the N@C coating phase in the form of disordered and crumpled N-doped carbons at the SiC support.
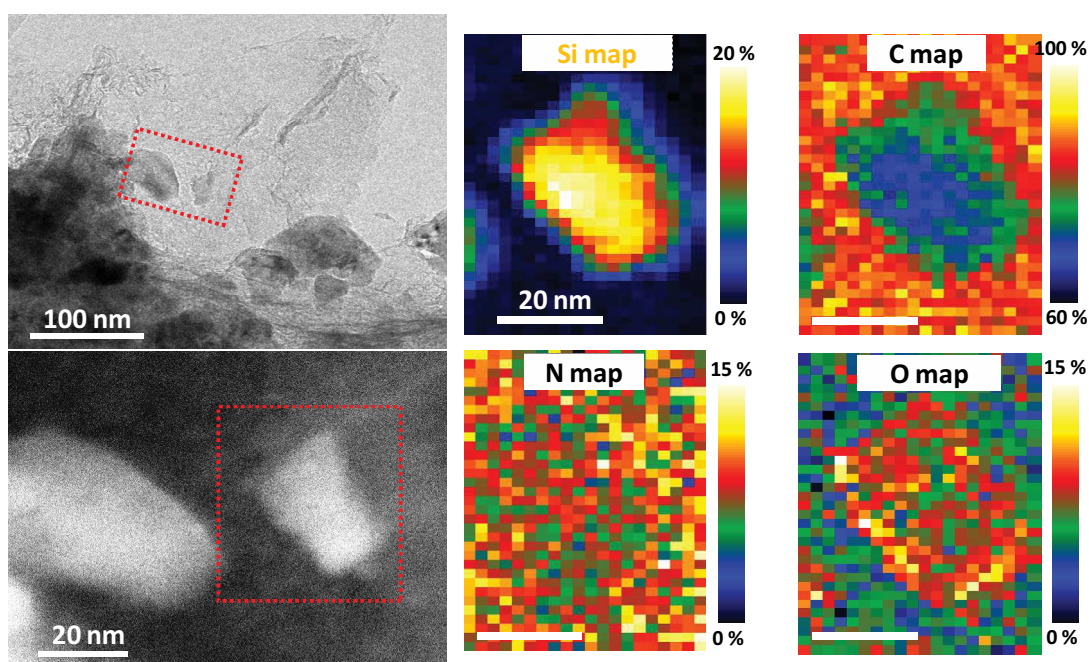
Fig. S8. Morphology of ^{A}N@C/SiC$_p^2$ [**III**] sample (Table S1, entry 3). An overview bright field TEM image (Top left). A high-angle annular-dark-field image (STEM-HAADF) which was taken from the area marked by the red dashed-line box in the top left image (Bottom left). Elemental maps of Silicon, Carbon, Nitrogen and Oxygen, respectively taken from the area highlighted by the red dashed-line box in the bottom-left image (Four color images on the right side). The colors correspond to the relative atomic composition ratio indicated by the adjacent vertical color bars.
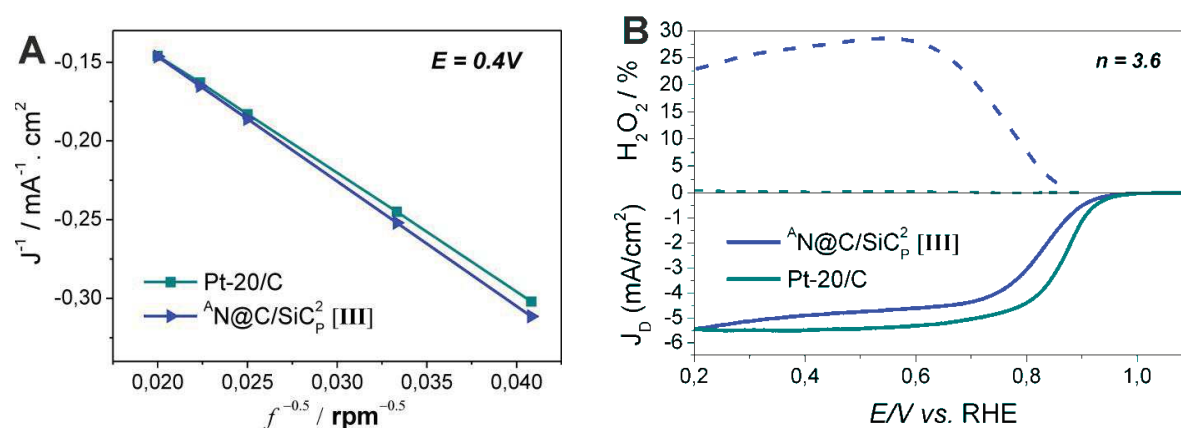
Fig. S9. (A) K-L plots for [**III**] and the reference 20 wt.% Pt/C catalysts as obtained from the respective LSVs at 0.4 V (vs. RHE). Parameters used: O_2 concentration (C), 1.15×10^{-3} mol.L^{-1}; O_2 diffusion coefficient (D), 1.95×10^{-5} cm^2.s^{-1}; kinematic viscosity (ν) of the electrolyte solution, 0.008977 cm^2.s^{-1}. **(B) [down]** RRDE current - potential curves at 25 °C for ORR in O_2 saturated 0.1 M KOH solution recorded by using a rotating ring-disk GC electrode [GC disk, A = 0.238 cm^2] with **(B) [top]** Pt ring [A = 0.234 cm^2]. Both samples ([**III**] and 20 wt.% Pt/C) are measured at an angular rotation rate (f) of 1600 rpm.
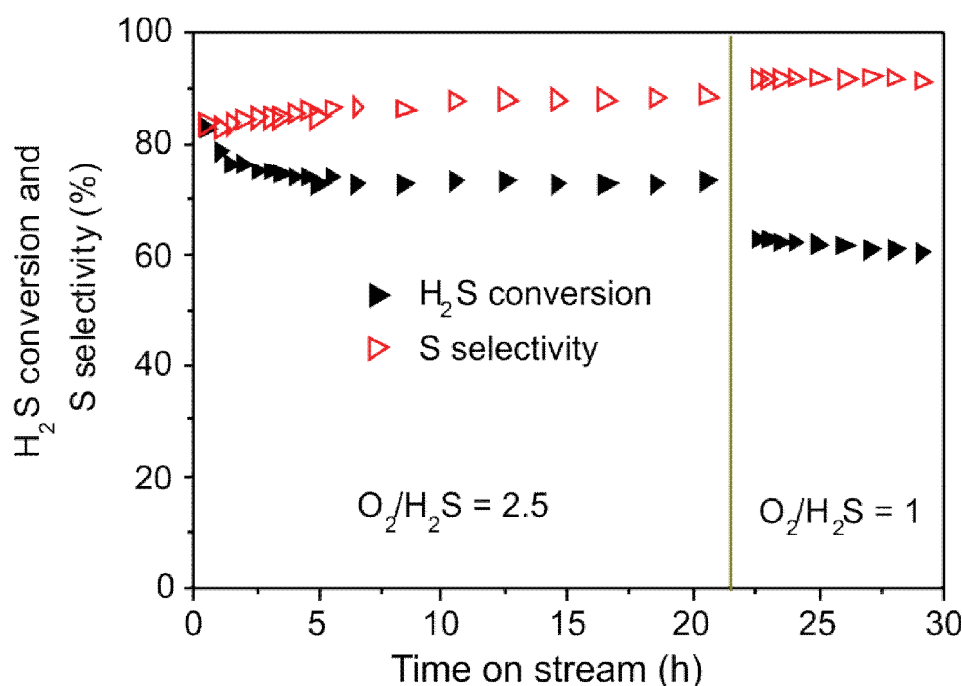
Fig. S10. H_2S conversion and sulfur selectivity on $^AN@C/Al_2O_{3B}{}^2$ catalyst (**VI**) under two O_2/H_2S molar ratio. Reaction conditions: M_{catal} = 1 g; T= 230 °C, WHSV = 0.6 h^{-1}.

References

[1]   J. Chlistunoff, J. Phys. Chem. C 115 (2011) 6496.

[2]   R.-J. van Putten, J.C. van der Waal, E. de Jong, C.B. Rasrendra, H.J. Heeres, J.G. de Vries, Chem. Rev. 113 (2013) 1499.

[3]   F.W. Lichtenthaler, A. Brust, E. Cuny, Green Chem. 3 (2001) 201.

[4]   F.W. Lichtenthaler, Acc. Chem. Res. 35 (2002) 728.

CHAPTER 4

Carbon nanotubes containing oxygenated decorating defects as metal-free catalyst for the partial oxidation of H$_2$S

HNO$_3$ | 250 °C
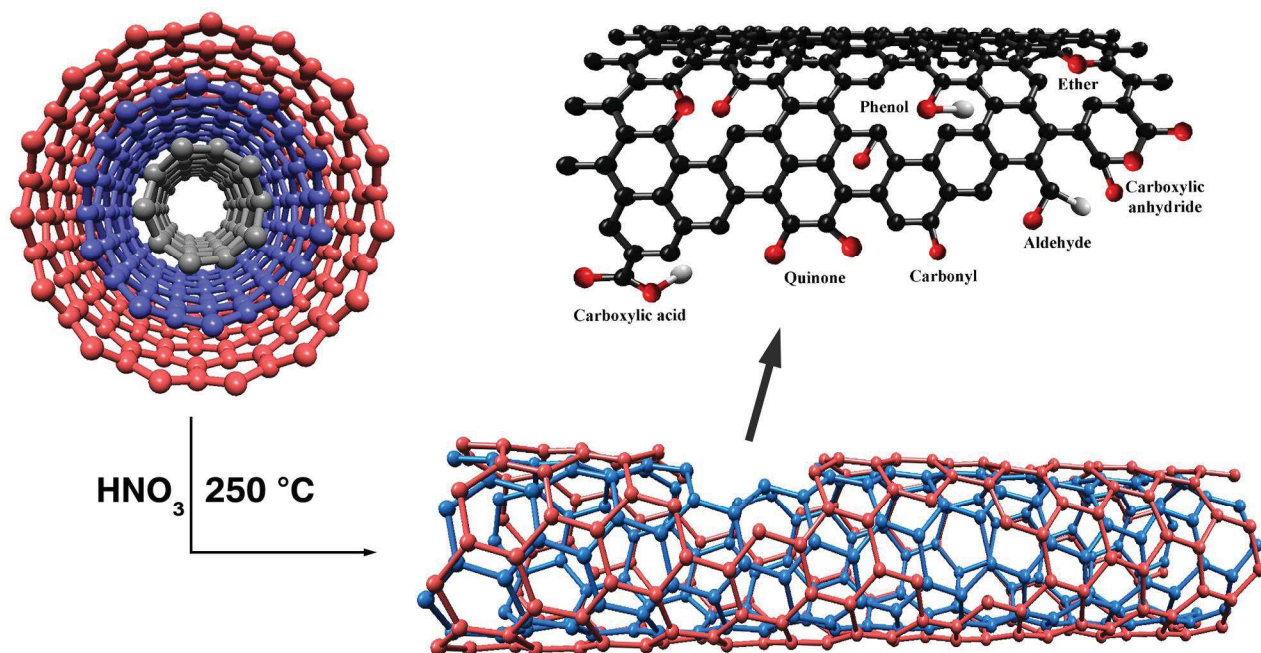
Carbon nanotubes containing oxygenated decorating defects as metal-free catalyst for the partial oxidation of H₂S

Cuong Duong-Viet[a,b], Housseinou Ba[a], Lai Truong-Phuoc[a], Yuefeng Liu[a],

Lam Nguyen –Dinh[c], Jean-Mario Nhut[a], Cuong Pham-Huu[a*]

(a) Institut de Chimie et Procédés pour l'Energie, l'Environnement et la Santé (ICPEES), ECPM, UMR 7515 du CNRS-Université de Strasbourg, 25 rue Becquerel, 67087 Strasbourg Cedex 02, France.

(b) Ha Noi university of Mining and Geology, Co Nhue 2 – Bac Tu Liem – Ha Noi.

(c) The University of Da-Nang, University of Science and Technology, 54 Nguyen Luong Bang, Da-Nang, Viet-Nam

Corresponding author: cuong.pham-huu@unistra.fr (C. Pham-Huu)

Abstract

In this study, we report on the influence of gaseous HNO_3 treatment, with various time and temperature, on the creation of oxygenated functional groups and defects on the CNTs side-wall. According to the characterization results the gaseous acid treatment at high temperature, i.e. 250 °C, leads to a significant increase of the oxygenated functional groups and defects on the tube wall along with a specific surface area improvement. The as-synthesized catalyst was further used as a metal-free catalyst in the selective oxidation of H_2S in the waste effluents. The desulfurization activity is extremely high and stable as a function of time on stream which indicates the high efficiency of these oxidized un-doped carbon nanotubes as metal-free for selective oxidation process. The high catalytic performance was attributed to both the presence of structural defects on the carbon nanotubes wall which acting as an adsorption center for the reactant and the oxygenated functional groups which could be act as the active sites.

Keywords: CNTs oxidized, selective oxidation of H_2S.

4.1. Introduction

Carbon nanomaterials, i.e. nanotubes (CNTs) and nanofibers (CNFs), have received an ever increasing scientific interest for being used as catalyst support or directly as metal-free catalysts in numerous relevant catalytic processes [1–6]. When used as catalyst support the defects and oxygenated functional groups present on the surface of these carbon nanomaterials play a key role to anchor metal and/or oxides nanoparticles active phase, which contribute to prevent excessive sintering of the metal and/or oxide nanoparticles during the course of the reaction, or also to stimulate the metal-free reactions themselves [7–9]. The defects and oxygenated functional groups density on the CNTs surface can be enhanced by submitting the materials to oxidative process either in the presence of oxygen containing gas or in the presence of difference oxidation agents such as H$_2$O$_2$ [10], O$_3$ [11], KMnO$_4$ [12], (NH$_4$)$_2$S$_2$O$_8$ [13] and H$_2$SO$_4$ and/or HNO$_3$ [14–18]. Among these oxidation processes the gas-phase treatment seems to be the most efficient and appropriate to introduce defects and oxygenated functional groups without destroying the size and shape of the carbon nanomaterials [19,20]. However, these oxygen/defects functionalized carbon nanomaterials have mostly employed as catalyst support while they have rarely been tested directly as metal-free catalyst where defect sites and/or oxygen functionalities could play a pivotal role to activate the reactant.

Recently, nitrogen-doped CNTs composite has been reported to be an efficient metal-free catalyst for selective oxidation processes. In some catalytic processes the doped carbon nanomaterials exhibit even a better catalytic performance compared to traditional catalysts such as selective dehydrogenation of ethylbenzene to styrene, either in the direct or oxidative dehydrogenation processes [21], selective oxidation [22–24], oxygen reduction reaction (ORR) [25–27] or in other catalytic processes [28,29], just to cite a few. The catalytic activity was attributed to the dissociative adsorption of the oxygen molecule on the carbon localized close to the nitrogen site according to the pioneering work of Dai and co-workers [30]. Such N-CNTs also exhibit an extremely high stability as a function of time on stream even under severe reaction conditions such as low temperature, high gaseous space velocity and low oxygen-to-reactant molar ratio. However, nitrogen-doping requires the use of nitrogen precursors which are relatively toxic and also, the low yield of the doping also leads to a high amount of post-reaction waste to be treated. It is of interest to find other methods to prepare such metal-free catalyst where low temperature and easy scale up process are used. The method should also provide lower waste which needs additional treatment, or even better, waste that can be easily recycled for subsequence use.

Recently, Song et al. [31] reported that the defective MWCNTs is active for benzene hydroxylation to phenol reaction in the presence of H$_2$O$_2$. In this study the catalytic performance can be directly correlated with the number of defects on the surface of the CNTs.

Another study of Waki et al. [32] also indicated that the defects such as pentagon-heptagon pair and edge plane defects can modify the electronic structure of the carbon allowing an improvement of the ORR performance of the catalyst. The activity performance is mainly attributed to the creation of new active sites on the surface of the oxidized CNTs due to the removal of high temperature CO desorbing functionalities. Su and co-workers have also reported that prismatic planes of carbon-based material associated with oxygen molecules could efficiently catalyze the oxidation of butane into acrylic acid [33].

Very recently, Wu et al. [34,35] have reported an important role of carbonyl group, which were generated by oxidation process of CNTs using H_2O_2 as gaseous oxidant, in the catalytic reduction of nitrobenzene and nitroarene. According to the results obtained the activity performance of these functionalized CNTs is clearly related to the presence of carbonyl groups present on the surface of the CNTs while the carboxylic group and anhydride played negative roles. However, it is expected that surface oxygen species are mainly linked with the defect sites present on the CNTs surface and thus, the catalytic performance could be originated from such dual sites and not solely to the oxygenated functional groups.

In the present article we report on the use of gaseous oxidative HNO_3 to create surface defects with exposed prismatic planes and decorated with oxygen functionalized groups on the CNTs wall which will be further acting as active sites for the selective oxidation of H_2S in the waste stream effluents. The catalytic sites could be attributed to the presence of oxygen species such as carbonyl, carboxyl groups decorating the structural defects present on the CNTs surface. It is worthy to note that as far as the literature results are concerned no such catalytic study using oxidized CNTs directly as metal-free catalyst has been reported so far.

4.2. Experimental

4.2.1. CNTs preparation

The carbon nanotubes were synthesized according to the Chemical Vapor Deposition (CVD) method reported previously [36,37]. The synthesis process is the following: firstly, γ-Al_2O_3 support was impregnated with an aqueous solution containing $Fe(NO_3)_3$ (20 wt.% Fe) by an incipient wetness impregnation method. The as-prepared Fe/Al_2O_3 sample was dried at room temperature for overnight and oven-dried at 110°C for 24 h. It was then calcined in air at 350 °C for 2 h in order to transform the nitrate precursor into its corresponding oxide. The Fe_2O_3/Al_2O_3 catalyst was then reduced under hydrogen flow (200 mL.min^{-1}) at 400 °C for 2 h and then, the reaction temperature was raised to 750 °C (heating rate of 10 °C/min) and the H_2 flow was replaced by a C_2H_6/H_2 mixture. The C_2H_6 and H_2 flow rates were fixed at 50:50 sccm.min^{-1}. The synthesis was lasted for 3 h, and the reactor was cooled to room temperature under argon.

After synthesis the raw product was treated with a solution of NaOH (5M) at 110 °C for 24 h in order to remove the alumina support. The resulting material was washed several times with distilled water until neutral pH and then treated with a solution of aqua regia at 110 °C for 17 h in order to remove the remaining iron particles. It was then washed with distilled water until neutral pH and dried at 100 °C.

4.2.2. Gaseous HNO$_3$ treatment of CNTs

The as-received pristine CNTs were first thermally treated under flowing argon for 1 h at 900 °C to remove the polyaromatic impurities on the surface. For the gaseous acid treatment 1g of CNTs was loaded inside the reactor (5 x 100 mm) and heated to the desired temperature between 150 °C and 275 °C by an external furnace. The treatment temperature was controlled by a thermocouple inserted inside the furnace. The reactor containing CNTs was connected to a round bottom flask filled with 150 mL of HNO$_3$ with a concentration of 65 %. The temperature of the round bottom flask was fixed at 125 °C and keep under magnetic stirring. The gaseous acid passed through the CNTs bed was further condensed in another flask which can be re-used for the process. The sample was treated at different temperatures and also with different durations at a given temperature in order to rule out the influence of these treatments on the final catalyst microstructure and chemical properties for subsequence catalytic activity.

4.2.3. Characterization techniques

The TEM analysis was carried out on a JEOL 2100F working at 200 kV accelerated voltage, equipped with a probe corrector for spherical aberrations, and a point-to-point resolution of 0.2 nm. The sample was grinded and then dispersed by ultrasounds in an ethanol solution for 5 minutes and a drop of the solution was deposited on a copper grid covered with a holey carbon membrane for observation.

The scanning electron microscopy (SEM) was carried out on a JEOL 2600F with a resolution of 5 nm. The sample was deposited onto a double face graphite tape in order to avoid the problem of charging effect during the analysis.

The specific surface area of the support and the catalyst, after reduction, was determined in a Micromeritics sorptometer. The sample was outgassed at 250 °C under vacuum for 14 h in order to desorb moisture and adsorbed species on its surface. The measurements were carried out using N$_2$ as adsorbent at liquid N$_2$ temperature at relative pressures between 0.06 and 0.2.

The X-ray photoelectron spectroscopy (XPS) measurements of the support and catalyst were performed by using a MULTILAB 2000 (THERMO) spectrometer equipped

with an AlKα anode (hν = 1486.6 eV) with 10 min of acquisition to achieve a good signal to noise ratio. Peak deconvolution was performed with the "Avantage" program from the Thermoelectron Company. The C1s photoelectron binding energy was set at 284.6 ± 0.2 eV relative to the Fermi level and used as reference to calibrate the other peak positions.

4.2.4. Catalytic application

The catalytic selective oxidation of H_2S by oxygen (Eq. (4.1)) was carried out in an apparatus working isothermally at atmospheric pressure. The temperature was controlled by a K-type thermocouple and a Minicor regulator. The gas mixture was passed downward through the catalyst bed. Before the test, the reactor was flushed with helium at room temperature until no trace of oxygen was detected at the outlet. The helium flow was replaced by the one containing steam. The catalyst was slowly heated up to the reaction temperature, and then the wet helium flow was replaced by the reactant mixture. The gases (H_2S, O_2, He) flow rate was monitored by Brooks 5850TR mass flow controllers linked to a control unit. The composition of the reactant feed was H_2S (1 vol.%), O_2 (0.63%, 1.25% or 2.5 vol.%), H_2O (30 vol.%) and He (balance). The use of a relatively high concentration of steam in the feed is motivated by the will to be as close as possible to the industrial working conditions as the steam formed during the former Claus units is not removed before the oxidation step and remains in the treated tail gas. The steam (30 vol.%) was fed to the gas mixture by bubbling a helium flow through a liquid tank containing water maintained at 85 °C. The O_2-to-H_2S molar ratio was varied from 0.63 to 2.5 with a WHSV fixed at 0.6 h^{-1}. It is worth to note that the WHSV used in the present work is extremely high regarding the usual WHSV used in the industrial process for this kind of reaction, i.e. 0.09 h^{-1} (GHSV: 1500 h^{-1}).

$$H_2S \ + \ \tfrac{1}{2} O_2 \ \rightarrow \ 1/n \ S_n \ + \ H_2O \qquad \Delta H = - \ 222 \ kJ.mol^{-1} \qquad (4.1)$$

The reaction was conducted in a continuous mode and the sulphur formed during the reaction was vaporized, due to the relatively high partial pressure of sulphur at these reaction temperatures, and was further condensed at the exit of the reactor in a trap maintained at room temperature.

The analysis of the inlet and outlet gases was performed on-line using a Varian CP-3800 gas chromatography (GC) equipped with a Chrompack CP-SilicaPLOT capillary column coupled with a thermal catharometer detector (TCD), allowing the detection of O_2, H_2S, H_2O and SO_2.

4.3. Results and discussion

4.3.1. Characteristics of the acid treated CNTs

In this work, the CNTs after acid treated are noted as follows: O-CNT-(X) for the treatment temperature-(Y) for the treatment duration in hour, for example: O-CNT-250-24 indicates that the raw CNTs were treated at 250°C for 24 h under gaseous HNO₃. The Raman spectra of the different samples obtained as a function of temperature and duration are presented in Fig. 4.1A and C. Raman spectra of all samples display two peaks localized at 1343 cm^{-1} (D-band) and 1573 cm^{-1} (G-band). The G-band corresponds to the sp^2 carbon atoms in the graphene sidewalls, while the D-band was attributed to the sp^3 carbon atoms localized at the defect sites on the surface of the tubes and amorphous carbon [16, 36].
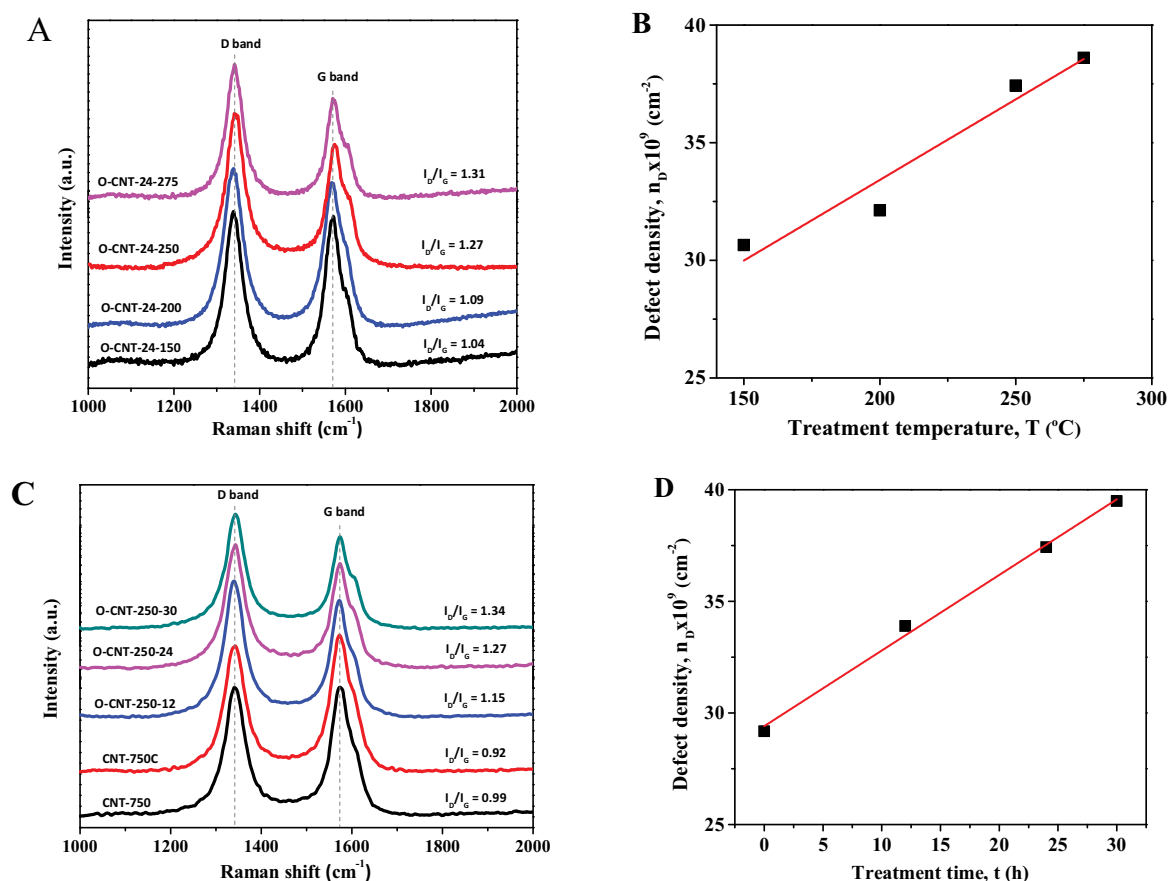
Fig. 4.1. (A) Raman spectra and I_D/I_G band ratio of the acid treated CNTs materials as a function of the treatment temperature (C) and duration (the temperature was fixed at 250°C). The Raman spectra of the pristine CNTs (noted CNT-750) and the same after carbonization step (CNT-750C) are also reported for comparison. (C, D) Defect density was calculated by Cançado's equation corresponding the I_D/I_G intensity ratio of oxidized CNTs.

The I$_D$/I$_G$ intensity ratio was usually used to estimate the amount of defects in the tubes. The I$_D$/I$_G$ intensity ratio of oxidized CNTs as a functional of treatment temperature and duration are presented in Fig. 4.1A and C. According to the Raman results increasing the acid treatment temperature and duration leads to an increase of the I$_D$/I$_G$ ratio which indicates that more defects have been incorporated inside the CNTs structure. In order to confirm such tendency the amount of defect density will be calculated from the Raman data. Cançado et al. [38] have proposed an empirical equation to calculate the amount of defect density n$_D$ (cm^{-2}) on the surface of the CNTs based on the Raman data:

$$n_D = \left(7.3 \pm 2.2\right) x10^9 E_L^4 \left(\frac{I_D}{I_G}\right) \qquad (4.2)$$

Where: E_L is the terms of excitation energies and I$_D$ and I$_G$ are the intensity of the Raman spectrum. In this work the excitation energies was fixed at 2.33 eV.

The density of defects (n$_D$) determined on the different samples according to Cançado's equation are presented in Fig. 4.1B and D. Such results clearly indicate that increasing the severity of the acid treatment, *i.e.* temperature or duration, leads to a monotonous increase of the defects inside the carbon nanotubes compared to the pristine CNTs and CNTs after carbonization step. Thus, it is worthy to note that the defect density is controllable by adjusting the treatment conditions and the role of these defects to mediate desulfurization process will be discussed in light of the catalytic results presented below.

The microstructure of the CNTs, as-synthesized, after carbonization step and after acid treatment, is analyzed by TEM and the results are presented in Fig. 4.2. TEM micrograph of the carbonized CNTs evidences the high graphitized microstructure of the tube along with the presence of a thin layer of amorphous carbon on the outer wall (Fig. 4.2A). The amorphous carbon presence on the tube surface could be formed during the cooling process under the presence of the reactant mixture. Indeed, it is expected that at temperature lower than the synthesis one some hydrocarbon can still be decomposed leading to the formation of amorphous carbon instead of CNTs due to the insufficient growth temperature. No defects are observed along the tube wall of the material which is in good agreement with the Raman results reported above. The selectivity towards the CNTs formation is extremely high under the used reaction conditions as no carbon nanoparticles were observed within the sample.

The acid treatment leads to a significant structural modification of the pristine CNTs according to the TEM analysis. At low acid treatment temperature (< 250 °C) or with a short treatment time (< 12 h), the TEM micrographs evidence the formation of structural nanoscopic defects on the tube wall (Fig. 4.2B and C) while the main shape of the tube remains unmodified. At higher acid treatment temperature and longer duration a significant modification of the CNTs structure is observed. Indeed, at higher treatment temperature (>

250 °C) and higher duration (> 12 h) a significant part of the tubes was destroyed according to the TEM micrographs recorded on the O-CNT-275-24 (Fig. 4.2D and E) and O-CNT-250-30 (Fig. 4.2F).
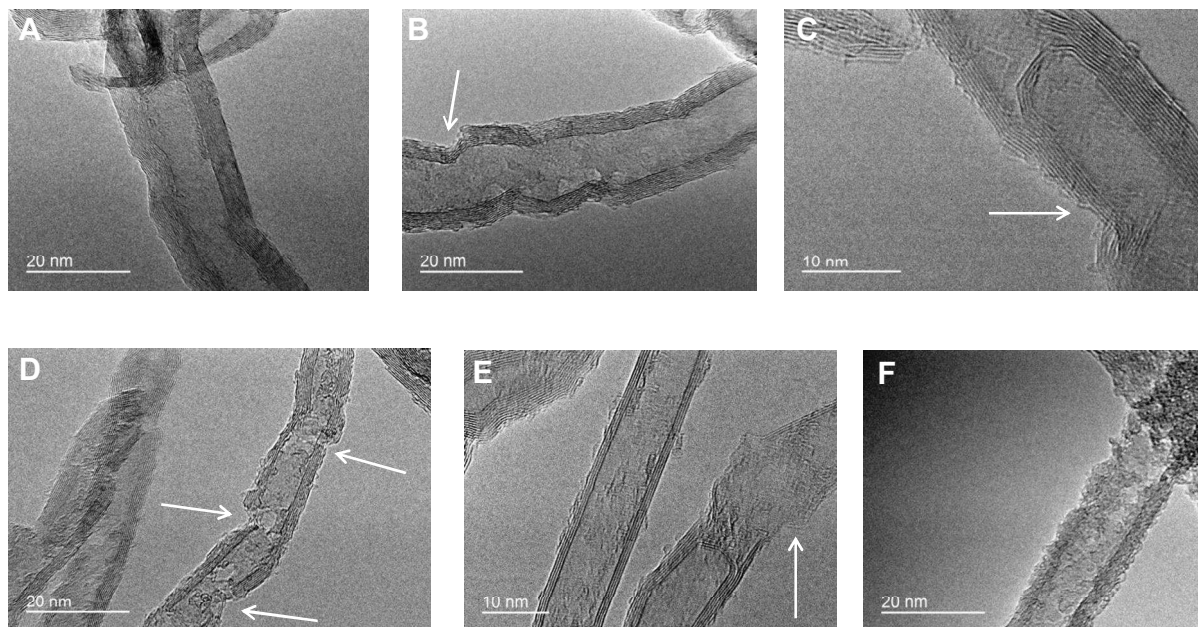

Fig. 4.2. Representative TEM micrographs: (A) Pristine graphitized CNTs, and (B), (C), (D), (E) and (F) oxidized CNTs as function of treatment temperature and duration. Sidewall defects are indicated with arrows.

These results are in good agreement with those of the Raman analysis presented above. Similar results have also reported by other research groups during their investigations on the influence of the gaseous acid treatment on the CNTs integrity [16,32]. Recently, Zhou et al. [39] have also reported the presence of defects on the CNTs wall even after a mild treatment in the presence of HNO_3.

The gaseous acid treatment also induces an overall oxidation of carbon matrix leading to a significant weight loss of the material. The weight loss calculated on the basis of the initial weight and the one after acid treatment as a function of the treatment duration and temperature is presented in Fig. 4.3. The weight loss during the acid treatment process is accounted for the corrosion of the tubes, and also to the removal of amorphous carbon layer presence on the tube wall and some carbon encapsulated residual growth catalyst; this later is expected to be relatively low taken into account the initial weight amount of the growth catalyst in the final composite. The weight loss increases with the treatment temperature and duration, especially for temperature > 225 °C or duration longer than 24 h. It is expected that the low temperature weight loss could be assigned to the removal of the amorphous carbon or

catalyst residue, since they are considered to be more reactive than the graphitic wall of the carbon nanotubes while the high temperature weight loss is linked with the formation of structural defects on the tube wall. Indeed, under a more severe treatment, *i.e.* longer duration or higher temperature, the weight loss becomes significantly, i.e. the weight loss recorded for the sample after being treated at 275 °C for 24 h or 40 h are 33 % and 43 %, respectively. This result can be attributed to the higher corrosion of the tubes wall and also to the tube breaking according to the TEM analysis presented above. The weight loss during the oxidative treatment under gaseous HNO_3 has already been reported by several groups in the literature [15, 20, 38].
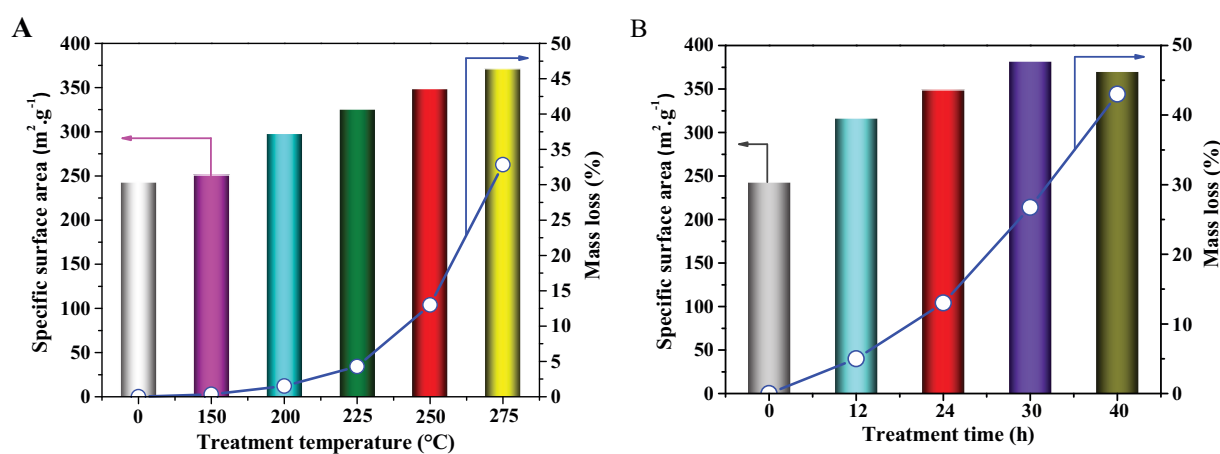
Fig. 4.3. Weight loss (open circles) and specific surface area (bares) modification of the acid treated carbon-based materials as a function of the treatment temperature with a duration fixed at 24 h (A) and duration at a fixed temperature of 250 °C (B).

The generation of defects along the tube wall during the acid treatment step also significantly increases the overall specific surface area of the as-treated materials. The specific surface area of the acid oxidized CNTs steadily increased as a function of the acid treatment step, i.e. temperature and duration, as evidenced in Fig. 4.3. The specific surface area of O-CNT-250-24 and O-CNT-275-24 are 1.6 times higher than that of the graphitized CNTs, *i.e.* 371 and 382 $m^2.g^{-1}$ instead of 243 $m^2.g^{-1}$. According to the results in Fig. 4.3B, the specific surface area of the acid treated CNTs reached a maximum after 30 h of treatment at 250 °C. The increase of the specific surface area could be directly attributed to the creation of defects on the tube wall leading to a higher adsorption sites for nitrogen. However, at higher treatment duration the specific surface is decreased and such result could be assigned to the

destruction of the tubes morphology or to the formation of amorphous carbon species with lower adsorption sites.

The amount of oxygen engaged in the different oxygenated functional groups is analyzed by means of the XPS technique and the results are presented in Fig. 4.4.
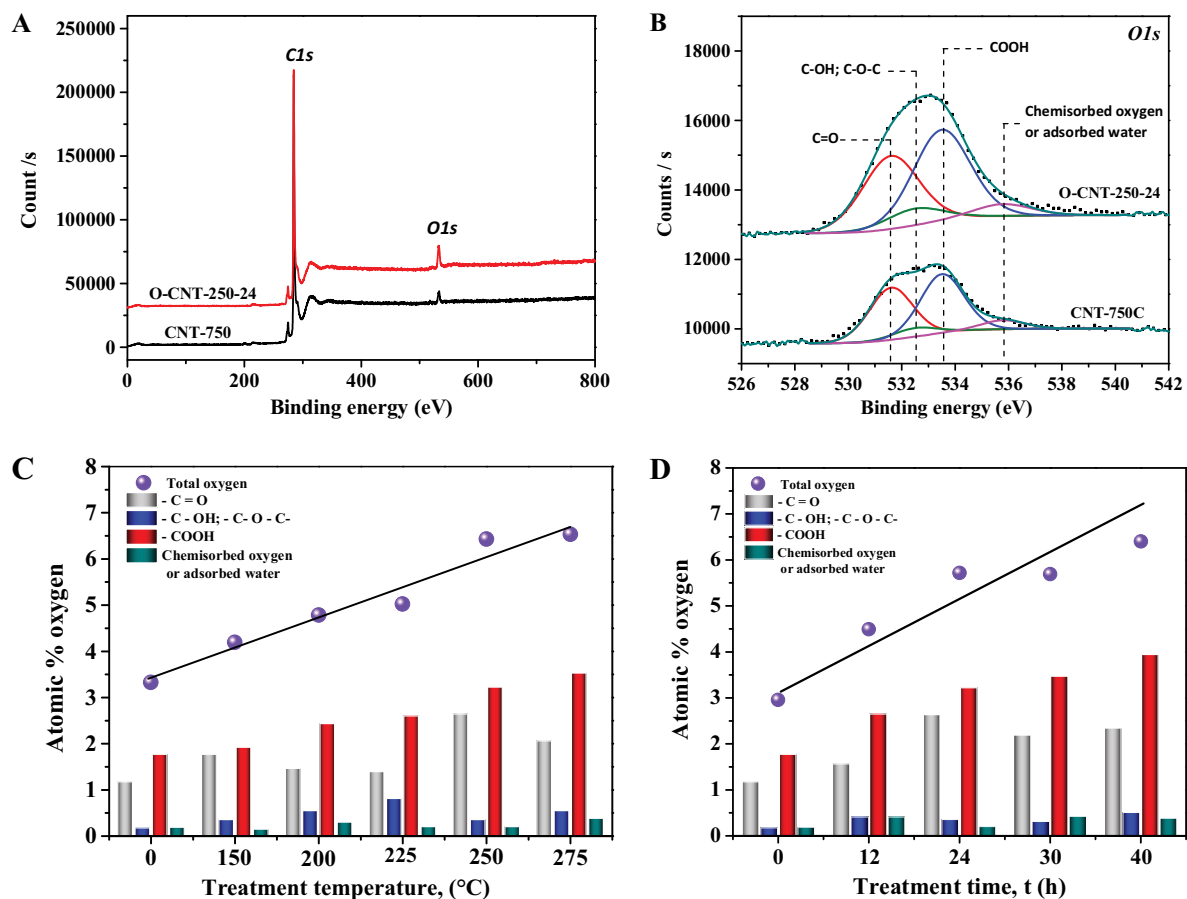
Fig. 4.4. (A) Survey XPS of O-CNT-250-24 in comparison with pristine graphitized CNTs, (B) deconvolution O1s present the oxygen species on the surface of the CNTs wall, (C, D) Oxygen species distribution of the acid treated carbon-based materials as a function of the treatment duration and temperature in comparison with the pristine graphitized CNTs.

Only strong C1s and O1s peaks are observed in a survey spectra (Fig. 4.4A) indicate that residual catalyst are completely removed from the CNTs. The deconvoluted O1s spectrum in Fig. 4.4B shows that it consists of four peaks which can be assigned to the =C=O (ketone, aldehyde, quinone…), -C-OH, -C-O-C- (alcohol, ether) and -O-C=O (carboxylic, ester) oxygen species. According to the XPS results presented in Fig. 4.4C and D the acid treatment leads to a significant increase of the total amount of oxygen, on the topmost layers

of the treated CNTs, from 3.5 to about 6 at.%. The oxygen engaged in the different functional groups steadily increases as increasing the treatment temperature and treatment duration while the chemisorbed oxygen and/or adsorbed water remain virtually unchanged.

In Fig. 4.5 the atomic percent of oxygen incorporated inside the CNTs versus the density defects, as a function of the treatment temperature (Fig. 4.5A) and duration (Fig. 4.5B), is presented. According to these results the oxygen and the defect density increase almost linearly with the acid treatment temperature up to 250 °C and duration of 24 h. Higher treatment temperature, i.e. 275 °C, or longer duration, i.e. > 24 h at 250 °C, lead to an almost unchanged values of the oxygen and defects density while the tube morphology is strongly damaged. According to the results one can stated that the optimized treatment conditions are: 250 °C for 24 h, which allow one to tailor O-CNTs with a highest amount of oxygen, defects and specific surface area without significant tube damage or breaking.
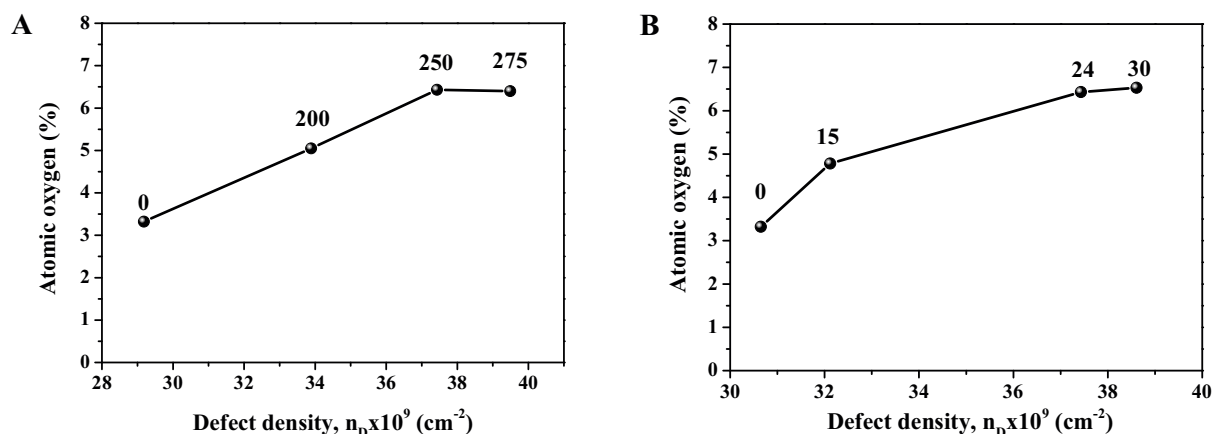
Fig. 4.5. (A) Amount of oxygen incorporated and defect density as a function of the acid treatment temperature. The treatment duration is keep at 24 h. (B) Amount of oxygen incorporated and defect density as a function of the acid treatment duration. The treatment temperature is keep at 250 °C.

4.3.2. Selective oxidation of H₂S

In order to assess in detail the role of defect sites and/or oxygenated functional groups on the desulfurization performance of the acid oxidized CNTs, desulfurization tests were carried out on the different treated catalysts at different temperatures and durations and the results are presented in Fig. 4.6. The tests were carried out for at least 30 h and the average desulfurization performance is reported. According to the results the acid treatment process leads to the formation of active metal-free catalysts for desulfurization reaction compared to the pristine graphitized CNTs (Fig. 4.6A and B). The CNTs treated during 24 h at 250 °C

displays the highest desulfurization performance. The results obtained also indicate that both H_2S conversion and sulfur yield increase as a function of the defect density (n_D), i.e. specific surface area (Fig. 4.6C and D), and also to the total amount of oxygen (Fig. 4.6E) for the samples treated at a temperature lower than 250 °C or with a duration shorter than 25 h.
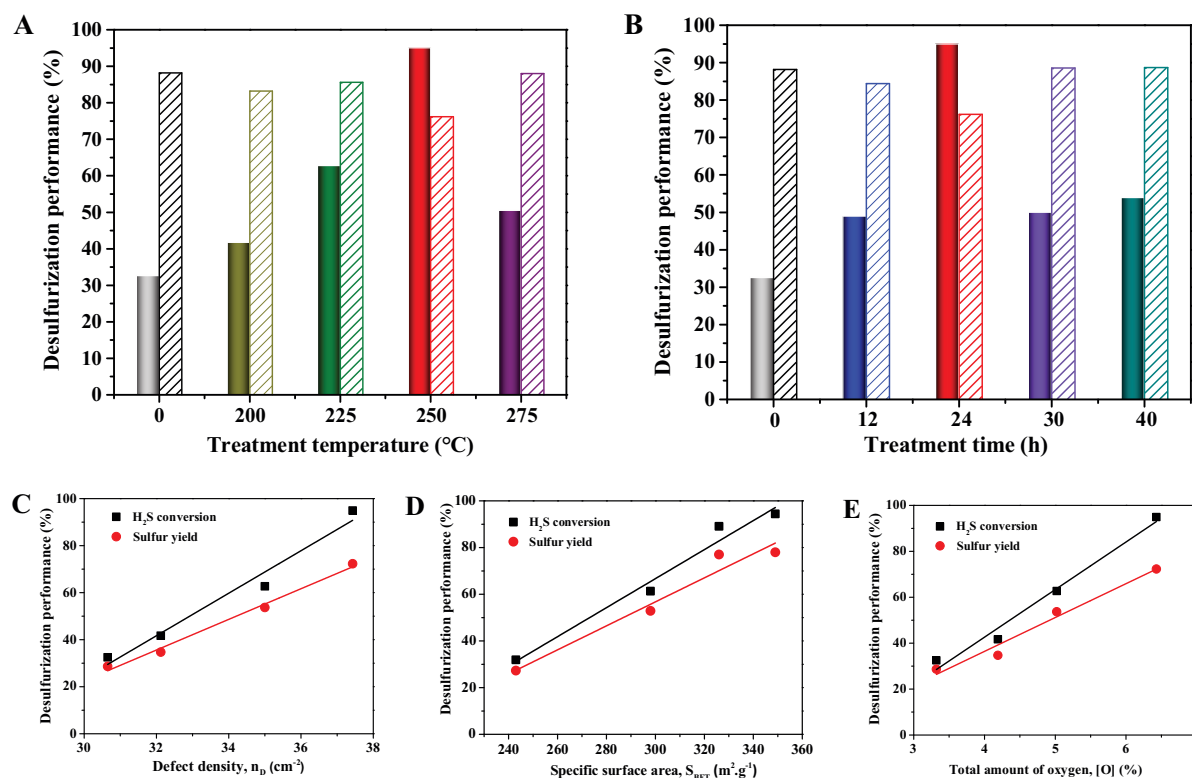
Fig. 6. (A, B) Desulfurization activity on the O-CNTs catalysts treated at different temperatures and durations under gaseous HNO_3. H_2S conversion and sulfur yield of O-CNTs catalysts as function of the defect density (C) or surface specific area (D) and total amount of oxygen (D). Reaction conditions: catalyst weight = 0.3 g; reaction temperature = 230 °C; WHSV = 0.6 h^{-1}; O_2-to-H_2S molar ratio = 2.5.

As obtained results, the increasing of the desulfurization activity firstly could be attributed to the high defect sites present on the tube wall which could play a role of adsorption center for the reactants. The high open porous structure of the O-CNTs catalyst, which provides a high effective surface contact between the reactant and the active sites compared to the CNTs graphitized, also represents a net advantage for performing the catalytic reaction. The improved desulfurization performance could also be attributed to the present of oxygenated functional groups, on or around the defect sites present on the surface of the CNTs after acid treatment. Among these different oxygenated functional groups, the carbonyl group seems to be the most important, while the other group such as carboxylic and

anhydride played negative roles for selective oxidation of H_2S according to the results reported by Su and co-workers [34,35] on the oxygen-treated CNTs for the hydrogenation of arenes. The results obtained in Fig 4.5C and D evidence that on the catalysts treated under severe conditions, *i.e.* longer duration or at higher temperature, both the carboxylic groups and total amount of oxygen still increase while the activity performance decreased (Fig. 4.6A and B). However, it is worthy note that the CNTs morphology was drastically changed at these treatment conditions due to the excessive oxidation and thus, could be at the origin of the loss of the catalytic performance.

In contrast, the decreasing of the sulfur selectivity compared to that obtained on the CNTs graphitized ones could be attributed to secondary reactions between the re-adsorbed sulfur on the defect sites and the excess of oxygen under the applied reaction conditions. Indeed, such low sulfur selectivity could be attributed to the presence of adjacent prismatic planes in the defect which could bind stronger the intermediate sulfur species leading to a secondary total oxidation process to yield SO_2 [41].

The long term desulfurization test was carried out under the optimum reaction conditions that we have reported in previous articles [23,24,41] at 230 °C and with a WHSV fixed at 0.6 h^{-1} on the graphitized CNTs and the same after an acid treatment, O-CNT-250-24. The desulfurization results as a function of time on stream are presented in Fig. 4.7.
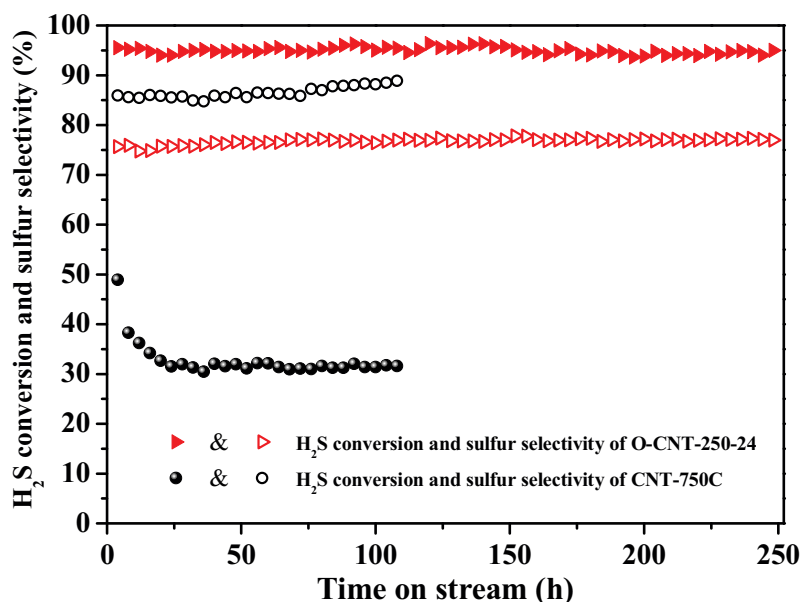

Fig. 4.7. Desulfurization conversion, sulphur selectivity on the O-CNT-250-24 compared to the CNTs graphitized (CNT-750C). Reaction conditions: catalyst weight = 0.3 g; reaction temperature = 230 °C; WHSV = 0.6 h^{-1}; O_2-to-H_2S molar ratio = 2.5.

According to the results, the desulfurization performance of the acid treated O-CNT-250-24 catalyst displays a significant improvement compared to the graphitized CNT catalyst at the same reaction conditions, *i.e.* conversion of 95 % instead of 32 %. No deactivation was observed on both catalysts as a function of time on stream indicates the high resistance of the catalysts towards active phase loss by both sintering and blocking. In contrast, the O-CNT-250-24 exhibits slightly lower sulfur selectivity compared to that obtained on the CNTs graphitized, *i.e.* 75 instead of 85 %. Such lower sulfur selectivity could be attributed to the high desulfurization activity or to the re-adsorption of the intermediate sulfur species on the oxygenated defects followed by secondary reaction leading to the formation of SO₂ product. The desulfurization results obtained clearly showed that the catalytic performance of the CNTs catalyst is strongly improved after an acid treatment process which introduces both oxygen functionalized groups and defects density on the catalyst surface.

The best O-CNT-250-24 catalyst will be further evaluated under different reaction conditions in order to map out the influence of the structural defects and the oxygenated functionalities on the desulfurization performance and stability.

The effect of the reaction temperature on the desulfurization performance of the O-CNT-250-24 catalyst was performed with the WHSV fixed at 0.6 h^{-1} and the O₂-to-H₂S molar ratio at 2.5. The catalyst was evaluated first at 230 °C for 40 h of test and then the reaction temperature was lowered to 210 °C and 190 °C for subsequently 30 h of test, respectively.
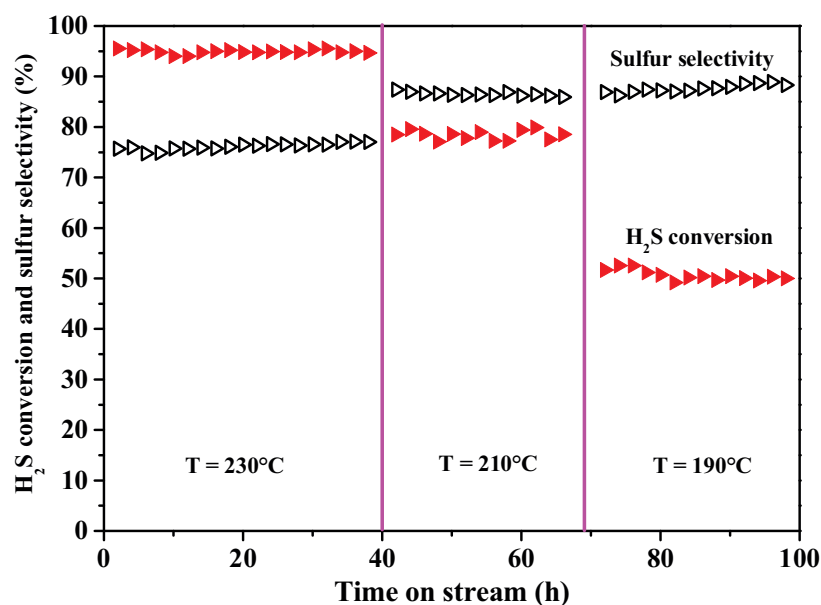

Fig. 4.8. Desulfurization activity and sulfur selectivity of the O-CNT-250-24 as a function of the reaction temperature. Reaction conditions: catalyst weight = 0.3 g; WHSV = 0.6 h^{-1}; O₂-to-H₂S molar ratio = 2.5.

According to the results presented in Fig. 4.8 the H$_2$S conversion decreases as decreasing the reaction temperature while the sulphur selectivity increase in a reverse way. However, at 190°C the H$_2$S conversion loss is more pronounced while the sulphur selectivity remains almost unchanged. Such result could be explained by the fact that the sulphur selectivity observed under these reaction conditions represents the intrinsic selectivity towards sulphur on the O-CNT-250-24 catalyst and thus, cannot be lowered due to the rate of re-adsorption and secondary oxidation.

The desulfurization test was also realized with high weight hourly space velocity, i.e. at 0.6, 0.9 and 1.2 h^{-1}, at 230°C. The results obtained are displayed in Fig. 4.9. According to the results the O-CNT-250-24 displays a relatively high H$_2$S conversion even at high space velocity, i.e. 85 % at 1.2 h^{-1}. Such a high desulfurization performance could be attributed to the high effective surface area and surface exposure active sites of the catalyst which significantly enhance the reactant adsorption. The high space velocity also leads to an improvement of the sulfur selectivity due to the high escaping rate of the intermediate sulfur from the active sites.
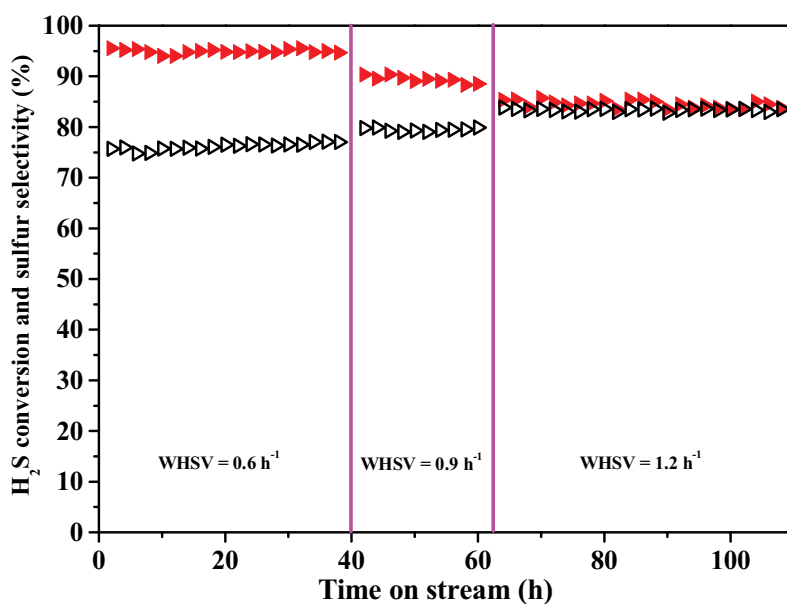
Fig. 4.9. Desulfurization activity and sulfur selectivity of the O-CNT-250-24 as a function of the WHSV. Reaction conditions: catalyst weight = 0.3 g; reaction temperature = 230 °C; O$_2$-to-H$_2$S molar ratio = 2.5.

The influence of the O$_2$-to-H$_2$S molar ratio on the desulfurization performance was also studied in order to confirm the high activity of the O-CNTs to generate active oxygen species for oxidizing H$_2$S compounds. The results obtained at different O$_2$-to-H$_2$S molar

ratios, i.e. 2.5, 1.25 and 0.63, as a function of time on stream are presented in Fig. 4.10. The decreasing of the O_2-to-H_2S molar ratio led to a monotonous decrease of the H_2S conversion, however, this later remains very high (about 82 %) even at the lowest O_2-to-H_2S molar ratio at 0.63 and under a relatively high space velocity. The catalyst also exhibits an extremely high stability for all the reaction conditions which indicates that deactivation by removal of the oxygenated functional groups on the catalyst surface is negligible.
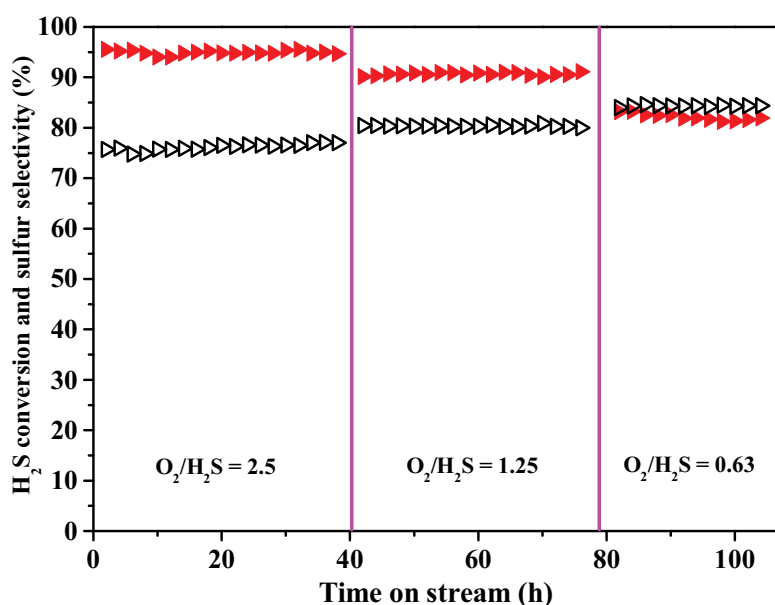
Fig. 4.10. Desulfurization activity and sulfur selectivity of the O-CNT-250-24 as a function of the O_2-to-H_2S molar ratio. Reaction conditions: catalyst weight = 0.3 g; reaction temperature = 230 °C; WHSV = 0.6 h^{-1}.

On the other hand, the sulfur selectivity slightly increased as decreasing the O_2-to-H_2S molar ratio due to the lower oxygen available for oxidizing the formed sulfur. These results indicated that the O-CNTs catalyst exhibits a high activity for oxygen dissociation which provides enough oxygen to perform the selective oxidation of H_2S even at low oxygen concentration in the reactant mixture and under a relatively high space velocity. The sulfur selectivity of about 85 % was obtained at an O_2-to-H_2S ratio of 0.6. Such sulfur selectivity is the highest value that one can obtain on the acid treated catalyst due to the consecutive reaction between the re-adsorbed sulfur and the oxygen in the flow. Similar results have also been observed during the study about the influence of the reaction temperature and space velocity reported above.

The results obtained above clearly indicate that the oxygenated functionalized and defects introduced by the acid treatment can act as hybrid metal-free sites for the oxidation of

H_2S into elemental sulfur similarly to what was observed on the nitrogen-doped carbon nanotubes (N-CNTs) [39].

Fig. 4.11. (A) Desulfurization performance on the pristine CNTs and N-CNTs catalysts and the same after acid treatment at 250 °C for 24 h. Reaction cond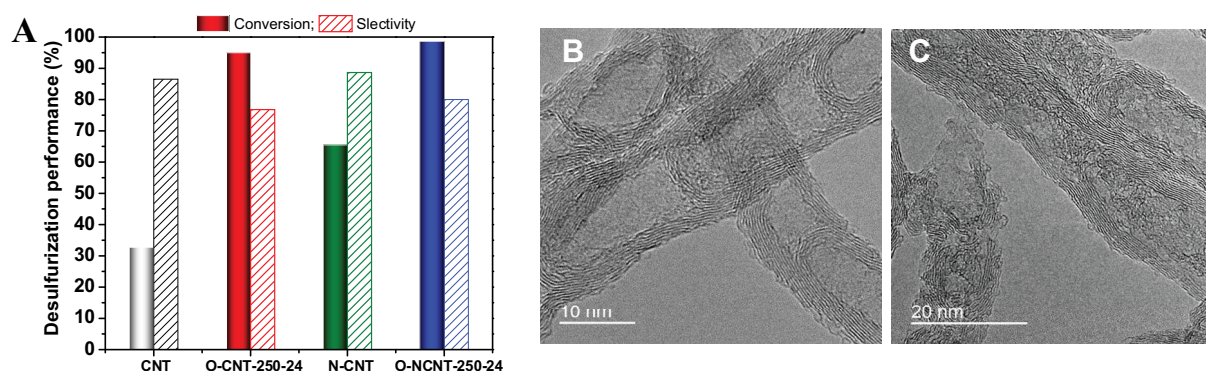itions: catalyst weight = 0.3 g; reaction temperature = 230 °C; WHSV = 0.6 h^{-1}. (B and C) Corresponding TEM micrographs of the N-CNTs and CNTs after acid treatment at 250 °C for 24 h.

In order to assess if the presence of nitrogen doping could have any influence on the overall desulfurization performance the same acid treatment was applied for the N-CNTs sample. The N-CNTs synthesized according to our previous report [36] were treated under the same conditions as those used for the CNTs and the catalyst was further evaluated in the partial oxidation of H_2S under the same reaction conditions and the results are presented in Fig. 4.11. The pristine CNTs catalyst exhibits a relatively low desulfurization performance, *i.e.* 32 %, while the same, after being treated in an aqueous solution of HNO_3 (65 vol.%), exhibits a significant improved desulfurization activity which could be attributed to the dissociative adsorption of oxygen on the prismatic planes present at the defects of the CNTs. Similar results have also been reported by Schlögl and co-workers [33] during the selective oxidation of n-butane into acrylic acid on CNTs catalysts. The introduction of nitrogen into the carbon matrix leads to a significant improvement of the desulfurization activity compared to the un-doped CNTs. thin the presence of nitrogen doping the H_2S conversion was increased from 32 to 65 % under similar reaction conditions. Such results confirm the catalytic role of nitrogen doping in the desulfurization performance of the doped metal-free catalyst. The desulfurization performance of the N-CNTs, after a treatment by a gaseous HNO_3 at 250 °C and 24 h, is significantly increased confirming the important role of oxygenated decorating defects generated by the treatment on the catalytic performance. According to the results the

desulfurization activity is almost similar between the O-CNTs and the O-N-CNTs catalysts, *i.e.* 95 instead of 97 % of H₂S conversion, while the sulfur selectivity is somewhat slightly higher on the O-N-CNTs catalysts.

4.3.3. Characteristics of the spent catalysts

The specific surface area of the spent O-CNT250-24 catalyst, measured after more than 300 h of the reaction selective oxidation under different reaction conditions is about 1.7 times lower than that of the fresh catalyst, i.e. 187 instead of 316 $m^2.g^{-1}$, as presented in Fig. 4.12A. Such result could be attributed to the deposition of some solid sulfur with low specific surface area within the catalysts porosity which lowering of the overall specific surface area of the catalysts. In order to verify such hypothesis regeneration was performed on the spent catalyst by submitting it to a thermal treatment under helium at 320 °C and 450 °C for 2 h to vaporize the trapped sulfur [41]. After the thermal treatment the catalyst surface area was almost recovered which confirming the hypothesis advanced above.
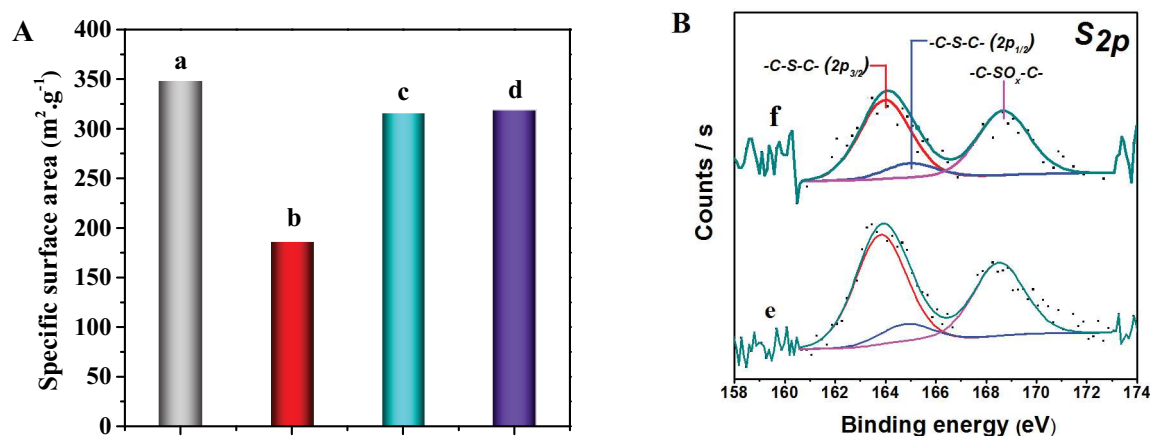
Fig. 4.12. (A) N₂ adsorption-desorption isotherms of O-CNT-250-24 catalyst before (a) – after desulfurization (b) test and after thermally following He flow at 320 °C (c) and at 450 °C (d) for 2 h. (B) XPS S$_{2p}$ spectra on catalyst surface after about 300 h of desulfurization test (e) and after thermally following He flow at 450 °C for 2 h (f).

The XPS analysis carried out on the spent catalyst, after more than 300 h on stream, evidences the presence of some sulfur species on the spent catalyst surface. The S2p$_{3/2}$ (163.8 eV) and S2p$_{1/2}$ (164.8 eV) peaks are ascribed to sulphide groups (-C-S-C) and the C-SO$_x$-C

peak (168.5 eV) is also observed as displayed in Fig. 4.12B and summarized in Table 4.1. Such sulfur deposition was attributed to the relatively low reaction temperature, ≤ 230 °C, in the present study which is not able to vaporize the totality of the solid sulfur formed during the reaction on the catalyst surface. It is expected that the thermal treatment under helium at high temperature allows the removing of a significant part of the deposit sulfur from the catalyst porosity. However, according to the XPS results 0.44 %.at (about 50% of the sulfur present on the spent catalyst surface) is still present. This result indicates that during the treatment part of the deposited sulfur could incorporate into the CNTs network. However, this residual solid sulfur seems not to influence in a noticeable way the desulfurization activity as no deactivation was observed.

Table 4.1. The atomic percentage and sulfur species percentages of spent catalyst obtained by XPS after reaction oxidation of H₂S in comparison with them before test.

Samples	C	O	S	-C-S-C- S (Sp$_{3/2}$)	-C-S-C-S (Sp$_{1/2}$)	-C-S$_{ox}$-C-
O-CNT-250-24	93.32	6.68	-	-	-	-
O-CNT-250-24-OS [*]	94.25	4.97	0.79	0.43	0.07	0.29
O-CNT-250-24-R320 [**]	95.37	4.09	0.56	0.22	0.20	0.14
O-CNT-250-24-R450 [***]	95.49	4.08	0.44	0.17	0.18	0.09

Notes: (*): O-CNT-250-24 catalyst after 300 h of oxidation of H₂S test.

(**): O-CNT-250-24 catalyst after 300 h of oxidation of H₂S test and regeneration at 320° C for 2 h under He flow.

(***): O-CNT-250-24 catalyst after 300 h of oxidation of H₂S test and regeneration at 450 °C for 2 h under He flow.

The influence of the regeneration step on the desulfurization performance was investigated and the results are presented in Fig. 4.13. According to the catalytic results the desulfurization performance, expressed in terms of H₂S conversion, remains unchanged which indicate that the deposit sulfur hardly influences the desulfurization performance.
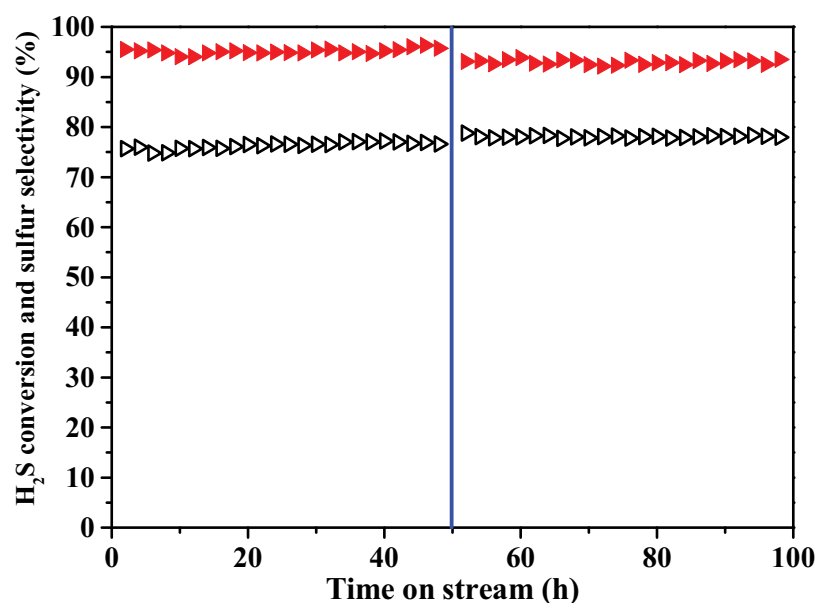
Fig. 4.13. Desulfurization activity on the O-CNT-250-24 before (A) and after thermal treatment under helium at 450 °C for 2 h (B). Reaction conditions: catalyst weight = 0.3 g; reaction temperature = 230 °C; WHSV = 0.6 h^{-1}, O$_2$-to-H$_2$S = 2.5.

4.3.4. Discussion

The treatment of the CNTs by a gaseous nitric acid had induced the formation of a large number of microstructural defects on the tube wall along with the incorporation of oxygen functional groups on the carbon nanotubes surface, probably next or on the defect sites. A combination of catalytic results and surface characterization by XPS indicates that both the oxygenated functional groups and the nanoscopic defects generated along the tube wall with exposed prismatic planes are mostly responsible for the observed metal-free activity. In addition, the formation of the defects on the tube wall also greatly contributes to an enhancement of the material specific surface area which provides high effective surface contact for the reactants.

The as-synthesized O-CNT-250-24 catalyst exhibits an extremely high and stable catalytic activity in the partial oxidation of H$_2$S into elemental sulfur in a fixed-bed reactor. Such high catalytic stability could be attributed to the stability of the defects in the tube wall at the used reaction temperature. On the other hand, the present of defects also lead to a rapid re-adsorption of the intermediate sulfur and thus, the secondary reaction leading to the formation of SO$_2$ is not negligible and accounted to about 15 % of the overall sulfur selectivity. It is worthy to note that the desulfurization performance remains stable despite the presence of some solid sulfur deposited during the course of the reaction, due to the relatively

low reaction temperature, *i.e.* $\geq$ 230 °C, which significantly decreases the catalyst specific surface area from 350 to 187 $m^2.g^{-1}$. It is expected that such solid sulfur is mostly deposited on the intact wall of the tube with higher hydrophobic character compared to the prismatic planes and thus, only hardly impact the overall desulfurization activity. Similar results have also been reported for the low-temperature desulfurization process on CNTs with dual hydrophilic/hydrophobic character [42]. Such residual solid sulfur deposited can be efficiently removed by a thermal treatment under helium at 320 °C according to the data collected. XPS analysis seems to indicate that during the regeneration process some sulfur may be incorporated in the CNTs matrix. XPS analysis also indicates that part of the oxygen incorporated into the acid treated CNTs was removed during the course of the reaction and also during the regeneration process (Table 4.1). Such oxygen loss could be attributed to loosely attached oxygen which is not directly involved in the catalytic process while the remained oxygen is strongly anchored on defects playing a role of catalytic sites.

The results obtained in the present study have evidence one pivotal fact in the development of metal-free catalysts: the surface functionalization and the density of defects play an extremely importance role in the catalytic process. According to the results the presence of hetero-atoms doping is not a *sine qua none* conditions in the synthesis of a highly active and stable metal-free catalyst and that the carbon surface containing oxygen decorated defects alone could also fulfill the request. The role of oxygen decorated defects acting as catalytic sites observed in this study is similar to that reported on metal-driven catalyst where the formation of carbon defects decorated with oxygen inside the parent metal oxide significantly improve the overall catalytic performance of the systems for performing dissociative adsorption of hydrogen [43,44]. The main advantage of the O-CNTs system in the present work is its extremely low sensitivity towards oxidation due to the lack of metal unlikely to that of the metal-oxygen-carbon defective systems which displaying an extremely high reactivity towards over oxidation. The results obtained also evidences the synergistic role of the nitrogen doping on the desulfurization performance. It is expected that a combination of nitrogen doping and oxygen decorated defect sites could represent an interesting option for the development of a new generation of metal-free catalysts with improved catalytic performance.

The detailed investigation of the desulfurization performance has also pointed out the relatively high re-adsorption rate of the formed sulfur which favors the complete oxidation process leading to the formation of SO_2.

4.4. Conclusion

In summary, we have shown that oxidation with gaseous HNO_3 can be an efficient pre-activation step to generate active metal-free catalysts, either without or with heteroatoms doping for performing partial oxidation process. According to the obtained results the nanodefects created on the CNT wall and the formation of oxygenated functional groups during the gaseous acid treatment could directly act as active phase for metal-free selective oxidation processes. According to the results the prismatic planes decorated with oxygenated groups are able to perform dissociative adsorption of oxygen for performing the partial oxidation of H_2S into elemental sulfur. The as-treated metal-free catalyst displays a relatively high desulfurization performance along with an extremely high resistance towards deactivation as a function of time on stream which could be attributed to the high stability of the oxygen decorated defects playing the role of active sites. It is expected that the results obtained here will contribute to the future development of metal-free carbon-based catalysts with better catalytic performance and stability compared to the traditional metal and oxides supported ones.

Acknowledgements

References

[1]   D.S. Su, S. Perathoner, G. Centi, Chem. Rev. 113 (2013) 5782.

[2]   P. Serp, M. Corrias, P. Kalck, Appl. Catal. Gen. 253 (2003) 337.

[3]   J.-P. Tessonnier, D.S. Su, ChemSusChem 4 (2011) 824.

[4]   C. Pham-Huu, M.-J. Ledoux, Top. Catal. 40 (2006) 49.

[5]   J. Amadou, K. Chizari, M. Houllé, I. Janowska, O. Ersen, D. Bégin, C. Pham-Huu, Catal. Today 138 (2008) 62.

[6]   M.J. Ledoux, R. Vieira, C. Pham-Huu, N. Keller, J. Catal. 216 (2003) 333.

[7]   J. Zhang, X. Liu, R. Blume, A. Zhang, R. Schlögl, D.S. Su, Science 322 (2008) 73.

[8]   J.-M. Nhut, R. Vieira, L. Pesant, J.-P. Tessonnier, N. Keller, G. Ehret, C. Pham-Huu, M.J. Ledoux, Catal. Today 76 (2002) 11.

[9]   J. Zhang, D. Su, A. Zhang, D. Wang, R. Schlögl, C. Hébert, Angew. Chem. Int. Ed. 46 (2007) 7319.

[10]   Y. Peng, H. Liu, Ind. Eng. Chem. Res. 45 (2006) 6483.

[11]   J.M. Simmons, B.M. Nichols, S.E. Baker, M.S. Marcus, O.M. Castellini, C.-S. Lee, R.J. Hamers, M.A. Eriksson, J. Phys. Chem. B 110 (2006) 7113.

[12]   H. Hiura, T.W. Ebbesen, K. Tanigaki, Adv. Mater. 7 (1995) 275.

[13]   K.J. Ziegler, Z. Gu, J. Shaver, Z. Chen, E.L. Flor, D.J. Schmidt, C. Chan, R.H. Hauge, R.E. Smalley, Nanotechnology 16 (2005) S539.

[14]   I. Gerber, M. Oubenali, R. Bacsa, J. Durand, A. Gonçalves, M.F.R. Pereira, F. Jolibois, L. Perrin, R. Poteau, P. Serp, Chem. – Eur. J. 17 (2011) 11467.

[15]   K.A. Wepasnick, B.A. Smith, K.E. Schrote, H.K. Wilson, S.R. Diegelmann, D.H. Fairbrother, Carbon 49 (2011) 24.

[16]   S. Osswald, M. Havel, Y. Gogotsi, J. Raman Spectrosc. 38 (2007) 728.

[17]   N.P. Blanchard, R.A. Hatton, S.R.P. Silva, Chem. Phys. Lett. 434 (2007) 92.

[18]   B. Smith, K. Wepasnick, K.E. Schrote, H.-H. Cho, W.P. Ball, D.H. Fairbrother, Langmuir 25 (2009) 9767.

[19]   W. Xia, C. Jin, S. Kundu, M. Muhler, Carbon 47 (2009) 919.

[20]   C. Li, A. Zhao, W. Xia, C. Liang, M. Muhler, J. Phys. Chem. C 116 (2012) 20930.

[21]   J. Zhang, D.S. Su, R. Blume, R. Schlögl, R. Wang, X. Yang, A. Gajović, Angew. Chem. Int. Ed. 49 (2010) 8640.

[22]   L.T.-P. Duong-Viet Cuong, Appl. Catal. Gen. (2014).

[23]   C. Duong-Viet, H. Ba, Y. Liu, L. Truong-Phuoc, J.-M. Nhut, C. Pham-Huu, Chin. J. Catal. 35 (2014) 906.

[24]   K. Chizari, A. Deneuve, O. Ersen, I. Florea, Y. Liu, D. Edouard, I. Janowska, D. Begin, C. Pham-Huu, ChemSusChem 5 (2012) 102.

[25]   K. Gong, F. Du, Z. Xia, M. Durstock, L. Dai, Science 323 (2009) 760.

[26]   L. Truong-Phuoc, C. Duong-Viet, W.-H. Doh, A. Bonnefont, I. Janowska, D. Begin, E.R. Savinova, P. Granger, C. Pham-Huu, Catal. Today (n.d.).

[27]   G. Tuci, C. Zafferoni, A. Rossin, A. Milella, L. Luconi, M. Innocenti, L. Truong Phuoc, C. Duong-Viet, C. Pham-Huu, G. Giambastiani, Chem. Mater. 26 (2014) 3460.

[28]   X. Li, X. Pan, L. Yu, P. Ren, X. Wu, L. Sun, F. Jiao, X. Bao, Nat. Commun. 5 (2014).

[29]   B. Zhong, J. Zhang, B. Li, B. Zhang, C. Dai, X. Sun, R. Wang, D.S. Su, Phys. Chem. Chem. Phys. 16 (2014) 4488.

[30]   D. Yu, E. Nagelli, F. Du, L. Dai, J. Phys. Chem. Lett. 1 (2010) 2165.

[31]   S. Song, H. Yang, R. Rao, H. Liu, A. Zhang, Catal. Commun. 11 (2010) 783.

[32]   K. Waki, R.A. Wong, H.S. Oktaviano, T. Fujio, T. Nagai, K. Kimoto, K. Yamada, Energy Environ. Sci. 7 (2014) 1950.

[33]   B. Frank, R. Blume, A. Rinaldi, A. Trunschke, R. Schlögl, Angew. Chem. Int. Ed. 50 (2011) 10226.

[34]   S. Wu, G. Wen, J. Wang, J. Rong, B. Zong, R. Schlögl, D.S. Su, Catal. Sci. Technol. 4 (2014) 4183.

[35]   S. Wu, G. Wen, R. Schlögl, D.S. Su, Phys. Chem. Chem. Phys. 17 (2014) 1567.

[36]   K. Chizari, I. Janowska, M. Houllé, I. Florea, O. Ersen, T. Romero, P. Bernhardt, M.J. Ledoux, C. Pham-Huu, Appl. Catal. Gen. 380 (2010) 72.

[37]   G. Gulino, R. Vieira, J. Amadou, P. Nguyen, M.J. Ledoux, S. Galvagno, G. Centi, C. Pham-Huu, Appl. Catal. Gen. 279 (2005) 89.

[38]   L.G. Cançado, A. Jorio, E.H.M. Ferreira, F. Stavale, C.A. Achete, R.B. Capaz, M.V.O. Moutinho, A. Lombardo, T.S. Kulmala, A.C. Ferrari, Nano Lett. 11 (2011) 3190.

[39]   W. Zhou, S. Sasaki, A. Kawasaki, Carbon 78 (2014) 121.

[40]   S. Kundu, W. Xia, W. Busser, M. Becker, D.A. Schmidt, M. Havenith, M. Muhler, Phys. Chem. Chem. Phys. 12 (2010) 4351.

[41]   D.-V. Cuong, L. Truong-Phuoc, T. Tran-Thanh, J.-M. Nhut, L. Nguyen-Dinh, I. Janowska, D. Begin, C. Pham-Huu, Appl. Catal. Gen. 482 (2014) 397.

[42]   N. Keller, C. Pham-Huu, M.J. Ledoux, Appl. Catal. Gen. 217 (2001) 205.

[43]   P. Delporte, C. Pham-Huu, M.J. Ledoux, Appl. Catal. Gen. 149 (1997) 151.

[44]   C. Pham-Huu, P.D. Gallo, E. Peschiera, M.J. Ledoux, Appl. Catal. Gen. 132 (1995) 77.

CHAPTER 5

Conclusions and Perspectives

Carbon materials (CNTs, CNFs) have hold numerous potential applications in electronic (electrocatalysis, batteries), mechanical, energy storage and heterogeneous catalysis… due to their unique physical and chemical properties such as: *(i)* high resistance to acid/basic media, *(ii)* possibility to control, up to certain limits, the porosity and surface chemistry of the solid and, *(iii)* easy recovery of the active phase, especially those constituted by precious metals, by burning the support. Recently, heteroatoms (nitrogen, boron, oxygen…) doped carbon nanotubes (X-CNTs) are receiving more and more scientific attention due to their altered physico-chemical properties with respect to polarity, conductivity and reactivity as compared to un-doped CNTs. Up to now, two approaches were employed and investigated for the synthesis of heteroatom doped CNTs, either directly during synthesis of CNTs (in-situ method) or by post-treatment of the as-synthesized CNTs (ex-situ method). For both approaches various methods such as arc-discharge, laser-ablation, chemical vapour decomposition (CVD), and organo-metallic functionalization have been employed.

The main different between the doped-CNTs and the un-doped ones is that the former is an active metal-free catalyst in several relevant reactions while the later is less. The literature reports indicated that heteroatoms, especially nitrogen, play an important role in providing an active center for performing the reaction. Other report suggested that the presence of both oxygenate functionalities and defects on the surface of CNTs are at the origin of the catalytic performance on the un-doped CNTs. However, there are scarce reports that systematically investigate the relation between these physical-chemical properties of the doped and un-doped CNTs to their catalytic performances.

In this thesis the main objective has been focused on the influence of both the nitrogen doping and the defects, decorated with oxygenated groups, on the catalytic performance for the partial oxidation of H_2S. The role and the intrinsic activity of each component, i.e. doping and defects, were discussed in detail according to the characterization data and the catalytic performance.

5.1. Synthesis and characterizations of nitrogen-doped carbon nanotubes decorated silicon carbide (N-CNT/SiC) by in-situ method

N-CNTs and N-CNT/SiC composite were synthesized directly by a CVD method with iron loaded on different supports, *i.e.* α-Al_2O_3 and SiC extrudates, as a growth catalyst. $C_2H_6/NH_3/H_2$ mixture was employed as carbon and nitrogen precursors. The synthesis conditions were described in detail in Chapter 2. According to the obtained results, the optimized synthesis parameters for the synthesis of N-CNT/SiC composite are the following: Fe-7 wt.% catalyst loaded on SiC support, $C_2H_6/NH_3/H_2$ = 50/50/20 (mL.min^{-1}), reaction

temperature of 750 °C, and duration of 90 min. The results indicated that the N-CNTs yield decreased as increasing the synthesis temperature and duration. The optimized N-CNTs yield was about 40 wt.% (750 °C and 90 minutes) on the N-CNTs/SiC as at yield higher than 60 wt.% (synthesis temperature < 720 °C and/or synthesis duration > 120 min), the macroscopic structure was partly destroyed after the removal iron catalyst by acid due to the breakdown of the grain boundary by the formed nanotubes. On the other hand, at synthesis temperature of 750 °C and synthesis duration for 90 min the surface specific area seem to be the most relevant for obtained N-CNT/SiC composite with the maximum value of 150 m^2/g (instead of 25 m^2.g^{-1} of the initial SiC support) along with the higher total nitrogen content.

5.2. Synthesis and characterizations of nitrogen-doped carbon phase on macroscopic supports by ex-situ method

We have successfully synthesized the porous nitrogen-doped carbon-based composites (N@C) with exceptionally high nitrogen content from non-toxic raw materials (food raw materials), *i.e.* ammonium carbonate, glucose and citric acid, by an ex-situ method. The N@C layer can be formed on different kinds of macroscopic supports such as alumina and silicon carbide as a function of the downstream catalytic applications. The method also allows one to incorporate a relatively large amount of nitrogen inside the carbon phase, *i.e.* > 10 wt.%, along with a large improvement of the final composite surface area , *i.e.* 149 m^2.g^{-1} instead of 29 m^2.g^{-1} for the pristine SiC. On the other hand, XPS measurement unveil remarkably high N-contents (normalized to the mass of N-doped mesoporous carbon deposit on the SiC matrix), spanning from 14 wt.%, for samples treated in air at 450 °C, to 8.8 wt.% for the high temperature (900 °C under argon) annealed composites. It is worthy noted that the nature and content (wt.%) of the N-species within each N@C phase is tunable as a function of several factors: *(i)* the ammonium carbonate molar fraction in the impregnating solution; *(ii)* the number of soaking/drying cycles; *(iii)* the applied thermal treatment(s).

5.3. Modification and characterizations of oxidized carbon nanotubes

One common approach for the surface functionalization of carbon nanotubes is based on the use of oxidative agents in liquid- or gas-phase. However, compared to the classical treatment in liquid-phase, the vapor treatment does not require any post-treatment additional process such as filtration, washing and drying, which are time and cost consuming for the process. As reported in Chapter 4, we have successfully carried out the gas-phase functionalization of the carbon nanotubes using vapor HNO$_3$. According to the obtained results the gas-phase functionalization of CNTs creates both defects and oxygenated functional groups on the surface of the treated CNTs. The generation of defects along the tube wall significantly increases as a function of the treatment temperature and

duration. The increasing of defects also led to an increasing of the surface specific area up to 1.6 times compared to the pristine CNTs, *i.e.* 382 $m^2.g^{-1}$ instead of 243 $m^2.g^{-1}$, while the amount of oxygen slightly increase from 3.5 to about 6 at.%. It is worthy note that at higher treatment temperature, *i.e.* 275 °C, or longer duration, i.e. > 24 h at 250 °C, the values of the oxygen and defects density almost unchanged while the tube morphology is strongly damaged leading to the mass loss up to 33 wt.% and 43 wt.% at 275 °C for 24 h or at 250 °C for 40 h, respectively. According to the results one can stated that the optimized treatment conditions under vapor HNO_3 are 250 °C for 24 h, which allow one to obtain O-CNTs with a highest amount of oxygen, defects and specific surface area without significant tube damage or breaking.

5.4. Catalytic performance test for selective oxidation reaction of H_2S into elemental sulfur

The different metal-free catalysts, which were either synthesized using in-situ or ex-situ method, were tested in the selective oxidation of H_2S into elemental sulfur. The influence of the nitrogen doping and defect sites on the desulfurization performance is summarized in Fig. 5.1.

According to the results all the metal-free catalysts display a relatively high desulfurization performance along with an extremely high resistance towards deactivation as a function of time on stream and under different reaction conditions. The metal-free desulfurization performance outperforms the one obtained on the industrial iron-based supported on SiC catalyst. The very high activity and stability of these metal-free carbon nanomaterials could be attributed to the high stability of the heteroatoms (oxygen presents on the defects and nitrogen as doping) in the CNTs matrix which plays the role of active site.

According to the obtained results, the macroscopic shaping of N-CNTs significantly improves the desulfurization activity performance in comparison with that obtained on the unsupported one, *i.e.* H_2S conversion of 95.7 % on N-CNTs/SiC and 86.3 % obtained on N@C/SiC compared to 33.4 % in the case of unsupported N-CNTs. The high activity of the supported N-CNTs could be attributed to the higher effective surface of the catalyst which significantly improves the reactant and active sites contact. In addition, it is worthy to note that the supported catalyst also allows one to overcome the problems linked with the handling and the transport of the nanoscopic un-supported N-CNTs catalyst. Finally, this hybrid metal-free catalyst with controlled macroscopic shape can be efficiently employed in a fixed-bed configuration without facing the problem linked with the pressure drop across the catalytic bed as generally encountered with the unsupported ones.

Table 5.1. Summarized the influence of physical-chemical properties of carbon nanomaterials as metal-free catalysts on catalytic performance of the selective oxidation of H_2S into elemental sulfur.

Sample	C	O	N	SSA ($m^2 \cdot g^{-1}$)	Active sites	H_2S conv. (T=230 °C)	S selec. (T=230 °C)	H_2S conv. (T=190 °C)	S selec. (T=190 °C)
Fe(3 wt.%)/SiC	-	-	-	25	Fe	31.1	92.3	16.9	88.0
CNTs	96.7	3.3	-	180	Defects, oxygen functional groups	32.7	86.5	-	-
O-CNTs	93.3	6.7	-	382	Defects, oxygen functional groups	94.9	76.8	50.6	87.6
N-CNTs	92.2	4.4	2.4	215	Defects, oxygen- and nitrogen functional groups	65.5	86.7	33.4	89.1
N-CNT/SiC	86.3	9.6	4.1		Defects, oxygen- and nitrogen functional groups	-	-	95.7	74.1
N@C/SiC	-	-	8.11	149	Defects, oxygen- and nitrogen functional groups	-	-	86.3	77.3

[*] Atomic percentage normalized to the un-doped/doped CNTs (active phase).

[**] Desulfurization conditions: M_{cata} (active phase) = 300 mg; $[H_2S]$ = 1 vol.%; $[H_2O]$ = 30 vol.%; O_2-to-H_2S = 2.5; WHSV = 0.6 h^{-1}.

(-) Undefined or not show in the thesis.

The results obtained also indicated that the desulfurization catalytic performance is also influenced by both the defects and oxygenated functional groups on the surface of the CNTs pretreated with a gaseous HNO_3. The H_2S conversion increased as the defects and oxygenated functional groups increase, *i.e.* the H_2S conversion of the HNO_3 treated carbon nanotubes is about 3 times higher compared to the untreated CNTs catalyst, 94.9 % instead of 32.7 %, respectively. The sulfur selectivity lost of about 10 % on the O-CNTs catalyst could be attributed to the secondary reactions between the formed sulfur and the oxygen present in excess leading to a higher production of SO_2 compared to the untreated ones.

On the other hand, the spent catalyst analysis observed some surface area lost which could be attributed to the presence of solid sulfur deposited in the pores of the active phase or supports during the course of the reaction. However, as no deactivation occurred, even after more than 300 h of test, one can speculate that such a solid sulfur deposition has no effect on the overall density of the active site.

5.5. Perspectives

The results obtained in this Ph.D thesis have opened a new opportunities for the development of carbon-based metal-free catalysts. It is expected that such catalyst will find extensive development in the future in other relevant catalytic processes where traditional catalysts, based on supported metal or oxides, suffer from achieving high catalytic performance and long-term stability. The different perspectives which can be envisioned are described in the following.

The optimization study will be continued on the detailed characterization of the role of the defects decorated with the oxygenated functional groups, generated during the treatment in the presence of gaseous HNO_3, in order to build up a direct relationship between these defect sites and the desulfurization activity. For the moment, the full exploitation of such pre-treatment on the catalytic performance of these CNTs containing defects materials is still far from being fully achieved and its is expected that optimization process is still needed.

A detailed study will be also dedicated to the understanding of the N@C, synthesized from food stuffs by an ex-situ method, physical and microstructural properties regarding the subsequence optimization process. Indeed, despite the large investigation devoted to this system within the framework of this Ph.D a large part of the characterization data is still missing, i.e. acid-base properties as a function of the nitrogen doping concentration, porous accessibility, diffusion problem, which calls for a detailed investigation. The characterization data will allows one to build up the direct relationship between the physical properties of the catalyst and its desulfurization performance. Such relationship will also allow one to optimize the catalyst surface properties for the above mentioned reaction.

The ability of the N@C catalyst to dissociate oxygen upon adsorption will be further developed in other reactions such as hydrogenation or oxygen reduction which represent an important class of catalytic processes for both petrochemical and fine chemical fields.

Annex

Publications and Communications

I. Published articles

1. **Few-layer graphene decorated with homogeneous magnetic Fe₃O₄ nanoparticles with tunable covering densities.**
    W. Baaziz, L. Truong-Phuoc, C. Duong-Viet, G. Melinte, I. Janowska, V. Papaefthymiou, O. Ersen, S. Zafeiratos, D. Begin, S. Begin-Colin, C. Pham-Huu.
    J. Mater. Chem. A, 2014, 2, 2690-2700.

2. **Tunable electrocatalysts for the oxygen reduction reaction in alkaline medium by functionalization of carbon nanotubes with pyridine-based frameworks.**
    G. Tucci, C. Zafferoni, A. Rossin, A. Milella, L. Luconi, M. Innocenti, M. L. Foresti, L. Truong-Phuoc, C. Duong-Viet, C. Pham-Huu, G. Gambastiani.
    Chemistry of Materials, 26, 3460-3470, 2014.

3. **Nitrogen-doped carbon nanotubes decorated silicon carbide as a metal-free catalyst for partial oxidation of H₂S.**
    C. Duong-Viet, L. Truong-Phuoc, T. Tran-Thanh, J. M. Nhut, L. Nguyen-Dinh, I. Janowska, D. Begin, C. Pham-Huu.
    Applied Catalysis A: General, 482, 397-406, 2014.

4. **Carbon nanotubes doped with nitrogen decorated silicon carbide for catalytic applications.**
    C. Duong-Viet, H. Ba, Y. Liu, L. Truong-Phuoc, J. M. Nhut, C. Pham-Huu.
    Chinese Journal of Catalysis, 35, 906-913, 2014.

5. **Influence of the reaction temperature on the oxygen reduction reaction on nitrogen-doped carbon nanotubes catalysts.**
    L. Truong-Phuoc, C. Duong-Viet, W.H. Doh, A. Bonnefont, I. Janowska, D. Begin, P. Granger, C. Pham-Huu.
    Catalysis Today, 249, 236-243, 2015.

6. **One-pot synthesis of nitrogen-doped carbon composite by electrospinning as metal-free catalyst for oxidative reaction.**
    Y. Liu, C. Duong-Viet, A. Hébraud, G. Schlatter, J. Luo, O. Ersen, J.M. Nhut, C. Pham-Huu.
    ChemCatChem, accepted (2015). DOI: 10.1002/cctc.201500353

7. **A highly N-doped carbon phase "dressing" of macroscopic supports for catalytic applications.**

H. Ba, Y. Liu, L. Truong-Phuoc, C. Duong-Viet, X. Mu, W.H. Doh, T. Tran-Thanh, W. Baaziz, L. Nguyen-Dinh, J.M. Nhut, I. Janowska, D. Begin, P. Granger, G. Tuci, G. Giambastiani, F. Banhart, M.J. Ledoux, C. Pham-Huu.

Chemical communications (2015), DOI: 10.1039/C5CC05259A

8. **Self-sustained nitrogen-doped carbon nanotubes as-metal-free catalyst for selective oxidation**

H. Ba, C. Duong-Viet, Y. Liu, J-M. Nhut[a], P. Granger[b], M. J. ledoux, C. Pham-Huu[a],*

Compte Rendu de Chimie, Accepted 2015

II. Articles under preparation

1. **Carbon nanotubes containing oxygenated decorating defects as metal-free catalyst for the partial oxidation of H_2S.**

C. Duong-Viet, L. Truong-Phuoc, H. Ba, J. M. Nhut, Y. Liu, P. Granger, C. Pham-Huu.

Journal of Catalysis, under preparation (2015).

2. **Nitrogen-enriched carbon nanospheres decorated silicon carbide as a superior metal-free catalyst for styrene production.**

H. Ba, Y. Liu, C. Duong-Viet, M. Iltis, J. Luo, L. Truong-Phuoc, J.M. Nhut, P. Granger, C. Pham-Huu.

Apply catalysis A, under preparation (2015).

3. **Minute made of N-S co-doped carbon metal-free active phase.**

H. Ba, C. Duong-Viet, J.M. Nhut, L. Truong-Phuoc, C. Pham-Huu.

Chemical Communication, under preparation (2015).

III. Book's chapter

Nitrogen-doped carbon nanotubes composites as metal-free catalysts

C. Duong-Viet, H. Ba, L. Truong-Phuoc, Y.F. Liu, J. P. Tessonnier, J.M. Nhut, P. Granger, C. Pham-Huu.

Nanocarbon for catalysis, Elsevier Book series, under preparation (2015).

IV. Patents

1. **Procédé pour la mise en œuvre des structures mésoporeuses à base de composites de carbure de silicium recouvert par une couche de carbone pour l'échantillonnage passif des composés organiques semi-volatils.**

   Levi M., Ba H., Duong-Viet C., Millet M., Pham-Huu C.

   Demande de brevet Européen en cours.

V. Oral presentations

➢ **Keynote presentation:**

1. **Exploring new routes for 1D and 2D carbon synthesis.**

   T. Tran-Thanh, H. Ba, C. Duong-Viet, J.M. Nhut, D. Begin, I. Janowska, P. Bennefont, E.R. Savinova, C. Pham-Huu.

   Carbocat VI, 22-25 June 2014, Trondheim – Norway.

➢ **Oral presentation:**

2. **Low-temperature synthesis of macroscopic porous nitrogen-doped carbon composite with high doping content and exclusive localization.**

   H. Ba, Y. Liu, C. Duong-Viet, J.-M. Nhut, O. Ersen, D. Begin, I. Janowska, C. Pham-Huu.

   Carbocat VI, 22-25 June 2014, Trondheim – Norway.

3. **Carbon nanotubes containing defects as metal-free catalyst.**

   C. Duong-Viet, H. Ba, L. Truong-Phuoc, W.D. Doh, Y. Liu, J.M. Nhut, D. Begin, I. Janowska, P. Granger, C. Pham-Huu.

   7th IWAMSN 2014, 2 – 6 November 2014, Ha Long – Viet Nam.

VI. Posters

1. **Nitrogen-doped carbon nanotubes decorated silicon carbide as a metal-free for selective oxidation of H_2S.**

   C. Duong-Viet, L. Truong-Phuoc, J.-M. Nhut, L. Nguyen-Dinh, I. Janowska, D. Begin, C. Pham-Huu.

   Carbocat VI, 22-25 June 2014, Trondheim – Norway.

2. **Bare nitrogen doped carbon nanotubes as efficient catalyst in oxygen reduction reaction.**

L. Truong-Phuoc, C. Duong-Viet, J.M. Nhut, I. Janowska, D. Begin, P-A. Bonnefont, E. Savinova, C. Pham-Huu.

Carbocat VI, 22-25 June 2014, Trondheim – Norway.

3. **Catalyseur "sans métaux" à base de nanotubes de carbone pour l'oxydation sélective de l'H₂S en soufre élémentaire.**

C. Duong-Viet, L. Truong-Phuoc, J.-M. Nhut, C. Pham-Huu.

Les Doctoriales d'Alsace 2014.

4. **Nitrogen-doped carbon nanotubes as metal-free catalyst.**

C. Duong- Viet, L. Truong-Phuoc, T. Tran-Thanh, H. Ba, J.M. Nhut, C. Pham-Huu.

ORPE 2014, 8-10 November 2014, Ha Noi – Viet Nam.

Résumé

Les nanotubes de carbone (NTCs) dopés avec différents hétéroéléments tels que l'oxygène et l'azote connaissent un intérêt croissant dans le domaine de la catalyse hétérogène comme leur utilisation en tant que catalyseur sans métaux. L'objectif de cette thèse consiste à la synthèse et la caractérisation de matériaux catalytiques à base de NTC dopés à l'azote supportés sur du carbure de silicium SiC par voie in situ (CVD) et ex-situ méthodes. Une autre approche a été utilisée pour la fonctionnalisation de la surface des nanotubes de carbone et basées sur l'utilisation d'un agent oxydant (HNO_3) en phase gazeuse. Ce procédé d'oxydation crée non seulement des défauts sur la surface des nanotubes de carbone mais également décore leur surface avec des groupes fonctionnels oxygénés. Les NTCs dopés à l'oxygène et à l'azote ainsi synthétisés ont été caractérisés par différentes techniques (XPS, MEB, MET, BET, ATG). Ces catalyseurs carbonés présentent des performances remarquables en termes d'activité et de sélectivité en soufre, et une très grande stabilité sous flux en fonction du temps dans la réaction d'oxydation partielle de l'H_2S en soufre élémentaire, et ce, même à vitesse spatiale de gaz élevée (WHSV) et faible rapport O_2/H_2S. L'influence des différentes propriétés physico-chimiques et les défauts présents sur la surface des NTC sur les performances catalytiques ont été étudiée et discutée dans le cadre de ce travail.

Abstract

Carbon nanotubes (CNTs) containing different doping such as oxygen and nitrogen composites have received more and more scientific attention as metal-free catalyst in the field of heterogeneous catalysis. The aim of this thesis is related to the synthesis and characterization of nitrogen-doped CNTs decorated on SiC support using both *in-situ* (CVD with NH_3) and *ex-situ* (N@C) methods. Other approach was employed for the surface functionalization of CNTs is based on the use of oxidative agent (HNO_3) in gas phase. This oxidation process not only creates defects on the CNTs surface but also decorates their surface with oxygenated functional groups. The as-synthesized oxygen- and nitrogen-doped CNTs are characterized by different techniques (XPS, SEM, TEM, BET, TGA). The carbon based catalysts exhibit outstanding performances in term of activity and sulfur selectivity, and very high stability with time on stream in the partial oxidation of H_2S into elemental sulfur even at high gas space velocity (WHSV) and low O_2-to-H_2S molar ratio. The influence of the physical-chemical properties and defects present on the CNTs surface on the catalytic performance was thoroughly investigated and discussed within the framework of this work.